Development, physico-chemical characterization and biological evaluation of silk fibroin/hyaluronic acid freeze-dried sponges for the trapping of Glioblastoma cells

Mathie Najberg

▶ To cite this version:

Mathie Najberg. Development, physico-chemical characterization and biological evaluation of silk fibroin/hyaluronic acid freeze-dried sponges for the trapping of Glioblastoma cells. Human health and pathology. Université d'Angers; Universidad de Santiago de Compostela, 2019. English. NNT : 2019ANGE0040 . tel-04835591

HAL Id: tel-04835591
https://theses.hal.science/tel-04835591v1

Submitted on 13 Dec 2024

THESE DE DOCTORAT DE

L'UNIVERSITE D'ANGERS
COMUE UNIVERSITE BRETAGNE LOIRE
ET DE
L'UNIVERSITE DE SAINT-JACQUES DE COMPOSTELLE

ECOLE DOCTORALE N° 605
Biologie Santé
Spécialité : « *Sciences Pharmaceutiques* »

Par
Mathie NAJBERG

Development, physicochemical characterisation and biological evaluation of silk fibroin/hyaluronic acid freeze-dried sponges for the trapping of glioblastoma cells

Thèse présentée et soutenue à Angers, le 18/10/2019
Unité de recherche : CRCINA, Inserm U1232 GLIAD, Angers, France
I+D en formas de dosificación y sistemas de liberación de medicamentos (GI-1645), Saint-Jacques de Compostelle, Espagne
Thèse N° : 181293

Rapporteurs avant soutenance :

Dr. Thierry VIROLLE
DR2 Inserm, Université Côte d'Azur, France

Dr. Miguel ABAL
Senior scientist, Nasasbiotech, Spain

Composition du Jury :

Dr. Thierry VIROLLE, Rapporteur
DR2 Inserm, Université Côte d'Azur, France

Dr. Miguel ABAL, Rapporteur
Senior scientist, Nasasbiotech, Spain

Dr. Maria MARLOW, Examinatrice
Associate professor, University of Nottingham, United Kingdom

Dr. Emmanuel GARCION, Directeur de thèse
DR2 Inserm, Université d'Angers, France

Dr. Carmen ALVAREZ-LORENZO, Co-directrice de thèse
Professeure d'Université, University of Santiago de Compostela, Spain

RÉSUMÉ

Le glioblastome (GBM) est une tumeur dévastatrice du système nerveux central. Malgré un traitement agressif, les récidives sont inévitables et l'application d'une stratégie thérapeutique efficace deumeure un défi. Le concept révolutionnaire de piège à cellules cancéreuses peut offrir de nouvelles opportunités. L'objectif est d'attirer et de confiner les cellules cancéreuses résiduelles entourant la cavité chirurgicale dans un implant polymère biomimétique délivrant des molécules chimioattractantes. Le SDF-1α, également appelé CXCL12, se lie sélectivement au récepteur CXCR4 à la surface des cellules de GBM infiltrantes et peut être utile pour induire le recrutement de ces cellules. Des éponges lyophilisées ont été préparées en combinant de la fibroïne de soie (SF), de l'acide hyaluronique (HA), de la poly-L-lysine (PLL) et de l'héparine (hep) réticulée avec N-(3-diméthylaminopropyl)-N'-éthylcarbodiimide (EDC) et du N-hydroxysulfosuccinimide (NHS). Les éponges ont montré une porosité élevée (près de 90%) avec des diamètres de pores moyens de 60 µm et contenait jusqu'à 95% d'eau une fois hydraté et un module de Young inférieur à 6 kPa. De plus, l'addition de SF dans la formulation a permis d’augmenter la stabilité des éponges dans le PBS comparé à l’éponge HA-PLL. Les éponges SF-HA et SF-HA-hep étaient capables de conserver 75% et 93% de la protéine SDF-1α respectivement après 7 jours dans du PBS supplémenté en enzymes (hyaluronidase et héparinase). Des études in vivo ont montré que les éponges SF-HA et SF-HA-hep étaient bien tolérées dans le cerveau des rats et que l’éponge SF-HA-hep ne libérait pas de SDF-1α dans le cerveau après 7 jours.

mots-clés : Piège à cellules tumorales; biomimétisme cérébral; implant poreux; éponges composites

ABSTRACT

Glioblastoma (GBM) is a devastating tumour of the central nervous system. Despite an aggressive treatment, recurrence is inevitable, and the application of an effective therapeutic strategy remains a challenge. The breakthrough concept of cancer cell trap may offer new hopes and opportunities. The goal is to attract and confine the residual cancer cells surrounding the surgical cavity in a biomimetic polymeric scaffold delivering chemoattractive molecules. The stromal cell-derived factor-1α (SDF-1α), also called CXCL12, binds selectively to the CXCR4 receptor on the surface of infiltrative GBM cells and may be useful for inducing chemotaxis and the recruitment of residual GBM cells. In this work, series of freeze-dried sponges were prepared by combining silk fibroin (SF), hyaluronic acid (HA), poly-L-lysine (PLL) and heparin crosslinked with N-(3-dimethylaminopropyl)-N′-ethylcarbodiimide hydrochloride (EDC) and N-hydroxysulfosuccinimide sodium salt (NHS). Sponges showed high porosity (near 90%) with mean pore diameters ca. 60 µm and contained up to 95% water once hydrated. They presented a soft texture close to the one of a brain with a Young’s Modulus down to 6 kPa. Moreover, addition of SF in the formulation yielded sponges with greater stability in PBS than the HA-PLL sponges. SF-HA and SF-HA-hep sponges were able to retain 75% and 93% of the SDF-1□ protein respectively after 7 days in PBS supplemented with enzymes (hyaluronidase and heparinase). In vivo studies showed that the SF-HA and SF-HA-hep sponges were well tolerated in rats’ brain and that the SF-HA-hep sponge did not release SDF-1α after 7 days in the brain.

keywords : Tumour cell trap; brain biomimicry; porous scaffold; composite sponges

Présidence de l'université
40 rue de rennes – BP 73532
49035 Angers cedex
Tél. 02 41 96 23 23 | Fax 02 41 96 23 00

université
angers

ENGAGEMENT
DE NON PLAGIAT

Je, soussigné(e) Mathie Najberg
déclare être pleinement conscient(e) que le plagiat de documents ou d'une partie d'un document publiée sur toutes formes de support, y compris l'internet, constitue une violation des droits d'auteur ainsi qu'une fraude caractérisée.
En conséquence, je m'engage à citer toutes les sources que j'ai utilisées pour écrire ce rapport ou mémoire.

signé par l'étudiant(e) le **15** / **07** / **2019**

ACKNOWLEDGMENTS

Firstly, I want to thank my supervisors Dr. Emmanuel Garcion and Dr. Carmen Alvarez-Lorenzo. They opened me the doors of two excellent and different laboratories and gave me the opportunity to develop an extremely interesting, challenging and multidisciplinary project. I received from them a constant trust and freedom in the realisation of this work and my choices have always been respected and discussed as an equal collaborator and not as an unexperienced student. You also both have been extremely supportive personally when I needed it and I will always be grateful. I also want to thank the members of my thesis committee Dr. Jean-Paul Issartel, Dr. Benjamin Lemasson and Dr. José-Luis Cenis for their time and feedback at each stage of my PhD. Your suggestions pushed me to see this work from different perspectives, and to implement my knowledge and research plan. Also, I want to acknowledge Dr. Thierry Virolle, Dr. Miguel Abal, and Dr. Maria Marlow for accepting to be part of my jury.

I want to thank particularly Dr. José-Luis Cenis, your emails always make me smile and encourage me. Thank you also for welcoming me in your laboratory at IMIDA as well as Salva, Ana and Abel and for passing me on your knowledge and passion about silk. I also want to thank Liliane for welcoming me in your house during my stay in La Alberca. You all helped me during this difficult time of my life while you barely knew me, and I will always be grateful.

As the scope of my thesis is very broad, I am grateful to have received assistance from a long list of kind-hearted people in Angers and in Santiago. From Santiago, I would like to thank Ruben Varela Calvino for all the time and his precious help for optimising the SDS-PAGE. Angel Concheiro Nine, Carlos Garcia Gonzalez, Mariano Marletta Vasquez and also Fernando for their welcome and help during my stay in Santiago as well as all the other members of the laboratory. From Angers I would like to thank Romain Mallet for the SEM, Rodolphe Perrot for the confocal imaging and Cathrine Guillet for the flow cytometry. I am very grateful to Clément Tétaud for his precious help with the in vivo experiments as well as to Audrey Rousseau for her expertise in histology. With my master’s in chemistry, I could never have done this thesis without the patience of Claire Loussouarn who taught me cellular culture and introduced me to the world of the biology and many thanks to Sylvie Avril, Laurence Sindji and Anne Clavreul for helping me all along. Thanks to Edward for his insights on gliobliostama treatment.

I would like to deeply thank my interns Céline Bourré, Théodore Taillé and Rosalie Moreau. You were the best students I could have asked for. You helped me a lot with my thesis, but you also made me grow personally.

To Muhammad, by accepting to work on this project, I knew I will be working with you. I was anxious and exited at the idea of not being the only PhD student started on this new idea that was the tumour trap. Right away we clicked, we work so well together it will be hard to work without you! You also became one of my closest friends, these three years would have not been the same without you.

A Víctor, Clara, Mariana, muchas gracias para el tiempo pasado a Santiago con vosotros. No es fácil vivir en un país extranjeros, pero con vosotros estaba como a mi casa.

To my colleagues and friends Hélène, Nela, Déborah, Muhammad, Charlotte, Assia, Shubaash, to the members of the “bureau des licornes” et “les amis des toilettes”, Janske, Baptiste, Adélie, Florence, Jamal, Lila. Thank you for sharing the hard and awesome times of the PhD journey with me.

Many thanks to all the nanofar students and in particular Chiara, Banhu, Maruti, Raneem, Batabile, Paul, Natalja, for the amazing sharing of cultures. Being part of the nanofar family means never be alone wherever you are.

Many thanks to the crow holding the key to allow me access to the world’s knowledge.

Finally, I would like to thank my extended family and in particular my parents, my brother and sisters (Sarah, Marie, Hugo) and their husbands and wife, Florence and Jacques-Yves, and my stress releasers Loki and Emile.

To my father

TABLE OF CONTENTS

Abbreviations

ADC	Aphidicholin
AF-SDF-1	Aleafluor647 labelled SDF-1
ATR-FTIR	Attenuated total reflection Fourier transformed infrared
BBB	Blood brain barrier
BCNU	Bis-chloroethylnitrosourea
BMP	Bone morphogenic protein
BMSC	Bone marrow stromal cells
BSA	Bovine serum albumin
CAF	Cancer-associative fibroblast
CAR	Chimeric antigen receptor
CED	Convection enhanced delivery
CNS	Central nervous system
CSC	Cancer stem cell
CSF	Colony-stimulating factor
CTC	Circulating tumor cell
DMEM	Dubelcco's modified eagle's medium
ECM	Extracelular matrix
EDC	N-(3-dimethylaminopropyl)-N′-ethylcarbodiimide hydrochloride
EGF	Epidermal growth factor
EMT	Epithelial-mesenchymal transition
EpCAM	Epithelial cell adhesion molecule
Eph	Erythropoietin-producing human hepatocellular carcinoma
EtOH	Ethanol
FBS	Fetal bovine serum
FDA	Food and drug administration
FITC	Fluorescein isothiocyanate
GBM	Glioblastoma
GlcA	B-D-glucuronic acid
GlcN	A-D-glucosamine
HA	Hyaluronic acid
hep	Heparin
HS	Heparan sulfate
IdoA	A-L-iduronic acid
MC	Methylcellulose
MGMT	O^6-methylguanine-DNA methyltransferase
MMP	Matrix metalloproteinase
MRI	Magnetic resonance imaging
NHS	N-hydroxysulfosuccinimide sodium salt
NPC	Neural progenitor cell
PARP	Polyadp ribose polymerase
PBS	Phosphate buffer saline
PCL	Polycaprolactone
PDL	Poly-D-lysine
PEG	Poly(ethylene glycol)

PLGA	Poly(lactide-co-glycolic acid)
PLL	Poly-L-lysine
RFP	Red fluorescent protein
SDF	Stromal cell derived factor
SDS-PAGE	SDS-poly(acrylamide) gel electrophoresis
SEM	Scanning electron microscopy
SF	Silk fibroin
SRT	Stereotactic radiotherapy
TMZ	Temozolomide
TTF	Tumor-treating field
WHO	World health organization
XL	Crosslinked
PFA	Paraformaldehyde
NGS	Normal goat serum
HE	Hematoxylin and eosin
SB	Soudan black B

CHAPTER I: INTRODUCTION

Table of content

CHAPTER I

Introduction

1. Cancer, glioma and glioblastoma

1.1. The cancer and solid tumours

Damages to the DNA can be caused by viruses or environmental factors like chemicals, fumes or UV light for example. In normal conditions, cells are able to repair damages done to the DNA which can create errors. If the lesions create an important damage, the cell undergos apoptosis. If the lesions are small, the cell can survive and proliferate normally, and mutations appear. They can either be recessive and do not represent a risk for the organism or be dominant and create a new trait. Repetitive aggressions can lead to multiple mutations and drive to the apparition of a tumour, characterised by an anarchic proliferation of cells. The tumour can either be noncancerous (benign) or cancerous (malignant).

Defining cancer is no easy task, that is why Hanahan and Weinberg proposed, in 2000, 6 hallmarks of cancer. They have been revisited in 2011 with the addition of 4 more (1). These hallmarks are biological capabilities acquired during the development of tumours:

- Sustaining proliferative signalling

Cancer cells sustain proliferative signalling in two different ways. They can produce themselves growth factors (autocrine loop) or they can activate healthy cells in their environment which answers by sending them growth factors (paracrine loop).

- Evading growth suppressors

The proteins retinoblastoma and p53 act as regulators and decide if the cell proliferates or activates the senescence or apoptosis programs. These two proteins are frequently mutated in cancers.

- Avoiding immune destruction

Cancerous cells are able to avoid the immune system by secreting immunosuppressive factors like the TGF-β. They can also recruit inflammatory cells with immunosuppressive properties like the regulatory T cells (Treg) and myeloid-derived suppressor cells (MDSCs).

- Tumour-promoting inflammation

Inflammation contributes to the acquisition of hallmarks by bringing bioactive molecules like growth factors, survival signals, pro-angiogenic factors, enzymes modifying the extracellular matrix (ECM) and facilitating angiogenesis, invasion and metastasis.

- Enabling replicative immortality

Cancerous cells can replicate indefinitely unlike normal cells.

- Inducing angiogenesis

Angiogenesis allows tumours to create its own capillary system to be supplied in oxygen and nutrients, necessary to its development.

- Genome instability and mutation

The probability of mutations development advantageous for the survival of cancerous cells is increased by defaults in the genome maintenance and DNA repair mechanisms.

- Resisting cell death

Apoptosis is regulated in cells by signals pro- (Bax and Bak proteins for example) and anti-apoptotic (like the proteins of the Bcl-2 family). Cancerous cells establish strategies to bypass apoptosis by increasing the expression of anti-apoptotic signals or by deregulating pro-apoptotic signals among other strategies.

- Deregulating cellular energetics

In normal conditions, energy is mainly generated by the Krebs cycle. However, in hypoxic condition, like in most of the tumours, the main energy production is generated by the cytoplasmic glycolysis.

- Activating invasion and metastasis

Cancerous cells are able to modify their structure and their environment as well as being able to detach from the other cells and from the ECM to invade tissues. This phenomenon is favoured by the epithelial-mesenchymal transition (EMT).

In addition to these hallmarks, tumours interact with their environment and recruit normal cells, creating a tumour microenvironment. Properties of tumours therefore differ depending on the type of cells they are originated from but also on the organ they are implanted in.

1.2. The glioma and glioblastoma

Brain tumours are classified from grade I to IV depending on their degree of malignancy; the grade IV describing tumours with the worst prognostic, according to the World Health Organization (WHO) classification of the central nervous system (CNS) (2).

- Grade I (benign tumours) corresponds to slow growing tumours with a delimited border.
- Grade II corresponds to slow growing tumours with an undelimited border.
- Grade III (malign tumours) corresponds to anaplastic tumours, *i.e.* presenting abnormal cells, and with a higher development rate than lower grade tumours.
- Grade IV tumours possess different cell types that proliferate fast and with a spontaneous necrotising tendency. They are not defined and infiltrate the brain.

Glioma is a type of tumour derived from the supportive tissue of the brain called glia, composing 90% of the brain. Gliomas are divided in three groups: oligodendrogliomas (derived from the oligodendrocytes), oligoastrocytomas (derived from oligodendrocytes and astrocytes) and astrocytomas (derived from astrocytes).

Astrocytomas are divided in four grades: pilocytic astrocytoma (grade I), diffuse astrocytoma (grade II), anaplastic astrocytoma (grade III) and multiform glioblastoma (grade IV).

Gliomas are identified and treated based on common histopathological criteria. However, they might not accurately predict clinical outcome (3). The 2016 WHO classification of tumours of the CNS therefore combines histology with molecular parameters (4). In the new classification, diffuse gliomas include grade II and III astrocytic tumours, grade II and III oligodendrogliomas, grade IV glioblastoma and related diffuse gliomas of childhood (Figure 1. 1). They are classified according to the mutation of the isocitrate dehydrogenase (IDH), ATRX, TP53 genes and codeletion of 1p/19q. A NOS designation implies that there is insufficient information to assign a more specific code, it designates tumours that cannot be classified in a more narrowly defined group.

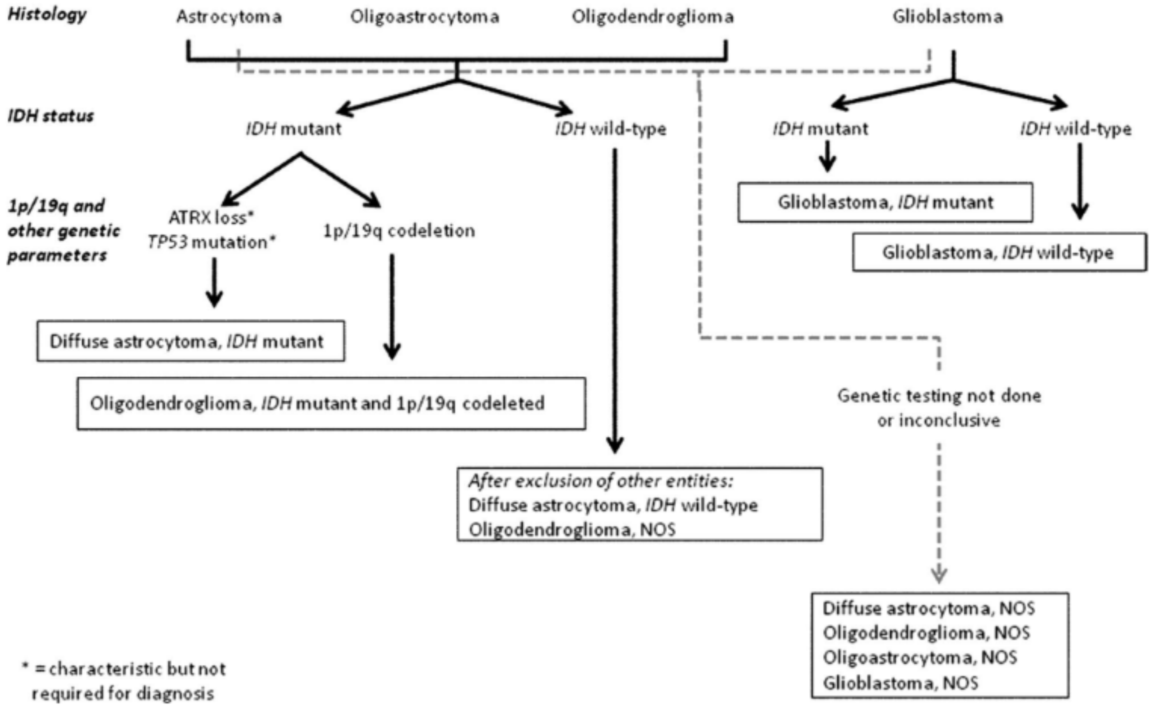

Figure 1. 1: Simplified classification of diffuse gliomas based on histological and genetic features. Adapted from (4).

Glioblastoma multiforme (GBM) is an infiltrating tumour of the CNS known since the beginning of the nineteenth century (5). It is the most lethal form of glioma since it always grows rapidly as a highly malignant tumour. GBM can be primary or secondary (result from the evolution of a tumour of an inferior grade). GBMs are divided into three groups according to the 2016 CNS WHO (4). The first group has IDH-wildtype, which corresponds most frequently with primary GBM in patients over 55 years old and it represents about 90% of the cases (6). The second group has IDH-mutant, which corresponds to secondary GBM, arises in younger patients and represents about 10% of the cases (6). The third group is the NOS, where a full IDH evaluation cannot be performed. IDH-mutant GBM has a higher median of survival (31 months) compared with IDH-wildtype GBM (15 months).

According to a study conducted worldwide from 2006-2011 on all newly diagnosed and histologically confirmed cases of primary central nervous system tumours, incidence of GBM is of 2.1/100,000 worldwide, 2.9 in Europe and 3.3 in France (7). GBM can occur at every age but in 70% of the cases patients are between 45 and 70 years old. Neurologic signs are not specific, reflecting an intracranial hyperpressure (headache and vomiting) often associated to behaviour changes or neurological defects depending on the affected zone of the brain. GBM can be detected by CT-scanner (computed tomography) or MRI (magnetic resonance imaging) as an infiltrative lesion infiltrating the brain parenchyma and necrotic zones (8). Use of contrasting agents like iodized compounds visible by X-ray for the CT-scanner or gadolinium for the MRI are needed. Figure 1. 2 shows MRI of a patient with GBM. The mass appears irregular, with an undulating ring or wavy margin, and its inner aspect is shaggy and irregular. Imaging can be associated with magnetic resonance spectroscopy (MRS) which allows to estimate the proliferation rate of tumour cells as well as the necrosis. GBM are characterised by an increase of the peak of choline (cellular hyperplasia and inflammation), lactate (hypoxia) and lipids (membrane alteration, necrosis) as well as a decrease of the peak of N-acetyl-aspartate (loss or displacement of neurons) and creatine (oxygen regulation) (9). A stereotactic biopsy or a craniotomy followed by histological analysis has to be performed to confirm the diagnostic.

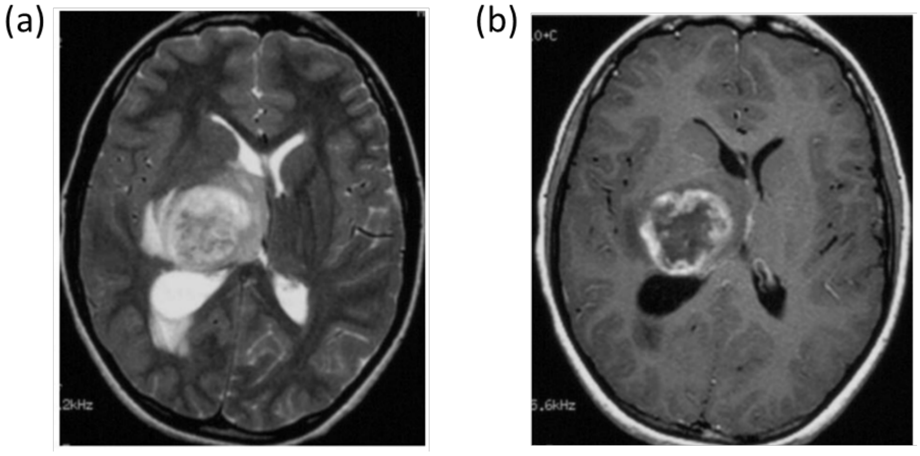

Figure 1. 2: Diagnostic of GBM by MRI. (a) Axial non-enhanced T2-weighted MRI of a GBM shows a large heterogeneous mass. (b) Axial gadolinium-enhanced T1-weighted MRI image of a GBM shows the irregular mass. The ring has a characteristically undulating or wavy margin, and its inner aspect is shaggy and irregular. Figure adapted from Smirniotopoulos *et al.* (8).

2. Current treatments of the glioblastoma

The term ''glioblastoma multiform'' was first coined by Percival Bailey and Harvey Cushing in 1926 (5). At this time, the only treatment was surgery. In 1949, Netsky and co-workers (10) studied the longevity of patients with GBM in order to gain knowledge on the tumour. They reported a mean survival of 8.3 months with near 80% of the patients dying within 20 months after the diagnostic. Today, 70 years later, the median of survival is of less than 15 months with 5% of the patients living more than 5 years after diagnostic (11). Nowadays, the treatment consists in a surgical resection removing the maximum of the tumour followed by radiotherapy in the region of the cavity post-surgery and chemotherapy with an alkylating agent, the temozolomide (Témodal®) (TMZ) (12). The surgery only allows a median of survival of about 6 months, combined with radiotherapy the median of survival is prolonged until 12.1 months. Addition of TMZ leads to a median of survival of 14.6 months.

2.1. Surgery

The surgery is a major element in the treatment of GBM. The post-operative tumour residue being often at the origin of the recurrence of the tumour, resection needs to be as large as possible without leading to unacceptable neurological deficits. Chaichana *et al.* (13) have studied the correlation between the percent of resection and survival over 259 patients. A resection of more than 70% of the tumour volume showed statistically significant improvement in overall survival and seizure control. However, surgery is not always an option, depending on the age of the patient, his/her health state, the size, localisation of the tumour and the technical availabilities for the surgery. Results suggest that repeat surgery at GBM recurrence confers a significant overall survival advantage (14).

Visual delimitation of the tumour's margins in combination with common surgical technics allows completer and more accurate resection of the tumour, leading to better outcomes for the patient. Different aids are at the disposal of the surgeon. Confocal intraoperative microscopy can be used to differentiate more precisely tumour cells from healthy tissue with the use of near infrared, fluorescence markers (like 5-aminolevulinic acid-induced porphyrin, indocyanine green or fluorescein sodium) (15). Other technics include intraoperative MRI and diffusion tensor imaging MRI (16–18).

2.2. Concomitant radiotherapy and chemotherapy

Nowadays, the standard treatment for GBM after surgery follows the protocol described by Stupp *et al.* in 2005 (12) and consists in a concomitant radiotherapy and chemotherapy following the surgery. GBM patients' need to wait for at least 4 weeks after the surgical resection before starting the TMZ and radiotherapy regimen to allow the tissues to heal (19). This period might be extended depending on the hospital schedule. Fractionated radiotherapy (30 times 2 Gy) is combined with a daily chemotherapy with TMZ for 6 weeks. It is then followed by adjuvant care therapy for 6 cycles of 5 days with 4 weeks gaps (Figure 1. 3).

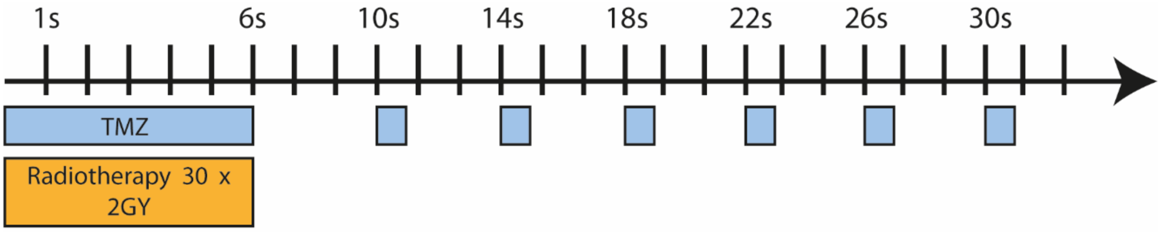

Figure 1. 3: Recommended therapy timeline. Fractionated radiotherapy (30 times 2 Gy) is combined with a daily chemotherapy with TMZ for 6 weeks. It is then followed by adjuvant care therapy with TMZ for 6 cycles of 5 days with 4 weeks gaps (12).

X-ray radiotherapy is administered in the area of the resection cavity post-surgery with a 2 cm gap in the surrounding healthy tissues. Ionising radiation induces simple strand and double strand breaks in the DNA of proliferating cells.

TMZ is an alkylating agent that generates DNA damages and drives targeted cells to apoptosis. It targets in particular the O^6-methylguanine by adding a methyl group. Before 2005, chemotherapy of GBM was done with nitrosoureas or procarbazine. TMZ was developed and received an accelerated approval in 1999 for GBM patients refractory to these two chemotherapeutic agents. TMZ is available in oral formulation with an equivalent bioavailability compared with the intravenous formulation, the last one being therefore rarely used in clinical practice (20). Treatment through oral delivery offers tremendous advantages compared with the intravenous one since in implies less interference in the daily life of patients. Since 2005, TMZ is used as the first-line treatment for GBM. Monika *et al.* (21) analysed 206 patients GBM including 46 patients that had the O^6-methylguanine-DNA methyltransferase (MGMT) promotor methylated. This enzyme repairs DNA by removing methyl groups. Therefore, if the MGMT is not present in the tumour cells, it leads to a better sensibility toward TMZ. For patients with the MGMT promotor methylated treated with radiotherapy and TMZ, the median of survival was of 21.7 months compared with 15.3 months for patients without the mutation. This mutation is found in 30% of the gliomas (22).

2.3. Challenges of glioblastoma therapy

The median of survival has not been prolonged since 2005 despite numerous studies and GBM remains incurable, recurrence of the tumour being inevitable (23). Researchers face many obstacles in their search for a cure including (i) its localisation, (ii) its heterogeneity (intrinsic and extrinsic), (iii) its infiltrative nature as summarised in the Figure 1. 4.

2.3.1 Localisation of the tumour

The anatomical location of the tumour in the brain makes the treatment of GBM challenging. A complete surgical resection is indeed impossible without damaging areas of the brain leading to unacceptable neurological deficits.

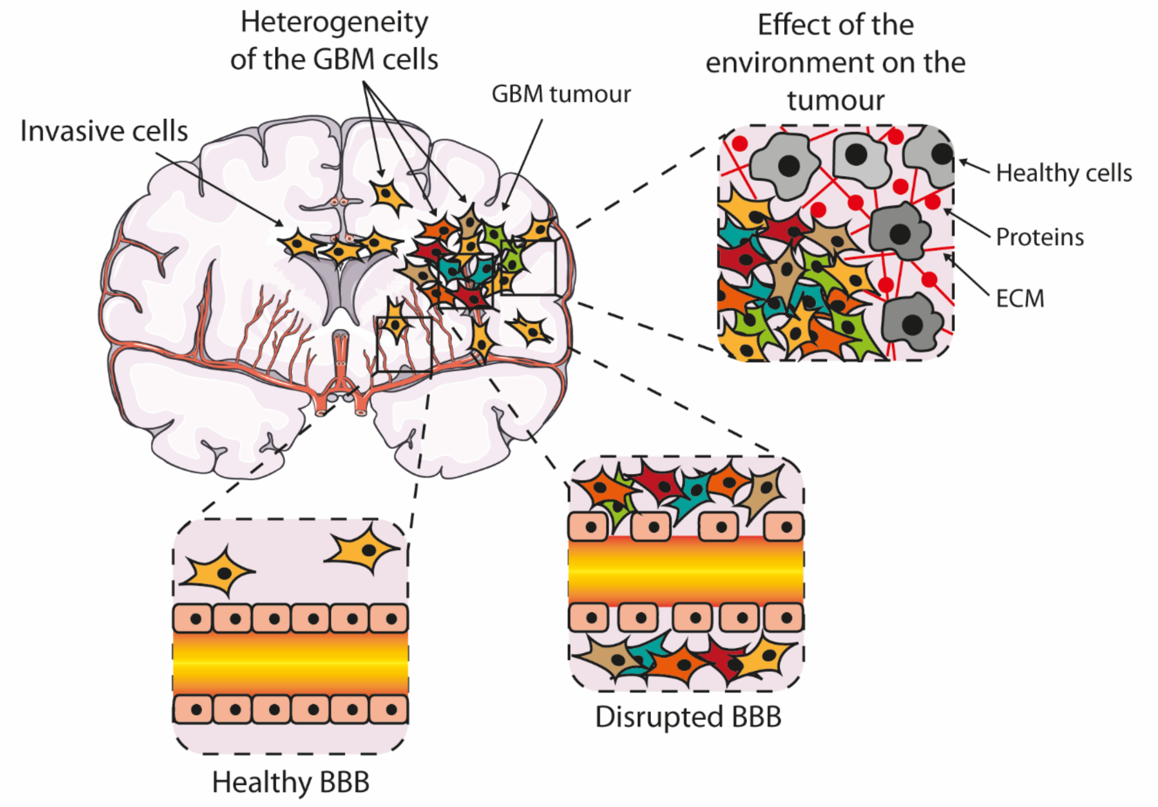

Figure 1. 4: GBM treatment faces many challenges due to the localisation of the tumour in the brain, its heterogeneity (intrinsic and extrinsic) and invasive nature.

Moreover, it is difficult to deliver drugs to the CNS at therapeutic concentration in particular because of the blood-brain barrier (BBB). In healthy patients it is constituted by a continuous layer of endothelial cells linked together by tight junctions and supported by adhesions and interactions with basement membranes, brain pericytes, astrocytes, and neurons (24). For GBM patients, it is often partially disrupted at the tumour site (25). Drugs administered systemically might be able to extravasate the BBB. However, they are unable to reach single infiltrating cells since this area has an intact or moderately altered BBB (26).

2.3.2 Heterogeneity of the glioblastoma

GBM is heterogenous considering the tissue (environment), the type of cells, and the molecular and genetic point of view making its classification no easy task and resulting in low predictability of the tumour response to the treatments (27–30). Because of this heterogeneity, treatments are not completely adapted to GBM and some cells always survive, leading to recurrence of the tumour. To increase the efficiency of radiotherapy, attempts have been made to increase doses, alter fraction schemes and use radiosensitisers but it unfortunately led to no improvements (31). Since the first use of intravenous chemotherapeutics in the 1940s, nearly every new class of drug that has reached the market (more than 60) has been tested in GBM patients (20). Alkylating agents are subjected by the same chemoresistance pathways as TMZ as their mechanism of action is similar; therefore, their effectiveness is often limited (23). Only one third of the patients are responsive to the treatment while some patients display innate or acquired chemoresistance. A study showed that increasing the dosage of TMZ did not improve the efficacy of the treatment (32). The chemoresistance of alkylating chemotherapeutics is mediated by different mechanisms including DNA repair pathways, deregulation of apoptosis regulating genes or tumour cells overexpression of proteins such as galectin-1 or epidermal growth factor (EGF) receptor (33).

A subpopulation of GBM is constituted of cancer stem-cells (CSCs). Stem cells have three properties: (i) self-renewal, *i.e.,* at cell division, at least one daughter retains the same biologic properties of the parent cell; (ii) the capability to develop into multiple lineages; (iii) the potential to proliferate extensively (34). They are therefore referred to as “tumour-initiating cells’’. CSCs are suspected to resist therapeutic intervention via several mechanisms including ABC transporter expression (35), aldehyde dehydrogenase (ALDH) activity (36), B-cell lymphoma-2 (BCL2) related chemoresistance (37), enhanced DNA damage response (38) and activation of key signalling pathways (39). These mechanisms have been reviewed elsewhere (40).

2.3.3 Infiltrative nature of the glioblastoma

It has been observed than tumour recurrence occurs in 90% of the cases within 2 cm of the resection cavity (41). This phenomenon can be explained by the invasion ability of glioblastoma cells. GBM is indeed also known as the ‘’octopus tumour’’ (42). GBM cells are able to infiltrate the surrounding normal parenchyma in the early stage of the tumour development. GBM cells are able to migrate and presence of genes associated to invasion and migration like CLEC18B (43), EGFLAM (44), HOXC10 (45) and circular RNAs like circ_0029426 (46) has been correlated with poor patient survival. The migration of GBM cells is not random and occurs mostly along white matter tracks (47) and blood vessels (48). Lagerweij and co-workers (49) have studied the migration of GBM cells and its relationship with blood vessels in an *ex vivo* murine model. Figure 1. 5 shows a large and diffuse infiltrative tumour from a GBM8 glioblastoma xenograft model in mice. Cells have migrated away from the tumour core into the deep grey matter, the white matter and even the contralateral side. Figure 1. 5-B shows that a large number of cells migrated collectively through white matter tracts like the corpus callosum. Moreover, solitary cells were identified away from the tumour site in close proximity with blood vessel (Figure 1. 5-D), demonstrating that GBM cells migrate along blood vessels as suggested in former studies.

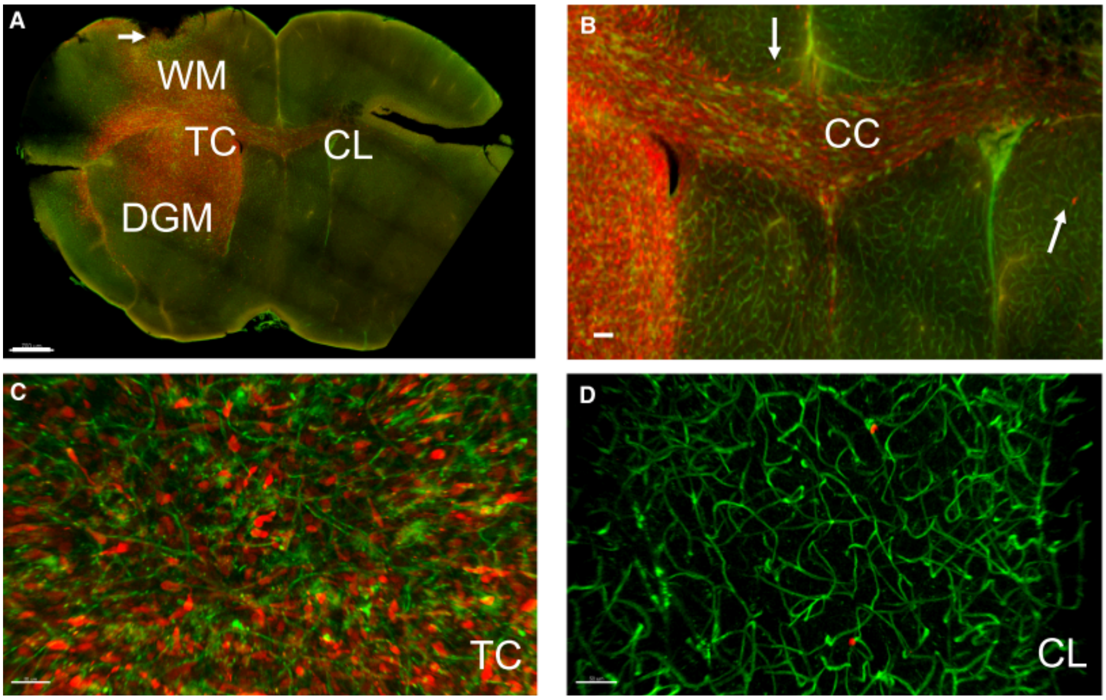

Figure 1. 5: Diffuse, invasively growing GBM8 tumour (anti-RFP-Ax594, *red*) and brain vasculature (lectin^{tomato}-DyLight488, *green*). (a) Tumour cells have migrated into the healthy brain parenchyma, away from the tumour core (TC) into the contralateral (CL) hemisphere, into the deep grey matter (DGM), and into the subarachnoid space (arrows). (b) Zoom showing the presence of GBM cells in the corpus callosum (CC). (c) Zoom of the tumour core showing tumour cells in close proximity with blood vessels. (d) Zoom showing distantly migrated solitary tumour cells in close proximity with blood vessels. Figure adapted from Lagerweij *et al.* (49).

GBM cells prefer existing routes of migration like blood vessels and white matter tracts as explained earlier but are also able to migrate into high density ECM like the brain parenchyma. It is composed of a high density of neurons and glia in a softer matrix and therefore display physical resistance to migrating cells. GBM cells have therefore to actively remodel the ECM to migrate (50–52). They are able to secrete proteases to degrade the ECM and create routes (53). They are shown to be able to upregulate hyaluronan, osteopontin, vitronectin, collagens, and tenascin-C and downregulate thrombospondin and versican (47,54–56). Since GBM cells are able to use different routes of migration, it implies that different signalling cues must be available. This context-dependent invasion signalling is getting more and more appreciated, but much still remains to be elucidated.

CSCs are a subpopulation of GBM and are known to be resistant to radiotherapy and chemotherapy but can also differentiate and be the cause of the recurrence of the tumour as explained earlier (section 2.3.2) but also to be highly invasive (57). This hypothesis is corroborated by the observation that mesenchymal GBM is enriched in CSCs. Mesenchymal GBM is a glioblastoma subtype characterised by the overexpression of genes characteristic of the migratory cells of the undifferentiated mesenchyme. This subtype accounts for approximately 30% of primary GBMs and has been related with a higher invasive potential and worse prognosis than other subtypes (58).

GBM cells are able to take different routes of migration which suggests that numerous signalling pathways are involved. However, the information available on the signalling pathways is limited due to a lack of adequate *in vitro* and *in vivo* models and thus only a few are known. Erythropoietin-producing human hepatocellular carcinoma (Eph) receptors type A and B typically bind A-type ephrins and B-type ephrins respectively (59). Eph receptors and ephrins mediate cell-to-cell signalling that control spatiotemporal organisation of tissues; in particular, they regulate cell migration and axon guidance. Several studies point out EphA and EphB signalling to GBM invasion. Indeed, Eph/ephrin pathways are overexpressed in invasive GBM cells but not in the tumour core (60–63). Interestingly, Wang *et al.* (64) showed that EphB2 overexpression increases invasion but also inhibits proliferation while its silencing increases proliferation and decreases invasion of GBM cells. The stromal derived factor-1α (SDF-1α), also called CXCL12 is a chemokine composed of 68 amino acids that bind to the CXC chemokine receptor 4 (CXCR4) (65). In healthy tissues, SDF-1α plays a role in recruiting immune cells at the site of injury but also in the development of the CNS (66,67). However, CXCR4 is also overexpressed in invasive GBM cells (68–70). It has been shown that overexpression of the CXCR4 in GBM cells is associated with poor prognosis (71). Data showed that CXCR4 and SDF-1α mRNA are colocalized in glioblastoma and their expression increases with the tumour grade (72).

Moreover, a gradient of this chemokine induces an attraction of cells expressing the CXCR4 receptor (73,74).

In sum, the high invasion ability of GBM is one of the main challenges in the look for a cure. On the bright side, GBM cells do not intravasate into blood vessels, metastasis from GBM in other organs are therefore extremely rare (75).

3. Innovative treatments

A plethora of clinical trials are currently ongoing aimed to improve the dark prognostic of GBM. At the date of the 5th of July 2019, 1380 clinical trials for GBM are registered in clinicaltrials.gov and 478 are active. Most of them are conducted in the US or in Europe. However, in many cases, the clinical end point is to stabilise the disease, improve the quality of life of the patients and maybe slightly extend their life but not complete remission. It must be noted that complementing treatments controlling seizures, increased intracranial pressure, deep vein thrombosis and embolism like anticonvulsant drugs, corticosteroids, and anticoagulant drugs are of prime importance as they occur in up to 30% of patients with primary brain tumours (31).

In conclusion, despite a highly active research on the subject, prognosis for GBM has not changed significantly in the last 90 years. Research is hopefully continuing to finally tackle this disease. Some innovative strategies aiming to overcome the challenges of GBM are outlined below.

3.1. Overcoming the blood-brain barrier

One of the challenges in GBM treatment is the localisation of the tumour in the brain. Indeed, despite the surgical challenge, obtaining a therapeutic concentration of drug at the site of the tumour is difficult because of the BBB. The BBB is known to be disrupted at the site of the GBM, which is demonstrated by the fact that gadolinium used for MRI imaging is accumulating in the tumour. However, the GBM infiltrate the surrounding tissues and does not disrupt the BBB there. Different strategies can be applied to pass the BBB: (i) designing drugs that can cross it, (ii) disrupting the BBB and (iii) injecting or implanting the drug directly at the site of the tumour.

3.1.1 Crossing the blood-brain barrier

The BBB is one of the main obstacles when it comes to deliver drugs into the brain. Some molecules are known to be able to cross it like TMZ, lomustine, semustine or carmustine. However, studies showed that levels of TMZ in the brain are only 20% of systemic drug levels (76).

Another strategy consists in modifying compounds or incorporating them in nanocarriers to reach the brain parenchyma by passive or active targeting of the BBB endothelial cells (77). The passive targeting is the transport of nanocarriers through leaky tumour capillary fenestrations into the tumour interstitium and cells by convection or passive diffusion, followed by their selective accumulation thanks to the enhanced permeability and retention (EPR) effect (78). The active targeting consists in using ligands to bind selectively receptors overexpressed by tumour cells or tumour vasculature. However, passing the BBB remains a challenge and appropriate targets for active targeting are still lacking.

In 2011, another treatment was approved by the FDA for the treatment of recurrent GBM: the tumour treating fields (TTFs) (79). They are low intensity alternating electric fields that selectively target proliferating cells by disrupting mitosis. Since it uses an electric field instead of a drug, TTF is not affected by the presence of the BBB. The NovoTTF-100A device (Optune®) is the first TTF device approved and is currently used as a concomitant therapy to TMZ following surgical resection and radiotherapy, both for newly diagnosed and recurrent supratentorial GBM (80).

3.1.2 Disrupting the blood-brain barrier

Groups have focused their attention in disrupting the BBB. It can be done for example by administration of chemical agents such as mannitol and adenosine A_{2A} agonist (81). Regadenoson is an FDA-approved A_{2A} receptor agonist and was tested on five patients in order to improve the concentration of TMZ in the brain (82). Although it was found in rodents to help increasing the crossing of the BBB by TMZ, no significant increase was observed in patients.

Recently, a system has been developed using the help of ultrasounds. SonoCloud® is a system that delivers ultrasounds locally by implanting the device in the resection cavity and is currently under clinical trial in phase I/IIa (83). So far, results showed that it is well tolerated by patients with recurrent GBM and that the procedure is safe.

3.1.3 Bypassing the blood-brain barrier: local delivery strategies

One way to overcome the BBB is to inject or implant the drug directly in the brain, at the tumour site. Locoregional delivery of therapeutics can be performed using injectable or implantable systems with sustained release characteristics. The goal is to prevent the growth of cancer cells that cannot be restricted by surgery. GBM cells are highly infiltrative but are not able to pass into the lymphatic system. They are therefore unable to form metastases outside the CNS (27). Moreover, in more than 90% of the cases, recurrence appears within a few centimetres of the resection cavity. Local delivery strategies can therefore increase the concentration of drugs at the tumour site, avoiding systemic side effects without disrupting the BBB or modifying the drug chemical structure.

Early strategies used the direct injection of chemotherapeutics into the tumour resection cavity or into the ventricle via repeated injections with needles or catheters (84). This simple method can be used to inject large volumes of drugs. However, the depth of the drug distribution is often limited at less than 3 mm from the injection site and repeated surgery are needed, increasing the risk of side effects such as intracranial haemorrhage and infections. Another approach that has been widely studied is the use of convection enhanced delivery (CED). It delivers drugs via a catheter under positive pressure inserted into the tumour under stereotactic guidance. This device allows to distribute the drug further into the brain (2-3 cm) (85). Nevertheless, the reservoir needs to be refilled continually, the drug distribution depends on the infusion parameters (volume, duration and rate of the infusion) and therefore need to be controlled, and neurotoxicity can be induced by leakage of the drug into the cerebrospinal fluid (86). Advancements in catheter design, placement and imaging techniques might help overcome these challenges.

Another strategy is the craniotomy-based drug delivery, *i.e.* the use of scaffolds (such as gels, films, 3D scaffolds, nano- or microparticles) loaded with drugs that can be implanted or injected in the resection cavity and that are capable of sustainably release drugs in the surrounding. Implants can either be biodegradable or not, the first one being preferred since non-degradable implants have to be removed surgically.

The only approved drug delivery implant of newly diagnosed and recurrent GBM by regulatory agencies is the Gliadel® wafer. It is composed of a biodegradable copolymer of 1,3-bis-(p-carboxyphenoxy)propane and sebacic acid in a 20:80 ratio (polifeprosan 20) loaded with bis-chloroethylnitrosourea (BCNU). 1 wafer contains 7.7 mg of BCNU and up 8 wafers can be placed in the cavity of resection in order to cover as much as possible the cavity. Prolonged overall survival was observed compared with placebo treated patient (13.9 months and 11.6 months, respectively) (87). Low systemic toxicity was observed (gastrointestinal disorders, asthenia, fever and depression) but serious local side effects included seizures, intracranial hypertension, meningitis, cerebral edema, impaired neurosurgical wound healing and wafer migration. A retrospective study after 10 years of use at Johns Hopkins Hosital (Baltimore, USA) on 1013 patients with malignant brain astrocytoma was conducted (88) and showed that there was indeed a small increase in the percentage of complication for Gliadel® patients but it was not found significant. Other groups tried to improve the efficacy of polymer implants by using different polymers or drugs. All-trans retinoic acid (ATRA) was encapsulated in polymeric particles and incorporated in a 3D printed hydrogel mesh (89). Rapamycin, an anti-proliferative agent effective in recurrent breast cancer, has been associated with a biodegradable caprolactone-glycolide polymer beads and tested *in vivo* in combination with radiotherapy for the local treatment of GBM (90). OncoGel® is a system composed of an *in situ* forming gel (ReGel™) loaded with paclitaxel and was tested in a phase I/II trial for GBM patients (91). The gel is degraded in 4 to 6 weeks as it releases paclitaxel. So far, the study has only been done on 4 patients and therefore no conclusions were given on the efficacy of this treatment yet. Microspheres are also studied for the local treatment of GBM, encapsulating paclitaxel (92) or 5-fluorouracil (93) for example. 5-fluorouracil was encapsulated in poly(lactide-co-glycolic acid) (PLGA) microspheres and studied in a phase II trial, but they failed to show an increase in the overall survival.

Synthetic or natural polymers can be used. On one hand, synthetic polymers are easier to control (polydispersity, reproducibility) which explain why most of the implants in clinical studies for GBM treatment are synthetic. On the other hand, the use of natural polymers is interesting for their facilitation in tissue integration and sites allowing for cell interaction. Collagen, chitosan, hyaluronic acid, and silk fibroin are natural polymers extensively studied for their interesting properties for production of biocompatible scaffold. Collagen and hyaluronic acid can be used for their biomimicry properties and chitosan and silk fibroin for their slow degradation *in vivo*. They are not favored for treatment of GBM today but extensively studied for brain regeneration applications.

3.2. Fighting glioblastoma despite its heterogeneity

One of the main challenges of the GBM resides in its heterogeneity. Drugs are effective on some of the cells, but a population shows radio- and/or chemo-resistance. Different strategies are being put in place by researchers in order to find a way to eliminate all the subpopulations constituting the GBM.

Evasion of the host immune system is one the hallmarks of cancers and GBM makes no exception. Focus is therefore being made to ablate the immune evasion ability of this cancer by educating the host immune system, creating a vaccine. A vaccine would induce potent anti-tumour immunity with long lasting immunological memory while sparing healthy tissues (94). Various strategies are being studied. First, it is possible to inhibits proteins responsible for immune evasion such as programmed cell death protein I (PD-I) and cytotoxic T-lymphocyte-associated protein 4 (CTLA-4) (95). CheckMate 143, using nivolumab, is the first death pathway inhibitor in a large randomized clinical trial for GBM but failed to show a prolongation of the overall survival compared with the classical treatment (96). Nivolumab is today being tested in combination with other drugs or protocols in different clinical trials (97,98).

Secondly, chimeric antigen receptor (CAR) T cells are genetically modified to target surface tumour-associated antigens (99). CARs can be constructed to target any tumour-associated or tumour-specific antigen and can distinguish tumours from healthy cells. CARs are selected to be specific to one patient’s tumour. T-cell are taken from the patients, chemically modified and then injected back. For GBM, four promising antigens have been particularly studied in clinical trials: EGFRvIII, human epidermal growth factor receptor 2 (HER2), and IL receptor 13Ra2 (IL-13Ra2). Thirdly, dendritic cell therapy allows the targeting of multiple antigens (100). Dendritic cells are harvested from the patient and exposed to tumour lysates, RNA, peptides, and/or products from cancer stem cells before being injected back to the patient. Several clinical trials are ongoing. ICT-107 was tested in a phase II trial with 124 patients in association with the classical treatment and reported an increase in the overall survival (18.3 for ICT-107 vs 16.7 for the control) (101). DCVax®-L showed exciting results in its phase III study with a 3-year survival of 46.4% over 348 patients (102).

GBM is characterized by extensive angiogenesis (103). Therefore, some teams are working on vascular endothelial growth factors signalling inhibitors like vandetanib and sorafenib as well as protein kinase inhibitors such as enzastaurin and cilengitide (104). By inhibiting angiogenesis, tumour oxygenation is improved through vascular normalisation. Since radiotherapy is more efficient with an increasing oxygen concentration, allowing the formation of reactive oxygen species, anti-angiogenic drugs should act as radiosensitisers (105). However, they failed so far in preclinical and early-phase studies. The reason remains unclear although some explanations have been proposed like the inadequate dosage, the inaccuracy of preclinical models used to predict a response in human GBM but also inadequate timing with radiations (106). An anti-angiogenic humanised monoclonal antibody, the bevacizumab (Avastin®), was approved by the FDA in 2009 for the first-line treatment of recurrent GBM patients. However, phase III clinical trial, done on 637 patients between 2009 and 2018 showed no improvement of the median of survival (107). The progression-free survival was improved from 7.3 months for the classical treatment (TMZ + radiotherapy + placebo) to 10.7 (TMZ + radiotherapy + Bevacizumab) but did not reach significance criterion.

To overcome resistance to treatment, other groups have studied the targeting of DNA repair by polyADP ribose polymerase (PARP) by the use of a PARP inhibitor. It allows the increase of single strand breaks by blocking the base excision repair pathway, making the tumour cell unstable (108,109). Studies have demonstrated synergistic interactions between PARP inhibitors and TMZ and showed that they are radiosensitizers (110,111).

CSCs are a small population of cells within a tumour with self-renewal, tumorigenicity and differentiation capabilities (112). Their presence in human GBM was reported in 2004 by Galli *et al.* (113). They have been shown to contribute to tumour initiation and to be resistant to standard radio- and chemotherapy, making them of prime importance in the progression and recurrence of the tumour. Salinomycin was found to inhibits the growth of various immortalised cancer cells both *in vivo* and *in vitro* and to reduce the fraction of CSCs by more than a 100-fold compared with paclitaxel (114). Those promising results have led to intensive research in investing this molecule for potential clinical use for the treatment of GBM.

3.3. Inhibiting cell migration

Invasion of GBM cells in the healthy brain is one of the major issues in GBM treatment. Therefore, some groups have focussed their attention in developing inhibitors of migration. Galunisertib (LY2157299) is a TGF-β inhibitor tested against glioma in several clinical studies (115–117). However, association of Galunisertib combined with Lomustine in recurrent GBM failed to increase the overall survival. An ongoing phase I/II study combine Galunisertib with TMZ (115). KB004 is a recombinant monoclonal antibody against EphA3 and is studied in a phase I clinical trial for GBM patients. So far, inhibiting GBM invasion has not been very successful. It is indeed unlikely to have a considerable impact on this particular tumour since extensive invasion has already occurred at the time of diagnostic.

Challenges in the treatment of GBM as well as promising future options are a myriad and only a glimpse of all the possibilities were given here. We will now focus on an innovative strategy, the trapping of tumour cells.

4. The tumour trap strategy

One of the difficulties in treating GBM is its tendency to infiltrate the surrounding healthy tissues. Infiltrating cells, as well as circulating tumour cells, are a recurrent problem in many types of cancers. Recent advances pursue the trapping of these cancer cells within a confined area to facilitate their removal for therapeutic and diagnostic purposes. The different strategies that can be used to trap cancerous cells for therapeutic and analytic purposes have been reviewed.

This article has been published in **Frontiers in Pharmacology**.

Publication

Reversing the tumour target: Establishment of a tumour trap

Mathie Najberg, Muhammad Haji Mansor, Frank Boury, Carmen Alvarez-Lorenzo, Emmanuel Garcion

Frontiers in Pharmacology, 2019, 10, 1-12, doi: 10.3389/fphar.2019.00887

Reversing the tumor target: Establishment of a tumor trap

Mathie Najberg[1,2], Muhammad Haji Mansor[1,3], Frank Boury[1], Carmen Alvarez-Lorenzo[2], Emmanuel Garcion[1]*

[1]CRCINA, INSERM, Université de Nantes, Université d'Angers, Angers, France

[2]Departamento de Farmacología, Farmacia y Tecnología Farmacéutica, R + D Pharma Group (GI-1645), Facultad de Farmacia, Universidade de Santiago de Compostela, Santiago de Compostela, Spain

[3]Center for Education and Research on Macromolecules (CERM), Université de Liège, Liège, Belgium

Correspondence:

*Corresponding Author

emmanuel.garcion@univ-angers.fr

Keywords: tumour cell migration, tumour trap, biomimetic trap, cancer therapy, premetastatic niche recruitment.

Abstract

Despite the tremendous progress made in the field of cancer therapy in recent years, certain solid tumours still cannot be successfully treated. Alongside classical treatments in the form of chemotherapy and/or radiotherapy, targeted treatments such as immunotherapy that cause fewer side effects emerge as new options in the clinics. However, these alternative treatments may not be useful for treating all types of cancers, especially for killing infiltrative and circulating tumour cells (CTCs). Recent advances pursue the trapping of these cancer cells within a confined area to facilitate their removal for therapeutic and diagnostic purposes. A good understanding of the mechanisms behind tumour cell migration may drive the design of traps that mimic natural tumour niches and guide the movement of the cancer cells. To bring this trapping idea into reality, strong efforts are being made to create structured materials that imitate myelinated fibres, blood vessels, or pre-metastatic niches and incorporate chemical cues such as chemoattractants or adhesive proteins. In this review, the different strategies used (or could be used) to trap tumour cells are described and relevant examples of their performance are analysed.

Introduction

For many decades, surgery, radiotherapy and chemotherapy have served as the mainstay trident in the fight against cancer (Figure 1. 6 Scheme I). During this period, the prognosis of many types of cancer has been significantly improved (118–121). However, the widespread use of these treatments has also uncovered several major limitations. For example, the feasibility of surgery is very much dependent on the localization and the size of the tumour. The procedure is also contraindicated in patients with poor clinical performance. As for radiotherapy and chemotherapy, these treatments are often implicated with serious side effects that, in some cases, may outweigh their potential therapeutic benefits. Moreover, these treatments lack the capacity to prevent metastases, which are responsible for roughly 90% of cancer-associated deaths (122).

Numerous studies in the quest of improving cancer treatments are driven by the concept of “magic bullet’’ (Figure 1. 6 Scheme II-2) put forward by the German scientist Paul Ehrlich (123). If radio- and chemotherapy are considered as weapons of mass destruction, Ehrlich´s strategy can be regarded as the sniper of cancer therapy. This concept is mainly based on the idea of increasing the bioavailability and specificity of vector-associated active agents in the body, while limiting their premature degradation and toxicity. In the context of anti-cancer approaches, the success of selective therapies depends on the discovery of targeting elements that, when coupled with active ingredients and/or diagnostic cues, enable the recognition of well-characterized molecules, cells or tissues. For example, Adcetris® targets the antigen CD30 in the treatment of Hodgkin's lymphoma, and Kadcyla® targets HER2, which is present in about 20% of breast cancer patients (124). Nevertheless, the discovery of appropriate targets that are specific to tumor cells remains a challenging task, despite the significant advancements made in the field of genomics and proteomics in recent decades.

Fortunately, a plethora of new therapies are being approved regularly for the treatment of cancer. Among them is the use of locoregional therapies (Figure 1. 6 Scheme II-1) which includes Nanotherm® (MagForce) that involves injection of magnetic nanoparticles inside the tumour or into the resection cavity. A magnetic field is then applied to generate heat via the nanoparticles and kill the cancerous cells locally (125). It is currently licensed in

Europe for the treatment of brain tumours and has received FDA approval in February 2018 to be used in clinical trials involving prostate cancer patients (126). Another example is Optune® (Novocure Ltd), a tumor-treating field (TTF) device composed of electrodes that

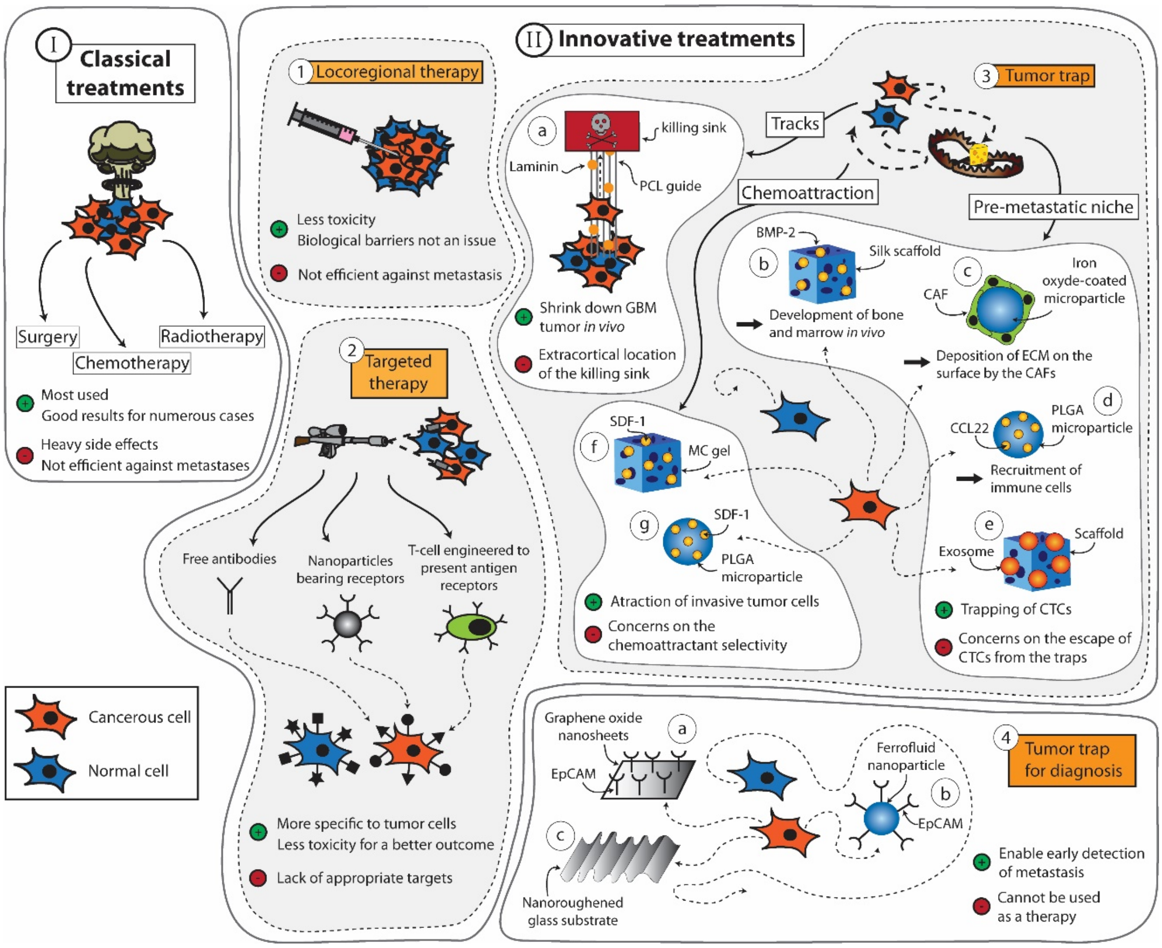

Figure 1. 6: Summary of the strategies that can be applied to fight cancers. (Scheme I) The classical treatments used for cancers are surgery, chemotherapy and radiotherapy. (Scheme II) Innovative treatments include (1) locoregional therapy, (2) targeted therapy and (3) tumor traps, among others. Tumor traps can be designed to take advantage of the migration pathways used by the tumor cells. It includes the use of tracks ((a) system developed by Jain *et al.* (127) using aligned PCL fibers coated with laminin). Tumor traps can be designed as synthetic pre-metastatic niches ((b) system developed by Seib *et al.* (128) using a silk scaffold loaded with bone morphogenic protein 2 (BMP-2) capable of developing bone and marrow *in vivo*, (c) system developed by De Vlieghere *et al.* (129) using iron oxide-coated microparticles encapsulating cancer-associative fibroblasts (CAFs) that deposit continuously ECM on the surface, (d) system developed by Azarin *et al.* (130) using poly(lactide-co-glycolic acid) (PLGA) through the induction of the immune system by the CCL22 chemokine, and (e) system developed by De la Fuente *et al.* (131) using a 3D scaffold loaded with exosomes). Finally, tumor traps can use chemoattractive molecules ((f) system developed by Giarra *et al.* (132) using a methylcellulose (MC) thermo-responsive hydrogel loaded with stromal derived factor-1 (SDF-1), and (g) the system developed by Haji Mansor *et al.* (133) using SDF-1 encapsulated in PLGA nanoparticles). (4) Tumor traps can also be used for the early detection of metastasis ((a) system developed by Yoon *et al.* (134) using graphene oxide nanosheets, (b) CELLSEARCH® CTC test (135) is a device using ferrofluid nanoparticles with EpCAM antibodies, and (c) system developed by Chen *et al.* (136) using a nanoroughened glass substrate).

can be placed on the patients' scalp and connected to a generator to deliver a low intensity electric field of 200 kHz (137). It is believed to exert anti-cancer effects by disrupting the division of tumor cells (138). The device has been approved for the treatment of glioblastoma and shown to increase the median survival from 15 months to 21 months when used on top of the standard treatments for this cancer (139). However, many countries and insurance companies do not cover the cost of this treatment and the clinical adoption of this technology remains limited due to concerns regarding the lack of understanding of the device's exact mechanism of action. Moreover, some skepticism exists toward the legitimacy of the device approval process due to the poor consideration of any placebo effect during the clinical trial phase (140).

Among the numerous classes of novel anti-cancer treatments entering the market, cancer immunotherapy is arguably the one that is currently attracting the highest level of attention (Figure 1. 6 Scheme II-2). This class of treatment aims to treat cancer through artificial stimulation of the patient's immune system (141). The most cutting-edge subset of this type of treatment is the chimeric antigen receptor (CAR) T-cell immunotherapy, which involves harvesting T-cells from a patient and genetically modifying these cells to express a receptor that can bind to a tumor antigen before injecting them back into the patient (142). CAR-T cell immunotherapy made its debut in the clinic in August 2017 when Kymriah® (Novartis) was approved by the FDA for the treatment of B-cell acute lymphoblastic leukemia (BCALL) (143). This was followed by the approval of Yescarta® (Gilead Sciences) in October the same year for the treatment of diffuse large B-cell lymphoma (144). Both Kymriah® and Yescarta® exert their effects by targeting CD19 antigen (145). However, there are numerous ongoing clinical studies that explore the feasibility of targeting other antigens including PD-L1 (ClinicalTrials.gov Identifier NCT03672305, NCT03198052, NCT03330834), EpCAM (ClinicalTrials.gov Identifier NCT03013712, NCT03563326, NCT02729493), and CD123 (ClinicalTrials.gov Identifier NCT03796390, NCT02937103, NCT03672851). Many of these trials also attempt to evaluate the efficacy of CAR-T cell immunotherapy against solid tumors to expand its indication beyond certain blood cancers. More comprehensive reviews on the current status and future directions of CAR T-cell immunotherapy as well as other subsets of cancer immunotherapy such as immune checkpoint inhibitors and cancer vaccines can be found elsewhere (146–148).

Despite the continuous increase in the number of novel anti-cancer treatments entering the clinic, local recurrence in previously healthy tissues seen in many cases of solid tumours remains an unsolved conundrum among clinicians and researchers alike. Development of new therapies for in situ control of the disease, while avoiding the problems of biological barriers and systemic toxicity, still proves to be a formidable task. Thus, in parallel to the innovative approaches mentioned above, the idea of trapping infiltrative or circulating tumour cells (CTCs) within a confined area to facilitate their removal for therapeutic or diagnostic purposes has risen (Figure 1. 6 Scheme II-3,4). Over the last years, this concept has developed progressively. The aim is two-fold: (a) to avoid the uncontrolled dissemination of tumour cells and (b) to efficiently prevent the phenomenon of epithelial-mesenchymal transition (EMT) or development of metastases. The concept is largely inspired by the “ecological trap” theory (149). By considering cancers as ecosystems, it is possible to develop tumour traps not only for the infiltrative tumour cells, but also for the CTCs that are responsible for metastasis. However, imitating the traditional features of a natural habitat or niche for tumour cells and directing their migration pathways presents numerous physical and biological challenges. The focus of this review will be on understanding the mechanisms of tumour cell migration and how this knowledge can be used to capture them, keeping in mind that different tumours are likely to utilize different mechanisms.

Migration of tumour cells

Tumour cells must cover a great distance on their journey to form metastases (Figure 1. 7). The first step of the process is to migrate away from the primary tumour. Tumour cells can follow aligned tracks (a), or gradients of chemoattractant in solution (chemotaxis) or fixed on a substrate (haptotaxis) through the extracellular matrix (ECM) (b). If the cross-sectional area of interfibrillar pores is more than 7 µm², degradation of the matrix is not needed for cell movement. Alternatively, a leader cell can open a path for the following cells by virtue of the matrix metalloproteinase (MMP) activity (c). The second step is to intravasate into the bloodstream or the lymphatic system in which the tumour cells will transit through the circulation. Third, cells extravasate to secondary tissues once they reach a location where they can adhere to the walls of the vessel. The fourth and final step deals with the formation of a secondary tumour. This only occurs if the environment is favourable to tumour growth. The different strategies implemented to mislead these cells into a trap are described in next sections. These strategies exploit the current knowledge on cancer cell migration and metastasis and the specificities of each type of tumour.

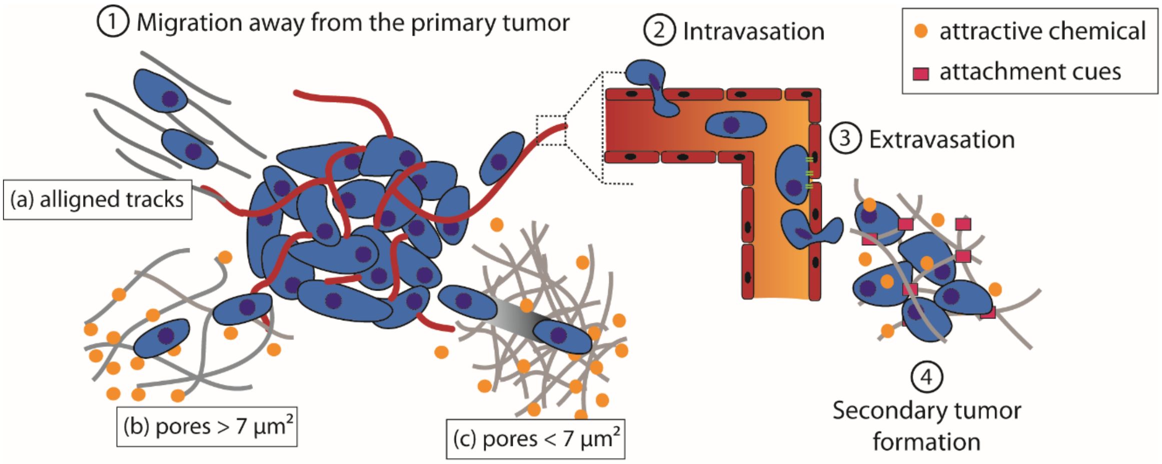

Figure 1. 7: Schematic representation of theorized paths of cancer cell migration away from the primary tumour. (1) Migration away from the primary tumour. Tumour cells can follow aligned tracks (a), or gradients of chemoattractant in solution (chemotaxis) or fixed on a substrate (haptotaxis) through the ECM. If the cross-sectional area of the interfibrillar pore is more than 7 µm², degradation of the matrix is not needed (b), otherwise, a leader cell creates a path for the following cells thanks to MMPs (c). (2) Tumour cells adhere to a vessel and intravasate to reach the blood or lymphatic stream in which they circulate. (3) Once they reach a location where they can adhere to the vessel wall, the cells extravasate. (4) If the environment is favourable, a secondary tumour grows.

Migration away from the primary tumour

The physical interactions between the ECM and cancer cells play a key role in allowing the cells to start migrating. Cancer cells may undergo an EMT to acquire a motile phenotype (150). This translates into the loss of intracellular adhesion molecules such as E-cadherin and cytokeratins, resulting in detachment of the cells from the primary tumor, and an overexpression of MMP on their surface that allows the cells to digest laminin and collagen IV to progress in the dense ECM (150). These changes are thought to be related to the stiffness of the matrix around the tumor, which is of higher values than that of normal tissues (151–154). For example, the stiffness of GBM tissues is of ~25 kPa while normal brain tissues have a stiffness of 0.1 to 1 kPa (155). Wang *et al.* investigated the effect of matrix stiffness on GBM cells and found that an increase in matrix rigidity could induce an upregulation of MMP-1, Hras, RhoA and ROCK1 (155), which are involved in increasing cell motility (156–159). Another physical factor that governs the dissemination of cancer cells is the architecture of the extracellular environment, which includes pores of a diameter ranging from less than 1 µm to 20 µm (160). Matrix degradation is usually required for cancer cell migration to occur when the cross-sectional area of the interfibrillar pore is less than 7 μm^2, which corresponds to about 10% of the nuclear cross-section of cancer cells (161). Above this value, cells can undergo deformation to migrate through the ECM.

Apart from the porosity of the ECM, the spatial arrangement of the matrix fibers near the primary tumor sites can also influence the motility of tumor cells; aligned fibers offer tracks that are more conducive to migration (162,163). These tracks are found along the ECM fibers in the interstitial space, between the muscle and nerve fibers, and along or within the vasculature of organs, among others (52). Moreover, it has been observed that leader tumor cells are able to align collagen fibers to assist the migration of the following cells (164). In addition to creating the required physical space, these tracks also facilitate cancer cell migration by providing relevant molecular guidance. For example, cancer cells can be guided towards laminin and hyaluronan molecules in the ECM by their integrins and CD44 receptors respectively, and also via haptotaxis by chemokines and growth factors immobilized along the tracks (52,165). Jain et al. took inspirations from these biological phenomena and designed a scaffold to guide GBM cells toward a killing sink in an extracortical location (Figure 1. 6 Scheme II-3-a) (127). They utilized aligned poly-L-lysine and laminin-coated polycaprolactone (PCL) nanofibers (10 µm thick) encased in a PCL / polyurethane support (2.4 mm diameter) to imitate the white matter tracts (41,48). The killing sink was composed of a collagen-based hydrogel conjugated to the chemotherapeutic agent cyclopamine. With this approach, the tumour mass of induced GBM in mice could be reduced. However, despite the positive results, this strategy as itself has limited clinical appeals as the establishment of an extracortical sink in human patients may invite numerous technical difficulties. Instead, exploiting the local (intracortical) migration of the cancer cells may be a more translatable strategy to develop an efficient tumour trap for this cancer.

Intravasation and tumour cell circulation

Tumor cells can circulate through the blood and lymphatic vessels on their journey to form a secondary tumor distant from the primary site (166). This requires the cells to intravasate by passing through the endothelial cell junctions. Intravasation into the blood vessels occurs frequently due to the leaky nature of tumor vasculature. In addition, it has been observed *in vivo* that metastatic cells are able to polarize toward blood vessels. A possible explanation to this phenomenon is that these cells have an increased expression of epidermal growth factor (EGF) and/or colony-stimulating factor 1 (CSF-1) receptors. Thus, they migrate toward a gradient of EGF or CSF-1 released by the macrophages lining the blood vessels (167,168). However, it is still easier for tumor cells to enter the lymphatic system as the surrounding ECM network is easier to penetrate and that the endothelial junctions are looser (169). Either route can lead to blood vessel dissemination since the lymphatic circulation drains into the blood. As the lymphatic fluid is filtered by the lymph nodes, tumor cells are invariably invading them, starting with the nearest (170).

Once in the blood circulation, the trajectory of the tumor cells is influenced by the blood flow, the diameter of the blood vessels and the intercellular adhesion (171). Two mechanisms can lead to the arrest of a CTC: physical occlusion and cell adhesion (Figure 1. 8). Physical occlusion occurs when the diameter of the blood vessel is smaller or equal to the one of the CTC (usually around 10 µm). This has been observed in the brain by real-time imaging in a mouse model model (172). Adhesion of CTCs to the vessel walls occurs when there is a balance between the adhesion force and the shear force exerted inside the blood vessel (173). When the shear force increases, the collisions between cells and the vessel wall increases, which in turn enhances the likelihood of cell adhesion. However, if the shear force is too high, turbulences may prevent the adhesion.

It is therefore possible to capture CTCs by designing a device with strong adhesive cues. Yoon et al. (134) designed a microfluidic device consisting of graphene oxide nanosheets fixed onto a patterned gold surface to capture CTCs in early-stage cancer for analytical purposes (Figure 1. 6 Scheme II-4-a). The nanosheets were functionalized with epithelial cell adhesion molecule (EpCAM) antibody to capture CTCs. Blood samples were retrieved from healthy donors and mixed with labelled human breast cancer cell lines MCF-7 and

Hs-578T and the human prostate cancer cell line PC-3. This microfluidic device captured more than 70% of the cancer cells in the prepared blood sample with high specificity. A similar principle was also implemented in the design of CELLSEARCH® CTC Test, the first and only clinically validated and FDA approved blood test for enumerating CTCs (135). It allows for early assessment of patient prognosis as well as follow up of the patient. The test constitutes the use of ferrofluid nanoparticles with epithelial cell adhesion molecule (EpCAM) antibodies that bind to CTCs (Figure 1. 6 Scheme II-4-b). Once magnetically separated from the rest of the blood sample, cells are stained to discriminate CTCs from leukocytes that can co-present in the sample. Working within the same domain of research, Chen et al. (136) designed a nanoroughened glass substrate to capture CTCs based on their stronger adhesion capacity compared to normal blood cells (Figure 1. 6 Scheme II-4-c). Such a working principle makes this device useful for capturing CTCs regardless of their surface marker expression profile, which is known to vary according to the type of cancer, patient demographics and the state of the disease. It is indeed well-discussed in the literature that the EMT process may lead to reduction in the epithelial EpCAM expression in CTC (174). The capture of CTC using EpCAM antibody alone may lead to an underestimation of the CTC number in the blood. With this device, more than 80% of cancer cells in whole blood samples from mice with induced breast cancer or lung cancer were captured independently of their EpCAM expression. Based on these findings, it is evident that a number of approaches can be adopted to capture CTCs to enable early detection of metastasis although most of them are still far from translation to the clinic.

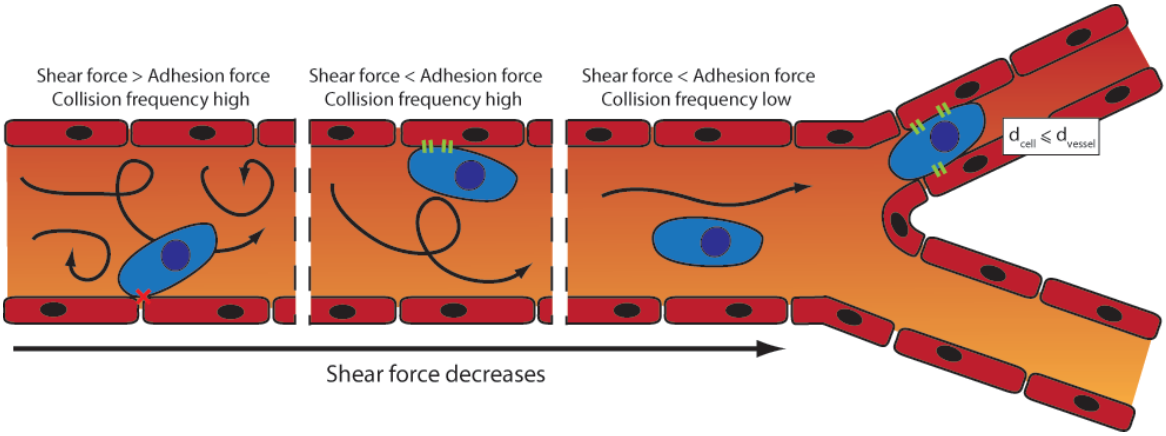

Figure 1. 8: Mechanisms of arrest of a CTC: the influence of the shear force and the blood vessel diameter on the site of CTC extravasation

Extravasation and secondary tumour formation

At the end of their time in blood circulation, the CTCs that survived and adhered to the blood vessel walls extravasate and a fraction of these proceeds to form a secondary tumor. It has been shown experimentally that only about 0.01% of the cells in the circulation system eventually contribute to metastatic colonization (175). The location at which they stop and grow into a secondary tumor is not believed to be randomly-determined, and the reasons driving the selection of a particular site are still being investigated. In 1889, Paget *et al.* hypothesized that metastasizing cancer cells are like seeds that can only grow in the proper soil (176). Indeed, it has been observed that invasive cancer cells tend to migrate toward certain preferred sites of metastasis; a phenomenon that has been coined as “tissue tropism” (128). More recent studies revealed that the formation of certain microenvironments termed as pre-metastatic niches is crucial to the subsequent formation of metastatic tumors. These microenvironments consist of inflammatory immune cells, stromal cells, ECM proteins, tumor-secreted exosomes and homing factors (177). Tumor-secreted exosomes are sent to prime the niche at a target organ (often lungs, liver, brain, bone and lymph nodes) by attracting bone-marrow derived cells (BMDCs) as well as increasing the proliferation of fibroblast-like stromal cells (178). BMDCs include $CD11b^+$ myeloid cells, myeloid-derived suppressor cells, neutrophils, tumor-associated macrophages and regulatory T cells. They are known to create an attractive site for metastasizing cells and the presence of VEGFR1-positive BMDCs can serve as a predictor for the arrival of tumor cells (179). Moreover, the establishment of a pre-metastatic niche is associated with an increased secretion of inflammatory cytokines and chemokines (180–182). The increasing understanding of the pre-metastatic niches and their roles in welcoming metastatic dissemination has inspired scientists to create synthetic niches as a means to trap migrating cancer cells.

Many different strategies have been explored to engineer pre-metastatic niches. For example, Seib et al. (128) developed a tumour trap for the metastasizing cells of breast and prostate cancer by imitating the red bone marrow microenvironment (Figure 1. 6 Scheme II-3-b). The strategy was adopted based on the knowledge that the bone was the preferred site of colonization in more than 60% cases of metastasis for primary breast cancer and 73% for primary prostate cancer (183). Evidence shows that red bone marrow attracts migrating cancer cells via chemotaxis with stromal derived factor-1 (SDF-1) (184) and CXCL16 (185). It also provides adhesion sites that interact with tumor cell surface molecules such as annexin2 (186), growth arrest-specific 6 (GASP-6) (187), CD44 (188), integrins (such as VLA-4, VLA-5 and LFA-1) and cadherins. Moreover, the bone marrow microenvironment is composed of osteoblasts, osteoclasts, stromal cells, stem cells and mineralized bone marrow surrounded by a rich vascular bed, making it a perfect site for tumor growth (189). To imitate the red bone marrow, Seib *et al.* designed a silk fibroin scaffold loaded with bone morphogenetic protein 2 (BMP-2) capable of developing bone and marrow *in vivo*. After implantation into the mammary fat pads of mice with induced breast or prostate tumor, no effect on the primary tumor growth was observed. However, metastatic growth could be seen taking place in the functionalized scaffolds, suggesting that it is possible to lure metastasizing cells into a trap by imitating the bone marrow microenvironment. A similar strategy was adopted by Bersani *et al.* (190). They utilized a polyacrylamide hydrogel coated with bone marrow stromal cells (BMSCs), which was able to capture metastasizing cells of prostate cancer.

De Vlieghere *et al.* (129) took a slightly different approach to mimic a pre-metastatic niche by developing traps made of iron oxide-coated microparticles encapsulating metabolically active cancer-associated fibroblasts (CAFs) (Figure 1. 6 Scheme II-3-c). The CAFs continuously deposited ECM composed of type I collagen and tenascine C, among others, creating an adhesive environment for disseminated cancer cells. The microparticles were implanted into the peritoneal cavities of mice with induced ovarian cancer. 24 hours after the implantation, the microparticles were magnetically removed and the adhesion of cancer cells on the microparticles was assessed. The treatment led to a delay in peritoneal metastasis and prolonged the animal survival.

Another variation in the strategy for recruiting metastasizing cancer cells was presented by Azarin et al. (130). They developed a microporous scaffold from poly(lactide-co-glycolic acid) (PLGA) scaffold for in vivo capture of metastasizing breast cancer cells through the induction of a local immune response (Figure 1. 6 Scheme II-3-d). Indeed, it has been shown that immune cells are implicated in tumor cell recruitment (191,192). Here, they have either recruited immune cells into the scaffold by grafting the chemokine CCL22, which is known to induce migration of immune cells but not tumor cells, or incorporated the $Gr1^{hi}CD11b^{+}$ immune cells directly into the PLGA scaffold. By doing this, they were able to reduce the number of breast cancer cells that metastasized to the lung by 88%. Similarly, Rao *et al.* (193) designed a PCL-based device with a slower degradation rate than PLGA scaffolds and investigated the immune response induced at the implantation site, the ability of the device to recruit metastatic cells for detection prior to colonization of organs as well as its influence on the survival of mice with induced breast cancer. Pelaez *et al.* (194) further developed the strategy to enable the elimination of the attracted metastatic cells by non-invasive focal hyperthermia. To do so, they coupled metal discs to PCL microparticles to allow heat generation through electromagnetic induction using an oscillating magnetic field. The heat generation could be modulated conveniently by changing the size of the disc or the type of metal.

It has been shown that exosomes, which are vesicles involved in the transfer of information between cells, play a role in homing CTCs in the pre-metastatic niche (178). De la Fuente *et al.* (131) harnessed the potential of this knowledge and designed a 3D scaffold with embedded exosomes extracted from the ascitic fluid of ovarian cancer patients (Figure 1. 6 Scheme II-3-e). The scaffold, called M-Trap, was implanted in the inner wall of the peritoneum of mice with a xenograft of human ovarian cancer in the peritoneal cavity. They showed that the scaffold could serve as the preferred site of metastasis while a peritoneal carcinometastasis was observed in the absence of the M-Trap. Moreover, an increase in the mean survival was observed in the presence of the M-Trap (from 117.5 to 198.8 days), which was further improved by the removal of the scaffold (mean of survival of 309.4 days). The safety and performance of the M-Trap is currently being evaluated in a clinical trial involving female patients with stage IIIC ovarian cancer (ClinicalTrials.gov Identifier NCT03085238).

Chemoattraction of tumour cells

Migrating cells can make directional choices when presented with different migration pathways. *In vitro*, it has been shown that neutrophil-like cells can navigate through a microfabricated maze by following a chemical gradient (195). Chemokines and their receptors are particularly involved in this navigation process. They are indeed responsible for the chemoattraction of various cells and could therefore be used to attract migrating tumor cells into a trap. Several receptors/chemokines have been identified to facilitate cancer cell migration. The most investigated one is SDF-1, also called CXCL12, which binds with high affinity to the CXCR4 and CXCR7 receptors. This chemokine is a pro-inflammatory mediator and is known to play a role in the recruitment of T cells, monocytes and lympho-hemopoietic progenitor cells (196). Its overexpression has been linked to an increase in the invasiveness of ovarian cancer (197), breast cancer (198,199) and GBM (73,200), among others (further details can be found elsewhere (201)). In addition, despite being less well-studied, CXCL16 and its receptor CXCR6 are also suspected to play a role in the migration of tumor cells. Wang *et al.* (202) have shown that the expression of CXCR6 increases with the grade of prostate cancer. These results were supported by Lu *et al*. (203) who observed that metastatic cells from prostate cancer over-express the CXCR6 receptor. Moreover, CXCL16 have been shown to induce the migration and enhance the proliferation of CXCR6-expressing cancer cells *in vitro* (182).

With this knowledge, several groups have tried to stop the migration of tumor cells by inhibiting chemokine receptors, particularly the CXCR4 receptor. A reduction in the migration of cancer cells has been observed *in vitro* (181,204,205). However, this has not been successfully replicated *in vivo*. Brennecke *et al.* found that the use of CXCR4 antibody 12G5 can reduce the number of osteosarcoma pulmonary metastases having a diameter of <0.1 mm but not those of larger dimensions (181). This finding can be explained by the fact that chemoattraction of cancer cells can be mediated by several pairs of chemokine-receptor interaction (for example, SDF-1 can bind either CXCR4 or CXCR7 or both and CXCR6 can be activated by CXCL16). In addition, cells can activate the so-called compensation mechanisms *in vivo* to maintain their migration capacity. Indeed, it has been observed that neural progenitor cells (NPCs) are able to migrate in response to SDF-1 via the activation of the CXCR7 receptor in response to the blockade of the CXCR4 receptor (206). Therefore, in order to stop the migration of tumor cells completely, all receptors implicated in *in vivo* chemoattraction should be identified and blocked, making the task nearly impossible. Moreover, this strategy could only work if the tumor cells have yet to begin migrating. In the particular case of GBM, cancer cells usually have already invaded the surrounding tissues at the time of diagnosis (41). Thus, it may be more useful to direct the migration of cells toward a desired location instead of blocking the migration process altogether.

Chemokines are already being used to attract cells into a scaffold for regenerative medicine purposes. The tumor trap concept can benefit from the existing knowledge in this field of application. Water-retaining polymer networks such as hydrogels and swellable matrices, which have been widely used in tissue engineering and regeneration, are pivotal platforms that are transferrable to the tumor trap application. For this purpose, biocompatible polymers capable of *in situ* formation of three-dimensional gels (207–209) or matrices (129,130,134,210–212) may be used to exert chemotaxis (based on a gradient of soluble attractant or repellent) or haptotaxis (based on a gradient of substrate-bound extracellular matrix proteins) (Figure 1. 9). Of particular interest is the potential exploitation of the CXCR4-SDF-1 axis due to its prominent roles in regulating the migration of many types of cancer cells (207,208,213,214). Examples of biomaterials used to deliver SDF-1 for regenerative medicine are presented in Table 1. 1. Recently, the development of SDF-1-releasing scaffolds to attract tumour cells has received increasing attention. Giarra et al. (132), designed a temperature-responsive gel loaded with SDF-1 based on methylcellulose (MC) or poloxamers with or without hyaluronic acid (HA) for the purpose of attracting CXCR4-expressing GBM cells (Figure 1. 6 Scheme II-3-f). Haji Mansor et al. (133), on the other hand, encapsulated the chemokine in nanoparticles composed of PLGA and a (PEG)-PLGA co-polymer to achieve sustained release (Figure 1. 6 Scheme II-3-g). However, in both papers, no in vivo assessment on the ability of SDF-1 to attract migrating cancer cells was performed.

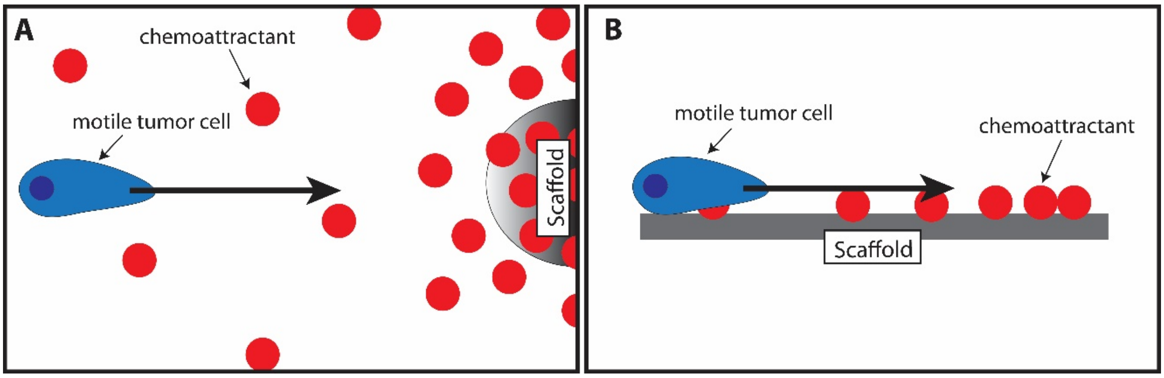

Figure 1. 9: Illustration of the use of scaffolds to attract motile tumour cells by (A) chemotaxis or (B) haptotaxis.

Table 1. 1: Strategies to load SDF-1 into different biomaterials.

Bonding strategy	**Type of biomaterial**	**Composition**	**Target site for regeneration**	**Ref**
Adsorption	Hydrogel	Hyaluronic acid	Cardiac tissue	(215)
		PPCN	Wound healing	(216)
	3D scaffold	Collagen	Cartilage	(217)
			Tendon	(218)
		Collagen/silk fibroin	Bone	(219)
		Hydroxyapatite	Bone	(220)
		Decellularized skeletal muscle	Muscle	(221)
		Collagen/PLA	Bone	(222)
		PLGA	Cartilage	(223)
	Membrane	PCL/gelatin	Bone	(224)
Immobilisation through specific heparin-mediated interaction	Hydrogel	Heparin/PEG	Cardiac tissue	(225)
			Blood vessel	(226)
			Cardiac tissue	(227)
	3D scaffold	Heparin/PLCL	Blood vessel	(228)
		Heparin/PGS	Blood vessel	(229)
		Heparin/PLLA	Blood vessel	(230)
Systems with nano/microparticles	Microspheres	Alginate	Bone	(231)
	Hydrogel/Nanoparticles	Hydrogel: CS/GP nano: CS/CMCS	Bone	(232)
	Microcapsules	Dex-GMA/gelatin/PNIPAAm	Wound healing	(233)
	Particles	PLGA	Cardiac tissue	(234)

PPCN: Poly (polyethylene glycol citrate-co-N-isopropylacrylamide); PLA: polylactide; PLGA: poly(lactic-co-glycolic) acid; PCL: polycaprolactone; PEG: poly(ethylene-glycol); PLCL: poly(L-lactide- co-e-caprolactone) (PLCL); PGS: poly(glycerol sebacate); PLLA: poly(l-lactic acid); CS: chitosan; GP: beta-glycerol phosphate disodium salt; CMCS: carboxymethyl-chitosan; Dex-GMA: glycidyl methacrylated dextran; PNIPAAm: poly(N-isopropylacrylamide).

Challenges associated with the clinical translation of the tumour trapping strategy

While promising preclinical results have been obtained from the use of tumour traps as a diagnostic and/or therapeutic tool, there are multiple issues that must be addressed before this approach can enter the clinic. Main concerns include identifying suitable means for in vivo monitoring of the recruitment of cancer cells into the scaffolds to allow one to decide on the optimal timepoint for killing the trapped cancer cells. Prolonged duration of cancer cell recruitment may lead to overcrowding of the tumour trap and subsequent cell escape, reducing the purpose of the synthetic niche to merely a "relay" for the cancer cells en route to their natural metastatic sites.

The incorporation of chemoattractant molecules such as SDF-1 into the tumor trap may also introduce additional complexities. In particular, there are concerns regarding the selectivity of SDF-1-mediated chemotaxis. Indeed, in addition to its role in recruiting cancer cells to local and distant sites of colonization, SDF-1 is also implicated in the homing of other cell lines such as immune cells and stem cells (196,219,223). Moreover, the potential off-target effects may also be exacerbated by the fact that this chemokine is known to be involved in various processes that support tumor progression, angiogenesis, metastasis and survival (235). It is therefore necessary to study in more detail the effect of injecting such proteins near tumor cells *in vivo* and to carefully evaluate the entire risks before moving to the clinic.

Further down the development timeline, the most effective way to kill the recruited cancer cells should be elucidated. It may be tempting to suggest direct removal of the trap to achieve an immediate eradication of the disease. However, this approach will necessitate an additional surgery, a requirement that may be very difficult to fulfil especially in patients who are terminally ill. A less invasive solution would be to use stereotactic radiotherapy (SRT). SRT is a treatment where radiation beam is directed to a well-defined spot, usually the tumour site, from many different angles around the body. The procedure ensures the targeted site receives much higher dose of radiation than the surrounding tissues. At the moment, SRT seems to be a viable option for killing the trapped cancer cells. This said, other selective approaches should also be considered and evaluated.

Conclusion

A good understanding of the escape pathways of a prey allows the hunter to capture it more efficiently; the same rule of thumb can be applied to tumor cells. Using this principle, it is possible to design tumor traps for diagnostic and/or therapeutic applications. For the latter purpose, it is necessary that the trapped cells are killed by the application of existing therapies. The different therapeutic strategies (surgery, chemotherapy, targeted therapy, …) may not be sufficient on their own to cure every cancer type but they can be used in combination to achieve the best clinical outcomes. Jain *et al.* used a chemotherapeutic agent in the form of cyclopamine alongside their tumor trap to shrink down the size of GBM tumors (127). It would also be interesting to combine the trap with radiosensitizers, focus x-ray or γ-ray microbeams. Since the trap would concentrate the tumor cells, the efficiency of chemo- and radio-therapies can potentially be improved while the associated side effects are likely to decrease. Immunotherapy, which can be broadly-described as the activation of immune cells to make them able to recognize and eliminate tumor cells, could also be used. Indeed, one of the major difficulties in immunotherapy is to make the cancer cells accessible to the activated immune cells. This is particularly true in the brain as there is a need to overcome the blood-brain barrier (236). If immune cells can be pre-loaded or attracted into the trap via chemoattraction, this will facilitate the killing of the trapped cancer cells. Indeed, immune cells are also sensitive to a gradient of chemokines such as SDF-1 (226) and can therefore be recruited into the trap together with the cancer cells of interest. Overall, this bio-integrative approach can be seen as counter-intuitive insofar as the factors governing the trapping of tumor cells are also involved in other signaling pathways that may lead to effects that are opposite to the initial will (237). Our current knowledge on the mechanisms driving the migration of cancerous cells might not be sufficient to develop a trap that only impact tumor cells in a safe manner. The translation to the clinic will therefore require further investigations on the efficacy and safety of such systems. Nevertheless, as Albert Einstein pointed out, "we do not solve problems with the modes of thought that have engendered them" and this unique approach therefore deserves further investigations.

ACKNOWLEDGEMENTS

This work was supported by the “Institut National de la Santé et de la Recherche Médicale” (INSERM), the University of Angers (Angers, France), the MINECO (SAF2017-83118-R), by the Agencia Estatal de Investigacion (AEI, Spain) and by the Federación Española de Enfermedades Raras (FEDER). It is also related to the LabEx IRON “Innovative Radiopharmaceuticals in Oncology and Neurology” as part of the French government “Investissements d’Avenir” program, to the INCa (Institut National du Cancer) MARENGO consortium “MicroRNA agonist and antagonist Nanomedicines for GliOblastoma treatment: from molecular programmation to preclinical validation through the PL-BIO 2014-2020 grant and to the MuMoFRaT project “Multi-scale Modeling & simulation of the response to hypo-Fractionated Radiotherapy or repeated molecular radiation Therapies” supported by “La Région Pays-de-la-Loire” and by the Cancéropôle Grand-Ouest (tumor targeting and radiotherapy network). Najberg was a Ph.D. student involved in the Erasmus Mundus Joint Doctorate program for Nanomedicine and pharmaceutical innovation (EMJD NanoFar) and received a fellowship from “La Région Pays-de-la-Loire”.

5. Objectives of the thesis

GBM is an infiltrating deadly tumour of the CNS. It is the most frequent, aggressive and lethal form of diffuse glioma. Its conventional treatment consists of a surgical resection of the tumour followed by a radio-chemotherapy using X-rays and TMZ. However, even with this aggressive treatment, the median of survival is less than 15 months. Indeed, recurrence of the tumour is today inevitable. It has been observed that tumour recurrence mostly occurs within 2 cm of the resection cavity which can be explained by the invasion ability of GBM cells. Therefore, the targeting of tumour cells infiltrated inside the brain, in particular in the margin of the resection cavity, is a major goal for the treatment of GBM. Infiltrative GBM cells overexpress the CXCR4 receptor. This receptor binds to the chemoattractant SDF-1α, also known as CXCL12. A gradient of this chemokine induces an attraction of cells expressing the CXCR4 receptor. Therefore, we hypothesized that it is possible to attract and confine infiltrative glioblastoma cells in a trap by implanting a scaffold inside the resection cavity liberating a gradient of SDF-1α. The aim of the thesis is therefore to design a novel scaffold releasing SDF-1α and consequently attracting and confining infiltrative glioblastoma cells from the surrounding tissue. In this study, freeze-dried sponges made of hyaluronic acid (HA), silk fibroin (SF) and heparin (hep) loaded with SDF-1α were developed.

For the design of a tumour trap, porous sponge scaffolds are of particular interest since a 3D porous structure promote cell attachment, migration and nutrient and waste transport. HA is the main constituent of the brain ECM. It can enhance cell mobility and invasion by interaction through the CD44 receptor. The main concern with HA for the purpose of this study is its quick degradation *in vivo*. SF from the silk worm *Bombix mori* is a naturally derived polymer which is known for its biocompatibility, relatively slow degradability, low inflammatory responses and versatile processing abilities. We therefore hypothesized that combining HA with SF would allow a fine tuning of the degradation time of the scaffold, SF being the main structural component with a slow degradation rate and HA increasing cellular invasion in the scaffold. Heparin/heparan sulfate is a component of the ECM and is present in the brain. It has been chosen to deliver SDF-1α since it is a natural binding molecule of the chemokine.

The general strategy is illustrated in the Figure 1. 10. After restriction of the tumour, the scaffold hydrated and shaped beforehand would be implanted in the cavity of resection. Slow release of SDF-1α overtime would attract GBM cells infiltrated in the healthy brain that the surgeon could not remove. After a time that needs to be determined, allowing cells to integrate the scaffold, a therapeutic strategy would be put in place to eliminate the cells. This therapy would be used in combination with the classical therapy with radiotherapy and TMZ. Over time, the scaffold would slowly degrade, leading to the complete recovery of the patient.

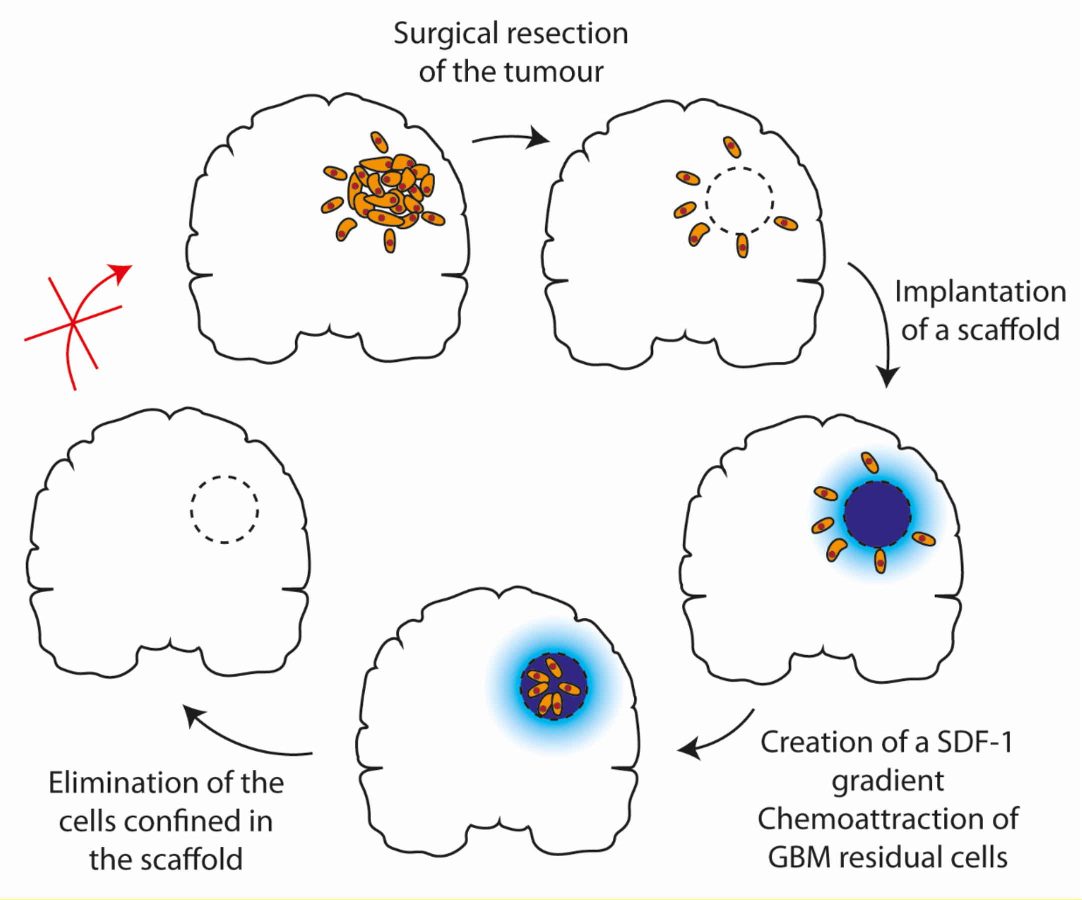

Figure 1. 10: Schematic representation of the general strategy of the tumour trap using a chemoattractant molecule such as SDF-1α.

The innovative aspect of this study is the development of a new strategy for GBM treatment using freeze-dried sponges made of a combination of SF, HA and hep loaded with a chemoattractive molecule, the SDF-1α.

The specific objectives of this work are:

1. Development of an appropriate model for the evaluation of the SDF-1α activity (Chapter II)
2. Development of a process to produce SF, HA and hep sponges (Chapter II)
3. Physicochemical characterisation of the polymers (Chapter II)
4. Biological evaluation *in vitro* and *in vivo* in a rat model (Chapter IV)
5. Identification of the best combination of polymers (SF, HA, SF-HA or SF-HA-hep) for our specific application (Chapter II and IV)

The scaffolds developed during this thesis could be used to understand better the interaction of SDF-1α with a GBM tumour *in vivo* and evaluate the feasibility of a tumour trap by chemoattraction with SDF-1α for GBM infiltrative cells. Ultimately, we hope that our results will contribute to the elaboration of the proof of concept and that our system will benefit the survival and quality of life of operable GBM patients.

REFERENCES

1. Hanahan D, Weinberg RA. Hallmarks of cancer: the next generation. Cell. 2011;144(5):646–74.
2. Louis DN, Perry A, Reifenberger G, von Deimling A, Figarella-Branger D, Cavenee WK, et al. The 2016 World Health Organization Classification of Tumors of the Central Nervous System: a summary. Acta Neuropathol. 2016;131(6):803–20.
3. Foote MB, Papadopoulos N, Diaz LA. Genetic Classification of Gliomas: Refining Histopathology. Cancer Cell. 2015;28(1):9–11.
4. Louis DN, Perry A, Reifenberger G, von Deimling A, Figarella-Branger D, Cavenee WK, et al. The 2016 World Health Organization Classification of Tumors of the Central Nervous System: a summary. Acta Neuropathol. 2016;131(6):803–20.
5. Bailey P, Cushing H. A classification of the tumors of the glioma group on a histogenetic basis : with a correlated study of prognosis. Philadelphia, PA: Lippincott; 1926.
6. Ohgaki H, Kleihues P. The Definition of Primary and Secondary Glioblastoma. Clin Cancer Res. 2013 Feb 15;19(4):764 LP – 772.
7. Darlix A, Zouaoui S, Rigau V, Bessaoud F, Figarella-Branger D, Mathieu-Daudé H, et al. Epidemiology for primary brain tumors: A nationwide population-based study. J Neurooncol. 2017;131(3):525–46.
8. Smirniotopoulos JG, Murphy M, Rushing EJ, Rees JH, Schroeder JW. Patterns of Contrast Enhancement in the Brain and Meninges. Radiographics. 2007;27(2):525–52.
9. Galanaud D, Nicoli F, Figarella-Branger D, Roche P, Confort-Gouny S, Fur Y Le, et al. Spectroscopie par résonance magnétique des tumeurs cérébrales. J Radiol. 2006;87(6):822–32.
10. Netsky MG, August B, Fowler W. The longevity of patients with glioblastoma multiforme. J Neurosurg. 1949;7(3):261–9.
11. Delgado-López PD, Corrales-García EM. Survival in glioblastoma: a review on the impact of treatment modalities. Clin Transl Oncol. 2016;18(11):1062–71.
12. Stupp R, Mason WP, van den Bent MJ, Weller M, Fisher B, Taphoorn MJB, et al. Radiotherapy plus Concomitant and Adjuvant Temozolomide for Glioblastoma. N Engl J Med. 2005;352(10):987–96.
13. Chaichana KL, Jusue-Torres I, Navarro-Ramirez R, Raza SM, Pascual-Gallego M, Ibrahim A, et al. Establishing percent resection and residual volume thresholds affecting survival and recurrence for patients with newly diagnosed intracranial glioblastoma. Neuro Oncol. 2014;16(1):113–22.
14. Lu VM, Jue TR, McDonald KL, Rovin RA. The Survival Effect of Repeat Surgery at Glioblastoma Recurrence and its Trend: A Systematic Review and Meta-Analysis. World Neurosurg. 2018;115:453-459.e3.
15. Lara-Velazquez M, Al-Kharboosh R, Jeanneret S, Vazquez-Ramos C, Mahato D, Tavanaiepour D, et al. Advances in brain tumor surgery for glioblastoma in adults. Brain Sci. 2017;7(12):1–16.
16. Wright J, Chugh J, Wright CH, Alonso F, Hdeib A, Gittleman H, et al. Laser interstitial thermal therapy followed by minimal-access transsulcal resection for the treatment of large and difficult to access brain tumors. Neurosurg Focus. 2016;41(4):E14.
17. Young RM, Jamshidi A, Davis G, Sherman JH. Current trends in the surgical management and treatment of adult glioblastoma. Ann Transl Med. 2015;3(9):121.
18. Yong RL, Lonser RR. Surgery for glioblastoma multiforme: Striking a balance. World Neurosurg. 2011;76(6):528–30.
19. Lawrence YR, Blumenthal DT, Matceyevsky D, Kanner AA, Bokstein F, Corn BW. Delayed initiation of radiotherapy for glioblastoma: How important is it to push to the front (or the back) of the line? J Neurooncol. 2011;105(1):1–7.
20. Thomas RP, Recht L, Nagpal S. Advances in the management of glioblastoma the role of TMZ and MGMT testing. Clin Pharmacol Adv Appl. 2013;5:1–9.

21. Hegi ME, Diserens A-C, Gorlia T, Hamou M-F, de Tribolet N, Weller M, et al. MGMT Gene Silencing and Benefit from Temozolomide in Glioblastoma . N Engl J Med. 2005;352(10):997–1003.

22. Silber JR, Mueller BA, Ewers TG, Berger MS. Comparison of 06-Methylguanine-DNA Methyltransferase Activity in Brain Tumors and Adjacent Normal Brain. Cancer Res. 1993;53(14):3416–20.

23. Brada M, Stenning S, Gabe R, Thompson LC, Levy D, Rampling R, et al. Temozolomide versus procarbazine, lomustine, and vincristine in recurrent high-grade glioma. J Clin Oncol. 2010;28(30):4601–8.

24. Abbott NJ. Blood-brain barrier structure and function and the challenges for CNS drug delivery. J Inherit Metab Dis. 2013;36(3):437–49.

25. Woodworth GF, Dunn GP, Nance EA, Hanes J, Brem H. Emerging Insights into Barriers to Effective Brain Tumor Therapeutics. Front Oncol. 2014;4(July):1–14.

26. Van Tellingen O, Yetkin-Arik B, De Gooijer MC, Wesseling P, Wurdinger T, De Vries HE. Overcoming the blood-brain tumor barrier for effective glioblastoma treatment. Drug Resist Updat. 2015;19:1–12.

27. Furnari FB, Fenton T, Bachoo RM, Mukasa A, Stommel JM, Stegh A, et al. Malignant astrocytic glioma: Genetics, biology, and paths to treatment. Genes Dev. 2007;21(21):2683–710.

28. Fischer I, Gagner J-P, Law M, Newcomb EW, Zagzag D. Angiogenesis in Gliomas: Biology and Molecular Pathophysiology. Brain Pathol. 2006;15(4):297–310.

29. Ulrich TA, De Juan Pardo EM, Kumar S. The mechanical rigidity of the extracellular matrix regulates the structure, motility, and proliferation of glioma cells. Cancer Res. 2009;69(10):4167–74.

30. Parker NR, Hudson AL, Khong P, Parkinson JF, Dwight T, Ikin RJ, et al. Intratumoral heterogeneity identified at the epigenetic, genetic and transcriptional level in glioblastoma. Sci Rep. 2016;6(September 2015):1–10.

31. Buckner JC, Brown PD, O'Neil BP, Meyer FB, Wetmore CJ, Uhm JH. Central Nervous System Tumors. Mayo Found Med Educ Res. 2007;82(10):1271–86.

32. Sun H, Du S, Liao G, Xie X, Ren C, Yuan YW. Do Glioma Patients Derive Any Therapeutic Benefit from Taking a Higher Cumulative Dose of Temozolomide Regimens? Med (United States). 2015;94(20):1–6.

33. Sarkaria JN, Kitange GJ, James CD, Plummer R, Calvert H, Weller M, et al. Mechanisms of chemoresistance to alkylating agents in malignant glioma. Clin Cancer Res. 2008;14(10):2900–8.

34. Buczacki S. Cancer Stem Cells. Encycl Cell Biol. 2015;3:807–12.

35. Zhou S, Schuetz JD, Bunting KD, Colapietro A-M, Sampath J, Morris JJ, et al. The ABC transporter Bcrp1/ABCG2 is expressed in a wide variety of stem cells and is a molecular determinant of the side-population phenotype. Nat Med. 2001;7(9):1028–34.

36. Cheung AMS, Wan TSK, Leung JCK, Chan LYY, Huang H, Kwong YL, et al. Aldehyde dehydrogenase activity in leukemic blasts defines a subgroup of acute myeloid leukemia with adverse prognosis and superior NOD/SCID engrafting potential. Leukemia. 2007;21(7):1423–30.

37. Konopleva M, Zhao S, Hu W, Jiang S, Snell V, Weidner D, et al. The anti-apoptotic genes Bcl-XL and Bcl-2 are over-expressed and contribute to chemoresistance of non-proliferating leukaemic CD34+ cells. Br J Haematol. 2002 Aug 1;118(2):521–34.

38. Cammareri P, Scopelliti A, Todaro M, Eterno V, Francescangeli F, Moyer MP, et al. Aurora-A Is Essential for the Tumorigenic Capacity and Chemoresistance of Colorectal Cancer Stem Cells. Cancer Res. 2010 Jun 1;70(11):4655 LP – 4665.

39. Bisson I, Prowse DM. WNT signaling regulates self-renewal and differentiation of prostate cancer cells with stem cell characteristics. Cell Res. 2009 Apr 14;19:683.

40. Mirzaei HR, Gharagozloo M, Rezaei A, Soleimani M, Kalantari H, Mirzaei H, et al. Mechanisms of chemoresistance in tumor-derived cancer stem cells. J Isfahan Med Sch. 2012;30(197):1–9.

41. Giese A, Bjerkvig R, Berens ME, Westphal M. Cost of migration: Invasion of malignant gliomas and implications for treatment. J Clin Oncol. 2003;21(8):1624–36.

42. Yamahara T, Numa Y, Oishi T, Kawaguchi T, Seno T, Asai A, et al. Morphological and flow cytometric analysis of cell infiltration in glioblastoma: A comparison of autopsy brain and neuroimaging. Brain Tumor Pathol. 2010;27(2):81–7.

43. Guo RM, Zhao C Bin, Li P, Zhang L, Zang SH, Yang B. Overexpression of CLEC18B Associates With the Proliferation, Migration, and Prognosis of Glioblastoma. ASN Neuro. 2018;10.

44. Chen J, Zhang J, Hong L, Zhou Y. EGFLAM correlates with cell proliferation, migration, invasion and poor prognosis in glioblastoma. Cancer Biomarkers. 2019;24(3):343–50.

45. Guan Y, He Y, Lv S, Hou X, Li L, Song J. Overexpression of HOXC10 promotes glioblastoma cell progression to a poor prognosis via the PI3K/AKT signalling pathway. J Drug Target. 2019;27(1):60–6.

46. Zhang G, Sun W, Zhu L, Feng Y, Wu L, Li T. Overexpressed circ_0029426 in glioblastoma forecasts unfavorable prognosis and promotes cell progression by sponging miR-197. J Cell Biochem. 2019;120(6):10295–302.

47. Bellail AC, Hunter SB, Brat DJ, Tan C, Van Meir EG. Microregional extracellular matrix heterogeneity in brain modulates glioma cell invasion. Int J Biochem Cell Biol. 2004;36(6):1046–69.

48. Bernstein JJ, Woodard CA. Glioblastoma cells do not intravasate into blood vessels. Neurosurgery. 1995;36(1):124–32.

49. Lagerweij T, Dusoswa SA, Negrean A, Hendrikx EML, de Vries HE, Kole J, et al. Optical clearing and fluorescence deep-tissue imaging for 3D quantitative analysis of the brain tumor microenvironment. Angiogenesis. 2017;20(4):533–46.

50. Cuddapah VA, Robel S, Watkins S, Sontheimer H. A neurocentric perspective on glioma invasion. Nat Rev Neurosci. 2014;15(7):455–65.

51. Osswald M, Jung E, Sahm F, Solecki G, Venkataramani V, Blaes J, et al. Brain tumour cells interconnect to a functional and resistant network. Nature. 2015;528(7580):93–8.

52. Gritsenko PG, Ilina O, Friedl P. Interstitial guidance of cancer invasion. J Pathol. 2012;226(2):185–99.

53. Rao JS. Molecular mechanisms of glioma invasiveness: the role of proteases. Nat Rev Cancer. 2003;3(July):489–501.

54. Pencheva N, de Gooijer MC, Vis DJ, Wessels LFA, Würdinger T, van Tellingen O, et al. Identification of a Druggable Pathway Controlling Glioblastoma Invasiveness. Cell Rep. 2017;20(1):48–60.

55. Zimmermann DR, Dours-Zimmermann MT. Extracellular matrix of the central nervous system: From neglect to challenge. Histochem Cell Biol. 2008;130(4):635–53.

56. Xia S, Lal B, Tung B, Wang S, Goodwin CR, Laterra J. Tumor microenvironment tenascin-C promotes glioblastoma invasion and negatively regulates tumor proliferation. Neuro Oncol. 2016;18(4):507–17.

57. Cheng L, Wu Q, Guryanova OA, Huang Z, Huang Q, Rich JN, et al. Elevated invasive potential of glioblastoma stem cells. Biochem Biophys Res Commun. 2011;406(4):643–8.

58. de Gooijer MC, Guillén Navarro M, Bernards R, Wurdinger T, van Tellingen O. An Experimenter's Guide to Glioblastoma Invasion Pathways. Trends Mol Med. 2018;24(9):763–80.

59. Himanen JP, Chumley MJ, Lackmann M, Li C, Barton WA, Jeffrey PD, et al. Repelling class discrimination: Ephrin-A5 binds to and activates EphB2 receptor signaling. Nat Neurosci. 2004;7(5):501–9.

60. Day BW, Stringer BW, Al-Ejeh F, Ting MJ, Wilson J, Ensbey KS, et al. EphA3 Maintains Tumorigenicity and Is a Therapeutic Target in Glioblastoma Multiforme. Cancer Cell. 2013;23(2):238–48.

61. Binda E, Visioli A, Giani F, Lamorte G, Copetti M, Pitter KL, et al. The EphA2 Receptor Drives Self-

Renewal and Tumorigenicity in Stem-like Tumor-Propagating Cells from Human Glioblastomas. Cancer Cell. 2012;22(6):765–80.

62. Miao H, Gale NW, Guo H, Qian J, Petty A, Kaspar J, et al. EphA2 promotes infiltrative invasion of glioma stem cells in vivo through cross-talk with Akt and regulates stem cell properties. Oncogene. 2015;34(5):558–67.

63. Teng L, Nakada M, Furuyama N, Sabit H, Furuta T, Hayashi Y, et al. Ligand-dependent EphB1 signaling suppresses glioma invasion and correlates with patient survival. Neuro Oncol. 2013;15(12):1710–20.

64. Wang SD, Rath P, Lal B, Richard JP, Li Y, Goodwin CR, et al. EphB2 receptor controls proliferation/migration dichotomy of glioblastoma by interacting with focal adhesion kinase. Oncogene. 2012;31(50):5132–43.

65. Janowski M. Functional diversity of SDF-1 splicing variants. Cell Adhes Migr. 2009;3(3):243–9.

66. Kitaori T, Ito H, Schwarz EM, Tsutsumi R, Yoshitomi H, Oishi S, et al. Stromal cell-derived factor 1/CXCR4 signaling is critical for the recruitment of mesenchymal stem cells to the fracture site during skeletal repair in a mouse model. Arthritis Rheum. 2009;60(3):813–23.

67. Kimura Y, Komaki M, Iwasaki K, Sata M, Izumi Y, Morita I. Recruitment of bone marrow-derived cells to periodontal tissue defects. Front Cell Dev Biol. 2014;2(May):1–6.

68. Ehtesham M, Winston JA, Kabos P, Thompson RC. CXCR4 expression mediates glioma cell invasiveness. Oncogene. 2006;25(19):2801–6.

69. Zhou Y, Larsen PH, Hao C, Yong VW. CXCR4 is a major chemokine receptor on glioma cells and mediates their survival. J Biol Chem. 2002;277(51):49481–7.

70. Zagzag D, Esencay M, Mendez O, Yee H, Smirnova I, Huang Y, et al. Hypoxia- and Vascular Endothelial Growth Factor-Induced Stromal Cell-Derived Factor-1α/CXCR4 Expression in Glioblastomas. Am J Pathol. 2008;173(2):545–60.

71. Yi L, Tong L, Li T, Hai L, Abeysekera IR, Tao Z, et al. Bioinformatic analyses reveal the key pathways and genes in the CXCR4 mediated mesenchymal subtype of glioblastoma. Mol Med Rep. 2018;18(1):741–8.

72. Rempel SA, Dudas S, Ge S, Gutiérrez JA. Identification and localization of the cytokine SDF1 and its receptor, CXC chemokine receptor 4, to regions of necrosis and angiogenesis in human glioblastoma. Clin Cancer Res. 2000;6(1):102–11.

73. Hira VVV, Verbovšek U, Breznik B, Srdič M, Novinec M, Kakar H, et al. Cathepsin K cleavage of SDF-1α inhibits its chemotactic activity towards glioblastoma stem-like cells. Biochim Biophys Acta - Mol Cell Res. 2017;1864(3):594–603.

74. Kim H, Roh HS, Kim JE, Park SD, Park WH, Moon J. Compound K attenuates stromal cell-derived growth factor 1 (SDF-1) -induced migration of C6 glioma cells. 2016;10(3):259–64.

75. Cunha MLV da, Maldaun MVC. Metastasis from glioblastoma multiforme: a meta-analysis. Rev Assoc Med Bras. 2019;65(3):424–33.

76. Ostermann S, Csajkag C, Buclin T, Leyvraz S, Lejeune F, Decosterd LA, et al. Plasma and cerebrospinal fluid population pharmacokinetics of temozolomide in malignant glioma patients. Clin Cancer Res. 2004;10(11):3728–36.

77. Karim R, Palazzo C, Evrard B, Piel G. Nanocarriers for the treatment of glioblastoma multiforme: Current state-of-the-art. J Control Release. 2016;227:23–37.

78. Danhier F, Feron O, Préat V. To exploit the tumor microenvironment: Passive and active tumor targeting of nanocarriers for anti-cancer drug delivery. J Control Release. 2010;148(2):135–46.

79. Davies AM, Weinberg U, Palti Y. Tumor treating fields: A new frontier in cancer therapy. Ann N Y Acad Sci. 2013;1291(1):86–95.

80. Stupp R, Wong ET, Kanner AA, Steinberg D, Engelhard H, Heidecke V, et al. NovoTTF-100A versus physician’s choice chemotherapy in recurrent glioblastoma: A randomised phase III trial of a novel

treatment modality. Eur J Cancer. 2012;48(14):2192–202.

81. Umlauf BJ, Shusta E V. Exploiting BBB disruption for the delivery of nanocarriers to the diseased CNS. Curr Opin Biotechnol. 2019;60:146–52.

82. Jackson S, Weingart J, Nduom EK, Harfi TT, George RT, McAreavey D, et al. The effect of an adenosine A2a agonist on intra-tumoral concentrations of temozolomide in patients with recurrent glioblastoma. Fluids Barriers CNS. 2018;15(1):1–9.

83. ClinicalTrials.gov [Internet]. Identifier NCT03744026, Safety and Efficacy of Transient Opening of the Blood-brain Barrier (BBB) With the SonoCloud-9 (SC9-GBM-01); 2019 April 8. Available from https://clinicaltrials.gov/ct2/show/NCT03744026?term=SonoCloud.

84. Chaichana KL, Pinheiro L, Brem H. Delivery of local therapeutics to the brain: working toward advancing treatment for malignant gliomas. Ther Deliv. 2015;6(3):353–69.

85. Hendricks BK, Cohen-Gadol AA, Miller JC. Novel delivery methods bypassing the blood-brain and blood-tumor barriers. Neurosurg Focus. 2015;38(3):E10.

86. Varenika V, Dickinson P, Bringas J, LeCouteur R, Higgins R, Park J, et al. Detection of infusate leakage in the brain using real-time imaging of convection-enhanced delivery. J Neurosurg JNS. 2008;109(5).

87. Bota DA, Desjardins A, Quinn JA, Affronti ML, Friedman HS. Interstitial chemotherapy with biodegradable BCNU (Gliadel®) wafers in the treatment of malignant gliomas. Ther Clin Risk Manag. 2007;3(5):707–15.

88. Attenello FJ, Mukherjee D, Datoo G, McGirt MJ, Bohan E, Weingart JD, et al. Use of Gliadel (BCNU) wafer in the surgical treatment of malignant glioma: A 10-year institutional experience. Ann Surg Oncol. 2008;15(10):2887–93.

89. Mirani B, Pagan E, Shojaei S, Duchscherer J, Toyota BD, Ghavami S, et al. A 3D bioprinted hydrogel mesh loaded with all-trans retinoic acid for treatment of glioblastoma. Eur J Pharmacol. 2019;854(October 2018):201–12.

90. Tyler B, Wadsworth S, Recinos V, Mehta V, Vellimana A, Li K, et al. Efficacy Study in an Experimental Malignant Glioma Model in Rats. Neuro Oncol. 2011;13(7):700–9.

91. ClinicalTrials.gov [Internet]. Identifier NCT00479765, A Phase 1 / 2 Dose Escalation Study of Locally-Administered OncoGel^{TM} in Subjects With Recurrent Glioma; 2014 May 15. Available from https://clinicaltrials.gov/ct2/show/study/NCT00479765?term=OncoGel&c.

92. Pradilla G, Wang PP, Gabikian P, Li K, Magee CA, Walter KA, et al. Local intracerebral administration of paclitaxel with the paclimer® delivery system: Toxicity study in a canine model. J Neurooncol. 2006;76(2):131–8.

93. Menei P, Capelle L, Guyotat J, Fuentes S, Assaker R, Bataille B, et al. Local and sustained delivery of 5-fluorouracil from biodegradable microspheres for the radiosensitization of malignant glioma: A randomized phase II trial. Neurosurgery. 2005;56(2):242–7.

94. Neagu MR, Reardon DA. An Update on the Role of Immunotherapy and Vaccine Strategies for Primary Brain Tumors. Curr Treat Options Oncol. 2015;16(11).

95. Mooney J, Bernstock JD, Ilyas A, Ibrahim A, Yamashita D, Markert JM, et al. Current approaches and challenges in the molecular therapeutic targeting of glioblastoma. World Neurosurg. 2019;129:90–100.

96. ClinicalTrials.gov [Internet]. Identifier NCT02017717; 2019, April 30. Available from https://clinicaltrials.gov/ct2/show/NCT02017717?term=NCT02017717&cond=Glioblastoma&rank=1.

97. ClinicalTrials.gov [Internet]. Identifier NCT02667587; 2019 June 28; Available from https://clinicaltrials.gov/ct2/show/NCT02667587?term=NCT02667587&cond=Glioblastoma&rank=1.

98. ClinicalTrials.gov [Internet]. Identifier NCT02617589, 2019 Jan. 15; Available from https://clinicaltrials.gov/ct2/show/NCT02617589?term=NCT02617589&cond=Glioblastoma&rank

=1.

99. Choi BD, Maus M V., June CH, Sampson JH. Immunotherapy for glioblastoma: Adoptive T-cell Strategies. Clin Cancer Res. 2019;25(7):2042–8.

100. Mooney J, Bernstock JD, Ilyas A, Ibrahim A, Yamashita D, Markert JM, et al. Current approaches and challenges in the molecular therapeutic targeting of glioblastoma. World Neurosurg. 2019;129:90–100.

101. ClinicalTrials.gov [Internet]. Identifier NCT01280552; 2017, March 20; Available from https://clinicaltrials.gov/ct2/show/NCT01280552?term=NCT01280552&cond=Glioblastoma&rank=1.

102. ClinicalTrials.gov [Internet]. Identifier NCT00045968; 2016, Oct 14; Available from https://clinicaltrials.gov/ct2/show/NCT00045968?term=NCT00045968&cond=Glioblastoma&rank=1.

103. Reijneveld JC, Voest EE, Taphoorn MJB. Angiogenesis in malignant primary and metastatic brain tumors. J Neurol. 2000;247(8):597–608.

104. Scaringi C, Enrici RM, Minniti G. Combining molecular targeted agents with radiation therapy for malignant gliomas. Onco Targets Ther. 2013;6:1079–95.

105. Mcgee MC, Hamner JB, Williams RF, Rosati F, Sims TL, Ng CY, et al. Improved intratumoral oxygenation through vascular normalization increases glioma sensitivity to ionizing radiation. Int J Radiat Oncol Biol Phys. 2010;76(5):1537–45.

106. Corso CD, Bindra RS. Success and Failures of Combined Modalities in Glioblastoma Multiforme: Old Problems and New Directions. Semin Radiat Oncol. 2016;26(4):281–98.

107. ClinicalTrials.gov [Internet]. Identifier NCT00884741, Temozolomide and Radiation Therapy With or Without Bevacizumab in Treating Patients With Newly Diagnosed Glioblastoma; 2018 Jan 30. Available from https://clinicaltrials.gov/ct2/show/results/NCT008847.

108. Bolderson E, Richard DJ, Zhou BBS, Khanna KK. Recent advances in cancer therapy targeting proteins involved in DNA double-strand break repair. Clin Cancer Res. 2009;15(20):6314–20.

109. Rouleau M, Patel A, Hendzel MJ, Kaufmann SH, Poirier GG. PARP inhibition: PARP1 and beyond. Nat Rev Cancer. 2010;10(4):293–301.

110. Javle M, Curtin N. The role of PARP in DNA repair and its therapeutic exploitation. Br J Cancer. 2011;105:1114–22.

111. Senra JM, Telfer BA, Cherry KE, McCrudden CM, Hirst DG, O'Connor MJ, et al. Inhibition of PARP-1 by Olaparib (AZD2281) Increases the Radiosensitivity of a Lung Tumor Xenograft. Mol Cancer Ther. 2011;10(10):1949–58.

112. Zuoren Yua,*, Timothy G. Pestellc, Michael P. Lisantic and RGP. Cancer stem cells. Int J Biochem Cell Biol. 2012;44(12):2144–51.

113. Galli R, Binda E, Orfanelli U, Cipelletti B, Gritti A, De Vitis S, et al. Isolation and Characterization of Tumorigenic, Stem-like Neural Precursors from Human Glioblastoma. Cancer Res. 2004;64:7011–21.

114. Gupta PB, Onder TT, Jiang G, Tao K, Kuperwasser C, Weinberg RA, et al. Identification of Selective Inhibitors of Cancer Stem Cells by High-Throughput Screening. Cell. 2009;138(4):645–59.

115. ClinicalTrials.gov [Internet]. Identifier NCT01220271, A Study Combining LY2157299 With Temozolomide-based Radiochemotherapy in Patients With Newly Diagnosed Malignant Glioma; 2017, Feb. 16. Available from https://clinicaltrials.gov/ct2/show/NCT01220271?t.

116. ClinicalTrials.gov [Internet]. Identifier NCT01682187, A Dose-Escalation Study in Participants With Recurrent Malignant Glioma; 2019, June 5. Available from https://clinicaltrials.gov/ct2/show/NCT01682187?term=NCT01682187&rank=1.

117. ClinicalTrials.gov [Internet]. Identifier NCT01582269, A Study in Recurrent Glioblastoma (GB); 2018, Dec. 4. Available from

https://clinicaltrials.gov/ct2/show/NCT01582269?term=NCT01582269&rank=1.

118. Iacobucci G. Cancer survival in England: rates improve and variation falls. BMJ. 2019;365(April):l1532.

119. Zeng H, Chen W, Zheng R, Zhang S, Ji JS, Zou X, et al. Changing cancer survival in China during 2003–15: a pooled analysis of 17 population-based cancer registries. Lancet Glob Heal. 2018;6(5):e555–67.

120. Brustugun OT, Grønberg BH, Fjellbirkeland L, Helbekkmo N, Aanerud M, Grimsrud TK, et al. Substantial nation-wide improvement in lung cancer relative survival in Norway from 2000 to 2016. Lung Cancer. 2018;122(February):138–45.

121. Trama A, Bernasconi A, McCabe MG, Guevara M, Gatta G, Botta L, et al. Is the cancer survival improvement in European and American adolescent and young adults still lagging behind that in children? Pediatr Blood Cancer. 2019;66(1):1–9.

122. Rankin EB, Giaccia AJ. Hypoxic control of metastasis. Science (80-). 2016;352(6282):175–80.

123. Strebhardt K, Ullrich A. Paul Ehrlich’s magic bullet concept: 100 years of progress. Nat Rev cancer. 2008;8:473–80.

124. Kim EG, Kim KM. Strategies and advancement in antibody-drug conjugate optimization for targeted cancer therapeutics. Biomol Ther. 2015;23(6):493–509.

125. Maier-Hauff K, Ulrich F, Nestler D, Niehoff H, Wust P, Thiesen B, et al. Efficacy and safety of intratumoral thermotherapy using magnetic iron-oxide nanoparticles combined with external beam radiotherapy on patients with recurrent glioblastoma multiforme. J Neurooncol. 2011;103(2):317–24.

126. MagForce. NanoTherm has the potential to tap into the US prostate cancer market as aunique focal treatment option. 2018.

127. Jain A, Betancur M, Patel GD, Valmikinathan CM, Mukhatyar VJ, Vakharia A, et al. Guiding intracortical brain tumour cells to an extracortical cytotoxic hydrogel using aligned polymeric nanofibres. Nat Mater. 2014;13:308–16.

128. Seib FP, Berry JE, Shiozawa Y, Taichman RS, Kaplan DL. Tissue engineering a surrogate niche for metastatic cancer cells. Biomaterials. 2015;51:313–9.

129. De Vlieghere E, Gremonprez F, Verset L, Mariën L, Jones CJ, De Craene B, et al. Tumor-environment biomimetics delay peritoneal metastasis formation by deceiving and redirecting disseminated cancer cells. Biomaterials. 2015;54:148–57.

130. Azarin SM, Yi J, Gower RM, Aguado BA, Sullivan ME, Goodman AG, et al. In vivo capture and label-free detection of early metastatic cells. Nat Commun. 2015;6:8094.

131. De La Fuente A, Alonso-Alconada L, Costa C, Cueva J, Garcia-Caballero T, Lopez-Lopez R, et al. M-Trap: Exosome-Based Capture of Tumor Cells as a New Technology in Peritoneal Metastasis. J Natl Cancer Inst. 2015;107(9):1–10.

132. Giarra S, Ierano C, Biondi M, Napolitano M, Campani V, Pacelli R, et al. Engineering of thermoresponsive gels as a fake metastatic niche. Carbohydr Polym. 2018;191(March):112–8.

133. Haji Mansor M, Najberg M, Contini A, Alvarez-Lorenzo C, Garcion E, Jérôme C, et al. Development of a Non-toxic and Non-denaturing Formulation Process for Encapsulation of SDF-1α into PLGA/PEG-PLGA Nanoparticles to Achieve Sustained Release. Eur J Pharm Biopharm. 2018;125(November 2017):38–50.

134. Yoon HJ, Kim TH, Zhang Z, Azizi E, Pham TM, Paoletti C, et al. Sensitive capture of circulating tumour cells by functionalized graphene oxide nanosheets. Nat Nanotechnol. 2013;8(10):735–41.

135. CELLSEARCH Circulating Tumor Cell, (2019), https://www.cellsearchctc.com/ (accessed May 25, 2019) [Internet]. 2019 [cited 2019 May 25].

136. Chen W, Allen SG, Reka AK, Qian W, Han S, Zhao J, et al. Nanoroughened adhesion-based capture of circulating tumor cells with heterogeneous expression and metastatic characteristics. BMC

Cancer. 2016;16(1):614.

137. Taphoorn MJB, Dirven L, Kanner AA, Lavy-Shahaf G, Weinberg U, Taillibert S, et al. Influence of treatment with tumor-treating fields on health-related quality of life of patients with newly diagnosed glioblastoma a secondary analysis of a randomized clinical trial. JAMA Oncol. 2018;4(4):495–504.

138. Giladi M, Schneiderman RS, Voloshin T, Porat Y, Munster M, Blat R, et al. Mitotic Spindle Disruption by Alternating Electric Fields Leads to Improper Chromosome Segregation and Mitotic Catastrophe in Cancer Cells. Sci Rep. 2015;5(December):1–16.

139. Stupp R, Taillibert S, Kanner A, Read W, Steinberg DM, Lhermitte B, et al. Effect of tumor-treating fields plus maintenance temozolomide vs maintenance temozolomide alone on survival in patients with glioblastoma a randomized clinical trial. JAMA - J Am Med Assoc. 2017;318(23):2306–16.

140. Fabian D, Eibl M del PGP, Alnahhas I, Sebastian N, Giglio P, Puduvalli V, et al. Treatment of glioblastoma (GBM) with the addition of tumor-treating fields (TTF): A review. Cancers (Basel). 2019;11(2):1–12.

141. Zhang H, Chen J. Current status and future directions of cancer immunotherapy. J Cancer. 2018;9(10):1773–81.

142. Feins S, Kong W, Williams EF, Milone MC, Fraietta JA. An introduction to chimeric antigen receptor (CAR) T-cell immunotherapy for human cancer. Am J Hematol. 2019;94(S1):S3–9.

143. FDA. FDA approval brings first gene therapy to the United States. 2017.

144. FDA. FDA approves CAR-T cell therapy to treat adults with certain types of large B-cell lymphoma. 2017.

145. Zheng PP, Kros JM, Li J. Approved CAR T cell therapies: ice bucket challenges on glaring safety risks and long-term impacts. Drug Discov Today. 2018;23(6):1175–82.

146. Sambi M, Bagheri L, Szewczuk MR. Current Challenges in Cancer Immunotherapy: Multimodal Approaches to Improve Efficacy and Patient Response Rates. J Oncol. 2019;2019:1–12.

147. Li Z, Song W, Rubinstein M, Liu D. Recent updates in cancer immunotherapy: A comprehensive review and perspective of the 2018 China Cancer Immunotherapy Workshop in Beijing. J Hematol Oncol. 2018;11(1):1–15.

148. Dougan M, Dranoff G, Dougan SK. Cancer Immunotherapy: Beyond Checkpoint Blockade. Annu Rev Cancer Biol. 2018;3(1):55–75.

149. van der Sanden B, Appaix F, Berger F, Selek L, Issartel J-P, Wion D. Translation of the ecological trap concept to glioma therapy: the cancer cell trap concept. Future Oncol. 2013;9(6):817–24.

150. Polyak K, Weinberg RA. Transitions between epithelial and mesenchymal states: acquisition of malignant and stem cell traits. Nat Rev Cancer. 2009;9(4):265–73.

151. Levental KR, Yu H, Kass L, Lakins JN, Egeblad M, Erler JT, et al. Matrix Crosslinking Forces Tumor Progression by Enhancing Integrin Signaling. Cell. 2009;139(5):891–906.

152. Wozniak MA, Desai R, Solski PA, Der CJ, Keely PJ. ROCK-generated contractility regulates breast epithelial cell differentiation in response to the physical properties of a three-dimensional collagen matrix. J Cell Biol. 2003;163(3):583–95.

153. Kumar S, Weaver VM. Mechanics, malignancy, and metastasis: The force journey of a tumor cell. Cancer Metastasis. 2009;28(1–2):113–27.

154. Paszek MJ, Zahir N, Johnson KR, Lakins JN, Rozenberg GI, Gefen A, et al. Tensional homeostasis and the malignant phenotype. Cancer Cell. 2005;8(3):241–54.

155. Wang C, Tong X, Yang F. Bioengineered 3D Brain Tumor Model To Elucidate the Effects of Matrix Stiffness on Glioblastoma Cell Behavior Using PEG-Based Hydrogels. Mol Pharm. 2014;11:2115–25.

156. Pulukuri S, Rao J. Martix matalloproteinase-1 promotes prostate tumor growth and metastasis. Int J. 2008;757–65.

157. Wu XY, Liu WT, Wu ZF, Chen C, Liu JY, Wu GN, et al. Identification of HRAS as cancer-promoting gene in gastric carcinoma cell aggressiveness. Am J Cancer Res. 2016;6(9):1935–48.

158. Liu X, Chen D, Liu G. Overexpression of RhoA promotes the proliferation and migration of cervical cancer cells. Biosci Biotechnol Biochem. 2014;78(11):1895–901.

159. Li D, Cao Y, Li J, Xu J, Liu Q, Sun X. MiR-506 suppresses neuroblastoma metastasis by targeting ROCK1. Oncol Lett. 2017;13(1):370–6.

160. Wolf K, Alexander S, Schacht V, Coussens LM, von Andrian UH, van Rheenen J, et al. Collagen-based cell migration models in vitro and in vivo. Semin Cell Dev Biol. 2009;20(8):931–41.

161. Wolf K, te Lindert M, Krause M, Alexander S, te Riet J, Willis AL, et al. Physical limits of cell migration: Control by ECM space and nuclear deformation and tuning by proteolysis and traction force. J Cell Biol. 2013;201(7):1069–84.

162. Paul CD, Mistriotis P, Konstantopoulos K. Cancer cell motility: lessons from migration in confined spaces. Nat Rev Cancer. 2017;17(2):131–40.

163. Provenzano PP, Inman DR, Eliceiri KW, Trier SM, Keely PJ. Contact Guidance Mediated Three-Dimensional Cell Migration is Regulated by Rho/ROCK-Dependent Matrix Reorganization. Biophys J. 2008;95(11):5374–84.

164. Provenzano PP, Eliceiri KW, Campbell JM, Inman DR, White JG, Keely PJ. Collagen reorganization at the tumor-stromal interface facilitates local invasion. BMC Med. 2006;4(1):38.

165. Aznavoorian S, Stracke ML, Krutzsch H, Schiffmann E, Liotta LA. Signal transduction for chemotaxis and haptotaxis by matrix molecules in tumor cells. J Cell Biol. 1990;110(4):1427–38.

166. Chiang SPH, Cabrera RM, Segall JE. Tumor cell intravasation. Am J Physiol - Cell Physiol. 2016;311(1):C1–14.

167. Wyckoff JB, Jones JG, Condeelis JS, Segall JE. A Critical Step in Metastasis : In Vivo Analysis of Intravasation at the Primary Tumor. Cancer Res. 2000;60:2504–11.

168. Wyckoff J, Wang W, Lin EY, Wang Y, Pixley F, Stanley ER, et al. A paracrine loop between tumor cells and macrophages is required for tumor cell migration in mammary tumors. 2004;64:7022–9.

169. Wong SY, Hynes RO. Lymphatic or Hematogenous Dissemination : Perspective How Does a Metastatic Tumor Cell Decide ? ND ES SC CE. Cell Cycle. 2006;5(8):812–7.

170. Nathanson SD. Insights into the mechanisms of lymph node metastasis. Cancer. 2003;98(2):413–23.

171. Wirtz D, Konstantopoulos K, Searson PCPPC. The physics of cancer: the role of physical interactions and mechanical forces in metastasis. Nat Rev Cancer. 2011;11(512):522.

172. Kienast Y, Von Baumgarten L, Fuhrmann M, Klinkert WEF, Goldbrunner R, Herms J, et al. Real-time imaging reveals the single steps of brain metastasis formation. Nat Med. 2010;16(1):116–22.

173. Zhu C, Yago T, Lou J, Zarnitsyna VI, McEver RP. Mechanisms for flow-enhanced cell adhesion. Ann Biomed Eng. 2008;36(4):1–18.

174. Hyun K-A, Koo G-B, Han H, Sohn J, Choi W, Kim S-I, et al. Epithelial-to-mesenchymal transition leads to loss of EpCAM and different physical properties in circulating tumor cells from metastatic breast cancer. Oncotarget. 2016;7(17):24677–87.

175. Fidler IJ. Metastasis: quantitative analysis of distribution and fate of tumour emboli labeled with 125I-5-iodo-2[prime]-deoxyuridine. J Natl Cancer Inst. 1970;45:773–82.

176. Paget S. The distribution of secondary growths in cancer of the breast. Lancet. 1889;133(3421):571–3.

177. Aguado BA, Bushnell GG, Rao SS, Jeruss JS, Shea LD. Engineering the pre-metastatic niche. Nat Biomed Eng. 2017;1(6):1–12.

178. Peinado H, Alečković M, Lavotshkin S, Matei I, Costa-Silva B, Moreno-Bueno G, et al. Melanoma exosomes educate bone marrow progenitor cells toward a pro-metastatic phenotype through MET. Nat Med. 2012;18(6):883–91.

179. Kaplan RN, Riba RD, Zacharoulis S, Bramley AH, Vincent L, Costa C, et al. VEGFR1-positive haematopoietic bone marrow progenitors initiate the pre-metastatic niche. Nature. 2005;438(7069):820–7.

180. Hiratsuka S, Watanabe A, Aburatani H, Maru Y. Tumour-mediated upregulation of chemoattractants and recruitment of myeloid cells predetermines lung metastasis. Nat Cell Biol. 2006;8(12):1369–75.

181. Brennecke P, Arlt MJE, Campanile C, Husmann K, Gvozdenovic A, Apuzzo T, et al. CXCR4 antibody treatment suppresses metastatic spread to the lung of intratibial human osteosarcoma xenografts in mice. Clin Exp Metastasis. 2014;31(3):339–49.

182. Darash-Yahana M, Gillespie JW, Hewitt SM, Chen YYK, Maeda S, Stein I, et al. The chemokine CXCL16 and its receptor, CXCR6, as markers and promoters of inflammation-associated cancers. PLoS One. 2009;4(8):e6695.

183. Weiss L. Comments on hematogenous metastatic patterns in humans as revealed by autopsy. Clin Exp Metastasis. 1992;10(3):191–9.

184. Taichman RS, Cooper C, Keller ET, Pienta KJ, Taichman NS, Mccauley LK. Use of the Stromal Cell-derived Factor-1 / CXCR4 Pathway in Prostate Cancer Metastasis to Bone. Cancer Res. 2002;62:1832–7.

185. Lee JT, Lee SD, Lee JZ, Chung MK, Ha HK. Expression analysis and clinical significance of CXCL16/CXCR6 in patients with bladder cancer. Oncol Lett. 2013;5(1):229–35.

186. Shiozawa Y, Havens AM, Jung Y, Ziegler AM, Pedersen EA, Wang J, et al. Annexin II/annexin II receptor axis regulates adhesion, migration, homing, and growth of prostate cancer. J Cell Biochem. 2008;105(2):370–80.

187. Shiozawa Y, Pedersen EA, Taichman RS. GAS6/Mer axis regulates the homing and survival of the E2A/PBX1-positive B-cell precursor acute lymphoblastic leukemia in the bone marrow niche. Exp Hematol. 2010;38(2):132–40.

188. Hill A, McFarlane S, Johnston PG, Waugh DJJ. The emerging role of CD44 in regulating skeletal micrometastasis. Cancer Lett. 2006;237(1):1–9.

189. Mishra A, Shiozawa Y, Pienta KJ, Taichman RS. Homing of cancer cells to the bone. Cancer Microenviron. 2011;4(3):221–35.

190. Bersani F, Lee J, Yu M, Morris R, Desai R, Ramaswamy S, et al. Bioengineered implantable scaffolds as a tool to study stromal-derived factors in metastatic cancer models. Cancer Res. 2014;74(24):7229–38.

191. Qian B-Z, Li J, Zhang H, Kitamura T, Zhang J, Campion LR, et al. CCL2 recruits inflammatory monocytes to facilitate breast-tumour metastasis. Nature. 2011;475(7355):222–5.

192. Qian B, Deng Y, Im JH, Muschel RJ, Zou Y, Li J, et al. A distinct macrophage population mediates metastatic breast cancer cell extravasation, establishment and growth. PLoS One. 2009;4(8):e6562.

193. Rao SS, Bushnell GG, Azarin SM, Spicer G, Aguado BA, Stoehr JR, et al. Enhanced survival with implantable scaffolds that capture metastatic breast cancer cells in vivo. Cancer Res. 2016;76(18):5209–18.

194. Pelaez F, Manuchehrabadi N, Roy P, Natesan H, Wang Y, Racila E, et al. Biomaterial scaffolds for non-invasive focal hyperthermia as a potential tool to ablate metastatic cancer cells. Biomaterials. 2018;166:27–37.

195. Skoge M, Wong E, Hamza B, Bae A, Martel J, Kataria R, et al. A worldwide competition to compare the speed and chemotactic accuracy of neutrophil-like cells. PLoS One. 2016;11(6):1–19.

196. Crump MP, Gong JH, Loetscher P, Rajarathnam K, Amara A, Arenzana-Seisdedos F, et al. Solution structure and basis for functional activity of stromal cell-derived factor-1; dissociation of CXCR4 activation from binding and inhibition of HIV-1. EMBO J. 1997;16(23):6996–7007.

197. Kajiyama H, Shibata K, Terauchi M, Ino K, Nawa A, Kikkawa F. Involvement of SDF-1alpha/CXCR4 axis in the enhanced peritoneal metastasis of epithelial ovarian carcinoma. Int J Cancer. 2008;122(1):91–

9.

198. Zhan Y, Zhang H, Liu R, Wang W, Qi J, Zhang Y. Eupolyphaga sinensis Walker Ethanol Extract Suppresses Cell Growth and Invasion in Human Breast Cancer Cells. Integr Cancer Ther. 2016;15(1):102–12.

199. Bachelder RE, Wendt MA, Mercurio AM. Vascular Endothelial Growth Factor Promotes Breast Carcinoma Invasion in an Autocrine Manner by Regulating the Chemokine Receptor CXCR4. Cancer Res. 2002;62(24):7203–6.

200. Barbero S, Bonavia R, Bajetto A, Porcile C, Pirani P, Ravetti JL, et al. Stromal cell-derived factor 1alpha stimulates human glioblastoma cell growth through the activation of both extracellular signal-regulated kinases 1/2 and Akt. Cancer Res. 2003;63(8):1969–74.

201. Kryczek I, Wei S, Keller E, Liu R, Zou W. Stroma-derived factor (SDF-1 / CXCL12) and human tumor pathogenesis. Am J Physiol - Cell Physiol. 2007;292(123):987–95.

202. Wang J, Lu Y, Wang J, Koch AE, Zhang J, Taichman RS. CXCR6 induces prostate cancer progression by the AKT/mammalian target of rapamycin signaling pathway. Cancer Res. 2008;68(24):10367–76.

203. Lu Y, Wang J, Xu Y, Koch AE, Cai Z, Chen X, et al. CXCL16 functions as a novel chemotactic factor for prostate cancer cells in vitro. Mol Cancer Res. 2008;6(4):546–54.

204. Zheng N, Chen J, Li T, Liu W, Liu J, Chen H, et al. Abortifacient metapristone (RU486 derivative) interrupts CXCL12/CXCR4 axis for ovarian metastatic chemoprevention. Mol Carcinog. 2017;56(8):1896–908.

205. Chittasupho C, Anuchapreeda S, Sarisuta N. CXCR4 targeted dendrimer for anti-cancer drug delivery and breast cancer cell migration inhibition. Eur J Pharm Biopharm. 2017;119:310–21.

206. Chen Q, Zhang M, Li Y, Xu D, Wang Y, Song A, et al. CXCR7 Mediates Neural Progenitor Cells Migration to CXCL12 Independent of CXCR4. Stem Cells. 2015;33:2574–85.

207. Addington CP, Heffernan JM, Millar-Haskell CS, Tucker EW, Sirianni RW, Stabenfeldt SE. Enhancing neural stem cell response to SDF-1alpha gradients through hyaluronic acid-laminin hydrogels. Biomaterials. 2015;72:11–9.

208. Schesny MK, Monaghan M, Bindermann AH, Freund D, Seifert M, Eble JA, et al. Preserved bioactivity and tunable release of a SDF1-GPVI bi-specific protein using photo-crosslinked PEGda hydrogels. Biomaterials. 2014;35(25):7180–7.

209. Shen Y, Abaci HE, Krupsi Y, Weng L, Burdick J a, Gerecht S. Hyaluronic acid hydrogel stiffness and oxygen tension affect cancer cell fate and endothelial sprouting. Biomater Sci. 2014;2:655–65.

210. Li W, Wang J, Ren J, Qu X. 3D graphene oxide-polymer hydrogel: Near-infrared light-triggered active scaffold for reversible cell capture and on-demand release. Adv Mater. 2013;25(46):6737–43.

211. Ding Y, Wang Y, Opoku-Damoah Y, Wang C, Shen L, Yin L, et al. Dual-functional bio-derived nanoparticulates for apoptotic antitumor therapy. Biomaterials. 2015;72:90–103.

212. Autier L, Clavreul A, Cacicedo ML, Franconi F, Sindji L, Rousseau A, et al. A new glioblastoma cell trap for implantation after surgical resection. Acta Biomater. 2018;84:268–79.

213. Andreas K, Sittinger M, Ringe J. Toward in situ tissue engineering: Chemokine-guided stem cell recruitment. Trends Biotechnol. 2014;32(9):483–92.

214. Goffart N, Kroonen J, Di Valentin E, Dedobbeleer M, Denne A, Martinive P, et al. Adult mouse subventricular zones stimulate glioblastoma stem cells specific invasion through CXCL12/CXCR4 signaling. Neuro Oncol. 2015;17(1):81–94.

215. Purcell BP, Elser JA, Mu A, Margulies KB, Burdick JA. Synergistic effects of SDF-1α chemokine and hyaluronic acid release from degradable hydrogels on directing bone marrow derived cell homing to the myocardium. Biomaterials. 2012;33(31):7849–57.

216. Zhu Y, Hoshi R, Chen S, Yi J, Duan C, Galiano RD, et al. Sustained release of stromal cell derived factor-1 from an antioxidant thermoresponsive hydrogel enhances dermal wound healing in diabetes. J Control Release. 2016;238:114–22.

217. Chen P, Tao J, Zhu S, Cai Y, Mao Q, Yu D, et al. Radially oriented collagen scaffold with SDF-1 promotes osteochondral repair by facilitating cell homing. Biomaterials. 2015;39:114–23.

218. Sun J, Mou C, Shi Q, Chen B, Hou X, Zhang W, et al. Controlled release of collagen-binding SDF-1α from the collagen scaffold promoted tendon regeneration in a rat Achilles tendon defect model. Biomaterials. 2018;162:22–33.

219. Hu Y, Ran J, Zheng Z, Jin Z, Chen X, Yin Z, et al. Exogenous stromal derived factor-1 releasing silk scaffold combined with intra-articular injection of progenitor cells promotes bone-ligament-bone regeneration. Acta Biomater. 2018;71:168–83.

220. Zhang B, Li H, He L, Han Z, Zhou T, Zhi W, et al. Surface-decorated hydroxyapatite scaffold with on-demand delivery of dexamethasone and stromal cell derived factor-1 for enhanced osteogenesis. Mater Sci Eng C. 2018;89(September 2017):355–70.

221. Rajabi S, Jalili-Firoozinezhad S, Ashtiani MK, Le Carrou G, Tajbakhsh S, Baharvand H. Effect of chemical immobilization of SDF-1α into muscle-derived scaffolds on angiogenesis and muscle progenitor recruitment. J Tissue Eng Regen Med. 2018;12(1):e438–50.

222. Ritz U, Gerke R, Götz H, Stein S, Rommens PM. A new bone substitute developed from 3D-prints of polylactide (PLA) loaded with collagen i: An in vitro study. Int J Mol Sci. 2017;18(12).

223. Wang Y, Sun X, Lv J, Zeng L, Wei X, Wei L. Stromal Cell-Derived Factor-1 Accelerates Cartilage Defect Repairing by Recruiting Bone Marrow Mesenchymal Stem Cells and Promoting Chondrogenic Differentiation <sup/>. Tissue Eng Part A. 2017;23(19–20):1160–8.

224. Ji W, Yang F, Ma J, Bouma MJ, Boerman OC, Chen Z, et al. Incorporation of stromal cell-derived factor-1α in PCL/gelatin electrospun membranes for guided bone regeneration. Biomaterials. 2013;34(3):735–45.

225. Prokoph S, Chavakis E, Levental KR, Zieris A, Freudenberg U, Dimmeler S, et al. Sustained delivery of SDF-1alpha from heparin-based hydrogels to attract circulating pro-angiogenic cells. Biomaterials. 2012;33(19):4792–800.

226. Krieger JR, Ogle ME, McFaline-Figueroa J, Segar CE, Temenoff JS, Botchwey EA. Spatially localized recruitment of anti-inflammatory monocytes by SDF-1α-releasing hydrogels enhances microvascular network remodeling. Biomaterials. 2016;77:280–90.

227. Baumann P, Balasubramanian V, Onaca-Fischer O, Sienkiewicz A, Palivan CG. Light-responsive polymer nanoreactors: a source of reactive oxygen species on demand. Nanoscale. 2013 Jan 7 [cited 2014 Sep 11];5(1):217–24.

228. Shafiq M, Kong D, Kim SH. SDF-1α peptide tethered polyester facilitates tissue repair by endogenous cell mobilization and recruitment. J Biomed Mater Res - Part A. 2017;105(10):2670–84.

229. Lee KW, Johnson NR, Gao J, Wang Y. Human progenitor cell recruitment via SDF-1α coacervate-laden PGS vascular grafts. Biomaterials. 2013;34(38):9877–85.

230. Yu J, Wang A, Tang Z, Henry J, Li-Ping Lee B, Zhu Y, et al. The effect of stromal cell-derived factor-1α/heparin coating of biodegradable vascular grafts on the recruitment of both endothelial and smooth muscle progenitor cells for accelerated regeneration. Biomaterials. 2012;33(32):8062–74.

231. Xu C, Xu J, Xiao L, Li Z, Xiao Y, Dargusch M, et al. Double-layered microsphere based dual growth factor delivery system for guided bone regeneration. RSC Adv. 2018;8(30):16503–12.

232. Mi L, Liu H, Gao Y, Miao H, Ruan J. Injectable nanoparticles/hydrogels composite as sustained release system with stromal cell-derived factor-1α for calvarial bone regeneration. Int J Biol Macromol. 2017;101:341–7.

233. Chen FM, Lu H, Wu LA, Gao LN, An Y, Zhang J. Surface-engineering of glycidyl methacrylated dextran/gelatin microcapsules with thermo-responsive poly(N-isopropylacrylamide) gates for controlled delivery of stromal cell-derived factor-1α. Biomaterials. 2013;34(27):6515–27.

234. Zamani M, Prabhakaran MP, Thian ES, Ramakrishna S. Controlled delivery of stromal derived factor-1α from poly lactic-co-glycolic acid core-shell particles to recruit mesenchymal stem cells for cardiac regeneration. J Colloid Interface Sci. 2015;451:144–52.

235. Teicher BA, Fricker SP. CXCL12 (SDF-1)/CXCR4 pathway in cancer. Clin Cancer Res. 2010;16(11):2927–31.

236. Lyon JG, Mokarram N, Saxena T, Carroll SL, Bellamkonda R V. Engineering challenges for brain tumor immunotherapy. Adv Drug Deliv Rev. 2017;114:19–32.

237. Komarova NL. Cancer: A moving target. Nature. 2015;525:198–9.

CHAPTER II: Development of freeze-dried sponges

Table of content

CHAPITRE II

Development of freeze-dried sponges

1. Introduction

The first step of the project was to design an ideal scaffold to trap tumour cells. SDF-1α is a chemokine that plays a key role in the recruitment of cells expressing the CXCR4 surface receptor. SDF-1α has drawn attention in various areas of study such as cancer metastasis, immune modulation and trafficking of stem cells. However SDF-1α bolus administration in the brain leads to poor results in the long term because of its rapid elimination (1). Encapsulating this chemokine in nanoparticles or immobilising it in scaffolds may prevent premature degradation and may provide sustained release for GBM cells. Moreover, to increase the efficacy of a scaffold, the construct has to be carefully tailored to the specific target tissue, here, the brain. SDF-1α is extensively studied for regenerative applications for its ability to attract stem cells. In particular, SDF-1α has been pointed out as a potent candidate to improve outcomes in brain injuries due to its well-described involvement in neural progenitor/stem-cells homing (2,3). The applications from cancer cell trap to regenerative medicine are substantially different but it is possible to learn from this field to design a tumour trap. To do so, two main features need to be considered: (i) the choice of the architecture and (ii) the choice of polymers.

Various architectures can be considered such as micro- or nanofibers, micro- or nanoparticles, 3D printed scaffolds, sponges and hydrogels. They all have their pros and cons in terms of injectability, biomimicry or processing. The architecture and physico-chemical properties of the scaffolds should closely mimic those of the targeted tissue. The brain is made up of 80% water and has a Young's modulus of less than 1 kPa (4–6). Soft hydrogels are good candidates to mimic these features. The scaffold should also be decorated with pores that are small enough to support 3D cell-cell contacts and large enough to allow good diffusion of nutrients, oxygen and bioactive factors. Indeed, we hypothesised that the scaffold should be an attractive environment for tumour cells in order to avoid them to escape the trap before their elimination. Pore sizes between 20 and 160 µm have been identified as adequate for regenerative medicine (7) and we hypothesised that it will be beneficial for the trapping of tumour cells as well. In this context, freeze-dried sponges that can turn to porous hydrogels once hydrated are promising.

Polymers should be chosen carefully for their physico-chemical properties, availability but also for their biocompatibility and processability. Natural polymers were chosen because of their biomimicry abilities.

Hyaluronic acid (HA) is an unbranched polysaccharide in the family of the glycosaminoglycans. It is constituted by a linear chain containing repeating disaccharide units of *N*-acetyl-D-glucosamine and D-glucuronic acid linked by β-1,4-glycosidic bonds (Figure 2. 1-A) (8). At physiological pH, each carboxyl group are deprotonated, HA is therefore negatively charged and highly hydrophilic. HA can reach a very high molecular weight of 10^8 Da while other glycosaminoglycans reach up to 10^4 Da (9). The first pharmaceutical-grade HA was produced from rooster combs and human umbilical cords by Balazs *et al.* in 1979 (10). HA is used since the early 1980s for implantable intraocular lenses, becoming a major product in ophthalmology for its safety and protective effect on corneal endothelium (11–13). HA is also used for the treatment of joint (14,15), skin disease (16), wound healing (17,18) and for plastic surgery (19,20). Moreover, HA is used in drug delivery systems (21–24). HA is one of the main constituents of the brain ECM (25) and is known to enhance cell mobility and invasion by interacting with the CD44 receptor as well as the CD168 receptor (26). The main concern with HA as a scaffold is its quick degradation *in vivo.* It is caused by two mechanisms: the first one is mediated by enzymes (hyaluronidases) and the second by oxidative damage due to reactive oxygen species (27). because of the hyaluronidase. The rate of degradation is dependent on the location, the size of the polymer chains and on its reticulation if it is crosslinked. It has been estimated that the half-life of HA in the skin is about 24h, in the eye about 30h, in the cartilage 1-3 weeks and in the vitreous about 70 days (28). Crosslinking of HA reduces its degradation rate *in vivo* and covalent crosslinking leads to the stronger mechanical properties (29). N-(3-dimethylaminopropyl)-N′-ethylcarbodiimide hydrochloride (EDC) and N-hydroxysulfosuccinimide sodium salt (NHS) can be used to activate the carboxyl groups of HA in order to react with a primary amine (30) (Figure 2. 1-C). This reaction can be performed in water and the by-products be washed away with water as well. In order to crosslink HA with this reaction, a reactant with at least two amine groups need to be used. Poly-L-lysine (PLL) (Figure 2. 1-B) was therefore chosen as it is also known to facilitate cellular adhesion via electrostatic interactions and may improve HA performance in this regard (31).

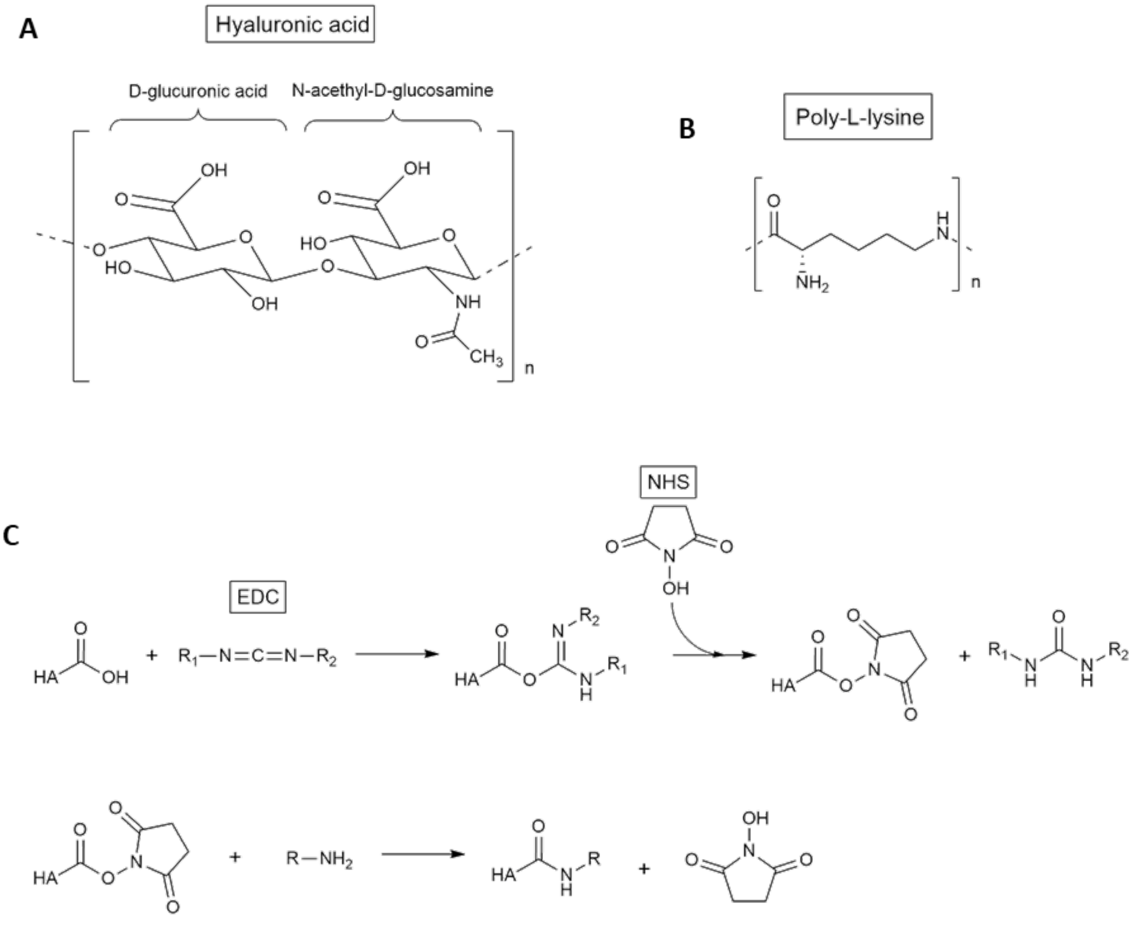

Figure 2. 1: Chemical structure of HA (A) and PLL (B). Crosslinking mechanism between the carboxyl of HA and the primary amine of another polymer such as PLL (C).

Silk is popularly known in the textile industry and can be produced by worms like *Bombyx mori* but also by spiders and butterflies. Silk fibres from *Bombyx mori* have been used for centuries as suture material and is still today the most common natural suture (32).

Variations in amino acid sequence exists between silks of different species, leading to structural and physical property differences. *Bombyx mori* silk is the most used and accessible and we will therefore only talk about this type. Silk fibres are constituted of silk fibroin (SF) coated with a glue-like protein called sericin. The raw silk fibre mass is composed of about 20–30% sericin and 70–80% SF (33). Since sericin causes inflammatory responses and prevent fibres to solubilise, it is necessary to undergo a degumming procedure to eliminate the sericin. It is typically done by boiling the cocoons of the worms in a sodium carbonate aqueous solution. SF is a protein composed of a heavy protein chain (~390 kDa) and a light protein chain (~25 kDa) which are connected by disulphide links (34). The primary amino acid sequence is composed of a repetition of Gly-X where X is typically alanine, sericin or tyrosine and the Gly-X motif exists in repeating hexamer units of GAGAGS, GAGAGY, GAGAGA or GAGYGA (35). The SF contains 12 domains with these repeating hexamer units separated by 11 short linker sequences composed of asparagine, aspartic acid, glutamic acid, lysine, phenylalanine, proline, threonine and tryptophan (composition of SF is shown in Table 2. 1). Carboxyl moieties as well as primary amines can be found on the backbone of SF on aspartic acid and glutamic acid, and arginine and lysine respectively. SF exists in different states such as the glandular state (silk I) which is mainly composed of random coil, the spun silk state found in the cocoons (silk II) with β-sheets secondary structure, and an air/water assembled interfacial silk (silk III), with a helical structure (36,37). The silk I structure is water soluble and is converted into silk II upon exposure to heat, physical spinning as well as changes in pH or exposure to organic solvents such as ethanol or methanol. The silk II structure is composed of asymmetrical β-sheet structures that are arranged so that strong hydrogen bonds as well as van der Waals forces generate a thermodynamically stable crystalline structure. It is insoluble in water as well as several solvents such as mild acids and alkaline conditions as well as chaotropes (molecules that can disrupt the hydrogen bonding network) like urea. SF has started to be used in biomaterials thanks to the discovery of a process using salts to obtain silk I, soluble in water, from the insoluble silk II of the cocoons. Lithium bromide (LiBr) is the most frequently used salt for dissolution of the silk fibroin and it was shown that a concentration of around 9 M lead to a degradation of the SF crystallites (38). Once in aqueous solution, SF can be processed to obtain hydrogels, sponges, films or nanofibers as well as nanoparticles via organic solvent-free processes (39). In order to enhance mechanical properties of the material produced with SF, it is possible to induce the formation of β-sheets with a process called annealing. Different technics can be used, leading to different β-sheet levels. Dipping in methanol is the most efficient method and lead to the formation of about 50% β-sheets for short term treatment and up to 56% for 4 days of treatment (40). Annealing with water vapours with increasing temperatures lead to an increasing formation of β-sheets (~14% at 4°C for 12h and ~60% at 90°C for 12h) (41). Annealing with vapours of ethanol for 2h lead to the formation of about 30% β-sheets (42). SF is known for its processability, biocompatibility, relatively slow degradability and low immunogenicity, it is therefore an interesting material for biomedical applications (37,43,44). Safety of SF hydrogels implanted into the mouse brain was shown by Fernández-García *et al.* (45). Previous studies revealed that sponges combining SF and HA have a higher stability than HA solely scaffolds and support the adhesion of cells to a greater extent than scaffolds made of either of the two polymers alone (46,47).

Table 2. 1: Composition of SF in amino acid

Amino acid	Residue (%)	Amino acid	Residue (%)
Glycine	44.7	Threonine	1.0
Alanine	25.7	Isoleucine	0.6
Serine	11.9	Leucine	0.5
Tyrosine	5.4	Proline	0.5
Valine	2.4	Arginine	0.5
Aspartic acid	1.6	Lysine	0.4
Phenylalanine	1.6	Histidine	0.2
Glutamic acid	1.1		

Heparin (hep) and heparan sulfate (HS) are glycosaminoglycans with various structures alternating 1→4-linked α-D-glucosamine (GlcN) and either β-D-glucuronic acid (GlcA) and α-L-iduronic acid (IdoA) (Figure 2. 2) (48). Moreover, sulfations may occur at C3 and C6 of GlcN and at C2 of the uronic acid. GlcN amine may be sulfonated, acetylated or unsubstituted. Therefore, 48 different disaccharides can be found in the HS chain. Hep is similar to HS and carry the same disaccharide variations but is more homogeneous with N-sulfonated and 6-O-sulfonated GlcN and 2-O-sulfonated IdoA occupying most of the chain (49). Hep is another component of the ECM present in the brain and is expressed in connective-tissue type mast cells while HS are expressed and secreted by most mammalian cells. Hep has various properties such as anticoagulant (50), release of lipoprotein lipase and hepatic lipase (51), inhibition of complement activation (52,53) and inhibition of angiogenesis and tumour growth (54–56). Moreover, it is known to strongly bind chemokines and its incorporation in a scaffold has been shown to facilitate the loading of SDF-1α (57–59). A gradient of SDF-1α is required to enable recruitment of cells expressing the CXCR4 receptor (60–64). Dutta *et al.* (1) investigated further the effect of SDF-1α presentation on the *in vivo* brain response. They showed that exogenous SDF-1α encapsulated in PLGA nanoparticles was mostly confined within 400 µm from the injection point but led to the production of endogenous SDF-1α in regions as far as 1200 µm from the site of administration. The spatiotemporal presentation of exogenous SDF-1α was a key factor in sustaining this behaviour. Therefore, we hypothesised that a scaffold that can highly retain SDF-1α may be useful to induce long-term production of endogenous SDF-1α and consecutively lead to an improved attraction of GBM infiltrative cells.

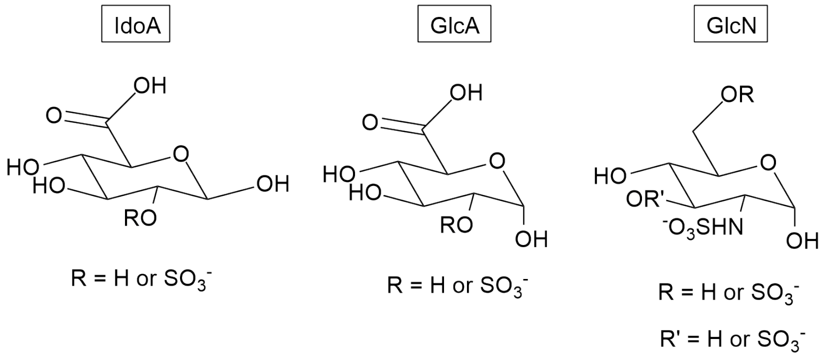

Figure 2. 2: HS and hep units.

In this study, sponges were designed to combine HA, SF and hep, each component playing a specific role. HA was chosen to improve cellular infiltration into the scaffold, SF was intended to function as the main structural component, and hep was included to increase the affinity of the scaffold to the protein of interest, SDF-1α, and protect it from premature brain clearance. Sponges with different compositions were produced from aqueous solutions by crosslinking the polymers with EDC and NHS followed by freeze-drying. First, optimisation of the crosslinking process was investigated as well as the annealing and the production of SF-HA and SF-HA-hep sponges. Then, miscibility conditions were investigated since SF may undergo phase separation in hydrophilic polymers dispersions (65). The composition was optimized to mimic the brain characteristics to the closest extent possible. Sponges architecture and physico-chemical characteristics (porosity, degradation, water uptake and stiffness) were therefore measured and SDF-1α release profile was studied.

2. Material and method

2.1. Materials

HA with a molecular weight of 200-400 kDa was purchased from Guinama (Valencia, Spain). PLL with a molecular weight of 150-300 kDa at 0.1 % (w/v) in H_2O was purchased from Sigma-Aldrich (St Louis, MO, USA). Heparin sodium salt from porcine intestinal mucosa with a molecular weight of 15,000 ± 2,000 Da was purchased from Calbiochem (Billerca MA, USA).

Hepes, bovine serum albumin (BSA), resazurin, hyaluronidase from bovine testes type I-S, heparinase I and III blend from *Flavobacterium heparinum* and sodium chloride were purchased from Sigma-Aldrich (St Louis, MO, USA). N-(3-dimethylaminopropyl)-N'-ethylcarbodiimide hydrochloride (EDC) and N-hydroxysulfosuccinimide sodium salt (NHS) were from Acros Organics (New Jersey, USA). Human SDF-1α was purchased from Miltenyi Biotec (Paris, France). Human SDF-1α labelled with AlexaFluor647 (AF-SDF-1α) was purchased from Almac Sciences (Craigavon, Northern Ireland).

2.2. Silk fibroin solution preparation

Solution of SF in water was produced by IMIDA (Murcia, Spain) under GMP conditions. Briefly, cocoons of the silkworms *Bombyx mori* (reared in IMIDA, Murcia, Spain) were chopped into 4 pieces then boiled in a 0.02 M Na_2CO_3 aqueous solution for 30 minutes to eliminate the sericin protein. Fibres were rinsed 3 times in distilled water and dried at RT for 3 days. They were dissolved in a 9.3 M LiBr solution for 3h at 60°C to generate a 20% (w/v) solution which was then dialysed against distilled water for 3 days at 4°C (Snakeskin Dialysis Tubing 3.5 KDa MWCO, Thermo Scientific). The obtained 8% (w/v) SF solution in water was stored at 4°C for less than 1 month.

2.3. Silk fibroin characterization by SDS-poly(acrylamide) gel electrophoresis (SDS-PAGE)

A SF stock solution at 10 mg/mL was prepared in water and diluted in 5x Laemmlie buffer (90 mmol of 0.5M Tris-HCl, pH 6.8, 20 % glycerol, 4 % SDS, 0.004 % bromphenol blue and 10 % β-mercaptoethanol) to obtain a final concentration of 6.25 µg/µL and boiled at 95°C for 5 min. An aliquot (10 µl) was added into the wells of the SDS gel. Electrophoresis was performed using a 4-20% gradient mini-protean TGX precast gel (Bio Rad). HiMark Pre-stained protein standards (Thermo Fisher) served as molecular weight marker. Electrophoresis was performed for 30 min at 70 V followed by a run at 110 V for 115 min with a Bio Rad Mini-PROTEAN® Tetra Vertical Electrophoresis Cell. After electrophoresis, the gel was stained with solution 1 % (w/v) Coomassie Brilliant Blue R- 250, 10 % (v/v) acetic acid, 40 % (v/v) methanol and distilled water over night, and then distained with 10 % (v/v) acetic acid, 40 % (v/v) methanol and distilled water for 5h.

2.4. Preparation of sponges and films

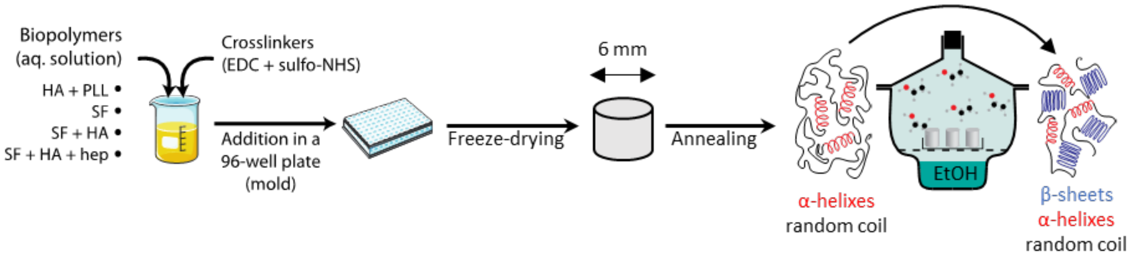

Figure 2. 3: Scheme describing the preparation of sponges by the freeze-drying method.

2.4.1 Optimisation of the HA-PLL sponge preparation

HA was dissolved in Hepes buffer ($C_{Hepes} = 20.10^{-3}$ M, $C_{NaCl} = 0.15$ M, pH = 7.4) to obtain a final concentration of 4% (w/v). A solution of HA 4% (w/v) and PLL 0.01% (w/v) was prepared by diluting 10 times PLL 0.1% (w/v) in the prepared HA solution in Hepes. Then, different quantities of crosslinking agents were added to obtain final concentrations of 0.5 mg/mL EDC and 0.18 mg/mL NHS (HA-PLL_{XL1}), 5 mg/mL EDC and 1.8 mg/mL NHS (HA-PLL_{XL2}), 30 mg/mL EDC and 11 mg/mL NHS (HA-PLL_{XL3}), 120 mg/mL EDC and 44 mg/mL NHS (HA-PLL_{XL4}) or nothing (HA-PLL_{XL0}). The solutions were poured immediately in a 96-well plate, covered, and allowed to crosslink 15h at 4°C. The gels were then frozen at -

20°C for 24h and freeze-dried in a Telstar® LyoQuest at -70°C and 0.01 mBar overnight. After freeze-drying, sponges were removed from the wells and stored in a desiccator with silica gel.

2.4.2 Optimisation of the SF sponge preparation

SF sponges were prepared by adding the SF into the wells of a 96-well plate. Solutions were frozen at -20°C for 24h and freeze-dried in a Telstar® LyoQuest at -70°C and 0.01 mBar overnight. After freeze-drying, sponges were removed from the wells and stored in a desiccator. Two annealing processes were tested: water and ethanol annealing as described respectively by Hu *et al.* (41) and Fan *et al.* (42). Water annealing consisted in putting the samples for 12h in a desiccator under vacuum with distilled water at the bottom at RT to create a highly humid atmosphere. For EtOH annealing, EtOH 70 % (v/v) in water was used instead of water and the desiccator was kept at atmospheric pressure, the samples were kept their 2h in that case.

Crosslinked SF sponges were also prepared by mixing the SF solution with EDC (final concentration of 5 mg/mL) and NHS (final concentration of 1.8 mg/mL). The solution is then added to a 96-well plate and SF is allowed to crosslink at 4°C for 24h before freeze drying in the same conditions than explained in section 2.4.1.

2.4.3 Film preparation

Dispersions of HA 4 % (w/v), SF 4 % (w/v) or SF 4 % (w/v) with HA 2 % (w/v) in hepes buffer (C_{Hepes} = 20.10^{-3} M, C_{NaCl} = 0.15 M, pH = 7.4) were prepared under magnetic stirring either 15 min, 2h or 15h. Films were prepared by pouring the dispersions in petri dishes and left to dry 24h at RT.

2.4.4 Optimisation of SF-HA and SF-HA-hep preparation

SF-HA sponges were prepared by mixing the SF 8 % (w/v) solution gently for 5h with an equivalent volume of HA 4 % (w/v) solution in Hepes buffer. For SF-HA-hep sponge, heparin sodium salt (C_f = 1 % (w/v)) was also added. SF-HA solutions were either directly poured in the 96-well plate and freeze-dried (SF-HA) or firstly crosslinked with EDC (final concentration of 5 mg/mL) and NHS (final concentration of 1.8 mg/mL) (SF-HA_{XL}). The sponges were then either annealed with ethanol (SF-HA(EtOH) and SF-HA$_{XL}$(EtOH)) as explained in section 2.4.2 or not annealed (SF-HA and SF-HA$_{XL}$).

SF-HA-hep sponges were either crosslinked with 5 mg/mL EDC and 1.8 mg/mL NHS (SF-HA-hep$_{XL}$(-)) or with 15 mg/mL EDC and 5.5 mg/mL NHS (SF-HA-hep$_{XL}$(+)).

2.5. Physico-chemical characterisation

2.5.5 Porosity evaluation

The porosity (P) of the dry sponges was calculated from Eq.1 and Eq.2, assuming that the polymer density was equal to 1. The thickness and diameter of the dry sponges were measured in triplicate using a digital caliper.

$$Sponge\ density\ (g.cm^{-3}) = \frac{Sponge\ mass\ (mg)}{Sponge\ volume\ (mm^3)} \qquad \text{Eq.1}$$

$$P\ (\%) = \left(1 - \frac{Sponge\ density\ (g.cm^{-3})}{Polymer\ density\ (g.cm^{-3})}\right) \times 100 \qquad \text{Eq.2}$$

2.5.6 Water uptake

The capability of the sponges to uptake water was evaluated, in triplicate, after immersion at RT in 3 ml of NaCl 0.9% (w/v). The sponges were withdrawn using tweezers, gently treated with blotting paper for 10s to remove the unabsorbed excess of medium, and weighed. The sponges were immediately returned to the corresponding vial and the weight measurements repeated until the hydration equilibrium was reached. For each composition, three sponges were measured. Water uptake was calculated as follows.

$$Water\ uptake\ (\%) = \frac{Hydrated\ sponge\ mass\ (mg) - Dry\ sponge\ mass\ (mg)}{Hydrated\ sponge\ mass\ (mg)} \times 100 \qquad \text{Eq.3}$$

2.5.7 Degradation

In vitro degradation of sponges was monitored in PBS with enzymes (0.3 mg/mL hyaluronidase (66) and 0.1 U/mL heparinase) at 37°C for 7 and 21 days. Sponges were cut to have similar sizes (about 6 mm diameter and 3 mm height) and weighed. After 7 or 21 days in 3 mL medium, the sponges were washed with milliQ water, snapped frozen in liquid nitrogen and then freeze-dried. Sponges degradation was calculated as percent of mass loss compared to original sponge mass (Eq.5). Degradation was measured on three sponges for each condition.

$$Degradation\ (\%) = \frac{Original\ sponge\ mass\ (mg) - degraded\ sponge\ mass\ (mg)}{Original\ sponge\ mass\ (mg)} \times 100 \qquad \text{Eq.5}$$

2.5.8 Scanning electron microscopy (SEM)

Sponge morphology was observed by scanning electron microscopy (SEM) with a SEM Evo LS15 (Zeiss, USA). Sponges were firstly hydrated in NaCl 0.9% (w/v) aqueous solution then, either directly or after 7 days at 37°C, snapped frozen in liquid nitrogen. To observe the interior morphology, sponges were cut transversely. Pores diameter were measured using ImageJ 1.50 software, at least 95 pores were measured per sponge.

2.5.9 Young's modulus measurement

Hydrated sponges were cut to obtain cylinders with a thickness of about 3 mm. The sponges were placed on the platform of a texture analyser (TA.TX Plus, Texture Technologies, USA) and compressed using a 2 cm cylinder probe. The sponges were compressed downward up to 1.5 mm with a speed of 1 mm/s. Each sponge was compressed 5 times with a sufficient time between each compression to allow elastic recovery of the shape whenever possible. The force needed to compress each sample was recorded over time. Three hydrated sponges were analysed for each composition. The Young's modulus was determined from the slope of the curve obtained by plotting the force (F) needed to compress the object divided by the cross-sectional area of the sponge (S) against the deformation of the sponge (ΔL) divided by the initial length of the sponge (L) as follows described by Eq.4 (Figure 2. 4) (67).

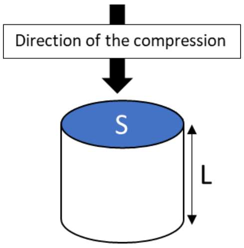

Figure 2. 4: The Young's modulus is calculated as the force (F) needed for a given surface (S) to deform a given length (L) of an object.

$$E\ (MPa) = \frac{F\ (N)/S\ (mm^2)}{\Delta L\ (mm)/L\ (mm)} \qquad \text{Eq.4}$$

2.5.10 Resolution of the internal structure of the sponges by fluorescence microscopy

Sponges were frozen in liquid nitrogen and immobilized in Tissue-Tek® (Sakura, USA). Cross sections with 30 µm thickness were obtained using a cryostat® (Leica CM3050 S Research Cryostat, Leica Biosystems Nussloch GmbH, Germany). Sections were placed on Starfrost® slides coated with gelatin and chrome alum. Sections were incubated 5 min with ActinRed (ThermoFisher) and the lamella mounted on the sections with fluorescence mounting medium (Dako, Agilent Technologies, USA). Finally, the slide was observed under a fluorescence microscope (Carl Zeiss Axioskop 2 MOT, Germany) with a rhodamine filter and pictures were taken with the same exposition time of 58 ms between slides.

2.5.11 FTIR analysis

Attenuated total reflection Fourier transformed infra-red (ATR-FTIR) analysis of sponges was performed with a Gladi-ATR equipped with a diamond crystal (Pike, Madison, WI, USA). For each measurement, 64 scans were recorded with a resolution of 4 cm^{-1}, and the wavelength ranged from 400 to 4000 cm^{-1}. The increase in crystallinity of SF sponges after ethanol annealing was evaluated by calculating the percentage of β-sheets applying the method described by Hu *et al.* (40). Briefly, Fourier self-deconvolution (FSD) of the IR spectra covering the amide I region (1595-1705 cm^{-1}) was performed using Opus 7.8 software (noise reduction factor of 0.3 and bandwidth of 2.5) followed by a curve fitting on this region. Peaks at 1616-1621, 1622-1627, 1628-1637, and 1697-1703 corresponded to β-sheets (40).

2.6. Analysis of SDF-1α uptake and release

2.6.12 Analysis of the distribution of SDF-1 in the sponges

SF-HA and SF-HA-hep sponges were hydrated in PBS and cut to obtain cylinders of 2 mm height and 3 mm diameter. Excess of PBS was removed of the sponges with Nunc paper. A drop of 3 µL of AF-SDF-1α (300 ng in PBS) was added on top of the sponges. To allow for interactions between the sponges and the SDF-1α, sponges were then incubated 1h at 4°C. A map of the fluorescence of the sponges (λ_{ex} = 625 nm; λ_{em} = 680 nm) was performed with a spectrophotometer (CLARIOstar®plus, BMG Labtech, Orthenberg, Germany). Each point was measured 500 µm apart.

2.6.13 Quantitative analysis of SDF-1α release by ELISA

SF-HA and SF-HA-hep sponges were hydrated in PBS and cut to obtain cylinders of 2 mm height and 3 mm diameter. Excess of PBS was removed of the sponges with Nunc paper. Then, the sponges were placed in Eppendorf tubes coated beforehand with Sigmacote® (Sigma-Aldrich, USA) in order to avoid non-specific adsorption of SDF-1α on the tubes. A drop of 3 µL of SDF-1α (300 ng in PBS) was added on top of the sponges then incubated at 4°C overnight. PBS (500 µL) with 0.1% BSA and enzymes (0.3 mg/mL hyaluronidase and 0.1 U/mL heparinase) was added in each tube and incubated at 37°C. The PBS was collected at defined time points (1h, 8h, 1d, 2d, 3d and 7d) and an equal volume of fresh medium was added back to the sponges. All solutions were collected and frozen at -20°C until they were assayed in duplicate using an ELISA kit (R&D Systems, Lille, France) in accordance with the manufacturer's instructions. This experiment was performed in triplicate.

2.7. Statistical analysis

The data were statistically analysed using an ANOVA test with Prism 7 software. In all statistical comparisons $p < 0.05$ was considered statistically significant.

3. Results and discussion

3.1. Silk fibroin characterisation

SF is composed of heavy molecular weight chains (H-chains) and light molecular weight chains (L-chains). In the gland of *Bombix mori*, the molecular weight of the H-chain is about 370 kDa and the L-chain is about 25 kDa (34). Depending on the process used to obtain the silk fibroin solution, the fibroin can be more or less degraded, which may have an impact on the properties of the materials produced (68). The molecular weight profile of the SF supplied by IMIDA (8% (w/v), stored at 4°C) was evaluated by means of SDS-PAGE with a 4-20% gradient gel (Figure 2. 5). The L-chain at 25 kDa was clearly observed.

The H-chain was recorded between 238 kDa and 460 kDa. Thus, the process used to produce the SF solution was able to retain the integrity of the protein.

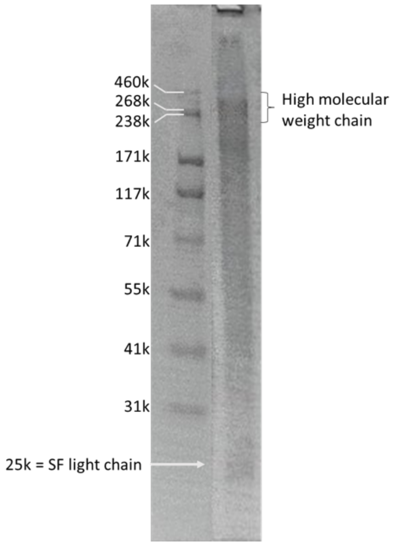

Figure 2. 5: Molecular weight analysis of the SF solution by SDS-PAGE showing the expected difference in electrophoretic mobility between the high molecular weight protein and the low molecular weight protein.

3.2. Crosslinking optimisation of HA-PLL sponges

HA-PLL sponges with 2% (w/v) HA and 0.01% (w/v) PLL were prepared with different concentrations of crosslinking agents (EDC and NHS) to determine which one is best. A sponge with a mixture of HA and PLL was produced instead of HA alone since the reaction with EDC and NHS is performed between a carboxylate and a primary amine (69). Carboxylate moieties are present on the HA chains but not the amine groups. Therefore, this crosslinking reaction does not proceed well for HA solely. PLL has been chosen since it is known to facilitate cellular adhesion via electrostatic interactions and may improve HA performance in this regard (31). Polymers were crosslinked for 15h and then freeze-dried. The porosity, water uptake, and texture were evaluated in order to determine the best formulation. First of all, after freeze-drying, the sponges were visually different (Figure 2. 6-A). Sponges with less than 5 mg/mL EDC and 1.8 mg/mL NHS (HA-PLL$_{XL0-1}$) disintegrated in a few minutes when immersed in NaCl 0.9% (w/v) aq. solution, it was therefore impossible to measure the water uptake for these two sponges. Above 5 mg/mL EDC and 1.8 mg/mL NHS (HA-PPL$_{XL3-4}$) the sponges did not retain the shape of the well after freeze-drying in the contrary of HA-PLL$_{XL2}$. This difference was also observed with the porosity, which decreased as the amount of crosslinkers increased (Figure 2. 6-B). The water uptake was also decreasing with the concentration of crosslinkers (Figure 2. 6-C). The HA-PLL$_{XL2}$ sponge uptook 95.5% ± 0.2% water, the HA-PLL$_{XL3}$ sponge 91.9% ± 0.8%, and the HA-PLL$_{XL4}$ sponge 82.2% ± 1.5%. Crosslinking is therefore compulsory, and the optimal concentration of crosslinking agent is 5 mg/mL EDC and 1.8 mg/mL NHS. The following sponges will therefore be prepared at this concentration. The HA-PLL$_{XL2}$ sponge will now be referred to as the HA-PLL sponge.

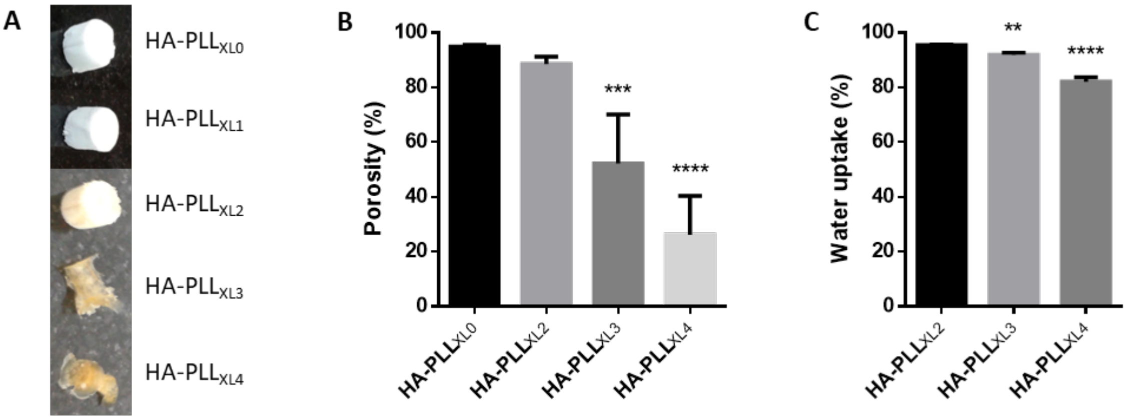

Figure 2. 6: Photos of dry HA-PLL$_{XL}$ sponges (A), porosity of dry HA-PLL$_{XL}$ sponges (B) and water uptake at the equilibrium in NaCl 0.9% (w/v) (C) for different concentrations of crosslinking agents. ANOVA analysis was performed against HA-PLL$_{XL0}$ for the porosity and against HA-PLL$_{XL2}$ for water uptake: ***p<0.001, ****p<0.0001.

3.3. Optimisation of the SF sponge preparation

SF sponges were prepared applying the freeze-drying method to identify the most adequate annealing method. After freeze-drying SF is mostly composed of random coils, which are soluble in water, and alpha helixes. Increasing the crystallinity of the protein by triggering β-sheets formation increases the insolubility of SF sponges and therefore slow down its degradation. However, if the crystallinity is too high, the swelling of the sponge would decrease. We therefore tested two methods previously reported that allow moderate increase in crystallinity: water annealing at RT for 12h (SF(H_2O)), and ethanol annealing at RT for 2h (SF(EtOH)). Methanol annealing, while highly used because of its efficiency, was not considered because of its high toxicity. The SF sponge without annealing lost its shape and led to a viscous system once in aqueous solution on the contrary of annealed sponges for both technics. For both technics, the porosity was similar and around 90% (Figure 2. 7-A). After complete swelling, SF(EtOH) uptook more water (92.2% ±0.5) than the SF(H_2O) sponge (85.3% ± 5.6%) (Figure 2. 7-B). Finally, both sponges showed elastic properties but SF(EtOH) was softer with a Young's modulus of 22 kPa for the SF(EtOH) sponge compared to 66 kPa for the SF(H_2O) sponge. For our purpose, the higher water uptake and softer the better, therefore, ethanol annealing has been chosen for the following experiments. Finally, the morphology of the sponges before and after annealing have been observed by SEM and no difference has been detected with an average pore size of 87 µm ± 29 µm for the SF sponge and 86 µm ± 25 µm for the SF(EtOH) sponge (Figure 2. 7-C). The interest of crosslinking the SF was also studied with a concentration of crosslinking agent of 5 mg/mL EDC and 1.8 mg/mL NHS. No effect was observed on the porosity (Figure 2. 7-B) but a decrease in water uptake (86% ± 5%) (Figure 2. 7-B) and in pore size (34 µm ± 15 µm) (Figure 2. 7-A) was observed. Crosslinking the SF was therefore not applied for the following studies.

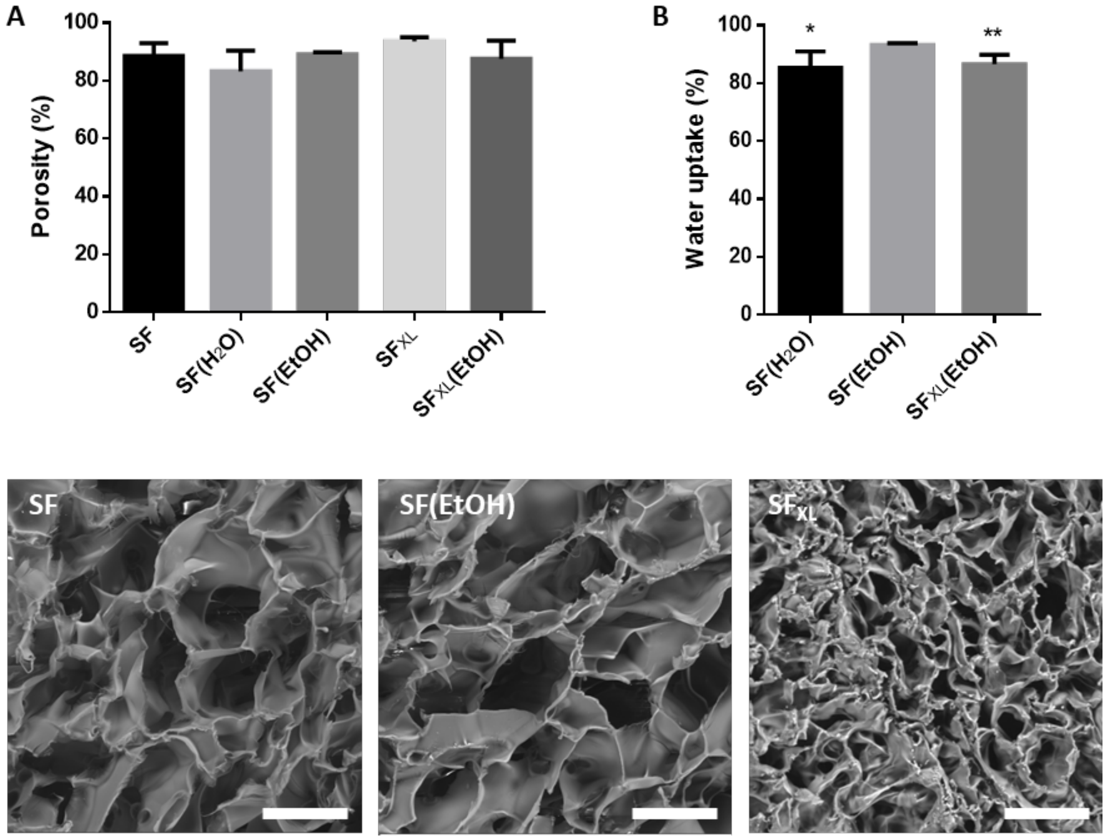

Figure 2. 7: Porosity of dry SF sponges (A), water uptake at the equilibrium in NaCl 0.9% (w/v) (B), and SEM images (scale = 100 µm) (C) for different annealing methods and crosslinking of SF sponges. ANOVA analysis was performed against SF(EtOH) for the water uptake: $^*p<0.05$, $^{**}p<0.01$.

3.4. Kinetic study of the interaction of SF with HA

Homogeneous dispersions of SF with hydrophilic polymers such as HA have been previously shown to be quite difficult to attain. Phase separation and/or specific interactions are quite prone to occur (46,65). Thus, the effect of the mixing time on the innerstructure of SF-HA systems was investigated by preparing films composed of either HA, SF or a blend of SF and HA mixed for 15 min, 2h or 15h were prepared (Figure 2. 8). The HA film displayed a rough surface while the SF film was reproducing the petri dish pattern. When mixed together for 15 min, two separate phases appeared in the form of globules with sizes ranging from 9.6 to 128.2 µm (38.7 ± 23.5 in average) that were clearly outlined by the second phase. The phase inside the globules had a similar topography to that of the SF film while the other phase seemed similar to that of the HA film. After 2h of mixing, the two phases were still distinguishable, but they became more well-mixed and had different textures compared to what was observed with 15 min of mixing time. The globules appeared rougher and the phase around them became thinner. Moreover, the sizes of the globules were significantly reduced to 2.4 - 19 µm. After an overnight mixing, the film adopted a much more homogeneous appearance. However, large aggregates could be seen to form extensively across the surface of the film. Therefore, sponges were prepared with an intermediate mixing time of about 5h.

3.5. Optimisation of the preparation of SF-HA and SF-HA-hep sponges

Sponges of SF 4% (w/v) alone and SF 4% (w/v) with HA 2% (w/v) sponges without further ingredients or also containing hep 1% (w/v) were prepared. In order to evaluate the importance of the crosslinking and of the annealing on sponges made of a blend of HA and SF, some systems were crosslinked with 5 mg/mL EDC and 1.8 mg/mL NHS for 15h at 4°C and some were subjected to annealing with ethanol. The SF-HA sponges without crosslinking and/or without annealing did not maintain their integrity after a few minutes in an aqueous solution, both steps are therefore necessary. In order to determine if the annealing of the SF-HA sponge had an influence on its structure, the porosity, pore size and morphology were analysed before and after ethanol annealing. The porosity of the sponges decreased slightly after annealing from 90.7% ± 2.6% to 87.4% ± 0.9% (Figure 2. 9-A). SEM images showed no difference in morphology but a statistically significant decrease in pore size (42 µm ± 16 µm before and 36 µm ± 14 µm after annealing). In conclusion, crosslinking and annealing of the SF-HA sponge is necessary but annealing had an effect on the structure of the sponges by decreasing the porosity and pore size of the sponges. For the following experiments, only SF-HA_{XL}(EtOH) will be considered and will be now called SF-HA for more simplicity.

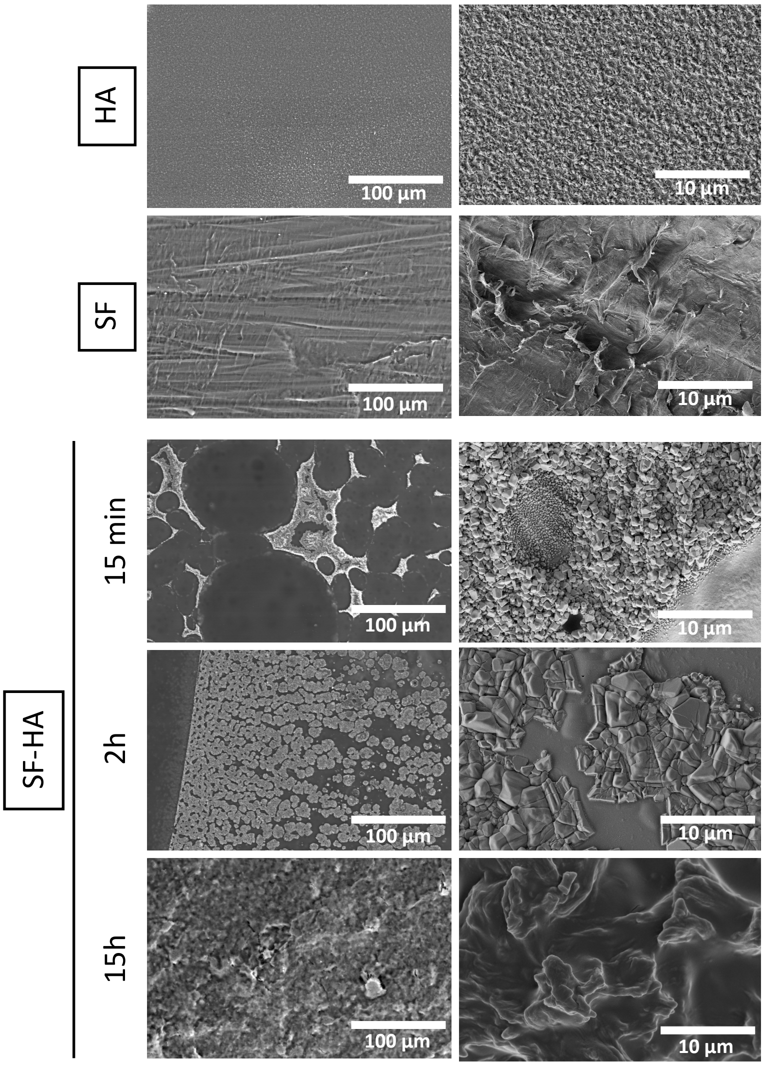

Figure 2. 8: SEM images of films prepared with either HA, SF or a blend of SF and HA mixed for 15 min, 2h or 15h.

The SF-HA-hep sponge with 5 mg/mL EDC and 1.8 mg/mL NHS (SF-HA-$hep_{XL(-)}$(EtOH)) showed a high degradation in PBS at 37°C for 7 days (Figure 2. 9-C) that was not seen for the SF-HA sponge. It can be explained by the higher total amount of polymer. Therefore, it was decided to use 15 mg/mL EDC and 5.5 mg/mL NHS (SF-HA-hep_{XL}(+)(EtOH)). The use of more crosslinkers did not affect the porosity of the sponges. Therefore, it was decided to use the SF-HA-hep_{XL}(+)(EtOH) for the following experiments. This sponge will now be called SF-HA-hep for more simplicity.

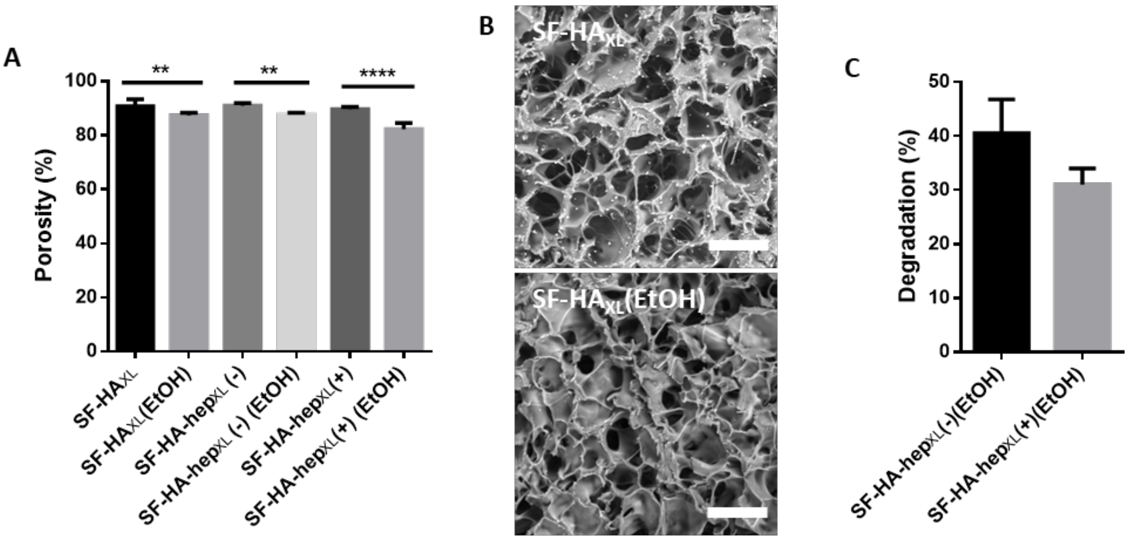

Figure 2. 9: Porosity of dry SF-HA$_{XL}$ and SF-HA-hep$_{XL}$ sponges before and after annealing (A), SEM images of the SF-HA$_{XL}$ sponge before and after annealing (scale = 100 µm) (B), and degradation in PBS at 37°C for 7 days of the SF-HA-hep$_{XL}$(-)(EtOH) sponge (C_{EDC} = 5 mg/mL, C_{NHS} = 1.8 mg/mL) and of the SF-HA-hep$_{XL}$(+)(EtOH) sponge (C_{EDC} = 15 mg/mL, C_{NHS} = 5 mg/mL) (C). ANOVA analysis: **p<0.01, ****p<0.0001.

3.6. Structural characterisation of the sponges

Four formulations have been selected, in regards to the optimisation studies, to explore further their characteristics: (i) the HA-PLL sponge made of HA 2% (w/v) with PLL 0.01% (w/v) and crosslinked with 5 mg/mL EDC and 1.8 mg/mL NHS, (ii) the SF sponge made of SF 4% and annealed with vapours of ethanol, (iii) the SF-HA sponge made of SF 4% (w/v) and HA 2% (w/v) annealed and crosslinked with 5 mg/mL EDC and 1.8 mg/mL NHS and (iv) the SF-HA-hep sponge made of SF 4% (w/v), HA 2% (w/v) and hep 1% (w/v) and crosslinked with 15 mg/mL EDC and 5.5 mg/mL NHS.

The microstructure of the sponges' walls was observed under fluorescence microscopy (Figure 2. 10). Antibodies used in immunofluorescence imaging like DAPI or ActinRed fixed in a non-specific manner to SF without interacting with HA. Indeed, a much stronger signal was observed for the SF sponge compared with the HA-PLL sponge. The walls of the SF sponge showed a smooth surface. Upon the addition of HA to SF, the walls of the pores became irregular and seemed to be formed by small fluorescent aggregates. The appearance of such aggregates was intensified upon the introduction of hep. The structure of SF-HA and SF-HA-hep sponges was formed by fluorescent aggregates that should therefore be SF-rich distributed in a non-fluorescent matrix that should be composed mainly of HA. Garcia-Fuentes *et al.* (65) studied the interaction between HA and SF in blends with different ratios. Results suggested that a phase separation occurs with a SF/HA ratio of 80:20 and 60:40 (w/w), with one phase containing HA alone while the other phase consisted of a mixture of HA and SF. The phase separation observed in the films prepared by us (a 2:1 SF/HA ratio was used here) as well as the structure observed in the walls of the sponges are consistent with those previous findings. We can therefore conclude that the polymer ratio as well as the mixing time are critical parameters when SF and HA are used to prepare 3D scaffolds.

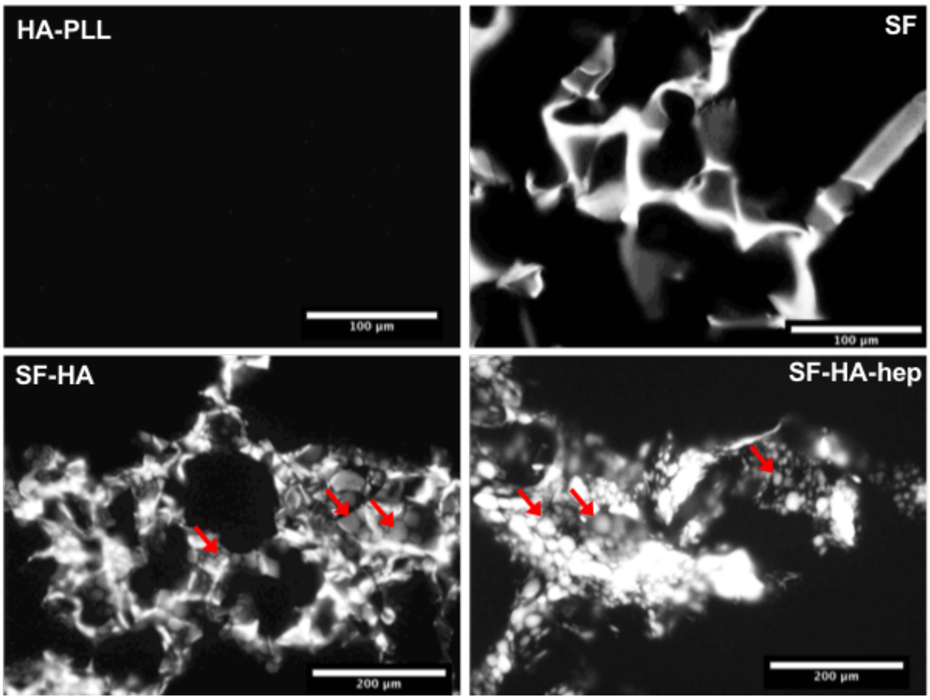

Figure 2. 10: Autofluorescence of the sponges under Rhodamine filter with the same exposure time of 58 ms. Red arrows indicate the presence of aggregates.

ATR-FTIR analysis was performed on the sponges before and after ethanol annealing to observe the changes in crystallinity (Figure 2. 10). After ethanol annealing, a shift from 1640 cm^{-1}, which corresponds to SF random coils, to 1621 cm^{-1}, which corresponds to SF β-sheets (40), was observed for all the sponges with SF. After ethanol annealing, all the sponges had a similar β-sheet content of about 28%. Without the annealing step, the structure of the sponges collapsed after a few minutes in an aqueous environment.

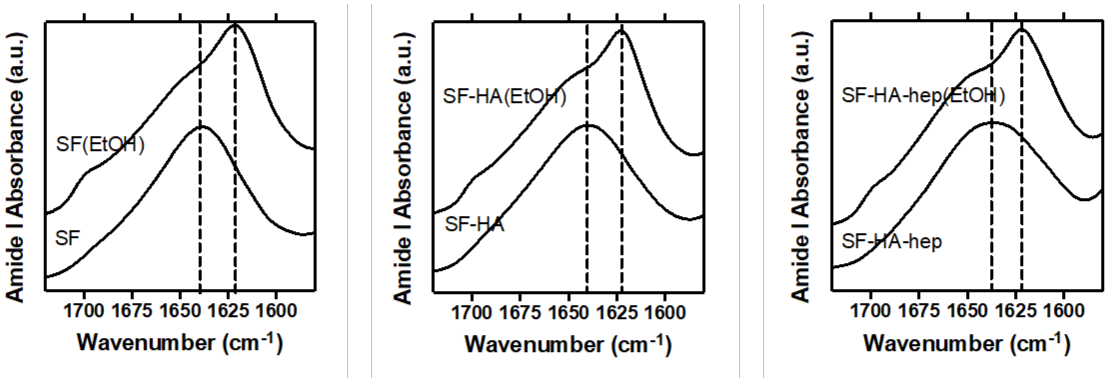

Figure 2. 11: FTIR absorbance spectra in the amide I region for sponges containing SF before and after ethanol annealing. Peak at 1621 cm^{-1} is typical of the β-sheet conformation of SF, while the peak at 1640 cm^{-1} corresponds to SF random coils.

All dry sponges exhibited high porosity, ranging from 82% for the SF-HA-hep sponge to 93% for the SF sponge. (Table 2. 2). The capability of the sponges to uptake water when immersed in NaCl 0.9% (w/v) aqueous solution was of 93% for the SF-HA-hep and the SF-HA sponges, and 95% for the HA-PLL sponge (Table 2. 2). Degradation of the sponges was monitored at 37°C during 7 and 21 days in PBS supplemented with enzymes (Figure 2. 12-A). Hyaluronidase and heparinase were selected since they are found *in vivo* and for their ability to degrade HA and hep. HA-PLL sponges were completely degraded after 7 days and produced a clear solution, while SF sponges maintained their integrity even after 21 days. SF-HA and SF-HA-hep showed intermediate degradability. Thus, in good agreement with previous reports, the mass loss in scaffolds composed of HA and SF blends can be attributed to the degradation of HA (46). Since HA degrades quicker than SF, the matrix has to be as homogeneous as possible to avoid the generation of scaffolds with distinct HA-rich compartments susceptible to rapid *in vivo* decomposition. An ideal scaffold for trapping GBM cells should be biodegradable to avoid the need for secondary surgery to remove the implant. Simultaneously, the degradation rate of the scaffold should match the rate of GBM migration so that the structure of the scaffold remains until the process is complete in order to eliminate the cells before scaffold degradation.

To confirm these results, the morphology of the sponges was observed using SEM before and after 7 days in PBS without any enzymes at 37°C (Figure 2. 12-B,C). These study conditions were selected to induce intermediate degradation of the HA-PLL sponge. At the end of this study, signs of degradations in the form of thinner walls and larger pores were clearly visible in HA-PLL sponges. Sponges made of SF and HA mixtures showed better preservation of morphology, confirming that the addition of SF to the sponges allowed for retention of the structure of the sponges in aqueous solutions. SEM images revealed good pore connectivity and an average pore size between 30 ± 13 µm for SF-HA and 87 ± 29 µm for SF. The structure of these porous sponges mimic the structure of the brain ECM that was described as a foam-like structure by Nicholson *et al.* (70). The pores were of various sizes ranging from 20 to 140 µm across the different sponge compositions studied in this work, which should be sufficiently small to support 3D cell-cell contacts, but large enough to allow good diffusion of nutrients, oxygen and bioactive factors for cell survival and growth (7).

Texture analysis was performed on hydrated sponges and Young’s modulus were calculated (Table 2. 2). All hydrated sponges showed textures within the same order of magnitude. The values of Young’s modulus recorded ranged between 6 kPa for HA-PLL and 22 kPa for SF. Sponges made from mixtures of SF and HA showed intermediate values. The brain has a Young’s modulus below 1 kPa (5,6). However, it is challenging to produce scaffolds that maintain their structural integrity with a Young’s modulus as low as the one of the brain. On the other hand, the stiffness of the material promotes better handling of the sponges. For example, the sponges could be conveniently cut into the desired dimensions to better fit the lesion at the intended site of implantation.

Table 2. 2: Porosity of dry sponges, water uptake in NaCl 0.9% aq. solution, and Young’s modulus after hydration.

Sponge	**Porosity (%)**	**Water uptake (%)**	**Young’s modulus (kPa)**
HA-PLL	91.9 ± 1.9	95.5 ± 0.2	6.0 ± 1.6
SF	92.7 ± 0.6	93.2 ± 0.5	21.7 ± 1.6
SF-HA	87.4 ± 1.0	92.8 ± 2.1	12.5 ± 7.8
SF-HA-hep	82.3 ± 2.2	92.9 + 2.2	13.1 ± 5.1

3.7. SDF-1α uptake and release

Since the SF-HA and SF-HA-hep sponges provided a good trade-off between the low rigidity of the HA-PLL sponge and the slow degradation of the SF sponge, they were chosen for the SDF-1α uptake and release studies.

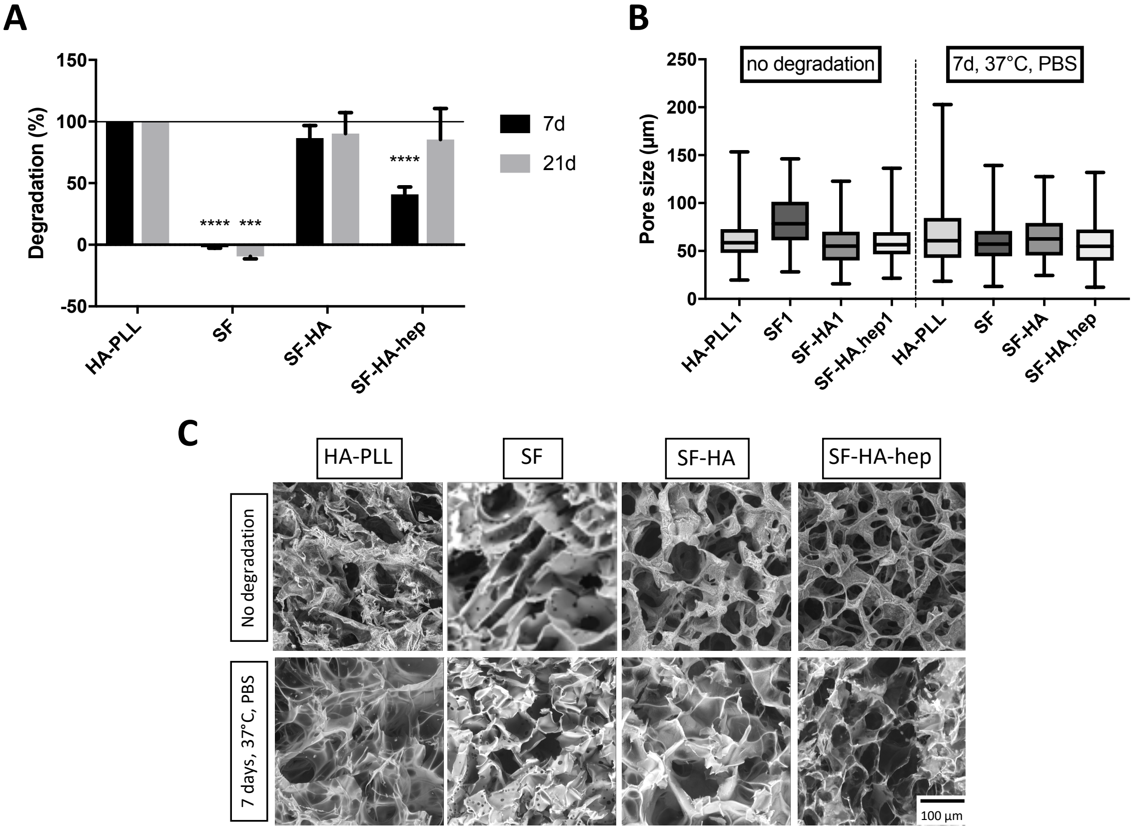

Figure 2. 12: (A) Degradation in PBS with enzymes (hyaluronidase and heparinase) at 37°C for 7 and 21 days of HA-PLL, SF, SF-HA and SF-HA-hep sponges. Paired comparisons were conducted between degradation of HA-PLL and the others with the same conditions. (B) Average pores size before and after incubation for 7 days in PBS at 37°C. At least 94 pores were measured per sponge. (C) SEM images of sponges; scale bar 100 µm. ANOVA analysis: ***p<0.001, ****p<0.0001.

SDF-1α was adsorbed on the SF-HA and SF-HA-hep sponges by simply hydrating the sponges with the protein dissolved in PBS. In order to determine the distribution profile of the protein inside the sponge, SDF-1α coupled to an AlexaFluor 647 was used. A fluorescence map was subsequently obtained (Figure 2. 13). We observed that the protein formed a radial concentration gradient from the center (where the drop was deposited) toward the edges of the sponges. Since it has been described that CXCR4 receptor-bearing cells can migrate in response to an SDF-1α concentration gradient, the radial distribution of SDF-1α in the sponge may be beneficial in facilitating extensive infiltration of stem cells into the sponge for tissue regeneration (3).

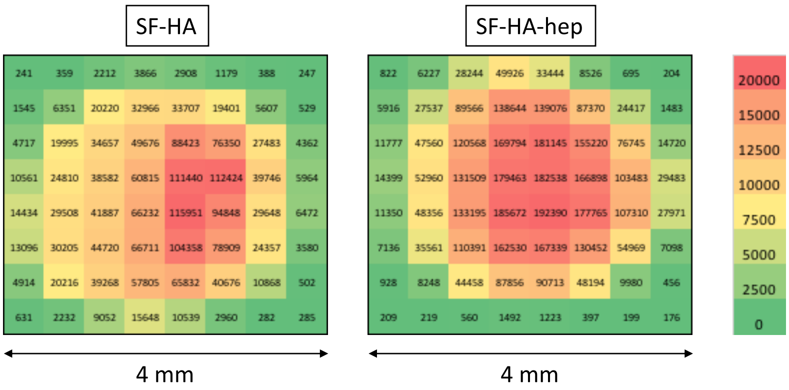

SF-HA

241	359	2212	3866	2908	1179	388	247
1545	6351	20220	32966	33707	19401	5607	529
4717	19995	34657	49676	88423	76350	27483	4362
10561	24810	38582	60815	111440	112424	39746	5964
14434	29508	41887	66232	115951	94848	29648	6472
13096	30205	44720	66711	104358	78909	24357	3580
4914	20216	39268	57805	65832	40676	10868	502
631	2232	9052	15648	10539	2960	282	285

SF-HA-hep

822	6227	28244	49926	33444	8526	695	204
5916	27537	89566	138644	139076	87370	24417	1483
11777	47560	120568	169794	181145	155220	76745	14720
14399	52960	131509	179463	182538	166898	103483	29483
11350	48356	133195	185672	192390	177765	107310	27971
7136	35561	110391	162530	167339	130452	54969	7098
928	8248	44458	87856	90713	48194	9980	456
209	219	560	1492	1223	397	199	176

Figure 2. 13: Representative image of the distribution of AF-SDF-1α in the SF-HA and SF-HA-hep sponges recorded via fluorescence detection.

SDF-1α release from SF-HA and SF-HA-hep in PBS with enzymes (hyaluronidase and heparinase) at 37°C was then monitored over 7 days (Figure 2. 14). For the SF-HA-hep sponge, a maximum release of 2.1 ± 0.8% was reached after 3 days. A significantly higher release was observed with the SF-HA sponge whereby a maximum release of 26 ± 16% was reached after 2 days. However, it is expected that, *in vivo*, release should continue over time in parallel with the degradation of the sponge. SDF-1α is a positively charged protein at physiological pH (isoelectric point (IEP) ~9.6) while HA and SF are negatively charged (IEP ~2.9 and ~4.6 respectively) (71,72), allowing the protein to bind to the sponges via electrostatic interactions. Moreover, heparin is known to form a strong complex with SDF-1α (73). SDF-1α was therefore expected to be better retained in the SF-HA-hep sponge than in the SF-HA sponge. However, the strong SDF-1α retention capacity displayed by the SF-HA-hep sponge has not been reported before to our knowledge. A strong retention of the protein inside the scaffold might have benefit effect for attraction of cells in the heart of the scaffold via haptotaxis as well as their retention over time.

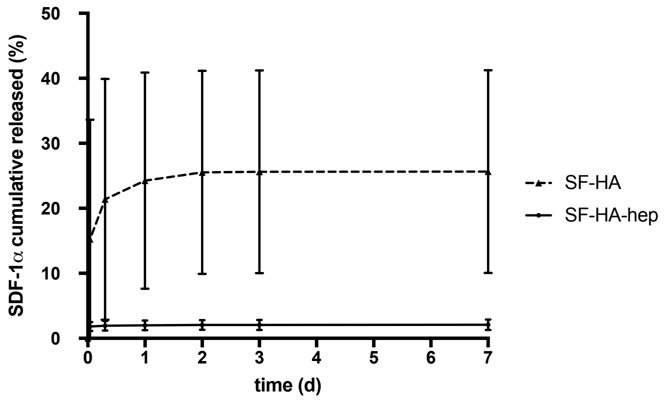

Figure 2. 14: SDF-1α cumulative release from the SF-HA and SF-HA-hep sponges during 7 days in PBS with enzymes. All values were expressed in percentage of the amount of SDF-1α added to the sponges.

4. Conclusion

In summary we demonstrated that by using mixtures of two biopolymers (SF and HA), it was possible to finely tune the properties of a biomaterial. Indeed, the SF-HA and SF-HA-hep sponges exhibited intermediate physicochemical properties (Young's modulus, degradation behaviour) compared to those of the SF or HA-PLL sponges. Considering their porous structure and ability to retain the chemokine SDF-1α, these SF and HA-based biomaterials may be of great use for the trapping of GBM cells.

REFERENCES

1. Dutta D, Hickey K, Salifu M, Fauer C, Willingham C, Stabenfeldt SE. Spatiotemporal presentation of exogenous SDF-1 with PLGA nanoparticles modulates SDF-1/CXCR4 signaling axis in the rodent cortex. Biomater Sci. 2017;5(8):1640–51.
2. Christie KJ, Turnley AM. Regulation of endogenous neural stem/progenitor cells for neural repair—factors that promote neurogenesis and gliogenesis in the normal and damaged brain. Front Cell Neurosci. 2013;6(January):1–18.
3. Imitola J, Raddassi K, Park KI, Mueller F-J, Nieto M, Teng YD, et al. Directed migration of neural stem cells to sites of CNS injury by the stromal cell-derived factor 1 /CXC chemokine receptor 4 pathway. Proc Natl Acad Sci. 2004;101(52):18117–22.
4. De Souza SW, Dobbing J. Cerebral Edema in Developing Brain : I . Normal water and cation Content in Developing Rat Brain and Postmortem Changes. Exp Neurol. 1971;32:431–8.
5. Nava MM, Raimondi MT, Pietrabissa R. Controlling Self-Renewal and Differentiation of Stem Cells via Mechanical Cues. J Biomed Biotechnol. 2012;2012:1–12.
6. Engler AJ, Sen S, Sweeney HL, Discher DE. Matrix elasticity directs stem cell lineage specification. Cell. 2006;126(4):677–89.
7. Mahumane GD, Kumar P, Du Toit LC, Choonara YE, Pillay V. 3D scaffolds for brain tissue regeneration: Architectural challenges. Biomater Sci. 2018;6(11):2812–37.
8. Weissmann B, Meyer K. The Structure of Hyalobiuronic Acid and of Hyaluronic Acid from Umbilical Cord. J Am Chem Soc. 1954;76(7):1753–7.
9. Fraser JRE, Laurent TC, Laurent UBG. Hyaluronan: Its nature, distribution, functions and turnover. J Intern Med. 1997;242(1):27–33.
10. Balazs EA. Ultrapure Hyaluronic Acid and the Use Thereof. U.S. Patent 4,141,973. 1979.
11. Ras E, Blackwell F. The Protective Effect of Na-Hyaluronate to Cornea1 Endothelium. 1980;119–27.
12. Percival SPB. Results of a clinical trial of sodium hyaluronate in lens implantation surgery. Am Intra-Ocular Implant Soc J. 1985;11(3):257–9.
13. Miller D, Stegmann R. Use of Na-hyaluronate in Anterior Segment Eye Surgery. Am Intra-Ocular Implant Soc J. 1980;6(1):13–5.
14. Auer JA, Fackelman GE, Gingerich DA, Fetter AW. Effect of hyaluronic acid in naturally occurring and experimentally induced osteoarthritis. Am J Vet Res. 1980;41(4):568–74.
15. Dougados M, Nguyen M, Listrat V, Amor B. High molecular weight sodium hyaluronate (hyalectin) in osteoarthritis of the knee: a 1 year placebo-controlled trial. Osteoarthr Cartil. 1993;1(2):97–103.
16. Pavicic T, Gauglitz GG, Lersch P, Schwach-Abdellaoui K, Malle B, Korting HC, et al. Efficacy of cream-based novel formulations of hyaluronic acid of different molecular weights in anti-wrinkle treatment. J Drugs Dermatology. 2011;10(9):990–1000.
17. Hellström S, Laurent C. Hyaluronan and healing of tympanic membrane perforations. An experimental study. Acta Otolaryngol. 1987;104(S442):54–61.
18. King SR, Hickerson WL, Proctor KG, Newsome AM. Beneficial actions of exogenous hyaluronic acid on wound healing. Surgery. 1991;109(1):76–84.
19. Duranti F, Salti G, Bovani B, Calandra M, Rosati ML. Injectable hyaluronic acid gel for soft tissue augmentation: A clinical and histological study. Dermatologic Surg. 1998;24(12):1317–25.
20. Bartlett S, Lin K, Bartlett S, Matsuo K, Livolsi V, Parry C, et al. Hyaluronic acid-filled mammary implants: An experimental study. Plast Reconstr Surg. 1994;94(2):306–15.
21. Borke T, Najberg M, Ilina P, Bhattacharya M, Urtti A, Tenhu H, et al. Hyaluronic Acid Graft Copolymers with Cleavable Arms as Potential Intravitreal Drug Delivery Vehicles. Macromol Biosci. 2017;(October):1700200.

22. Wang Q, Zhong Y, Liu W, Wang Z, Gu L, Li X, et al. Enhanced chemotherapeutic efficacy of the low-dose doxorubicin in breast cancer via nanoparticle delivery system crosslinked hyaluronic acid. Drug Deliv. 2019;26(1):12–22.

23. Tunesi M, Raimondi I, Russo T, Colombo L, Micotti E, Brandi E, et al. Hydrogel-based delivery of Tat-fused protein Hsp70 protects dopaminergic cells in vitro and in a mouse model of Parkinson's disease. NPG Asia Mater. 2019;11(1).

24. Guan J, Liu Q, Jin L, Xu H, Wu H, Zhang X, et al. Synergistic effect of Soluplus and hyaluronic acid on the supersaturation maintenance of lovastatin: The facilitated in vitro-in vivo performance and improved physical stability. Carbohydr Polym. 2019;222.

25. Rouslahti E. Brain extracellular matrix. Glycobiology. 1996;6(5):489–92.

26. Bellail AC, Hunter SB, Brat DJ, Tan C, Van Meir EG. Microregional extracellular matrix heterogeneity in brain modulates glioma cell invasion. Int J Biochem Cell Biol. 2004;36(6):1046–69.

27. Heldin P, Lin C-Y, Kolliopoulos C, Chen Y-H, Skandalis SS. Regulation of hyaluronan biosynthesis and clinical impact of excessive hyaluronan production. Matrix Biol. 2019;78–79:100–17.

28. Schiraldi C, La A, De M. Biotechnological Production and Application of Hyaluronan. Biopolymers. 2010;

29. Shimojo AAM, Pires AMB, Lichy R, Rodrigues AA, Santana MHA. The crosslinking degree controls the mechanical, rheological, and swelling properties of hyaluronic acid microparticles. J Biomed Mater Res - Part A. 2015;103(2):730–7.

30. Yang X, Wang X, Yu F, Ma L, Pan X, Luo G, et al. Hyaluronic acid/EDC/NHS-crosslinked green electrospun silk fibroin nanofibrous scaffolds for tissue engineering. RSC Adv. 2016;6(102):99720–8.

31. Mazia D, Schatten G, Sale W. Adhesion of cells to surfaces coated with polysine. Applications to electron microscopy. J Cell Biol. 1975;66(3):198–200.

32. Moy RL, Lee A, Zalka A. Commonly used suture materials in skin surgery. Am Fam Physician. 1991;44(6):2123–8.

33. Wray LS, Hu X, Gallego J, Georgakoudi I, Omenetto FG, Schmidt D, et al. Effect of processing on silk-based biomaterials : Reproducibility and biocompatibility. J Biomed Mater Res Part B. 2011;99B:89–101.

34. Yamada H, Nakao H, Takasu Y, Tsubouchi K. Preparation of undegraded native molecular fibroin solution from silkworm cocoons. Mater Sci Eng C. 2001;14(1):41–6.

35. Yamaguchi K, Kikuchi Y, Takagi T, Kikuchi A, Oyama F, Shimura K, et al. Primary structure of the silk fibroin light chain determined by cDNA sequencing and peptide analysis. J Mol Biol. 1989;210(1):127–39.

36. Jin HJ, Kaplan DL. Mechanism of silk processing in insects and spiders. Nature. 2003;424(6952):1057–61.

37. Vepari C, Kaplan DL. Silk as biomaterial. Prog Polym Sci. 2012;100(2):130–4.

38. Konishi T, Sakabe H, Arimoto H. The Elongation Recovery of Raw Silk by Lithium Bromide Aqueous Solution. J Sericultural Sci Japan. 1979;48(1):8–14.

39. Rockwood DN, Preda RC, Yücel T, Wang X, Lovett ML, Kaplan DL. Materials fabrication from Bombyx mori silk fibroin. Nat Protoc. 2011;6(10):1612–31.

40. Hu X, Kaplan D, Cebe P. Determining beta-sheet crystallinity in fibrous proteins by thermal analysis and infrared spectroscopy. Macromolecules. 2006;39(18):6161–70.

41. Hu X, Shmelev K, Sun L, Gil ES, Park SH, Cebe P, et al. Regulation of silk material structure by temperature-controlled water vapor annealing. Biomacromolecules. 2011;12(5):1686–96.

42. Fan Z, Zhang F, Liu T, Zuo BQ. Effect of hyaluronan molecular weight on structure and biocompatibility of silk fibroin/hyaluronan scaffolds. Int J Biol Macromol. 2014;65:516–23.

43. Mobini S, Taghizadeh-Jahed M, Khanmohammadi M, Moshiri A, Naderi M-M, Heidari-Vala H, et al. Comparative evaluation of in vivo biocompatibility and biodegradability of regenerated silk scaffolds reinforced with/without natural silk fibers. J Biomater Appl. 2016;30(6):793–809.

44. Thurber AE, Omenetto FG, Kaplan DL. In vivo bioresponses to silk proteins. Biomaterials. 2015;71(2015):145–57.

45. Fernández-garcía L, Marí-buyé N, Barios JA, Madurga R, Elices M, Pérez-rigueiro J, et al. Safety and tolerability of silk fibroin hydrogels implanted into the mouse brain. Acta Biomater. 2016;45:262–75.

46. Garcia-Fuentes M, Meinel AJ, Hilbe M, Meinel L, Merkle HP. Silk fibroin/hyaluronan scaffolds for human mesenchymal stem cell culture in tissue engineering. Biomaterials. 2009;30(28):5068–76.

47. Ren YJ, Zhou ZY, Liu BF, Xu QY, Cui FZ. Preparation and characterization of fibroin/hyaluronic acid composite scaffold. Int J Biol Macromol. 2009;44(4):372–8.

48. Zulueta MML, Lin SY, Hu YP, Hung SC. Synthetic heparin and heparan sulfate oligosaccharides and their protein interactions. Curr Opin Chem Biol. 2013;17(6):1023–9.

49. Rabenstein DL. Heparin and heparan sulfate: Structure and function. Nat Prod Rep. 2002;19(3):312–31.

50. Park JW, Jeon OC, Kim SK, Al-Hilal TA, Jin SJ, Moon HT, et al. High antiangiogenic and low anticoagulant efficacy of orally active low molecular weight heparin derivatives. J Control Release. 2010;148(3):317–26.

51. Fujita K, Sakamoto N, Kuzuya F. Effect of Heparin on Post Heparin Lipoprotein Lipase and Hepatic TG-lipase. Nippon Ronen Igakkai Zasshi Japanese J Geriatr. 1982;19(1):53–60.

52. Lappegård KT, Riesenfeld J, Brekke O-L, Bergseth G, Lambris JD, Mollnes TE. Differential effect of heparin coating and complement inhibition on artificial surface-induced eicosanoid production. Ann Thorac Surg. 2005;79(3):917–23.

53. Ekre H-PT, Fjellner B, Hägermark Ö. Inhibition of complement dependent experimental inflammation in human skin by different heparin fractions. Int J Immunopharmacol. 1986;8(3):277–86.

54. Yu Y, Xu C, Zhen L, Yang S, Zhou J, Yao J. Bio-inspired drug-dominated supramolecular nanocomplex based on low molecular weight heparin for progressive tumor therapy. Carbohydr Polym. 2019;220:30–42.

55. Shen X, Fang J, Lv X, Pei Z, Wang Y, Jiang S, et al. Heparin impairs angiogenesis through inhibition of microRNA-10b. J Biol Chem. 2011;286(30):26616–27.

56. Folkman J, Langer R, Linhardt RJ, Haudenschild C, Taylor S. Angiogenesis inhibition and tumor regression caused by heparin or a heparin fragment in the presence of cortisone. Science (80-). 1983;221(4612):719–25.

57. Prokoph S, Chavakis E, Levental KR, Zieris A, Freudenberg U, Dimmeler S, et al. Sustained delivery of SDF-1alpha from heparin-based hydrogels to attract circulating pro-angiogenic cells. Biomaterials. 2012;33(19):4792–800.

58. Krieger JR, Ogle ME, McFaline-Figueroa J, Segar CE, Temenoff JS, Botchwey EA. Spatially localized recruitment of anti-inflammatory monocytes by SDF-1α-releasing hydrogels enhances microvascular network remodeling. Biomaterials. 2016;77:280–90.

59. Bladergroen BA, Siebum B, Siebers-Vermeulen KGC, Kuppevelt TH Van, Poot AA, Feijen J, et al. In Vivo Recruitment of Hematopoietic Cells Using Stromal Cell–Derived Factor 1 Alpha–Loaded Heparinized Three-Dimensional Collagen Scaffolds. Tissue Eng Part A. 2009;15(7):1591–9.

60. Kucia M, Ratajczak J, Reca R, Janowska-Wieczorek A, Ratajczak MZ. Tissue-specific muscle, neural and liver stem/progenitor cells reside in the bone marrow, respond to an SDF-1 gradient and are mobilized into peripheral blood during stress and tissue injury. Blood Cells, Mol Dis. 2004;32(1):52–7.

61. Tweedy L, Susanto O, Insall RH. Self-generated chemotactic gradients - cells steering themselves. Curr Opin Cell Biol. 2016;42:46–51.

62. Jarocha D, Zuba-Surma E, Majka M. Dimethyl Sulfoxide (DMSO) Increases Percentage of CXCR4 + Hematopoietic Stem/Progenitor Cells, Their Responsiveness to an SDF-1 Gradient, Homing Capacities, and Survival . Cell Transplant. 2016;25(7):1247–57.

63. Wysoczynski M, Reca R, Ratajczak J, Kucia M, Shirvaikar N, Honczarenko M, et al. Incorporation of CXCR4 into membrane lipid rafts primes homing-related responses of hematopoietic stem/progenitor cells to an SDF-1 gradient. Blood. 2005;105(1):40–8.

64. Won YW, Patel AN, Bull DA. Cell surface engineering to enhance mesenchymal stem cell migration toward an SDF-1 gradient. Biomaterials. 2014;35(21):5627–35.

65. Garcia-Fuentes M, Giger E, Meinel L, Merkle HP. The effect of hyaluronic acid on silk fibroin conformation. Biomaterials. 2008;29(6):633–42.

66. Correia CR, Moreira-Teixeira LS, Moroni L, Reis RL, van Blitterswijk CA, Karperien M, et al. Chitosan Scaffolds Containing Hyaluronic Acid for Cartilage Tissue Engineering. Tissue Eng Part C Methods. 2011;17(7):717–30.

67. Lassoued N, Delarue J, Launay B, Michon C. Baked product texture: Correlations between instrumental and sensory characterization using Flash Profile. J Cereal Sci. 2008;48(1):133–43.

68. Nultsch K, Germershaus O. Silk fibroin degumming affects scaffold structure and release of macromolecular drugs. Eur J Pharm Sci. 2017;106(June):254–61.

69. Kuo JW, Swarm DA, Prestwich GD. Chemical Modification of Hyaluronic Acid by Carbodiimides. Bioconjug Chem. 1991;2(4):232–41.

70. Nicholson C, Syková E. Extracellular space structure revealed by diffusion analysis. Trends Neurosci. 1998;21:207–15.

71. Foo CWP, Bini E, Hensman J, Knight DP, Lewis R V., Kaplan DL. Role of pH and charge on silk protein assembly in insects and spiders. Appl Phys A Mater Sci Process. 2006;82(2):223–33.

72. Malay Ö, Bayraktar O, Batigün A. Complex coacervation of silk fibroin and hyaluronic acid. Int J Biol Macromol. 2007;40(4):387–93.

73. Sadir R, Baleux F, Grosdidier A, Imberty A, Lortat-Jacob H. Characterization of the stromal cell-derived factor-1alpha-heparin complex. J Biol Chem. 2001;276(11):8288–96.

CHAPTER III: Development of a cellular model as an evaluation tool

Table of content

CHAPTER III

Development of a cellular model as an evaluation tool

1. Introduction

The stromal derived factor-1α (SDF-1α), also called CXCL12 is a chemokine composed of 68 amino acids that bind to the CXC chemokine receptor 4 (CXCR4) (1). CXCR4 is overexpressed in invasive GBM cells (2–4). Goffart *et al.* (5) studied the implication of SDF-1α and the invasion ability of GBM cells. They demonstrated the expression of the CXCR4 receptor in three cell lines (U87MG, U373 and LN18) and two primary cultures of GBM tumour from patients. Moreover, the relationship between CXCR4 bearing cells and migration toward an SDF-1α gradient has been shown.

Primary cells are the best *in vitro* model in terms of reproduction of *in vivo* behaviour thanks to a preservation of an undifferenciated state and molecular repertoire of receptors as well as activated signaling pathways. However, they are complicated to use because of their heterogeneity and variability as well as isolation and maintenance in culture. In order to control better the experiments, we therefore decided to use a human GBM cell line, the U87MG cells. While it was reported by Goffart *et al.* (5) that U87MG ATCC HTB-14 cells express the CXCR4 receptor, the cells we brought from the same source, did not. Indeed, the CXCR4 receptor can be more or less expressed depending on the environment. In order to overcome intrinsic and extrinsic variations in CXCR4 expression in these cells, U87MG were transfected previously in our laboratory by Dr Delphine Séhédic with a lentivirus coding for this receptor, which resulted in the stable expression of the target CXCR4 in U87MG. The cells were transfected with two lentiviruses: one encoding CXCR4 and the red fluorescent protein (RFP) (U87MG-CXCR4$^+$)

and one control lentivirus (U87MG-CXCR4$^-$) (Figure 3. 1-AFigure 3. 1). Séhédic *et al.* (6) grew a chimeric tumour composed of U87MG-CXCR4$^+$ and -CXCR4$^-$ cells in mice. As shown in Figure 3. 1-B, U87MG-CXCR4$^-$ cells composed the core of the tumour while U87MG-CXCR4$^+$ cells infiltrated the healthy surrounding tissues, demonstrating once more the implication of the CXCR4 receptor in the invasive ability of the GBM.

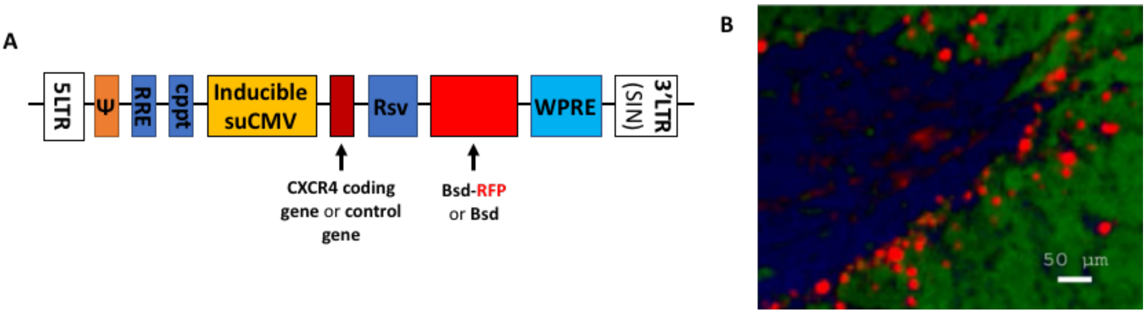

Figure 3. 1: (A) Schematic representation of lentivirus coding gene for CXCR4 or control gene, and (B) fluorescence spectral imaging analysis showing the infiltrative nature of CXCR4 positive cells (in red) from the tumour core (blue) to the healthy tissue (green). Adapted from (6).

In this study, the ability of SDF-1α to increase the migration of U87MG cells bearing the CXCR4 receptor was evaluated thanks to an agarose drop assay.

2. Materials and methods

2.1. Cell line

U87-MG cells (American Tissue Culture Collection, Rockville, Maryland, USA) were previously transfected to express or not the CXCR4 receptor by Séhédic *et al*. (6). Cells expressing the CXCR4 also expressed the red fluorescent protein (RFP). Cells expressing the receptor were named U87MG-CXCR4$^+$ and cells without the receptor were named U87MG-CXCR4$^-$. They were cultured at 37°C and 5% CO$_2$ in DMEM high glucose media (Sigma Aldrich) supplemented with 10% fetal bovine serum (FBS), and 1% penicillin/streptomycin and subcultured every 3-4 days.

2.2. Flow cytometry

U87MG-CXCR4$^+$ cells were regularly tested by flow cytometry to ensure that the CXCR4 receptor was not lost through the passages. Cells were first incubated with a CXCR4 primary antibody (5 µg/mL, CD184, BD Pharmingen) 1h at 4°C or with IgG2a (BD Biosciences, Le Pont de Claix, France). After being washed with PBS containing 5% FBS and

0.02% azide, cells were incubated with FITC-conjugated goat anti-mouse secondary antibody (Dako, Trappes, France) 30 min at 4°C. Subsequently, samples were analysed on a BD FACSCalibur™ fluorescent-activated flow cytometer and flow cytometry acquisition was performed on the BD CellQuest™ software (BD-Biosciences). Presence of the CXCR4 receptor and of the RFP was detected with the FITC and PE filter respectively.

2.3. Agarose drop assay

The ability of SDF-1α (Miltenyi Biotec) to attract cells with the CXCR4 receptor was evaluated using an agarose assay as described by Milner *et al*. (7). Briefly, a 24-well plate was previously coated with extracellular matrix from U87MG cells. To do so, wells were firstly coated with poly-D-lysine (PDL, Sigma) then U87MG cells were cultured in the wells for 48h and finally lysed with pure water, washed with PBS and air dried under sterile condition before use. Then, a 2 µL drop of low melting point low gelling temperature agarose (Sigma-Aldrich) at 1% (w/v) in PBS containing 100,000 cells was placed in the centre of a well of a 24-well plate previously coated with extracellular matrix from U87MG cells. The agarose was allowed to solidify by incubating the plate at 4°C for 10 minutes. Media, without serum and with or without the chemokine, was then carefully added on top of the agarose solid drops. Concentrations from 0 to 80 ng/mL of SDF-1α were tested on U87MG CXCR4$^+$ cells and U87MG CXCR4$^-$ cells. Plates were incubated for 3 days at 37°C and 5% CO_2. Pictures were finally taken using a microscope equipped with a camera and the distance of migration was measured at 4 points of the drop between the edge of the drop and the front of migration (as described in Figure 3. 2) with imageJ 1.52e software. In all cases, 9 drops were done for each condition.

Figure 3. 2: Schematic representation of the agarose drop assay. A drop of cells in agarose is deposited in a well and covered with media with or without SDF-1α. After 3 days, the distance of migration is measured at 4 points (red arrows) as the distance from the edge of the drop to the edge of the migration front.

The effect of cell proliferation on the migration was evaluated by means of an agarose drop assay with aphidicholin (ADC). ADC is a chemical which has the property of blocking cell proliferation (8). For this assay, SDF-1α was used with a concentration of 40 ng/mL and ADC with a concentration of 20 µg/mL.

2.4. Statistical analysis

The data were statistically analysed using an ANOVA test with Prism 7 software. In all statistical comparisons $p < 0.05$ was considered statistically significant.

3. Results and discussion

3.1. Flow cytometry

As shown in Figure 3. 3, 92% of the cells were in Q2 for the U87MG-CXCR4^{+} cells and 99% of the cells were in Q3 for the U87MG-CXCR4^{-} cells meaning that U87MG-CXCR4^{+} cells possessed the CXCR4 receptor with the RFP while the U87MG-CXCR4^{-} cells did not after 32 passages as they were constructed.

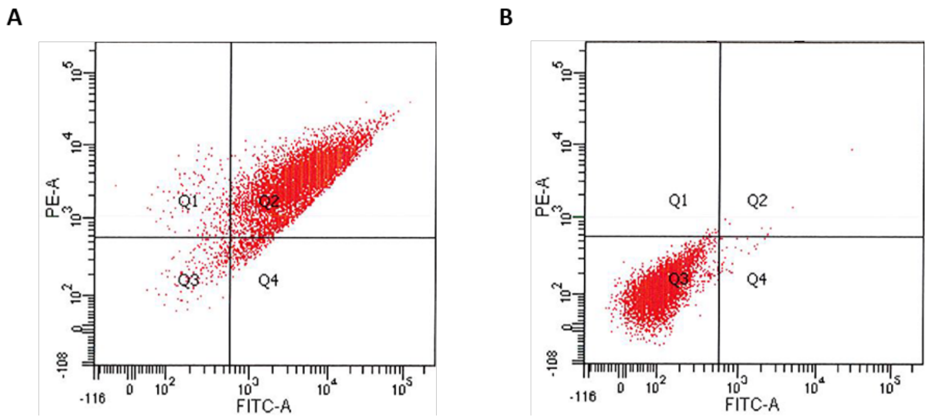

Figure 3. 3: Analysis of the U87MG-CXCR4^{+} (A) and U87MG-CXCR4^{-} (B) cells by flow cytometry. PE measures the RFP and FITC the CXCR4 receptor.

3.2. Migration assay

The migration of U87MG-CXCR4^{-} was not dependent of the SDF-1α concentration, as expected (Figure 3. 4-A), on the contrary of the migration of U87MG-CXCR4^{+}. The distance was found significantly different compared with the migration at 0 ng/mL for 20 and 40 ng/mL. A plateau was reached after 40 ng/mL of SDF-1α. Surprisingly, it was observed that, without SDF-1α, U87MG-CXCR4^{-} migrated further than U87MG-CXCR4^{+}. It was hypothesised that this phenomenon was due to a difference in the proliferation of the cells as the U87MG-CXCR4^{-} cells proliferated faster than the U87MG-CXCR4^{+} cells (data not showed). In order to test this hypothesis, a blocker of proliferation, the ADC, was used.

When the proliferation was blocked with ADC, almost no migration was observed without SDF-1α (139 µm ± 40 µm) while cells migrated in presence of 40 ng/mL SDF-1α (409 µm ± 29 µm) (Figure 3. 4-B). Moreover, we can see that the cells migrated less with ADC. The distance of migration for the experiments without ADC was therefore due to a combination of migration and proliferation.

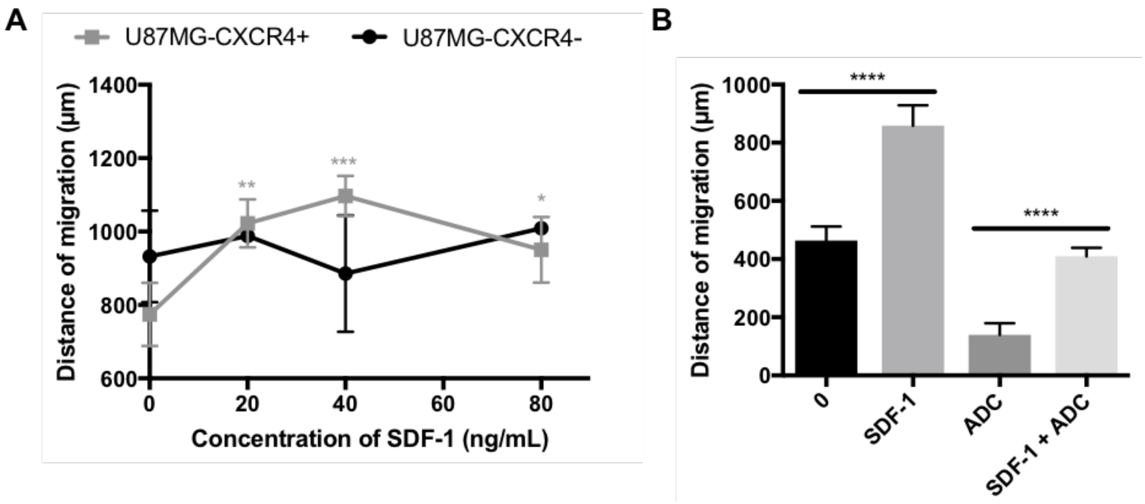

Figure 3. 4: Distance of migration from the agarose drop (A) with different concentrations of SDF-1α in the media between 0 and 80 ng/mL for U87MG-CXCR4^{+} and CXCR4^{-} cells, and (B) with 0 or 40 ng/mL SDF-1α and with or without ADC for U87MG-CXCR4^{+}. Paired comparisons were conducted against the corresponding condition without SDF-1α for (A). ANOVA analysis: *$p<0.0001$, **$p<0.0001$, ***$p<0.0001$, ****$p<0.0001$.

This assay is an interesting tool to evaluate the activity of SDF-1α along formulations. It was used to validate the activity of the protein along a process of encapsulation in PLGA nanoparticles and electrospinning developed by Muhammad Haji Mansor and published in European Journal of Pharmaceutics and Biopharmaceutics (9) (Annexe 1).

4. Conclusion

The agarose drop assay with U87MG-CXCR4^{+} cells can be used to evaluate the activity of SDF-1α after formulation, freeze-drying or storage for example. Moreover, it allowed us to validate the model, U87MG cells bearing the CXCR4 receptor migrating further in presence of SDF-1α on the contrary of the U87MG without the receptor.

REFERENCES

1. Janowski M. Functional diversity of SDF-1 splicing variants. Cell Adhes Migr. 2009;3(3):243–9.
2. Ehtesham M, Winston JA, Kabos P, Thompson RC. CXCR4 expression mediates glioma cell invasiveness. Oncogene. 2006;25(19):2801–6.
3. Zhou Y, Larsen PH, Hao C, Yong VW. CXCR4 is a major chemokine receptor on glioma cells and mediates their survival. J Biol Chem. 2002;277(51):49481–7.
4. Zagzag D, Esencay M, Mendez O, Yee H, Smirnova I, Huang Y, et al. Hypoxia- and Vascular Endothelial Growth Factor-Induced Stromal Cell-Derived Factor-1α/CXCR4 Expression in Glioblastomas. Am J Pathol. 2008;173(2):545–60.
5. Goffart N, Kroonen J, Di Valentin E, Dedobbeleer M, Denne A, Martinive P, et al. Adult mouse subventricular zones stimulate glioblastoma stem cells specific invasion through CXCL12/CXCR4 signaling. Neuro Oncol. 2015;17(1):81–94.
6. Séhédic D, Chourpa I, Tétaud C, Griveau A, Loussouarn C, Avril S, et al. Locoregional confinement and major clinical benefit of188Re-loaded CXCR4-targeted nanocarriers in an orthotopic human to mouse model of glioblastoma. Theranostics. 2017;7(18):4517–36.
7. Milner R, Edwards G, Streuli C, Ffrench-Constant C. A role in migration for the alpha V beta 1 integrin expressed on oligodendrocyte precursors. J Neurosci. 1996;16(22):7240–52.
8. Ikegami S, Taguchi T, Ohashi M, Oguro M, Nagano H, Mano Y. Aphidicolin Prevents Mitotic Cell DIvision by Interfering with the Activity of DNA Polymerase α. Vol. 275, Nature. 1978. p. 458–60.
9. Haji Mansor M, Najberg M, Contini A, Alvarez-Lorenzo C, Garcion E, Jérôme C, et al. Development of a Non-toxic and Non-denaturing Formulation Process for Encapsulation of SDF-1α into PLGA/PEG-PLGA Nanoparticles to Achieve Sustained Release. Eur J Pharm Biopharm. 2018;125(November 2017):38–50.

CHAPTER IV: Biological evaluation of SF-HA and SF-HA-hep sponges

Table of content

CHAPTER IV

Biological evaluation of SF-HA and SF-HA-hep sponges

1. Introduction

Sponges made of SF, HA and hep were produced and it was determined that the SF-HA and SF-HA-hep sponges were the most interesting as they were combining the softness of the HA-PLL sponge and the slow degradation of the SF sponge. The next step of the project was to study the interaction between GBM cells and the SF-HA and SF-HA-hep sponges as well as the safety of the sponges. To do so, biocompatibility of the SF-HA and SF-HA-hep sponges was evaluated *in vitro* and *in vivo*. Biodegradability of the sponges and release of SDF-1α as well as its effect on the brain were evaluated *in vivo*. Finally, the effect of SDF-1α loaded in the SF-HA and SF-HA-hep sponges on the behaviour of U87MG-CXCR4$^+$ cells was evaluated.

2. Materials and methods

2.1. Cell lines

U87MG cells (American Tissue Culture Collection, Rockville, Maryland, USA) were previously transfected to express or not the CXCR4 receptor by Séhédic *et al*. (1). Cells expressing the CXCR4 also expressed the red fluorescent protein (RFP) and were named U87MG-CXCR4$^+$. The mouse fibroblasts NIH/3T3, the U87MG and the U87MG-CXCR4$^+$ cells were cultured at 37°C and 5% CO_2 in DMEM high glucose media (Sigma Aldrich) supplemented with 10% fetal bovine serum (FBS), and 1% penicillin/streptomycin and subcultured every 3-4 days.

2.2. Cytocompatibility

The cytocompatibility of the sponges was evaluated using U87MG cells and NIH/3T3 cells. Following ISO standard 10993-5 two different culturing methods were used: direct contact and indirect contact (Figure 4. 1). The direct contact method allows for the physical interaction of the cells and the material while the indirect contact method allows for interaction of any leachable products with the cells. For both methods, cells were seeded in a 24-well plate with different densities depending on the type of cells and the duration of the assay and incubated 24h at 37°C and 5% CO_2 prior addition of the sponges. NIH/3T3 cells were seeded at a density of 40,000 cells/well in 500 µL for 24h and 10,000 cells/well for 72h. U87MG cells were seeded at a density of 80,000 cells/well in 500 µL for 24h and 20,000 cells/well for 72h.

Swollen SF, HA-PLL, SF-HA and SF-HA-hep sponges were firstly cut to obtain cylinders with 2 mm height and then sterilized under UV light for 1h. For evaluation of the washing technique, sponges were either washed for 24h in 15 mL PBS under stirring (PBS changed 5x) at RT or 5 times 30s in a sonicator in 15 mL PBS (PBS changed between each sonication) followed by 1h under stirring at RT. Immediately before use, sponges were washed 3 times with PBS under sterile conditions and then equilibrated in complete DMEM for 15 min.

For the direct contact method, sponges were directly added on top of the monolayer of cells in triplicates. Wells without sponges were used as control. After 24h or 72h incubation at 37°C and 5% CO_2, sponges were removed by aspiration and the media was replaced with 500 µL of resazurin 44 µM. Resazurin was also added in wells without cells to serve as blank. After 2h of incubation at 37°C, cell viability was estimated from the fluorescence intensity of the reduced product of resazurin, called resorufin, which is formed in the cytosol of alive cells. Fluorescence was measured using a ClarioStar microplate fluorometer (BMG Labtech GmbH, Ortenberg, Germany) at 545 nm excitation and 600 nm emission. All readings were normalised to those obtained with the control wells.

For the indirect contact method, suspended culture inserts (MilliCell, PET, 8 µm) were placed in the wells with sponges inside in triplicate. Inserts without sponges were used as control. 200 µL of media was added to cover completely the sponges. After 24h or 72h incubation at 37°C and 5% CO_2, inserts and sponges were removed and the media was replaced with 500 µL of resazurin 44 µM. The viability of the cells was evaluated with the same protocol than for the direct contact method.

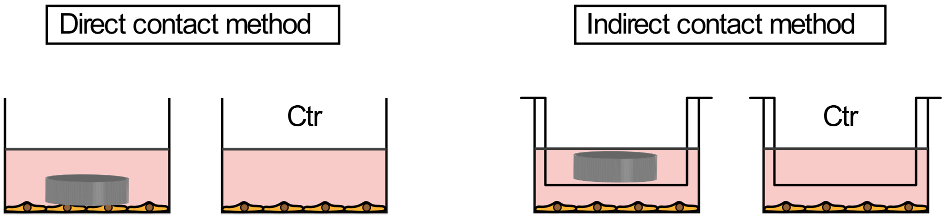

Figure 4. 1: Schematic representation of the direct contact and indirect contact method as well as their respective controls.

2.3. Cellular interaction with sponges

Sponges were swollen in PBS and sterilised 1h under UV light. Sponges were then washed 3 times with sterile PBS and equilibrated in complete media. To optimise the use of Sudan Black B (SB) to decrease the fluorescence of the sponge, 50,000 U87MG cells were deposited on the top of the sponge, placed in a well, and incubated 4h at 37°C and 5% CO_2 to allow cellular attachment before adding media to cover the sponges and incubate them 72h. Cells were then fixed with paraformaldehyde (PFA) 4% (w/v), permeabilised with 0.2% (w/v) Triton X-100 and saturated with normal goat serum (NGS) 10% (w/v). Sponges were covered with SB 0.3% (w/v) in 70% (v/v) ethanol for 30 min before or after immunomarking. The actin cytoskeleton of the cells was stained with ActinRed 555 (Thermo Fisher Scientific, Waltham, MA) and the nuclei with DAPI (Thermo Fisher Scientific, Waltham, MA). Stained cells were visualised using a confocal microscope Leica TCS SP8 AOBS (Leica Microsystems, Wetzlar, Germany).

In order to evaluate the effect of SDF-1α on U87MG overexpressing the CXCR4 receptor, 50,000 U87MG-CXCR4$^+$ cells were deposited on SF-HA or SF-HA-hep sponges prepared as explained in the paragraph above excepted that a 5 µL drop containing 150 ng of SDF-1α was deposited on top of the sponges for half of them. Sponges were incubated 1, 7, 14 or 28 days in DMEM without FBS and media was changed 2 times per week. Cells were finally fixed, permeabilised and stained as explained above.

2.4. Implantation of sponges in rat brain parenchyma

Fischer female rats aged 8-10 weeks were obtained from Janvier Labs (Le Genest-Saint-Isle, France). The protocol was approved by the Ethical Committee for Animal Experimentation of Région Pays de la Loire (authorization number #2015.20). Animals were anesthetised by intraperitoneal injection of a mixture of ketamine (100 mg/kg) and xylazine (13 mg/kg) and positioned in a Kopf stereotaxic instrument. A 10 mm-long incision was made along the midline to create access to the surface of the skull. Following this, a burr hole was drilled into the skull using a high-speed drill to expose the brain tissues underneath. A portion of the brain cortex was then cut using a biopsy punch device (Figure 4. 2-A) and subsequently removed using vacuum suction (Figure 4. 2-B) to create a cavity that was approximately 3 mm wide and 2 mm deep (Figure 4. 2-C). SF-HA and SF-HA-hep sponges were swollen in PBS, cut transversally to obtain 2 mm height cylinders, and sterilised with UV light for 1 hour the day before the surgery. The sponges were cut one by one immediately before implantation with a 3 mm diameter biopsy punch with a push-button (Figure 4. 2-D-F) and implanted in the cavity with the biopsy punch (Figure 4. 2-G,H). Following the implantation of the scaffold into the cavity, the wound was sutured (Figure 4. 2-I), and the rats were allowed to awaken without any further intervention. All rats became fully conscious and active between 1 and 2 hours after surgery and did not display any sign of distress. In control rats, the same surgical procedure was also performed, but no scaffold was implanted. Two groups of rats were set up non-concurrently: one group, consisted of 9 rats (3 implanted with SF-HA sponges, 3 implanted with SF-HA-hep sponges and 3 controls), was intended for the short-term study (sacrificed after 8 days) while the other group, consisted of 12 rats (4 implanted with SF-HA sponges, 4 with SF-HA-hep sponges and 4 controls), was intended for the long-term follow-up (sacrificed after 118 days).

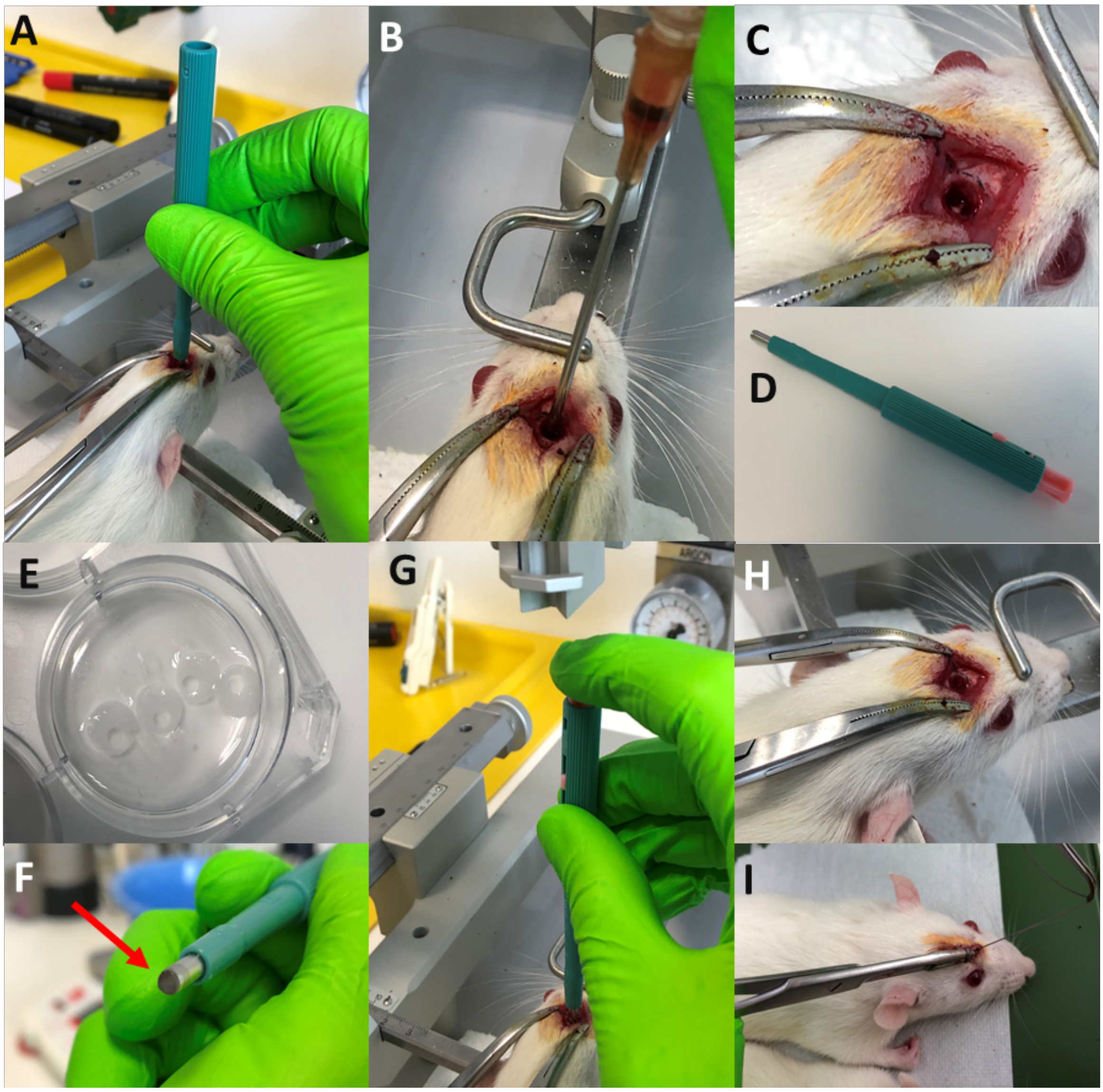

Figure 4. 2: Surgical procedure for sponge implantation in rats. (A) The brain was cut using a 3 mm diameter biopsy punch and (B) removed using vacuum suction creating (C) a resection cavity of 3 mm diameter and about 2 mm deep. (D) A 3 mm diameter biopsy punch with a push-button was used to (E) cut the swollen sponges. (F) The sponge stayed inside the biopsy punch. (G) It was implanted in the cavity by placing the biopsy punch inside it and pressing the button delicately. (H) The sponge implanted had exactly the same size than the cavity. (I) Finally, the wound was sutured.

2.5. MRI analysis

MRI analysis was performed on D1 and D6 for the short-term study and D6 and D76 for the long-term study, with a Bruker Biospec 70/20 system operating at 7T, under isoflurane (0.5% 1L/min O_2) anesthesia, with the monitoring of respiratory parameters. T2-weighted images were acquired with a multispin echo sequence [FOV = 30 x 30 mm, 9 axial 0.8 mm slices (gap = 0.1 mm), matrix 256 x 256, TR = 2.5 s, 25 TE = 30 ms].

2.6. Histology

Rats were sacrificed at 8 days and 118 days (4 months) after implantation. Brains were collected and fixed in formalin for 10 days, embedded in paraffin, sections were cut and stained with hematoxylin and eosin (HE).

2.7. *In vivo* release of SDF-1α in rat brains

To study the *in vivo* release of SDF-1α from the sponge to the brain, an SDF-1α coupled with AlexaFluor647 (AF-SDF-1α) at the C terminal (Almac, Scotland) was used. Only the SF-HA-hep sponge was used since the SF-HA sponge was completely degraded after 8 days. Sponges were swollen in PBS, cut transversally to obtain 2 mm height cylinders, and sterilised with UV light for 1 hour the day before the surgery. The sponges were cut one by one immediately before implantation with a 3 mm diameter biopsy punch with a push-button. Sponges were taken out of the biopsy punch, slightly dehydrated by plotting them on a gauze compress and rehydrated by adding 3 µL of AF-SDF-1α (150 ng) on the top of the sponge and finally implanted in the cavity as described in section 2.4. With this process, the full volume of AF-SDF-1α was absorbed by the sponge, resulting in a theoretical 100% loading. Rats were sacrificed after 7 days and brains were collected. Brains were frozen in isopentane between -20°C and -30°C and stored at -80°C. Brains were cut axially in the region of interest with a Cryostat Leica CM3050 S (Leica Biosystems, Nussloch, Germany) to obtain 10 µm thick slices that were deposited on gelatinated Superfrost slides (Thermo Fischer Scientific, Braunschweig, Germany). Slides were stored at -20°C until immunomarking.

2.8. Immunohistochemistry

Sections were permeabilised with PFA 4% (w/v) at 4°C for 20 min, permeabilised with 0.025% (w/v) Triton X-100 in PBS for 10 min and saturated with NGS 10% (w/v) in PBS for 2h. They were then incubated overnight at 4°C with polyclonal rabbit IgG anti-SDF-1 (Abcam, Cambridge) followed by 1h incubation at RT with the secondary antibody goat anti-rabbit AlexaFluor 488 (Cell Signaling Technology). Cell nuclei were stained with DAPI prior to mounting sections with Dako fluorescence mounting media (Dako, CA, USA) and coverslips. Stained sections were visualised using a confocal microscope Leica TCS SP8 AOBS (Leica Microsystems, Wetzlar, Germany).

2.9. Statistical analysis

The data were statistically analysed using an ANOVA test with Prism 7 software. In all statistical comparisons $p < 0.05$ was considered statistically significant.

3. Results and discussion

3.1. Cytocompatibility

Cytotocompatibility of the sponges has been evaluated via indirect and direct contact method at 24 and 72h with normal cells (mouse fibroblast cell line NIH/3T3) and glioblastoma cells (U87MG cell line) (Figure 4. 3-A-D). NIH/3T3 cells were chosen as they have been reported to be highly-sensitive to chemical-induced toxicities (2). The SF and HA-PLL sponges were found to be cytocompatible in every condition tested. For the SF-HA sponge, cytotoxicity was observed only after 72h with the direct contact method on NIH/3T3 cells (71 ± 14% viability). Moderate cytotoxicity was found for the SF-HA-hep sponge at 24h with the direct contact method on U87MG cells (76 ± 9% viability) and at 72h with the indirect contact method on NIH/3T3 (63 ± 19% viability), with the direct contact method on NIH/3T3 (39 ± 9% viability) and on U87MG (64 ± 9% viability). We can therefore consider the SF and HA-PLL sponge cytocompatible. Moreover, the SF-HA sponge is more cytocompatible than the SF-HA-hep sponge. Different washing techniques were tested to eliminate traces of crosslinkers to try to improve the cytocompatibility of SF-HA-hep sponges. The first one consisted in a 24h wash in PBS under mild agitation, the second one in a 5x30s sonication followed by 1h in PBS under mild agitation. The direct contact method at 72h with NIH/3T3 cells has been chosen to evaluate the effect of the washing, being the most sensitive to toxicity. However, no improvement was observed (Figure 4. 3-E). In order to determine whether EDC and NHS or the hep were responsible for this cytotoxicity, two new sponges were produced, and cytotoxicity was evaluated with the direct contact method at 72h with NIH/3T3 cells. The first one was composed of SF and HA crosslinked with the same concentration of crosslinkers than SF-HA-hep (C_{EDC} = 15 mg/mL, C_{NHS} = 5.5 mg/mL) and was called here SF-HA(+). The second one was composed of SF, HA and hep crosslinked with the same concentration of crosslinkers than SF-HA (C_{EDC} = 5 mg/mL, C_{NHS} = 1.8 mg/mL) and was called here SF-HA(+). Because of the low concentration of crosslinkers in the SF-HA-hep(-) sponge, this sponge lost its shape in the media. Sponges with the same concentration of crosslinkers showed the same cytotoxicity, a low concentration of crosslinker leading to an increase in viability (Figure 4. 3-E).

Free heparin is used as an anticoagulant and can therefore cause thrombocytopenia or haemorrhagic complications (3,4). However, when modified or covalently incorporated in scaffolds, it can be safely used for biomedical applications (5–7). EDC and NHS promote the formation of covalent crosslinks between a carboxyl and a primary amine but do not remain as part of the crosslink (see Figure 2.1-C). Therefore, there is no possibility of toxic substances being released into tissues from crosslink breakdown after implantation into patients as it can be washed away from the hydrogel with water (8). It is therefore used for the synthesis of hydrogel for different biomedical applications (9–11) and Qazvini *et al.* (12) described this crosslinking technique as non-toxic. However, we found that the crosslinkers were responsible for the cytotoxicity observed here. An appropriate washing protocol should therefore be found, or the crosslinking should be optimised to reduce the concentration of crosslinkers in the SF-HA-hep sponges. Since the cytotoxicity observed was mild (only found after 72h), the SF-HA-hep sponge biocompatibility was still tested *in vivo*.

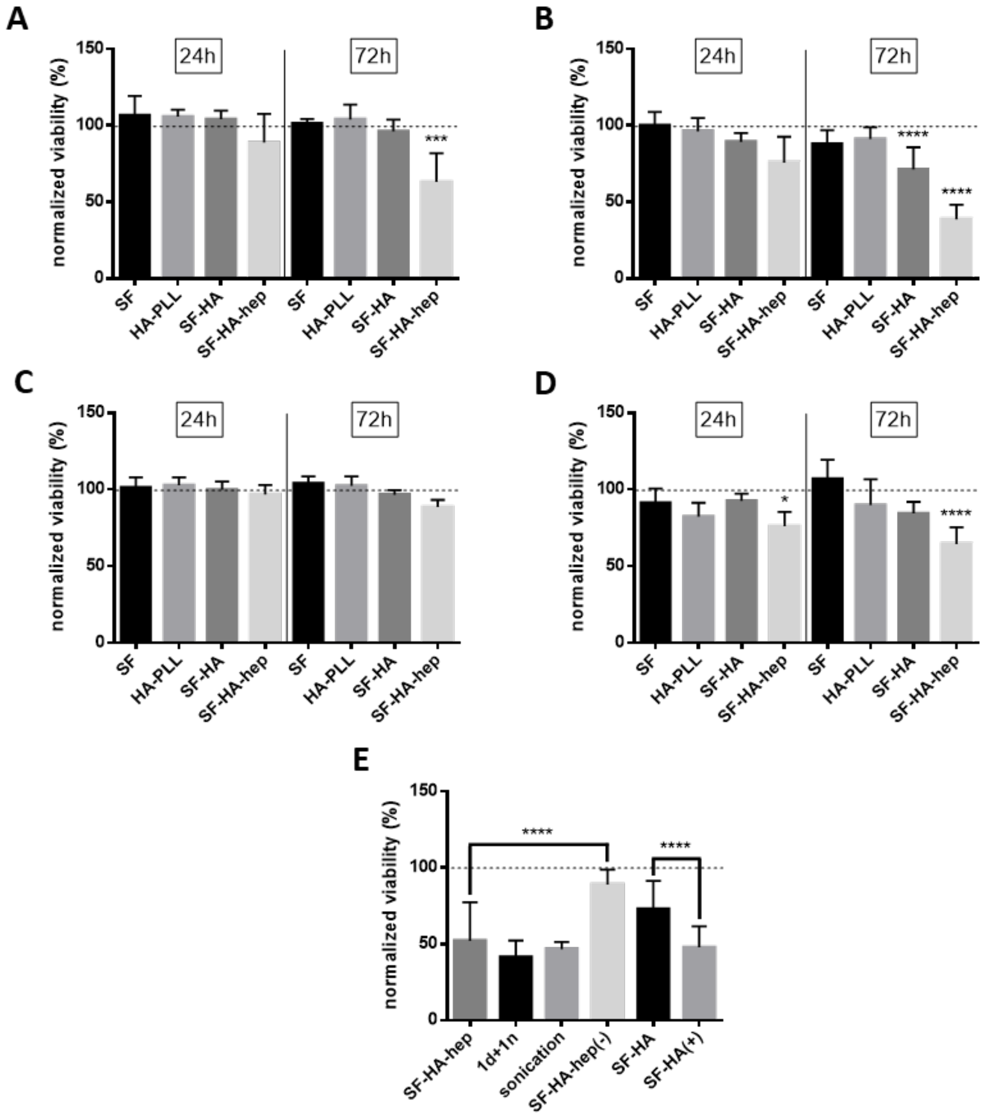

Figure 4. 3: Evaluation of the cytotoxicity of SF, HA-PLL, SF-HA and SF-HA-hep sponges by the indirect contact method (A,C) and the direct method (B,D) with NIH/3T3 cells (A,B) and U87MG cells (C,D) at 24h and 72h. Effect of the washing process as well as the concentration of crosslinkers on the cytotoxicity of cells (E). ANOVA analysis were done to compare the wells with sponges with the corresponding controls for A-D: *p<0.05, **p<0.01, ***p<0.001, ****p<0.0001.

3.2. Cellular interaction with the sponges

3.2.1 Decrease of the SF fluorescence with Sudan Black B

DAPI and ActinRed are used to mark the nuclei (in blue) and the actin skeleton (in red) of cells. However, they adsorbed unspecifically by SF as shown in Chapter 2 section 3.6, making it difficult to observe the cells in the sponges. According to a protocol described by Neo *et al.* (13), SB, a molecule used usually to stain lipids on tissues, can be used to decrease the fluorescence of the SF. U87MG cells deposited on SF-HA-hep sponges and incubated 72h were used to test the protocol. Three conditions have been tested: (i) immunomarking with DAPI and ActinRed (Figure 4. 4-A), (ii) incubation with SB before immunomarking (Figure 4. 4-B) and (iii) incubation with SB after immunomarking (Figure 4. 4-C). Without SB, cells were hardly distinguishable from the sponge while, when SB was used after immunomarking, ActinRed was quenched as well as the signal from the sponge. When sponges were incubated in SB before immunomarking, signal from the sponge was highly decreased and cells were therefore visible. This protocol worked better to decrease the red signal than the blue. This observation can be explained as SB is known to undergo strong hydrophobic interactions and interact with negatively charged structures like SF (14). Adding SB before staining should therefore block the adsorption of DAPI and ActinRed to the sponge.

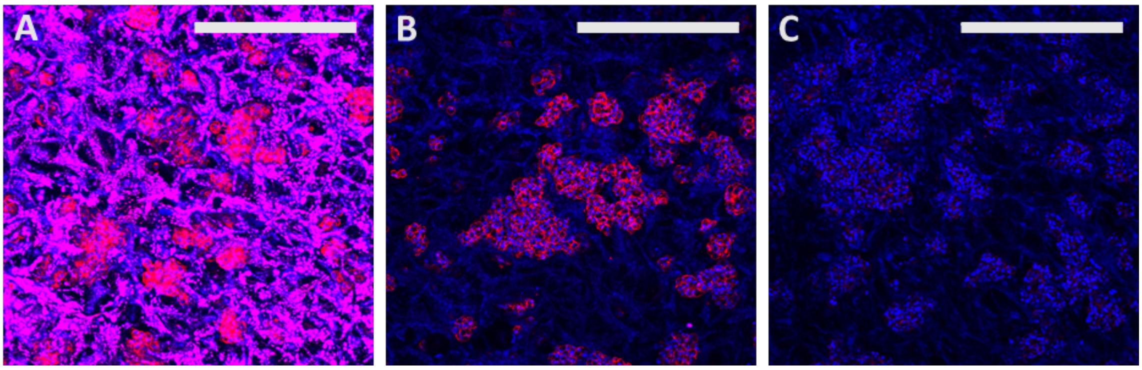

Figure 4. 4: U87MG cells incubated for 72h on SF-HA-hep sponges and marked following different protocols: without SB (A), with SB added before (B) and after (C) immunomarking with DAPI (nuclei, *blue*) and ActinRed (actin, *red*). Scale: 500 µm.

3.2.2 Morphology of U87MG-CXCR4$^+$ cells on sponges

In order to study the interaction between GBM cells and the sponges, U87MG-CXCR4$^+$ cells have been deposited on SF-HA and SF-HA-hep sponges with or without SDF-1α. After 1, 7, 14 and 28 days, cells were fixed with PFA, incubated in SB and stained with DAPI and ActinRed (Figure 4. 5). After 1 day (Figure 4. 5-A-D), cells were aggregated between each other with a round morphology and were situated principally on the top of the sponge (about 200 µm deep). Similar observations were done after 7 days (data not shown) while cellular aggregates seemed larger. After 14 days, cells were more dispersed in the sponge and aggregates were not found. Similar observations were done after 28 days and cells were found deeper in the sponges (Figure 4. 5-E-G). This showed that U87MG-CXCR4$^+$ cells were able to survive a month and interact with both SF-HA-hep and SF-HA sponges. This characteristic is essential to trap GBM cells as it suggests that cells would stay inside the trap until they can be eliminated. However, no differences were observed between the type of sponge and the presence of SDF-1α and a potential haptotaxis could not be quantified as cells were non-homogeneously dispersed on the sponges.

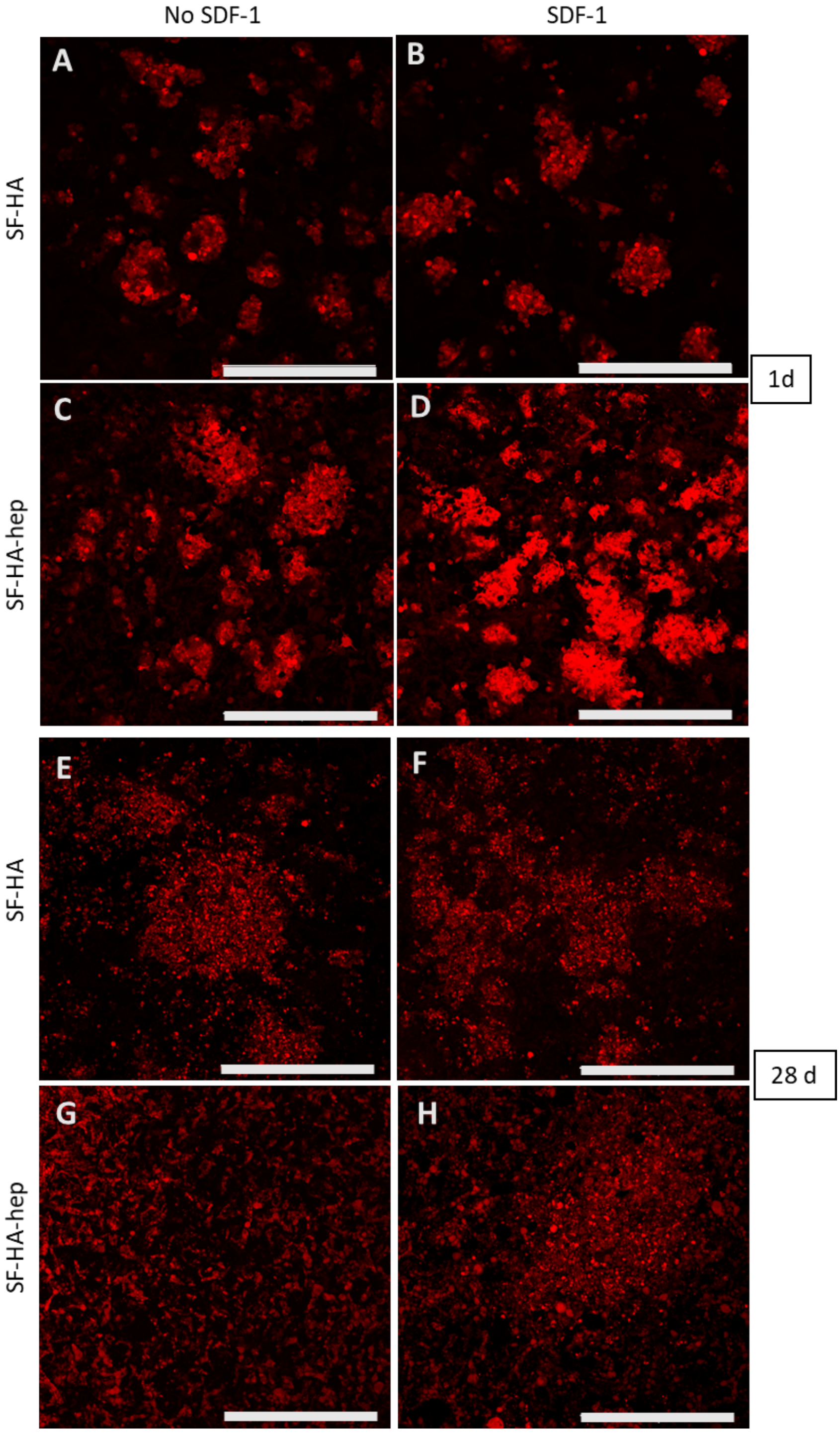

Figure 4. 5: Representative fluorescence images of U87MG-CXCR4$^+$ cells deposited on SF-HA (A,B,E,F) and SF-HA-hep (C,D,G,H) sponges with (B,D,F,H) or without (A,C,E,G) SDF-1α after 1 (A-D) and 28 days (E-H). Cells' cytoskeleton was stained with ActinRed. Scale: 500 µm.

3.3. *In vivo* biocompatibility and biodegradability

A resection cavity was formed using a 3 mm diameter biopsy punch. SF-HA and SF-HA-hep sponges were swollen in PBS, cut to have the same dimensions as the cavity, and implanted. A control consisted in the resection without implantation. All animals tolerated the surgical procedures and there was no evidence of neither systemic nor neurological disease in any animal throughout the course of the experiment. MRI images were taken 6 and 76 days after implantation. 3 rats per group were sacrificed 8 days after implantation and 4 rats per groups were sacrificed 4 months (118 days) after implantation. Brains were retrieved after sacrifice fixed in formalin, embedded in paraffin and sections were cut. Tissues were stained with HE for histological analysis.

Sponges could be observed by MRI 6 days after implantation (Figure 4. 6). After 76 days, a white spot was observed by MRI at the coordinate of the resection cavity which was interpreted as an infiltration of water inside the cavity. It seemed that the sponges were completely degraded at that time.

Eight days after implantation of the SF-HA-hep sponge, no signs of degradation were observed at the dissection. Some sponges were sticking to the skin covering the cavity and were therefore taken out of the brain when the brain was collected. When the sponges had stayed inside, they were systematically detached from the cavity upon slicing. They therefore appeared detached from the brain on the histology slides while the sponges were in contact with the brain tissue as they completely filled the cavity at the time of implantation. Sponges were infiltrated with neutrophils and pyocytes; necrosis was also found (Figure 4. 7). At the interface between the sponge and the brain tissue, an acute inflammatory response was observed with the presence of neutrophils, pyocytes, necrosis and neo-angiogenesis. Neutrophils are a type of phagocyte and one of the first responders of inflammatory cells to migrate toward a site of inflammation. A few hundreds micrometres away from the edge of the cavity, there were no signs of inflammation, and the rest of the brain was healthy. This reaction was considered as a normal reaction toward a foreign body. As a comparison, Gliadel® wafer, an approved implant for GBM treatment (see Chapter I, section 3.1.3), was implanted in monkeys and an histology analysis was performed over 72 days (15). They observed a narrow zone of necrosis as well as a subacute inflammatory response after 16 days that was no longer observed by day 72.

The SF-HA sponges implanted in rats were completely degraded after 8 days. Similarly to the control rats (cavity without sponge), a process of detersion (debris eliminated by the macrophages) and cicatrisation was observed as well as a local chronic inflammation with presence of macrophages and lymphocytes (Figure 4. 7). The rest of the brain was healthy.

After 118 days, slight chronic inflammation and hemosiderin-laden macrophages were observed in and/or at the edge of the cavity; no sign of inflammation was found away from the interface between the resection cavity and the brain for the three conditions studied (Figure 4. 8). Similarly, implantation of Gliadel® wafers in monkeys showed a chronic inflammation with a narrow zone of gliosis and hemosiderin-laden macrophages at the polymer-brain interface after 72 days of implantation.

Thus, the SF-HA-hep sponge seemed more immunogenic than the SF-HA sponge in the short term, but both sponges were completely degraded after 4 months with no difference compared to the control cavity. Moreover, only local reaction was observed and was similar to the implantation of Gliadel® wafers. Both sponges were therefore considered biocompatible and safe to use for brain implantation.

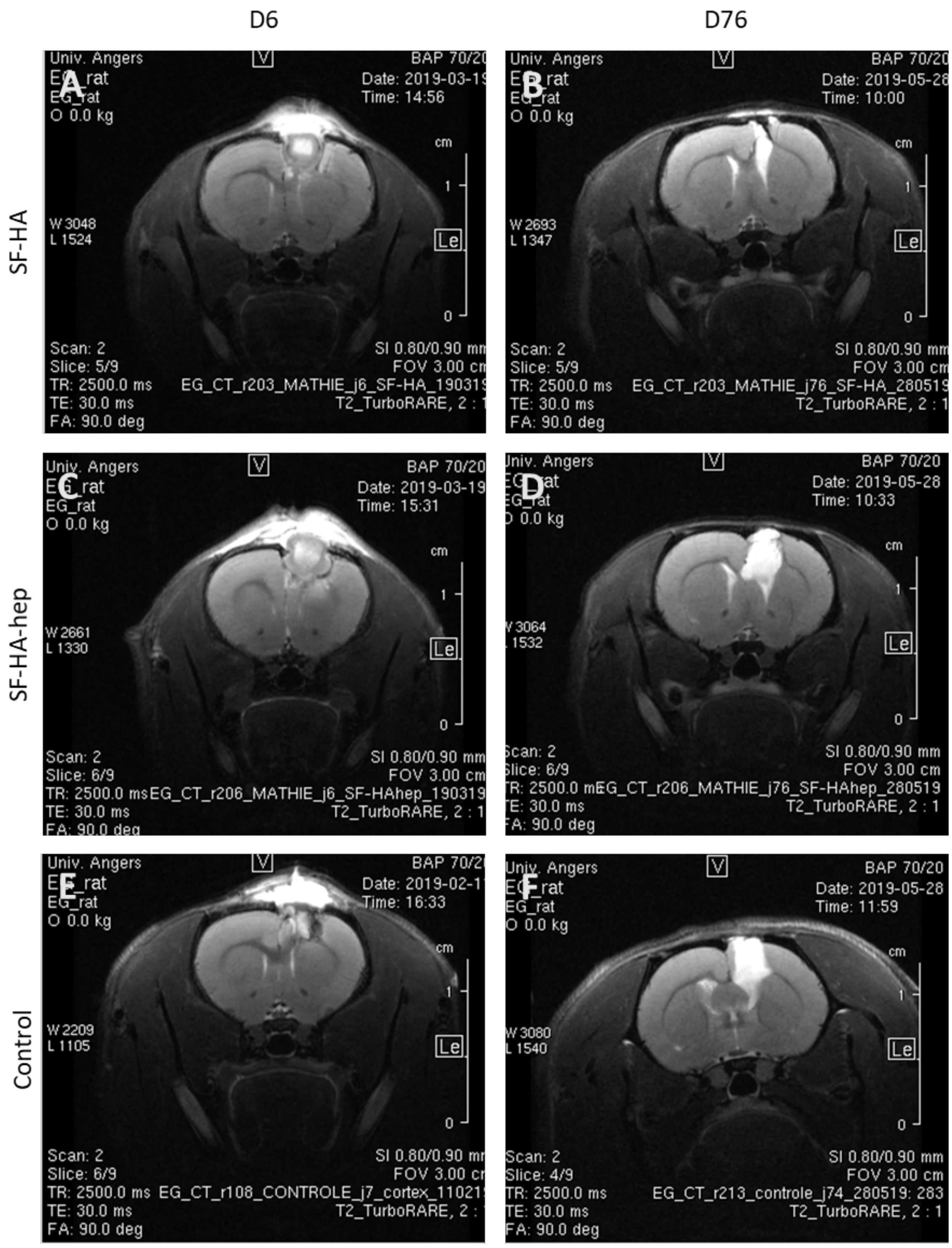

Figure 4. 6: Representative T2 MRI analysis of the rat’s brains 6 days (A,C,E) or 76 days (B,D,F) after implantation of the SF-HA (A,B) or the SF-HA-hep (C,D) sponges or nothing (control) (E,F).

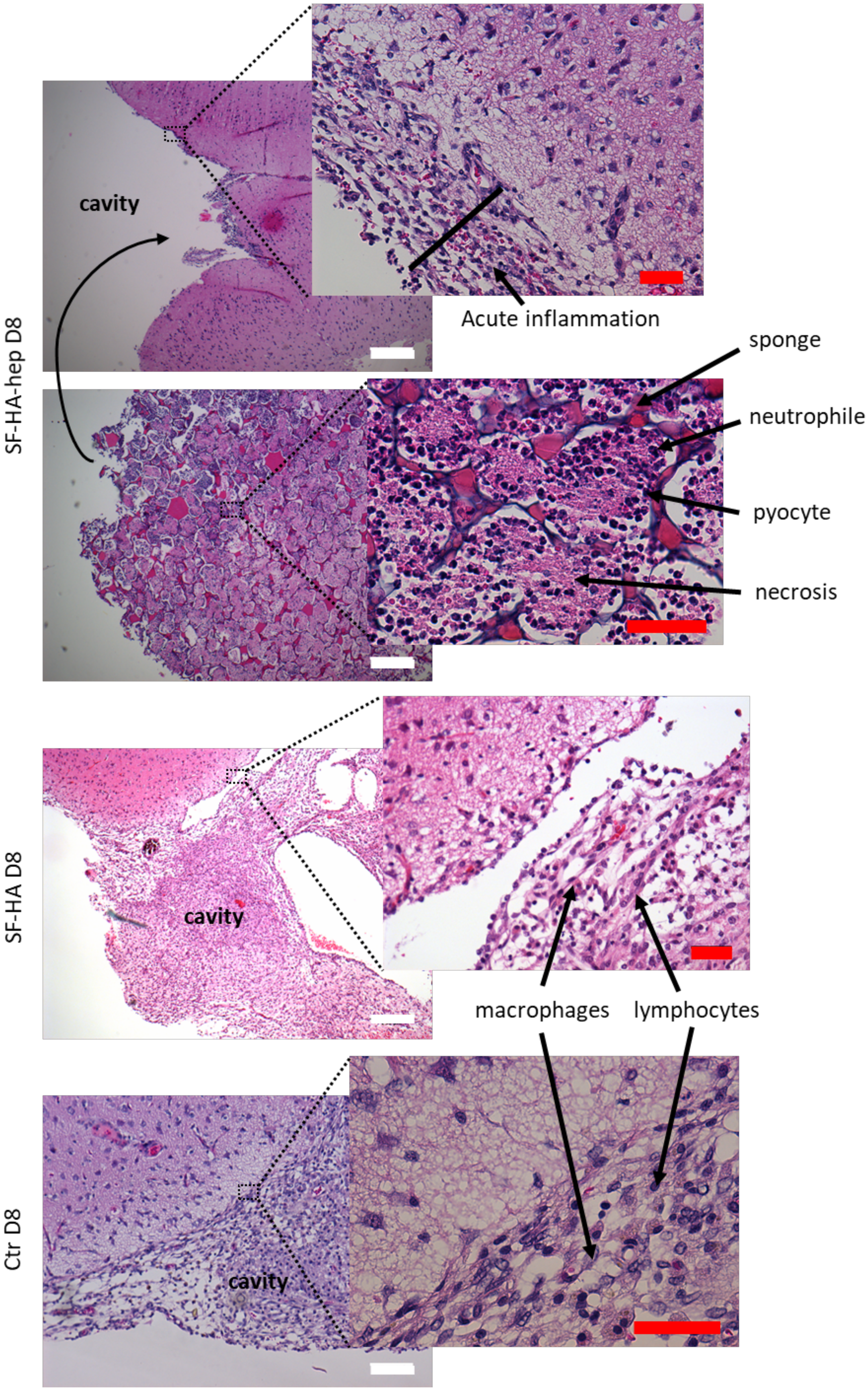

Figure 4. 7: HE stained-slide of a rat brain eight days after SF-HA-hep or SF-HA sponge implantation or after scrapping of the brain (control cavity with no sponge, Ctr D8). The white bar indicates 250 µm and the red 50 µm.

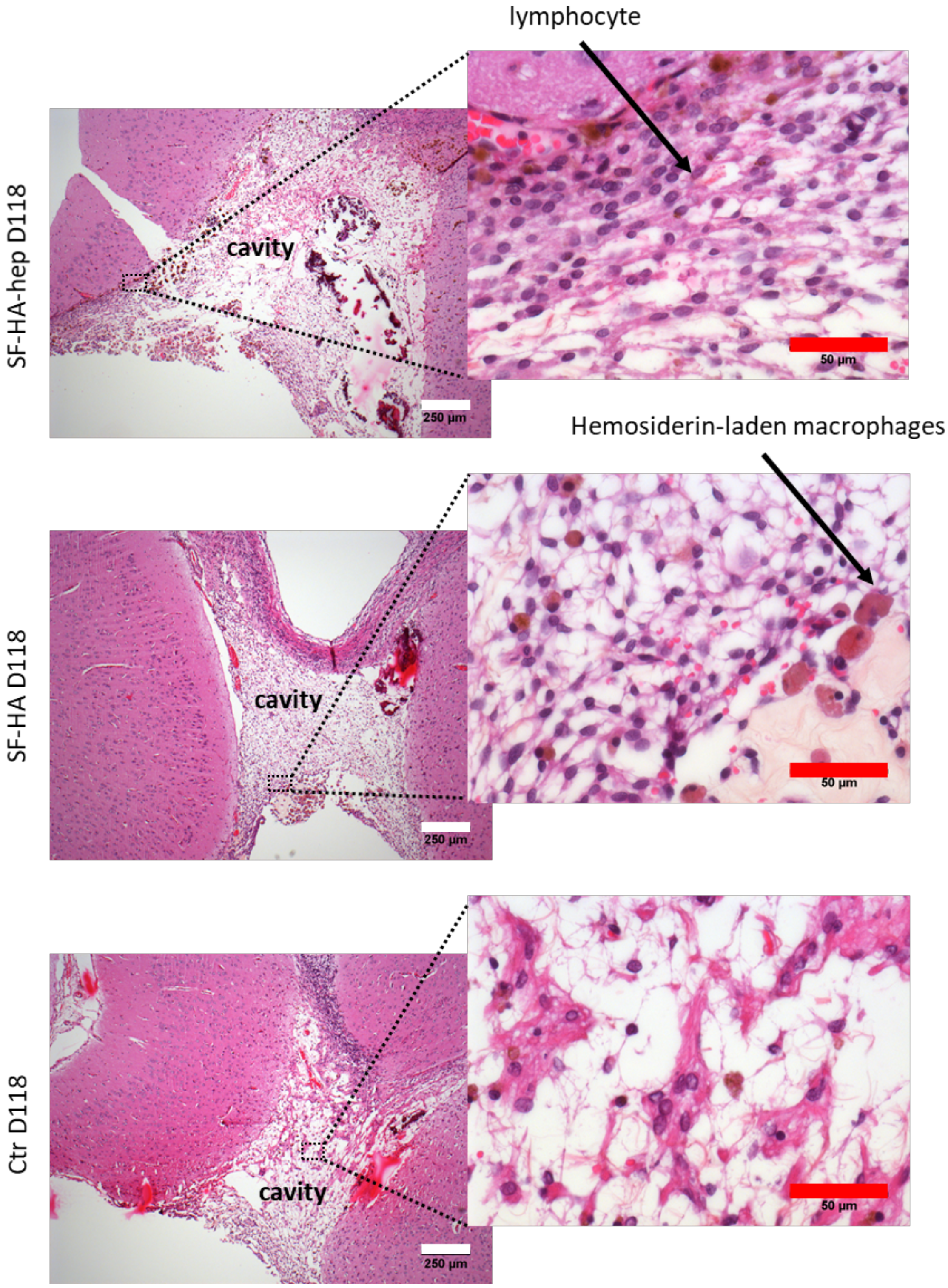

Figure 4. 8: HE stained-slide of a rat brain 118 days after SF-HA-hep or SF-HA sponge implantation or after scrapping of the brain (control cavity with no sponge, Ctr D118). The white bar indicates 250 µm and the red 50 µm.

3.4. *In vivo* release of SDF-1α

AF-SDF-1α was clearly visible inside the sponges after 8 days of implantation but was not detected in the brain tissues. Interestingly, it was not homogeneously spread along the sponge but distributed as droplets of about 20 µm diameter which corresponded to the internal structures observed in the sponges in Chapter II. We can therefore hypothesise that hep formed globules with SF inside the walls of the sponges and that AF-SDF-1α was adsorbed preferentially at those sites. More nuclei can be observed inside the sponge compared with the brain tissue. Considering the histological analysis made for SF-HA-hep sponges after 8 days, we can assume that it was due to an invasion of the sponge by inflammatory cells such as neutrophils. Endogenous SDF-1α was stained with an antibody coupled with FITC (green) and was distinguished from the exogenous SDF-1α as the latest was coupled with AlexaFluor 647 (red). Endogenous SDF-1α was found inside the sponge as well as at the margin of the cavity with or without the addition of AF-SDF-1α as well as in the control group but of less extent. It was probably produced as an inflammatory response in order to recruit immune cells. Indeed, histological analysis of the brains after 8 days (Figure 4. 7) showed recruitment of immune cells inside the sponge and at the sponge-brain interface such as neutrophils for the SF-HA-hep sponge but also macrophages for the cavity alone. It is known that such cells are able to produce SDF-1α in order to recruit more immune cells (16–18). It has been previously observed that injection of exogenous SDF-1α induces production of endogenous SDF-1α (19). However, this was not observed here at 8 days after implantation as it seems that the production of endogenous SDF-1α in the sponge without AF-SDF-1α was as strong as in the sponge with AF-SDF-1α though it was not possible to quantify it here. It can be explained by the absence of release from the SF-HA-hep sponge at this time.

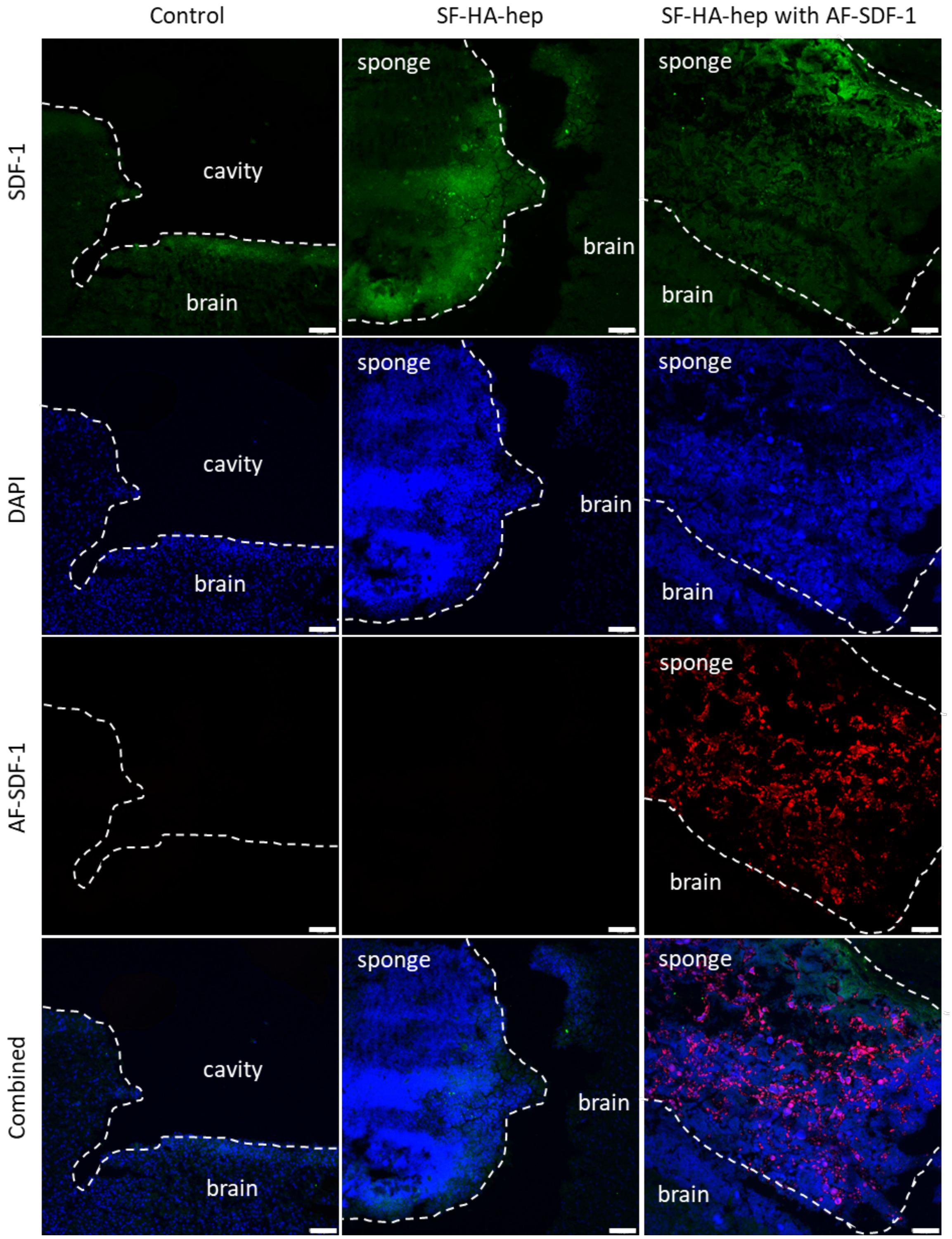

Figure 4. 9: Representative fluorescent images of the production of endogenous SDF-1α upon creation of a resection cavity (control), implantation of an SF-HA-hep sponge or implantation of an SF-HA-hep sponge loaded with AF-SDF-1α. The white bar indicates 100 µm.

4. Conclusion

In summary we demonstrated that both the SF-HA and the SF-HA-hep sponges were well tolerated by the rats although the SF-HA-hep sponge led to a decrease of cellular viability and a stronger immune reaction at short term. A strong difference in the degradation rate was observed as the SF-HA sponges implanted in the brains of rats were all completely degraded after 8 days while the structure of the SF-HA-hep sponges was intact at that time. Loading of SDF-1α into the sponges did not induce any visible reaction from U87MG-CXCR4$^+$ cells *in vitro* or from the brain *in vivo* which might be explained by the absence of SDF-1α release from the SF-HA-hep sponge.

REFERENCES

1. Séhédic D, Chourpa I, Tétaud C, Griveau A, Loussouarn C, Avril S, et al. Locoregional confinement and major clinical benefit of188Re-loaded CXCR4-targeted nanocarriers in an orthotopic human to mouse model of glioblastoma. Theranostics. 2017;7(18):4517–36.
2. Xia M, Huang R, Witt KL, Southall N, Fostel J, Cho MH, et al. Compound cytotoxicity profiling using quantitative high-throughput screening. Environ Health Perspect. 2008;116(3):284–91.
3. Sanders SW, Dukes GE, Gray P, Tolman KG. Toxicity of heparin in isolated rat hepatocytes. Biochem Pharmacol. 1984;33(14):2223–6.
4. Gurbuz HA, Durukan AB, Sevim H, Ergin E, Gurpinar A, Yorgancioglu C. Heparin toxicity in cell culture: A critical link in translation of basic science to clinical practice. Blood Coagul Fibrinolysis. 2013;24(7):742–5.
5. Zhao B, Zhao Z, Ma J, Ma X. Modulation of angiogenic potential of tissue-engineered peripheral nerve by covalent incorporation of heparin and loading with vascular endothelial growth factor. Neurosci Lett. 2019;705:259–64.
6. Rodrigues EM, Cornélio ALG, Godoi PH, da Costa PI, Rossa-Junior C, Faria G, et al. Heparin is biocompatible and can induce differentiation of human dental pulp cells. Int Endod J. 2019;52(6):829–37.
7. Choi W Il, Sahu A, Vilos C, Kamaly N, Jo SM, Lee JH, et al. Bioinspired Heparin Nanosponge Prepared by Photo-crosslinking for Controlled Release of Growth Factors. Sci Rep. 2017;7(1):1–9.
8. Gratzer PF, Lee JM. Control of pH Alters the Type of Cross-linking Produced by Treatment of Acellular Matrix Vascular Grafts. J Biomed Mater Res. 2001;58(2):172–9.
9. Fagerholm P, Lagali NS, Merrett K, Jackson WB, Munger R, Liu Y, et al. A biosynthetic alternative to human donor tissue for inducing corneal regeneration: 24-Month follow-up of a phase 1 clinical study. Sci Transl Med. 2010;2(46).
10. Xu X-F, Ren X-J, Gong D, Wang A-P, Xin Y, Wu Y, et al. Effect of carbodiimide cross-linking of decellularized porcine pulmonary artery valvular leaflets. Int J Clin Exp Med. 2014;7(3):649–56.
11. Tenkumo T, Vanegas Sáenz JR, Nakamura K, Shimizu Y, Sokolova V, Epple M, et al. Prolonged release of bone morphogenetic protein-2 in vivo by gene transfection with DNA-functionalized calcium phosphate nanoparticle-loaded collagen scaffolds. Mater Sci Eng C. 2018;92:172–83.
12. Taheri Qazvini N, Zinatloo S. Synthesis and characterization of gelatin nanoparticles using CDI/NHS as a non-toxic cross-linking system. J Mater Sci Mater Med. 2011;22(1):63–9.
13. Neo PY, Tan DJ-A, Shi P, Toh SL, Goh JC-H. Enhancing Analysis of Cells and Proteins by Fluorescence Imaging on Silk-Based Biomaterials: Modulating the Autofluorescence of Silk. Tissue Eng Part C Methods. 2015;21(2):218–28.
14. Pfüller U, Franz H, Preiß A. Sudan Black B: Chemical structure and histochemistry of the blue main components. Histochemistry. 1977;54(3):237–50.
15. Brem H, Tamargo RJ, Olivi A, Pinn M, Weingart JD, Wharam M, et al. Biodegradable polymers for controlled delivery of chemotherapy with and without radiation therapy in the monkey brain. J Neurosurg. 1994;80(2):283–90.
16. Nakayama E, Shiratsuchi Y, Kobayashi Y, Nagata K. The importance of infiltrating neutrophils in SDF-1 production leading to regeneration of the thymus after whole-body X-irradiation. Cell Immunol. 2011;268(1):24–8.
17. Wan X, Xia W, Gendoo Y, Chen W, Sun W, Sun D, et al. Upregulation of stromal cell-derived factor 1 (SDF-1) is associated with macrophage infiltration in renal ischemia-reperfusion injury. PLoS One. 2014;9(12):1–12.
18. Tu R, Peng Y, Wang Y, Tang X, Wang S. The stromal cell-derived factor 1/C-X-C chemokine receptor type 4 axis is important in neutrophil migration caused by cardiopulmonary bypass in children.

Interact Cardiovasc Thorac Surg. 2018;26(3):431–7.

19. Dutta D, Hickey K, Salifu M, Fauer C, Willingham C, Stabenfeldt SE. Spatiotemporal presentation of exogenous SDF-1 with PLGA nanoparticles modulates SDF-1/CXCR4 signaling axis in the rodent cortex. Biomater Sci. 2017;5(8):1640–51.

CHAPTER V: General discussion, Conclusion and Perspectives

Table of content

CHAPTRE V

General discussion, Conclusion and Perspectives

1. Main contributions

GBM is an infiltrating deadly tumour of the CNS. It is the most frequent, the most aggressive and the most lethal form of diffuse glioma. Its conventional treatment consists of a surgical resection of the tumour followed by a radio-chemotherapy using X-rays and TMZ (1). However, recurrence of the tumour is today inevitable. It has been observed that tumour recurrence mostly occurs within 2 cm of the resection cavity which can be explained by the invasion ability of GBM cells (2). Therefore, the targeting of tumour cells infiltrated inside the CNS, in particular in the margin of the resection cavity, is a major goal for the treatment of GBM. In parallel with researches considering the “magic bullet” principle, a new concept arises: the tumour trap (3).

The objective of this PhD project was to design a scaffold able to create a gradient of a chemoattractant protein, the SDF-1α in order to attract and trap infiltrative GBM cells. Indeed, the attraction of residual infiltrative cells could lead to the concentration of tumour cells inside a controlled environment, allowing a more efficient elimination of cancer cells with less side effects.

In this research we developed freeze-dried sponges made of SF, HA and hep and evaluated their mechanical properties, architecture, biocompatibility, and loading and release profile of the chemokine SDF-1α. The formulation was optimised in order to find the best candidate to trap tumour cells and carry out the proof of concept. Our major findings can be summarised as follows:

- Sponges made of a blend of SF and HA combine the stability of the SF with the softness of the HA;
- SF-HA and SF-HA-hep have properties adapted for brain implantation (high water uptake, softness, cytocompatibility);
- A reproducible ''biopsy punch'' tumour resection technique was used to implant the sponges in the brain of rats;
- The SF-HA and the SF-HA-hep sponges were well tolerated in the long-term *in vivo*;
- The integrity of the structure of the SF-HA sponge is maintained for less than a week *in vivo* while the SF-HA-hep degrade slower;
- SDF-1α formed a concentration gradient from the centre to the edge of the sponges;
- The release of SDF-1α from the SF-HA sponge is characterised by a burst release in the first 72 hours *in vitro* while the SF-HA-hep sponge does not release the protein *in vitro* and *in vivo* for a week;
- An agarose drop assay can be used to assess the activity of SDF-1α;
- Presence of SDF-1α lead to an increase of the migration of U87MG-CXCR4$^+$ cells but no response was observed once associated to the SF-HA and SF-HA-hep sponges.

2. Major Findings: Discussion

In this PhD work, we evaluated the parameters that we considered crucial for the development of a tumour trap for GBM cells. These included choosing a chemoattractant for the attraction of GBM infiltrative cells, choosing adapted polymers and architecture to develop a biocompatible scaffold that resembles the brain tissue, and evaluation of its mechanical properties, tolerability and degradability over time and its association with SDF-1α for its use as a tumour trapping device. Properties of the sponges produced as well as theoretical ideal parameters are summarised in Table 5. 1.

Table 5. 1: Theoretical ideal characteristics of a scaffold for brain tissue reconstruction taken from Mahumane *et al.* review (4) compared with the properties of the produced sponges.

Theoretical ideal characteristics		**HA-PLL**	**SF**	**SF-HA**	**SF-HA-hep**
Water composition	80%	95%	93%	93%	91%
Young's modulus	0.1-1 kPa	6 kPa	22 kPa	12.5 kPa	13 kPa
Porosity	~ 90%	92%	93%	87%	82%
Pore size	20-160 µm	20-153 µm	28-146 µm	16-123 µm	22-136 µm
Translational potential	Can be shaped or resized to the lesion	Yes	Yes	Yes	Yes
Biocompatible	No cytotoxicity *in vitro*	OK	OK	OK	OK (but lower cell viability)
	Tolerable *in vivo*	NT	NT	OK	Higher inflammatory reaction
Biodegradability	Slow degradation rate (more than a month)	100 % degraded in 7 days *in vitro*	Minor degradation *in vitro*	Intermediate degradation (90% in 3 weeks) *in vitro* and complete degradation in 8 days *in vivo*	Intermediate degradation (85% in 3 weeks) *in vitro* and slower degradation than SF-HA *in vivo*
SDF-1α release	Sustained release	NT	NT	25% release over 72h then plateau (*in vitro)*	2% release over 2 weeks *in vitro*, no evidence of release *in vivo*.

2.1. Choosing the polymers and architecture of the future trap

When this project started, no studies had been published about the use of SDF-1α to attract GBM cells. The protein is however studied, in association with scaffolds, for the regeneration of tissues. In both applications, the purpose is to attract cells in a scaffold. The scaffold should be a welcoming environment for the cells, so they do not leave it. For the case of regenerative medicine, host cells should then be able to grow and form new tissues while, for the tumour trap, the unwanted cells should be attracted to and confined in the scaffold until elimination. We therefore hypothesised that the parameters for a scaffold intended for brain regeneration should be the same as than for a brain tumour trap.

It is important to design the scaffold so it can be used for future clinical applications: (i) the sponges are made of cost-effective FDA approved components, (ii) a high number of sponges can be made in the same time using moulds thanks to a simple freeze-drying process, (iii) sponges can be shaped to fit the resection cavity of the patient, (iv) the trap is composed of a freeze-dried sponge and a protein meaning that the degradation of the sponge corresponds to the release of the protein and no traces will remain after degradation of all the natural components, (v) freeze-dried sponges can be easily stored an rehydrated just before the implantation and (vi) the mechanical properties are adapted for implantation in the brain. Freeze-dried sponge made of blends of HA, SF and hep were prepared by crosslinking them with EDC and NHS followed by freeze-drying. PLL was used to prepare sponges with only HA as the crosslinking was performed between a carboxyl and a primary amine and HA does not possess primary amines.

The physicochemical characteristics of the sponges made from different combinations of HA, SF and hep were evaluated to gain insight into the composition that may better perform as brain tissue scaffold. The theoretical ideal parameters for brain regeneration and the performances of the four sponges tested in this study are summarised in Table 5. 1. The ideal scaffold for brain regeneration, as described by Mahumane *et al.* (4), should mimic the brain tissues as closely as possible. The brain composition is 80% water (5). Here, we produced sponges with a water uptake capability that ranges between 95% (as in the case of HA-PLL sponges) and 93% (as in the case of SF-HA and SF-HA-hep sponges). It is important to highlight that the maximum swelling capacity of the sponge was reached within a few minutes in PBS and no further swelling was noticed afterwards. Sponges have to be swollen before implantation and there is no further swelling once in the brain. Implantation of dry sponges was not considered as the volume increases of about 30% when swollen which could create an unwanted pressure.

The brain has a Young’s modulus below 1 kPa (6,7). It is quite challenging to produce scaffolds that maintain their structural integrity with a Young’s modulus as low as the one of the brain. The Young’s modulus of a brain tumour is about 25 kPa (8), we therefore considered that the mechanical properties of the sponges should be between those of healthy and tumour tissues. The sponges have a Young’s modulus between ~6 kPa (HA-PLL sponge) and ~22 kPa (SF sponge), with an intermediate value of ~13 kPa recorded for the SF-HA and SF-HA-hep sponges. Sponges with a lower Young’s modulus could be produced by decreasing the degree of crosslinking, but, when tested, these sponges showed structural collapse once in aqueous media. Alternatively, the Young’s modulus may decrease if the β-sheet content of the SF decreases. However, it was shown that the decrease in the β-sheet content can lead to negative effects on the sponge stability (9). Thus, about 30% of β-sheet content was determined to be the minimum threshold to ensure maintenance of the structural integrity of the implant. It was therefore not possible to further decrease the Young's modulus with these sponges compositions and fabrication technique. On the other hand, the stiffness of the material promotes better handling of the sponges. For example, the sponges could be conveniently cut into the desired dimensions after hydration to better fit the lesion at the intended site of implantation. Moreover, the structure of these porous sponges mimic the structure of the brain ECM that was described as a foam-like structure (10). The pores were of various sizes ranging from 20 to 140 µm across the different sponge compositions studied in this work, which was described as ideal by Mahumane *et al.* (4) since they are sufficiently small to support 3D cell-cell contacts, but large enough to allow good diffusion of nutrients, oxygen and bioactive factors for cell survival and growth. Moreover, cells are able to migrate through pores that are larger than 10% of their nuclei cross-section (11). For tumour cells, it is about 7 μm^2, meaning that they can migrate through pores with a size above 1 µm without degrading the matrix. The ideal porosity was defined to be around 90% by Jurga *et al.* (12) and this was replicated in the sponges produced herein; namely, 82% and 93% for the SF-HA-hep sponge and SF sponge respectively. Moreover, it was observed after implantation of the SF-HA-hep sponge in the brain that immune cells were able to penetrate in the heart of the sponge; GBM cells should therefore be able to infiltrate the sponges.

2.2. Evaluating the degradation rate

We observed that the HA-PLL sponge was totally degraded after 7 days in PBS in the presence of relevant degrading enzymes (hyaluronidase and heparinase) at 37°C. The SF sponge however showed no sign of degradation even after 3 weeks of incubation under the same conditions. Relevantly, SF-HA and SF-HA-hep showed intermediate degradation rate with 90% SF-HA sponge and 85% SF-HA-hep sponge degraded after 3 weeks. Thus, in good agreement with previous reports, the mass loss in scaffolds composed of HA and SF blends can be attributed to the degradation of HA (13). Since the SF-HA and SF-HA-hep sponges provided a good trade-off between the low rigidity of the HA-PLL sponge and the slow degradation of the SF sponge, they were chosen for further *in vivo* studies. No differences in the degradation were observed *in vitro* between the SF-HA and the SF-HA-hep sponge; i*n vivo,* however, results showed that the SF-HA sponges were completely degraded after 8 days of implantation on the contrary of the SF-HA-hep sponge. MRI images taken after 2 months suggested that the SF-HA-hep sponges were degraded at that time but we do not know at what extent. Dissection after 4 months of implantation showed a complete degradation of the SF-HA-hep sponges. Deeper studies should be performed in order to determine the degradation rate of this type of sponge. In addition to compatible mechanical properties the scaffold should be biodegradable to avoid the need for secondary surgery to remove it. Simultaneously, the degradation rate of the scaffold should be slow enough to allow for the complete migration of GBM cells and their killing. It has been observed than tumour recurrence occurs in 90% of the cases within 2 cm of the resection cavity (2). Migration rate of four GBM cell lines (U87MG, SNB19, LN229 and U251) was measured in a 3D *in vitro* model by Dia *et al.* (14). They reported a migration speed between 0.5 ± 0.07 µm/min for the U87MG cells and 0.17 ± 0.02 µm/min for the U251 cells. These results are coherent with what was observed with the agarose drop assay (Chapter III) as the speed measured for U87MG-CXCR4$^+$ cells was about 0.2 µm ± 0.05 µm/min. Considering these results, GBM cells at 2 cm from the margin of the resection cavity should take between 1 and 3 months to migrate inside the trap. As radiation has an impact on the wound healing process, GBM patients' need to wait for at least 4 weeks after the surgical resection before starting the TMZ and radiotherapy regimen to allow the tissues to heal (15). Therefore, the structure of the sponges should stay intact over a month to let the cells migrate inside the sponge and to start the therapy to eliminate them. The SF-HA is therefore degrading too fast.

Casting mixed SF and HA solutions to obtain thin films allowed us to identify the mixing time as a control parameter for the overall structure of the generated construct. To our knowledge, the effect of this variable has not been reported before. Phase separation was evident for films prepared after a short mixing time (15 min). The phases seemed then to interact with each other, resulting in an increase in homogeneity in the polymer blend. Since aggregates started to form extensively after an overnight mixing, an intermediate mixing time of about 5 hours was chosen for the sponge preparation. In order to study the microstructure of the sponges' walls, fluorescence microscopy was used. We observed that antibodies coupled with fluorophores like DAPI or ActinRed could adsorb to the SF component of the sponges but not the HA-filled regions. The structure of SF-HA and SF-HA-hep sponges was formed by fluorescent aggregates that should therefore be SF-rich domains distributed in a non-fluorescent matrix composed mainly of HA. Garcia-Fuentes *et al.* (16) studied the interaction between HA and SF in blends with different ratios. Results suggested that a phase separation occurs with a SF/HA ratio of 80:20 and 60:40 (w/w), with one phase containing HA alone while the other phase consisting of a mixture of HA and SF. The phase separation observed in the films prepared by us (a 2:1 SF/HA ratio was used here) as well as the structure observed in the walls of the sponges are consistent with those previous findings. We can therefore conclude that the polymer ratio as well as the mixing time are critical parameters when SF and HA are used to prepare 3D scaffolds. Since HA degrades quicker than SF, the matrix has to be as homogeneous as possible to avoid the generation of scaffolds with distinct HA-rich compartments susceptible to rapid *in vivo* decomposition. This phenomenon has also been described for blends of SF with other polymers like polyethylene oxide (17) and dextran sulphate (18). However, fluorescent microscopy of the sponges showed us that the polymers were not yet distributed homogeneously with SF rich globules inside a HA matrix. Since HA degrades faster than SF, this would lead to a fast degradation of the structure of the sponge, leaving microparticles made mainly of SF. If the sponge is made of a homogenous blend of polymers (or one type of polymer), it is eroded from the surface to the core with walls becoming thinner, leaving the structure intact for a long time (Figure 5. 1-A). If the sponge is made of a non-homogeneous blend of polymers with slow degrading polymer globules inside a fast degrading matrix like here, the sponge degrades by leaving smaller pieces, the structure is therefore more quickly compromised (Figure 5. 1-B). If, on the contrary, the sponge is made of a non-homogeneous blend of polymers with fast degrading polymer globules inside a slow degrading matrix, more pores are created as the material degrade (Figure 5. 1-C). The ideal scenario should therefore either be the (A) or (C).

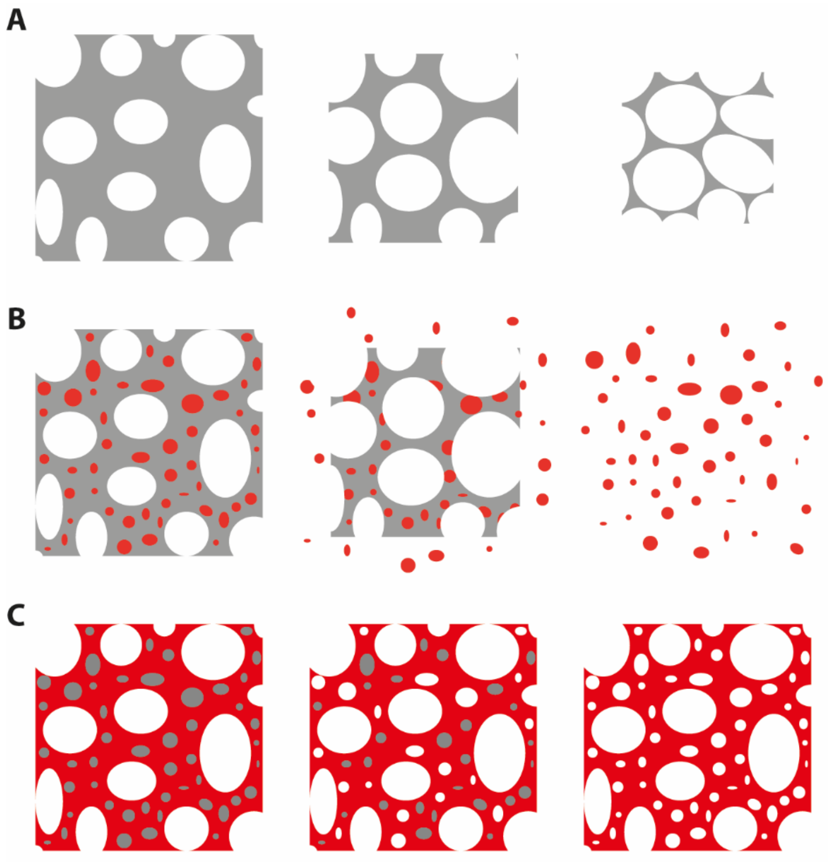

Figure 5. 1: Schematic representation of the degradation profile of sponges made of (A) a homogeneous polymer matrix, (B) slow degrading polymer globules inside a fast degrading matrix and (C) fast degrading polymer globules inside a slow degrading matrix.

2.3. Evaluating the tolerability of the formulation

The biocompatibility of a scaffold is a major concern for brain use and an accurate and methodical work needs to be performed in this sense to guarantee the safety of new products (19). Biocompatibility is a poorly defined term (20) but the most used is the one given by Williams in 1987 (21) as ''the ability of a material to perform with an appropriate host response in a specific application''. The biocompatibility therefore depends on the host (species, site of implantation, microenvironment) as well as on the material itself (shape, size, surface chemistry, roughness, design, morphology and porosity, composition, sterility, contact duration and degradation) (19,20,22,23). Showing that a material is biocompatible is therefore challenging as no material can perform with an appropriate response in all situation and each particular case has to be considered. Here, biocompatibility has been evaluated in the targeted tissue (the brain) but the microenvironment differs as no tumour is present and the species used was rat. However, it is a good model for preliminary experiments, and it allowed us to understand better the behaviour of the material in the brain. Immediately after implantation, a polymer-blood interface is created which leads to a non-specific adsorption of blood and tissue fluid proteins on the foreign material (24). Then, immune and inflammatory cells intervene by creating a fibrous capsule around the material in order to separate it from the body. It consists in a juxtaposition of astrocyte end feet and a thin layer of collagen (25). An example, observed by Autier *et al.* (26) at 1 month after implantation of a collagen scaffold, is given Figure 5. 2. This reaction does not mean that the material is not biocompatible but may prevent or decrease the release of drugs from the material for instance (20,22,27). Polymers can be chosen to avoid the formation of this capsule. In our case, it may prevent the release of SDF-1α and the migration of tumour cells inside our scaffold, a fibrous capsule should therefore be avoided. Fortunately, this reaction was not observed for any of our sponges.

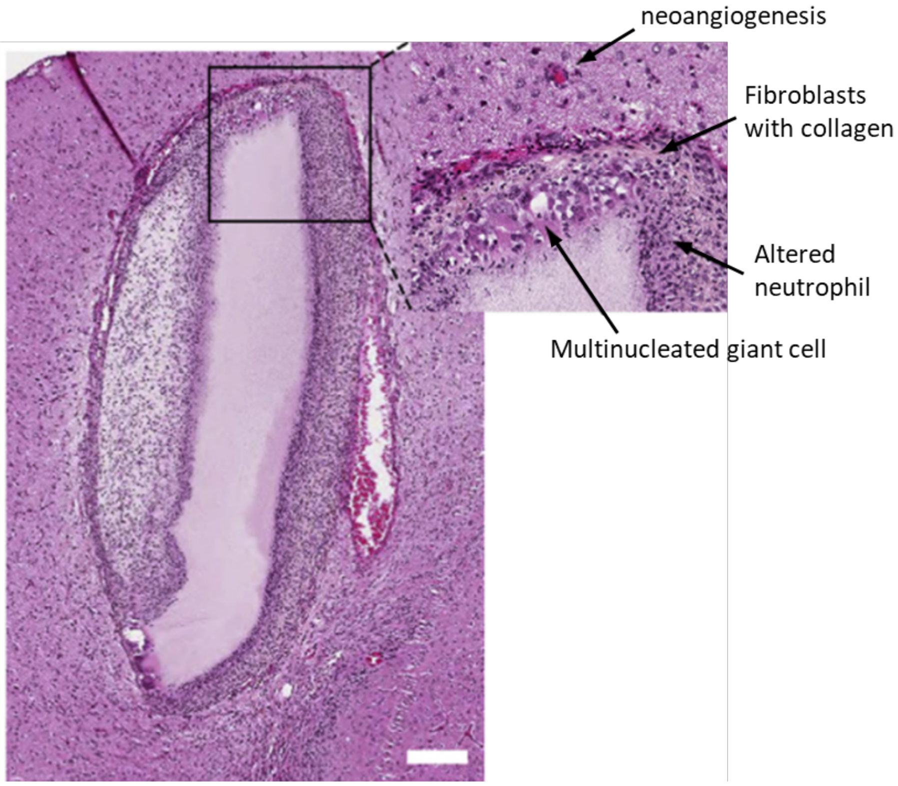

Figure 5. 2: Histological section of rat brain 1 month after implantation of a collagen scaffold showing a fibrous capsule observed by Autier *et al*. (26). The bar indicates 200 µm.

The acute inflammation is the immediate response to injury and consists in the recruitment of phagocytes (in particular neutrophils) (14), then, microglial cells, macrophages and foreign-body giant cells erode the material and eliminate it after a time lag depending on the material (composition and architecture) and on the implantation site. Changes in the microvasculature and neo-angiogenesis can be observed. The purpose of this reaction is to prevent the ongoing tissue damage, isolate and destroy the foreign material and activate the repair process. This reaction was observed for the SF-HA-hep sponge after 8 days of implantation. Acute inflammation was not observed for the SF-HA sponge as well as the for the resection without implantation whereas it probably occurred earlier. For the SF-HA-hep sponge, necrosis was also found. It usually occurs when the biomaterial is toxic for macrophages, leading to their death and to the release of enzymes in the surrounding tissue causing tissue damage. This reaction was probably due to the presence of residual crosslinking agents as they were shown to be the cause of the cytotoxicity effect in Chapter IV. It is therefore of prime importance to ensure their removal before implantation. Cleaning is usually done by a simple wash in water. However, even after washing 24h in PBS under mild agitation at RT or 5x30s sonication in PBS followed by 1h in PBS under mild agitation, no improvement in the cell viability was observed. Stronger washing techniques would however degrade the sponges, it is therefore not an option. Another solution might be to optimise the crosslinking process in order to obtain a similar crosslinking rate with a lower concentration of EDC/NHS. As explained in Chapter II, EDC/NHS promote the formation of covalent crosslinks between a carboxyl and a primary amine but do not remain as part of the crosslink, they can therefore be considered as catalysers and one molecule of EDC and NHS can form more than one link under the right conditions. The concentration of EDC and NHS should be quantified by HPLC for example before moving to the clinic.

The chronic phase response follows the acute phase. It is characterised by the proliferation of fibroblasts, producing collagen and proteoglycans in order to encapsulate the material, and macrophages to eliminate it.

All animals tolerated the surgical procedures and there was no evidence of either systemic or neurological disease in any animal throughout the course of the experiment. After 4 months of implantation, only a slight chronic inflammation at the cavity border was visible for the three conditions and both SF-HA and SF-HA-hep sponges were totally degraded. The SF-HA-hep sponge as well as the SF-HA sponge were therefore well tolerated although the SF-HA-hep lead to a more intense immune reaction.

2.4. Evaluating the effect of SDF-1α on GBM cells

SDF-1α was adsorbed on the SF-HA and SF-HA-hep sponges by simply hydrating the sponges with the protein dissolved in PBS. Thanks to the use of fluorophore-labelled SDF-1α, the protein was evidenced to form a radial concentration gradient inside the sponge. Since it has been described that CXCR4 receptor-bearing cells can migrate in response to an SDF-1α concentration gradient, the radial distribution of SDF-1α in the sponge may be beneficial in facilitating extensive infiltration of stem cells into the sponge for tissue regeneration. Adding the protein to the polymer blend before crosslinking was not considered for several reasons. First, the protein would have been crosslinked as well by the EDC and NHS since it possesses the carboxyl and primary amine implicated in the reaction. Secondly, SDF-1α might have been degraded through the process. Thirdly, adding SDF-1α on the freeze-dried sponge allows a 100% loading of the protein in the sponge, which is essential considering its price. Fourthly, it allows a precise control over the quantity added to each sponge. Indeed, because of the high viscosity of the HA solution, mixing is difficult and might lead to inhomogeneities. Moreover, the cut of the sponge is not precise and might result in differences in volumes. Finally, the storage of freeze-dried sponges is easy as they should be stored in a dry environment at RT. If SDF-1α is added before the production, stability of the protein during storage should be studied.

SDF-1α is a positively charged protein at physiological pH (isoelectric point (IEP) ~9.6) while HA and SF are negatively charged (IEP ~2.9 and ~4.6 respectively) (28,29), allowing the protein to bind quickly to the sponges via electrostatic interactions. Moreover, heparin is known to form a strong complex with SDF-1α (30). SDF-1α was therefore expected to be better retained in the SF-HA-hep sponge than in the SF-HA sponge. We indeed observed about 25% of loaded SDF-1α being released from the SF-HA sponge after 3 days while there was still 98% of SDF-1α retained in the SF-HA-hep sponge after 7 days in PBS with enzymes (hyaluronidase and heparinase). Release profiles from scaffolds described in the literature with similar compositions and SDF-1α loading protocol as adopted in this study are summarized in Table 5. 2. They all showed a much higher release although the SF-HA sponge was not far from the literature data. Differently, the strong

SDF-1α retention capacity displayed by the SF-HA-hep sponge has not been reported before.

Table 5. 2: SDF-1α release profiles from scaffolds with similar composition and SDF-1α loading protocol as adopted in this study.

Scaffold	Release profile	Ref.
SF freeze-dried sponge	~35% release within 24h	(31)
HA degradable hydrogel	~40% release after 2 days	(32)
StarPEG-hep hydrogel with or without MMP-cleavable sites	~20% release after 24h for non-cleavable gel ~40% release after 24h for cleavable gel	(33)
PEG-hep hydrogel	~25% release after 3 days	(34)
Collagen scaffold functionalized or not with hep	~80% release after 2 weeks without hep ~40% release after 2 weeks with hep	(35)

Different methods can be used to show that a material loaded with a chemoattractant is efficient to attract cells. Here, we developed an agarose drop assay were the distance of migration of cells from a drop of agarose can be measured. We observed that 40 ng/mL was necessary to cause a significant increase of the migration of the U87MG-CXCR4$^+$ cells; such high concentration was impossible to achieve considering the low release of the protein from the sponge. We therefore decided to observe if cells added on top of the sponges would migrate faster directly on the sponges loaded with the protein. We observed that cells were able to survive for a month in the sponges, but the migration was not quantifiable with this technique as cells were non-homogeneously dispersed in the sponge and no difference was observed with or without SDF-1α. This assay could be improved using spheroids. Preliminary tests have been conducted in the lab and it was shown that it was possible to prepare spheroids made of U87MG-CXCR4$^+$ cells as well as U87MG-CXCR4$^-$ cells, deposit one spheroid on top of the sponge and cultivate it for a week (Figure 5. 3). Because the edge of the spheroid is well delimitated, it would be possible to measure the distance of migration of single cells from the spheroids at the surface of the sponge as well as in depth by cutting the sponge transversally.

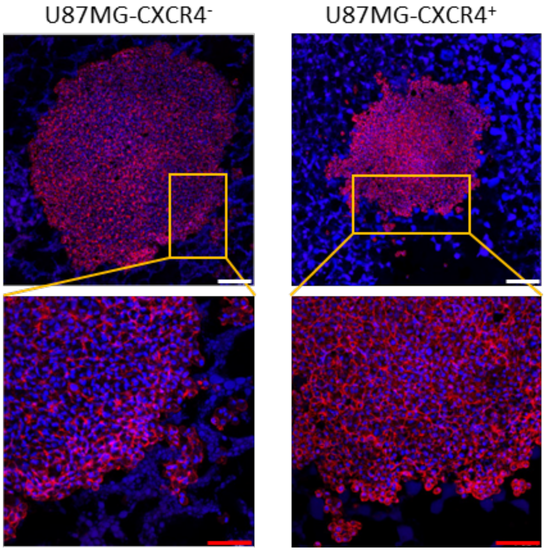

Figure 5. 3: Confocal fluorescence images of U87MG-CXCR4$^-$ and U87MG-CXCR4$^+$ spheroids after 1 week on SF-HA-hep sponges. Cells were stained with ActinRed and DAPI. Despite the use of SB to decrease the unspecific adsorption of the fluorophores on the sponge, the sponge was stained in blue by the DAPI (preliminary, non-published data). White bar indicates 100 µm and red bar 50 µm.

Because of the fast degradation of the SF-HA sponge, only the SF-HA-hep sponge was used to evaluate the release of the protein *in vivo*. We were expecting a faster release than *in vitro* because of the degradation of the sponge as well as possible competition mechanisms with other proteins but no release in the brain was observed after 8 days.

Injection of SDF-1α alone cannot be used because of its rapid elimination (36). Indeed, it has been reported that the SDF-1α half-life *in vivo* was 26 min when administered systematically (37). After injury, there is a peak of SDF-1α but it decreased dramatically by two weeks post injury (38). It therefore needs to be continued by a sustained release of the protein for a longer time. Use of nanoparticles to encapsulate SDF-1α could have been considered to achieve a sustained release. This approach has been studied by Haji Mansor *et al.* (39) with PLGA nanoparticles. They showed that SDF-1α was still active after processing as demonstrated in an agarose drop assay. A possible downside with the use of nanoparticle is its dispersion. Indeed, nanoparticles might go too far before releasing the protein (Figure 5. 4-A), creating multiple points of attraction. Little is known, however, on the mechanism behind chemoattraction. It has been reported that cells develop pseudopods (polymerisation of actin filaments) in the direction of the highest concentration of chemoattractant and retraction at the opposite direction, leaving to the movement of the cell in direction of the chemoattractant source (40). Moreover, it has been observed that injection in the brain of exogenous SDF-1α was confined within 400 µm of the injection site but induced SDF-1α expression over 2 cm from the injection site (36). These results suggested that the information is transferred by the cells as explained in Figure 5. 4-B. It can therefore be hypothesised that a local delivery of the protein can still have an effect at long distances. We observed the production of SDF-1α *in vivo* after 8 days of implantation of the SF-HA-hep sponge loaded with SDF-1α marked with a fluorophore. 8 days was chosen since the production of the protein in response to the surgery would be theoretically decreased, allowing us to observe the effect of the exogenous SDF-1α. However, no increase of the endogenous production of SDF-1α was detected. Since no SDF-1α was released from the scaffold at that time, we assumed that the minimal release required to induce a reaction was not met. The SF-HA-hep is therefore not suitable to attract GBM cells and a sponge with a higher release rate should be used.

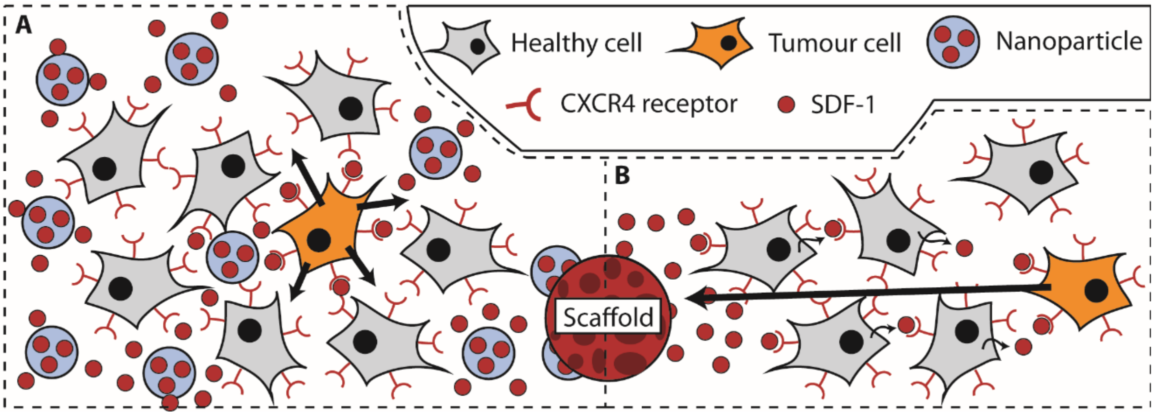

Figure 5. 4: Illustration of the possible downside of using nanoparticles to attract GBM cells (A) compared to the use of free SDF-1α (B).

3. Current and future perspectives

In this PhD thesis, we developed sponges made of SF, HA and hep. The SF-HA and SF-HA-hep sponges presented the most interesting physicochemical properties, associating the stability of the SF with the biomimicry of the HA. However, there are still several unmet limitations that should be addressed before considering a translation into the clinics. Indeed, *in vivo* data showed us that the SF-HA sponge degraded too fast (less than a week) while the SF-HA-hep sponge did not release the chemoattractant SDF-1α, the sponge should therefore be improved in light of these results. An animal model should be developed in order to conduct a proof of concept: is the sponge able to attract GBM-

CXCR4⁺ cells? Then, the risks should be assessed and the best method to kill the trapped cells should be evaluated. Once these steps done, the possible scale up of the sponge production should be considered. The different steps necessary to take the sponges developed during this PhD to the clinic are summarised in the Figure 5. 5 and discussed below.

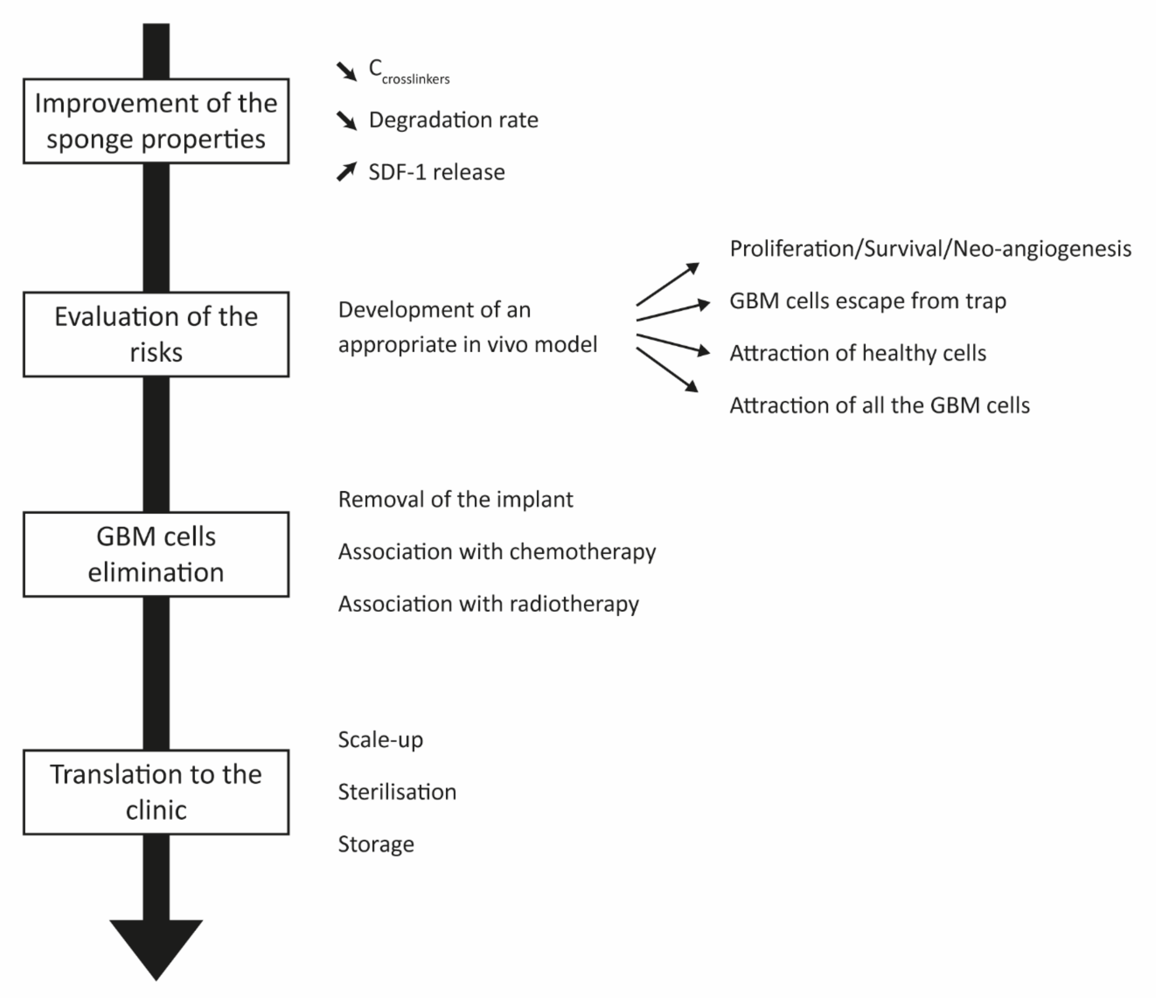

Figure 5. 5: Timeline of the project: from bench to bedside.

3.1. Improvement of the sponge properties

The biological evaluation of the sponges allowed us to understand better the relationship between physical and chemical properties and the biological response and to bring to light weaknesses in the design of the sponges. We learned that the higher quantity of EDC and NHS used in the SF-HA-hep sponges leads to cytotoxicity and higher immune response *in vivo*. We also observed that, while *in vitro* the degradation of SF-HA and SF-HA-hep was similar and they were both retaining their structure after one week, the *in vivo* results showed that the SF-HA sponge was fully degraded after 8 days of implantation. Finally, the SF-HA-hep sponge did not release SDF-1α *in vitro* and *in vivo* after a week. Nor the SF-HA sponge neither the SF-HA-hep one were therefore perfect for the tumour trap application but had both qualities. In the light of this knowledge, it should be possible to redesign a sponge ideal for our project.

3.1.1 Decreasing the quantity of crosslinkers

Increasing the stability of the material while reducing the concentration of EDC and NHS should be feasible. Indeed, the more the crosslinking rate, the more stable the material. Different parameters can be considered: (i) the reaction time, (ii) the temperature, (iii) the buffer used and its pH and (iv) the order of addition of the polymers.

EDC and NHS activate the carboxyl group in order to allow the nucleophilic attack by a primary amine, forming a covalent bond between the two polymers (HA contains carboxylic groups, SF and hep contain primary amines). EDC and NHS are retrieved and can be reused on another bond. Thus, if we increase the reaction time, it might increase the crosslinking rate. One of the major difficulties of this reaction is the viscosity of the HA, making the mixing of the polymers with EDC and NHS complicated. Viscosity can be decreased by heating, diluting more the HA or using HA with smaller chains (here we used HA with MW = 200-400 kDa). The activation buffer should not contain any primary amine or carboxyl group as they will compete with the activation reaction. Phosphate and acetate buffers may also reduce the reactivity of the EDC. In this study, we used Hepes buffer at pH 7.4 but MES ((2-(N-morpholino) ethanesulfonic acid)) buffer at pH 6 might give better results. It has been shown that mixing first the EDC and NHS with the carboxyl bearing polymer (here HA) to activate it then adding the primary amine bearing polymer can increase the yield of the reaction (41).

3.1.2 Decreasing the degradation rate

Decreasing the degradation rate of the SF-HA sponge is essential to obtain a sponge that retains its structure for at least one month. Firstly, it can be achieved by improving the crosslinking process as shown in section 3.1.1. As reported in section 2.2, while the presence of SF allowed to increase the stability of the sponges, the inhomogeneity of the blend between SF and HA creates an undesirable degradation profile. Indeed, while increasing the mixing time between the two polymers helped creating a more homogeneous matrix, SF-reached globules inside a HA matrix was observed. The main reason is that SF is a protein mainly hydrophobic with a highly organised 3D structure (42). In order to mix it properly with HA, the small hydrophilic parts need to have time to form hydrogen bridges with the HA chains (43). However, we saw that if the mixture was stirred for too long, aggregates were started to form. The high viscosity of the HA solution used might have been too high to achieve a proper blending. Using smaller chains of HA and/or a smaller concentration might be a solution. Indeed, Yan *et al.* (44) produced films with a uniform microstructure and no phase separation using a blend of HA 1.5% (w/v) with SF 1.5% (w/v) followed by crosslinking with EDC and NHS. However, they did not mention the duration of the mixing step. Moreover, since SF presented a slower degradation profile, a higher proportion of this polymer might help decreasing the degradation rate. Another solution that was not explored is to heat the polymers when stirred at a temperature to reduce the viscosity of the solution. If chosen, this would have to be carefully monitored as the rearrangement of the SF protein might lead to the creation of β-sheets and therefore to an increase in the inhomogeneity of the blend (9).

3.1.3 Increasing the release of SDF-1α

As we found, the SF-HA-hep did not release SDF-1α *in vitro* and *in vivo* for a week. The use of hep is therefore questioned. Moreover, due to the negative charges present on the SF and HA polymers, SDF-1α is able to bind via electrostatic charges to the sponge even without the hep. The more obvious solution to the problem would therefore be to use the SF-HA sponge once its stability issues are resolved. One reason for the use of hep was its protective properties over SDF-1α. Indeed, it has been shown that hep and HS protect SDF-1 from degradation, in particular by the CD26/dipeptidyl peptidase IV (45). Therefore, another solution would be to use less hep in the composition. Indeed, the SF-HA-hep sponge is composed of 57% SF, 28% HA and 15% of hep (w/w). Comparatively, Krieger *et al.* (34) used 10% hep and 90% PEG (w/w) and Bladergroen *et al.* (35) 3% hep and 97% collagen (w/w). Reducing its proportion to 5% might therefore be sufficient to protect the SDF-1α while allowing a higher release of the protein.

Controlling the release rate is of prime importance. If it is too slow, the concentration gradient might be insufficient to drive the chemotaxis of infiltrative GBM cells. If it is too fast, cells might undergo a receptor desensitisation/downregulation due to overstimulation (46).

3.2. Evaluation of the risks

Using SDF-1α to attract infiltrative GBM cells entails risks that have to be evaluated. Indeed, SDF-1α is also known to increase the proliferation and survival of tumour cells as well as neo-angiogenesis (47). It might therefore lead to an increase of the tumour aggressiveness if not controlled. A better understanding of the pathways might help to find a condition where only chemotaxis is activated (concentration, association with another protein, presentation of a specific sequence of the chemokine).

The optimal concentration of SDF-1α should be found if it exists. Indeed, if the concentration is too low, no attraction would be observed. If it is too high, it might lead to an acceleration of the secondary tumour growth and invasiveness.

Heparin sulphate (HS) was found to play a role in the modulation of SDF-1 activity (48). HS as well as hep are found in the extracellular matrix and bind to the chemokine. HS is also present on the cellular surface (49). This interaction provides positional information within tissues as local gradients, more robust than soluble ones. It has been shown that a chemokine-receptor interaction involves two distinct sites implicated in receptor binding and receptor activation (50). Chemokines can bind to HS through various configurations and binding epitopes, which give rise to different mode of association (51,52). This suggests that HS can modulate the activity of the chemokine.

Different isoforms of SDF-1 exists (α, β and γ), they are all composed of the same first 68 amino acid residues corresponding to the α isoform. The β isoform contains 5 more residues at the C-terminal and the γ isoform 30 more residues. SDF-1α contains one HS-binding motif, two for the SDF-1β and four for the SDF-1γ (Figure 5. 6). The CXCR4 binding motif is localised on the SDF-1α sequence (53). It was shown that SDF-1α functioned similarly regardless of whether it was bound to HS. In contrast, SDF-1γ, although binding to CXCR4 with a much higher affinity than that of SDF-1α, did not induce robust cell motility unless it was bound to HS. This mechanism is not well understood but it lets think that a modification of the protein or hiding a specific sequence might lead to different activations and therefore one isoform might favour chemotaxis against proliferation or survival.

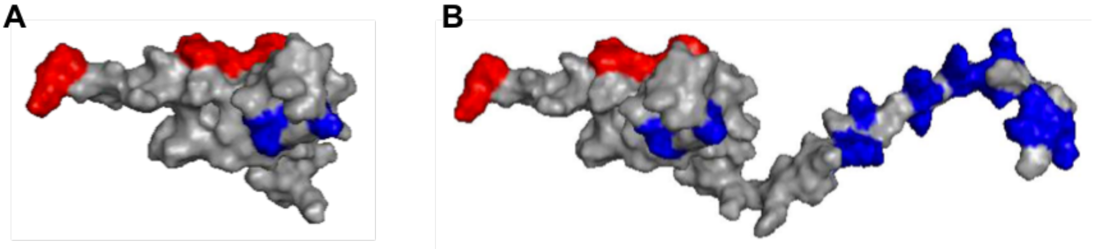

Figure 5. 6: Structures of (A) SDF-1α and (B) SDF-1γ. Amino acid residues known to contribute to binding to the CXCR4 receptor are shown in red and to HS are shown in blue. Adapted from (48).

SDF-1α was selected on this project as it is the most studied isoform but using a different one can be an alternative if it turns out that using SDF-1α presents too much risks. Other possibilities to attract GBM cells can also be considered. Only a few groups over the world are studying ways to trap GBM cells. The first publication to present such concept was made by Jain *et al*. in 2014 in *Nature Materials* and consisted in a guide made of aligned polymeric nanofibers that drive GBM cells to an extracortical location made of a cytotoxic gel (54). They were able to show a shrinkage of over 90% of the tumour in a rat model and are today working with the FDA in order to get approval for clinical studies by the end of 2019. The purpose of this device is to decrease the size of the tumour in order to make it more manageable. Though it might lead to an increase of the median of survival, especially for patients with advanced tumours that are not resectable due to their size, it would not be sufficient to completely cure the patients. The same group is also investigating the use of electrotaxis *i.e.,* the use of an electrical field to attract GBM cells and have shown *in vitro* that U87MG cells were responsive to electrotaxis (55). Other chemoattractant molecules could also be considered. Conditioned medium of stromal cells from the peritumoral zone of GBM called GASCs contains chemoattractants such as THBS1, SDF-1α, HGF and fibronectin (56) and was shown to increase the migration of the GBM cell line F98 at a higher extent than purified CXCL12 or THBS1 alone and could be easily used as a substitute for SDF-1α in our sponges (26).

Another risks that have too be studied is the escape of the GBM cells from the trap. To address this issue, several strategies can be considered. First, the trap can be designed such as cells are killed upon arrival in the trap (see section 3.3). Second, the timing of the treatment has to be studied in order to kill the cells after all of the infiltrated GBM cells penetrated inside the trap but before tumour cells proliferate and escape the trap. Additionally, an inhibitor of proliferation such as ribociclib® (57) could be loaded inside the sponge.

Finally, it will be necessary to study the attraction of healthy cells inside the sponge and evaluate the implications. Cells that can be attracted are cells with migration capacities possessing the CXCR4 receptor. In the adult brain, cells with the CXCR4 receptor are mostly immune cells and stem cells (58). Using SDF-1α might therefore increase the inflammation after implantation and the consequences should be evaluated. Stem cells niches in the adult brain are localised in the subgranular zone of the hippocampus, as well as the subventricular zone (59). The effect of the attraction of stem cells in the trap on the patient should be evaluated. Indeed, it might help reconstructing the brain in the resection area and therefore allow a better recovery of the patient from surgery (60,61). If the elimination of those cells after treatment, the subgranular zone of the hippocampus and the subventricular zone should be avoided.

In order to answer these issues, a pertinent animal model has to be developed. An ideal model should recapitulate the key histopathological, genetic and imaging features encountered in GBM's aggressive growth as well as being a reproducible and reliable. Researchers should consider different parameters while choosing an optimal GBM model: (i) The size/species of the animal; (ii) human GBM models are closer to the clinic situation but the use of athymic nude mice or rats lack of full tumour-immune microenvironment. (iii) The infiltrating capacity of GBM cells from the tumour mass to the brain parenchyma differs depending on the GBM cell line.

Hydrated sponges can be cut in order to fit a resection cavity and it is possible to obtain a cylinder with 3 mm diameter and 2 mm height. However, making it smaller is difficult; rats have therefore been chosen as they can bear a cavity of this size with no complications. In order to see if the sponges with SDF-1α are able to attract infiltrative cells, it would be interesting to develop a tumour with the U87MG-CXCR4$^+$ cells in the first instance. Since these cells produce RFP, it will be possible to evaluate their migration with fluorescence imaging. These cells have been previously grown in nude mice by Dr Delphine Séhédic

(62). The model should therefore be adapted for the rat and is currently under development by Clément Tétaud. In the second instance, a model closer to a real human GBM should be developed using primary cells from patients in order to address the risks discussed above.

3.3. How to kill cells once trapped

The first step of the project was to design a scaffold with the right properties to be used as a GBM trap. In order to make it functional it will be mandatory to find the most efficient way to kill the cells once inside the trap. The major interest of guiding these cells inside a controlled environment is that they are concentrated in a known location, focused and concentrated therapies can therefore be used with low side effects. Different techniques can be considered: (i) removal of the implant, (ii) association with chemotherapy, and (iii) association with radiotherapeutics. Some interesting approaches are being discussed. It is important to point out than some techniques could be combined.

The implant could be removed through a second surgery. It has been shown that patients undergoing repeated surgery after recurrence of the tumour have a higher median of survival. However, it is performed with high risks including wound dehiscence and infection after primary immune-suppressing adjuvant therapies (63,64). The timing would have to be study in order to remove the implant only once all the cells are inside but before it degrades and release the cells. This solution is therefore not preferred by surgeons and we were therefore advised to develop a scaffold that will degrade over time with no need of secondary surgery.

The sponge could be used as a trap and a local delivery system and a killing agent such as TMZ or bevacizumab could be integrated inside the trap. It would be interesting to confine it in the core of the implant so that only cells reaching it would be killed. A higher concentration inside the implant could overcome resistance mechanisms that are observed when cells are dispersed in the brain. The killing agent should be slowly released over time as the sponge degrade. A burst release would be undesirable as it could lead to high toxicity for the brain.

The tumour trap could benefit from advances in stereotactic radiosurgery such as the microbeam radiation therapy (65,66) or the Gamma Knife (67), able to deliver with high precision a radiosurgical therapeutic dose to a small target while sparing surrounding tissues. The sponge could also be associated with an internal radiation strategy. Indeed, a previous work conducted in our lab showed an 83% cure rate by injecting lipid nanocapsules encapsulating a β^- emitter, the Rhenium-188 (68). The radioelement could be retained inside the sponge, allowing a local elimination of attracted cells. GBM is considered radioresistant as recurrence occurs in the irradiation field in more than 90% of the cases (69). Radiosensitisers are therefore being developed to overcome this issue and one could be included in the sponge. For example, olaparib, a poly(ADP-ribose)polymerase inhibitor is considered as a promising radiosensitiser and is currently in phase I/IIa trial (70,71).

3.4. Translation to the clinic

The possible translation of the product needs to be considered early in a project. Different aspects should be studied: (i) the scale up of the sponge production and (ii) the sterilisation.

3.4.4 Scale-up

In order to scale-up the production of our sponges, the availability of SF and HA needs to be taken into consideration. They can both easily be produced in large scale for biomedical purposes and are already used in the clinic (72,73). HA for biomedical application is nowadays mostly produced by bacterial fermentation with *Bacillus subtilis* which allows a good control over the molecular weight distribution (74). Ensuring a good batch to batch reproducibility for the SF is necessary for the quality of the sponge production. SF is produced by dissolution of the cocoons of the silkworm *Bombyx mori*. If another species is used, the SF produced will be different. The dissolution process also needs to be controlled. This include the degumming (concentration of Na_2CO_3, boiling time), the dissolution itself (concentration of LiBr, temperature and time), and dialysis. IMIDA (Murcia, Spain) is producing the SF used here under GMP (good manufacturing practice) conditions.

Four critical steps are needed to produce the sponges: (i) polymer mixing, (ii) crosslinking, (iii) freezing, (iv) drying. For each step, the critical parameters identified in Table 5. 3 need to be studied to ensure the quality of the product. Sponges would have to be produced in a larger scale but also with a larger volume. Indeed, the resection cavity created in rats here is about 14 mm^3 while the mean resection cavity for humans is 7.8 cm^3 (75).

Table 5. 3: Critical parameters for each step of the sponge production to take into account during the scale-up.

Step	Critical parameters
Polymer mixing	Volume Mixing process Time Temperature
Cross-linking	Concentration Addition (one batch, drop by drop) Incubation time Incubation temperature
Freezing	Volume Temperature Container shape/material
Drying	Temperature Pressure Volume Container shape Containers disposition inside the freeze-dryer

3.4.5 Sterilisation

A major concern in the development of implants for human application is the sterility. It is necessary for the complete destruction or removal of all microorganisms (including spore-forming and non-spore-forming bacteria, viruses, fungi, and protozoa) that could contaminate pharmaceuticals or other materials and thereby constitute a health hazard. According to the international pharmacopoeia (76), autoclaving or hot air are the most reliable sterilisation techniques and should be used whenever possible. Other sterilisation methods include filtration, ionizing radiation (gamma and electron-beam radiation), and gas (ethylene oxide, formaldehyde). Whatever method of sterilisation is chosen, the procedure must be validated for each type of product or material, both with respect to the assurance of sterility and to ensure that no adverse change occurs within the product. The sterilisation can either be done on the polymers in solution and ensure the sterility during the full process or on the finished material.

Sterilisation techniques available for solutions includes autoclaving (121°C to 124°C at 200 kPa for 15 min 100% humidity) or filtration. Autoclaving the SF solution lead to protein aggregation and autoclaving of HA solution leads to depolymerisation (77,78). Sterilisation by filtration might be employed if the solution is thermosensitive. The solution has to go through a sterile bacteria-retaining filter with pore size not greater than 0.22 µm and be followed by an aseptic transfer of the sterilised solution to the final containers which should then be immediately sealed to exclude any recontamination. Because of the high viscosity of the HA solution, filtration is not an option. For the SF solution, it was shown that the concentration as well as the molecular weight profile was modified through filtration with a loss of the high molecular weight chains (77). Solution sterilisation has to be used only if post-processing sterilisation is not viable option, for example when it is loaded with biological molecules. In our case, we plan to add SDF-1α after sterilisation of the freeze-dried sponge. Sterilisation of the polymers before casting is therefore not needed.

Scaffolds can be sterilised by autoclaving, dry heat, γ irradiation, ethylene oxide and plasma.

Thermal sterilisation by dry heat or steam sterilisation by autoclaving are routinely used to sterilise medical devices but are generally unsuitable for biomedical polymers as it can cause major changes in mechanical and degradation properties (79). Dry heat requires higher temperature than autoclaving and a longer exposition time (160°C for 180 min or 180°C for 30 min) (76). It is more convenient for heat-stable, non-aqueous materials that cannot be sterilised by steam because of its deleterious effects or failure to penetrate. For SF scaffold, it has been used in the literature and led to a modification of the protein conformation, increasing the stiffness and strength of the material (39). Concerning HA scaffolds, it was shown that heat leads to chemical degradation and depolymerisation with a decrease in the average molecular weight as well as destruction of the porous structure because of plastic deformation (78,80).

Exposure to ionising radiation in the form of gamma radiation can be used (76). It is obtained by radioisotopes such as cobalt 60 or electrons energised by a suitable electron accelerator. This process is dangerous for the operator and only well-trained and experienced staff can monitor the process in specially designed installations. It has been observed that sterilisation of a SF scaffold by this technique resulted in an accelerated rate of degradation (77). This is probably due to the production of radicals by ionisation of water molecules and might therefore be reduced by performing γ irradiation under cold conditions or in presence of free radicals scavengers, such as ascorbic acid (81). The same observation was made for HA scaffolds (78).

Gas sterilisation usually involves ethylene oxide. It is highly flammable and highly toxic and is therefore mixed with an inert gas (76). It is possible that toxic residues remain on the material, especially on porous ones like sponges. The process is difficult to control and should only be considered if no other sterilisation procedure can be used.

Plasma treatment using hydrogen peroxide or argon has emerged in many hospital and research settings. No modification on the structure and mechanical properties of SF scaffolds nor on HA scaffolds has been observed with this technique (77,82).

UV irradiation was used here as it was shown to not affect SF and HA scaffold morphology and mechanical properties, and it is easy to use and commonly available in laboratories (77,82). However, while sufficient for preliminary studies, UV is not considered as a suitable sterilisation technique by the international pharmacopeia as it does not kill all microorganisms (76).

Considering the literature, it seems that plasma treatment does not alter the physicochemical properties and morphology of SF and HA scaffolds in the contrary of the other techniques. However, this assumption should be verified analysing the physicochemical properties, morphology, protein release and biological activity of the sponges before and after sterilisation as well as the efficacy of the sterilisation process.

4. Opinion on clinical perspectives

GBM represents one of the greatest challenges in oncology nowadays and the challenge in finding a cure is a daunting task. New, specific, and more effective drugs and/or multidrug synergistic approaches that allow targeting different tumorigenic pathways need to be discovered to reach the goal of eradicating GBM.

Sponges are still far from being adapted for a human application, and some ideas to achieve its translation were discussed. However, I personally believe that tumour trapping could represent a valid option in the future for GBM management in association with other treatments.

Using natural polymers might help to achieve biomimicry as well as approval from the regulatory authorities. However, natural polymers are more complex than synthetic polymers as different conformations might be achieved under different conditions. Though HA and SF are two highly studied polymers, interactions between each other are still misunderstood and it might lead to issues in the future, especially with the scale-up. I think that using natural polymers is the future of the biomaterials and efforts should be made to understand their behaviours better.

As previously mentioned in this PhD thesis, the ideal scaffold should (i) be soft and have mechanical properties close to the brain to avoid increased intracranial pressure; (ii) retain its structure for at least one month and degrade over time to avoid second surgery; and (iii) sustainably release SDF-1α.

We developed freeze-dried sponges made of crosslinked HA, SF and hep. These sponges mimicked the ECM of the brain as they could uptake more than 90% water with a porosity of about 90% and pore sizes between 20 and 150 µm. Mixing SF with HA allowed us to associate the softness of the HA with the strength of the SF. The sponges had a Young’s modulus close to the one of the brain but were stiff enough to be cut to the shape of the resection cavity. Testing the SF-HA and SF-HA-hep sponge *in vivo* taught us the limitations of these sponges. Indeed, the SF-HA sponge degraded too quickly (less than a week) while the SF-HA-hep sponge did not release the chemokine SDF-1α in the brain after a week.

In conclusion, this challenging and original project showed that sponges are a promising tool for the production of a first tumour trap for infiltrative GBM cells that can lead to a proof of concept. Several clinical limitations will need to be considered before dreaming the use of sponges in the clinics and partnerships will have to be developed with academic laboratories as well as with the industry to answer these challenges. However, in this PhD project we expanded the knowledge about the relationship between mechanical and biological properties and we are now able to design more appropriately the ‘‘perfect scaffold’’ for trapping tumour cells. Moreover, this project will help understand better the implications of the implantation of an SDF-1α delivery device in the brain and, hopefully, others will focus on its potential use for treating GBM.

REFERENCES

1. Chinot OL, Wick W, Mason W, Henriksson R, Saran F, Nishikawa R, et al. Bevacizumab plus radiotherapy-temozolomide for newly diagnosed glioblastoma. N Engl J Med. 2014;370(8):709–22.
2. Giese A, Bjerkvig R, Berens ME, Westphal M. Cost of migration: Invasion of malignant gliomas and implications for treatment. J Clin Oncol. 2003;21(8):1624–36.
3. van der Sanden B, Appaix F, Berger F, Selek L, Issartel J-P, Wion D. Translation of the ecological trap concept to glioma therapy: the cancer cell trap concept. Future Oncol. 2013;9(6):817–24.
4. Mahumane GD, Kumar P, Du Toit LC, Choonara YE, Pillay V. 3D scaffolds for brain tissue regeneration: Architectural challenges. Biomater Sci. 2018;6(11):2812–37.
5. De Souza SW, Dobbing J. Cerebral Edema in Developing Brain : I . Normal water and cation Content in Developing Rat Brain and Postmortem Changes. Exp Neurol. 1971;32:431–8.
6. Nava MM, Raimondi MT, Pietrabissa R. Controlling Self-Renewal and Differentiation of Stem Cells via Mechanical Cues. J Biomed Biotechnol. 2012;2012:1–12.
7. Engler AJ, Sen S, Sweeney HL, Discher DE. Matrix elasticity directs stem cell lineage specification. Cell. 2006;126(4):677–89.
8. Wang C, Tong X, Yang F. Bioengineered 3D Brain Tumor Model To Elucidate the Effects of Matrix Stiffness on Glioblastoma Cell Behavior Using PEG-Based Hydrogels. Mol Pharm. 2014;11:2115–25.
9. Hu X, Shmelev K, Sun L, Gil ES, Park SH, Cebe P, et al. Regulation of silk material structure by temperature-controlled water vapor annealing. Biomacromolecules. 2011;12(5):1686–96.
10. Nicholson C, Syková E. Extracellular space structure revealed by diffusion analysis. Trends Neurosci. 1998;21:207–15.
11. Wolf K, te Lindert M, Krause M, Alexander S, te Riet J, Willis AL, et al. Physical limits of cell migration: Control by ECM space and nuclear deformation and tuning by proteolysis and traction force. J Cell Biol. 2013;201(7):1069–84.
12. Jurga M, Dainiak MB, Sarnowska A, Jablonska A, Tripathi A, Plieva FM, et al. The performance of laminin-containing cryogel scaffolds in neural tissue regeneration. Biomaterials. 2011;32(13):3423–34.
13. Garcia-Fuentes M, Meinel AJ, Hilbe M, Meinel L, Merkle HP. Silk fibroin/hyaluronan scaffolds for human mesenchymal stem cell culture in tissue engineering. Biomaterials. 2009;30(28):5068–76.
14. Diao W, Tong X, Yang C, Zhang F, Bao C, Chen H, et al. Behaviors of Glioblastoma Cells in in Vitro Microenvironments. Sci Rep. 2019;9(1):1–9.
15. Lawrence YR, Blumenthal DT, Matceyevsky D, Kanner AA, Bokstein F, Corn BW. Delayed initiation of radiotherapy for glioblastoma: How important is it to push to the front (or the back) of the line? J Neurooncol. 2011;105(1):1–7.
16. Garcia-Fuentes M, Giger E, Meinel L, Merkle HP. The effect of hyaluronic acid on silk fibroin conformation. Biomaterials. 2008;29(6):633–42.
17. Jin HJ, Kaplan DL. Mechanism of silk processing in insects and spiders. Nature. 2003;424(6952):1057–61.
18. Ageitos JM, Pulgar A, Csaba N, Garcia-Fuentes M. Study of nanostructured fibroin/dextran matrixes for controlled protein release. Eur Polym J. 2019;114(February):197–205.
19. Fournier E, Passirani C, Montero-Menei CN, Benoit JP. Biocompatibility of implantable synthetic polymeric drug carriers: Focus on brain biocompatibility. Biomaterials. 2003;24(19):3311–31.
20. Ratner BD. Reducing capsular thickness and enhancing angiogenesis around implant drug release systems. J Control Release. 2002;78(1–3):211–8.
21. Williams D. Definitions in biomaterials. William D, editor. Progress in biomedical engineering. Amsterdam:Elsevier; 1987.

22. Castner DG, Ratner BD. Biomedical surface science: Foundations to frontiers. Surf Sci. 2002;500(1–3):28–60.

23. Babensee JE, Anderson JM, McIntire L V, Mikos AG. Host response to tissue engineered devices. Adv Drug Deliv Rev. 1998;33(1–2):111–39.

24. Williams DF. Tissue-biomaterial interactions. J Mater Sci. 1987;22(10):3421–45.

25. Menei P, Croué A, Daniel V, Pouplard-Barthelaix A, Benoit JP. Fate and biocompatibility of three types of microspheres implanted into the brain. J Biomed Mater Res. 1994;28(9):1079–85.

26. Autier L, Clavreul A, Cacicedo ML, Franconi F, Sindji L, Rousseau A, et al. A new glioblastoma cell trap for implantation after surgical resection. Acta Biomater. 2018;84:268–79.

27. Říhová B. Biocompatibility of biomaterials: Hemocompatibility, immunocompatibility and biocompatibility of solid polymeric materials and soluble targetable polymeric carriers. Adv Drug Deliv Rev. 1996;21(2):157–76.

28. Foo CWP, Bini E, Hensman J, Knight DP, Lewis R V., Kaplan DL. Role of pH and charge on silk protein assembly in insects and spiders. Appl Phys A Mater Sci Process. 2006;82(2):223–33.

29. Malay Ö, Bayraktar O, Batigün A. Complex coacervation of silk fibroin and hyaluronic acid. Int J Biol Macromol. 2007;40(4):387–93.

30. Sadir R, Baleux F, Grosdidier A, Imberty A, Lortat-Jacob H. Characterization of the stromal cell-derived factor-1alpha-heparin complex. J Biol Chem. 2001;276(11):8288–96.

31. Yang J wen, Zhang Y feng, Wan C yan, Sun Z yi, Nie S, Jian S juan, et al. Autophagy in SDF-1a-mediated DPSC migration and pulp regeneration. Biomaterials. 2015;44:11–23.

32. Purcell BP, Elser JA, Mu A, Margulies KB, Burdick JA. Synergistic effects of SDF-1α chemokine and hyaluronic acid release from degradable hydrogels on directing bone marrow derived cell homing to the myocardium. Biomaterials. 2012;33(31):7849–57.

33. Prokoph S, Chavakis E, Levental KR, Zieris A, Freudenberg U, Dimmeler S, et al. Sustained delivery of SDF-1alpha from heparin-based hydrogels to attract circulating pro-angiogenic cells. Biomaterials. 2012;33(19):4792–800.

34. Krieger JR, Ogle ME, McFaline-Figueroa J, Segar CE, Temenoff JS, Botchwey EA. Spatially localized recruitment of anti-inflammatory monocytes by SDF-1α-releasing hydrogels enhances microvascular network remodeling. Biomaterials. 2016;77:280–90.

35. Bladergroen BA, Siebum B, Siebers-Vermeulen KGC, Kuppevelt TH Van, Poot AA, Feijen J, et al. In Vivo Recruitment of Hematopoietic Cells Using Stromal Cell–Derived Factor 1 Alpha–Loaded Heparinized Three-Dimensional Collagen Scaffolds. Tissue Eng Part A. 2009;15(7):1591–9.

36. Dutta D, Hickey K, Salifu M, Fauer C, Willingham C, Stabenfeldt SE. Spatiotemporal presentation of exogenous SDF-1 with PLGA nanoparticles modulates SDF-1/CXCR4 signaling axis in the rodent cortex. Biomater Sci. 2017;5(8):1640–51.

37. Chopra A. 99mTc-S-acetylmercaptoacetyltriserine-stromal- derived factor 1α. J Nucl Med. 2008;49:963–969.

38. Yi X, Jin G, Zhang X, Mao W, Li H, Qin J, et al. Cortical Endogenic Neural Regeneration of Adult Rat after Traumatic Brain Injury. PLoS One. 2013;8(7):1–13.

39. Haji Mansor M, Najberg M, Contini A, Alvarez-Lorenzo C, Garcion E, Jérôme C, et al. Development of a Non-toxic and Non-denaturing Formulation Process for Encapsulation of SDF-1α into PLGA/PEG-PLGA Nanoparticles to Achieve Sustained Release. Eur J Pharm Biopharm. 2018;125(November 2017):38–50.

40. Insall RH. Understanding eukaryotic chemotaxis: a pseudopod-centred view. Nat Rev Mol Cell Biol. 2010;11(6):453–8.

41. Staros J V., Wright RW, Swingle DM. Enhancement by N-hydroxysulfosuccinimide of water-soluble carbodiimide-mediated coupling reactions. Anal Biochem. 1986;156(1):220–2.

42. Koh LD, Cheng Y, Teng CP, Khin YW, Loh XJ, Tee SY, et al. Structures, mechanical properties and applications of silk fibroin materials. Prog Polym Sci. 2015;46:86–110.

43. CHEN X, LI W, YU T. Conformation Transition of Silk Fibroin Induced by Blending Chitosan. J Polym Sci Part B Polym Phys. 1997;35:2293–6.

44. Yan S, Li M, Zhang Q, Wang J. Blend films based on silk fibroin/hyaluronic acid. Fibers Polym. 2013;14(2):188–94.

45. Sadir R, Imberty A, Baleux F, Lortat-Jacob H. Heparan sulfate/heparin oligosaccharides protect stromal cell-derived factor-1 (SDF-1)/CXCL12 against proteolysis induced by CD26/dipeptidyl peptidase IV. J Biol Chem. 2004;279(42):43854–60.

46. Abe P, Mueller W, Schütz D, MacKay F, Thelen M, Zhang P, et al. CXCR7 prevents excessive CXCL12-mediated downregulation of CXCR4 in migrating cortical interneurons. Development. 2014;141(9):1857–63.

47. Teicher BA, Fricker SP. CXCL12 (SDF-1)/CXCR4 pathway in cancer. Clin Cancer Res. 2010;16(11):2927–31.

48. Connell BJ, Sadir R, Baleux F, Laguri C, Kleman JP, Luo L, et al. Heparan sulfate differentially controls CXCL12a-And CXCL12g-mediated cell migration through differential presentation to their receptor CXCR4. Sci Signal. 2016;9(452):1–12.

49. Sarrazin S, William C. L, Jeffrey D. E. Heparan Sulfate Proteoglycans Stephane. Neoplasma. 1965;12(5):549–56.

50. Allen SJ, Crown SE, Handel TM. Chemokine:Receptor Structure, Interactions, and Antagonism. Annu Rev Immunol. 2007 Mar;25(1):787–820.

51. Monneau Y, Arenzana-Seisdedos F, Lortat-Jacob H. The sweet spot: how GAGs help chemokines guide migrating cells. J Leukoc Biol. 2016;99(6):935–53.

52. Lortat-Jacob H, Grosdidier A, Imberty A. Structural diversity of heparan sulfate binding domains in chemokines. Proc Natl Acad Sci. 2002;99(3):1229–34.

53. Laguri C, Sadir R, Rueda P, Baleux F, Gans P, Arenzana-Seisdedos F, et al. The novel CXCL12γ isoform encodes an unstructured cationic domain which regulates bioactivity and interaction with both glycosaminoglycans and CXCR4. PLoS One. 2007;2(10).

54. Jain A, Betancur M, Patel GD, Valmikinathan CM, Mukhatyar VJ, Vakharia A, et al. Guiding intracortical brain tumour cells to an extracortical cytotoxic hydrogel using aligned polymeric nanofibres. Nat Mater. 2014;13:308–16.

55. Lyon JG, Carroll SL, Mokarram N, Bellamkonda R V. Electrotaxis of Glioblastoma and Medulloblastoma Spheroidal Aggregates. Sci Rep. 2019;9(1):1–19.

56. Clavreul A, Guette C, Faguer R, Tétaud C, Boissard A, Lemaire L, et al. Glioblastoma-associated stromal cells (GASCs) from histologically normal surgical margins have a myofibroblast phenotype and angiogenic properties. J Pathol. 2014;233(1):74–88.

57. ClinicalTrials.gov [Internet]. Identifier NCT02345824, 2017, Feb. 16. Available from https://clinicaltrials.gov/ct2/show/NCT02345824?term=proliferation&cond=Glioblastoma&rank=2 .

58. Bajetto A, Bonavia R, Barbero S, Florio T, Schettini G. Chemokines and their receptors in the central nervous system. Front Neuroendocrinol. 2001;22(3):147–84.

59. Duan X, Kang E, Liu CY, Ming G li, Song H. Development of neural stem cell in the adult brain. Curr Opin Neurobiol. 2008;18(1):108–15.

60. Kim DH, Seo YK, Thambi T, Moon GJ, Son JP, Li G, et al. Enhancing neurogenesis and angiogenesis with target delivery of stromal cell derived factor-1α using a dual ionic pH-sensitive copolymer. Biomaterials. 2015;61:115–25.

61. Hickey K, Stabenfeldt SE. Using biomaterials to modulate chemotactic signaling for central nervous system repair. Biomed Mater. 2018;13(4).

62. Séhédic D, Chourpa I, Tétaud C, Griveau A, Loussouarn C, Avril S, et al. Locoregional confinement and major clinical benefit of188Re-loaded CXCR4-targeted nanocarriers in an orthotopic human to mouse model of glioblastoma. Theranostics. 2017;7(18):4517–36.

63. Lu VM, Jue TR, McDonald KL, Rovin RA. The Survival Effect of Repeat Surgery at Glioblastoma Recurrence and its Trend: A Systematic Review and Meta-Analysis. World Neurosurg. 2018;115:453-459.e3.

64. Brandes AA, Bartolotti M, Franceschi E. Second surgery for recurrent glioblastoma: Advantages and pitfalls. Expert Rev Anticancer Ther. 2013;13(5):583–7.

65. Serduc R, Bräuer-Krisch E, Siegbahn EA, Bouchet A, Pouyatos B, Carron R, et al. High-precision radiosurgical dose delivery by interlaced microbeam arrays of high-flux low-energy synchrotron x-rays. PLoS One. 2010;5(2):1–12.

66. Smyth LML, Day LR, Woodford K, Rogers PAW, Crosbie JC, Senthi S. Identifying optimal clinical scenarios for synchrotron microbeam radiation therapy: A treatment planning study. Phys Medica. 2019;60:111–9.

67. Bowden G, Faramand A, Niranjan A, Lunsford LD, Monaco E. Gamma Knife Radiosurgery for the Management of More Than 15 Cerebral Metastases. World Neurosurg. 2019;126:e989–97.

68. Cikankowitz A, Clavreul A, Tétaud C, Lemaire L, Rousseau A, Lepareur N, et al. Characterization of the distribution, retention, and efficacy of internal radiation of 188Re-lipid nanocapsules in an immunocompromised human glioblastoma model. J Neurooncol. 2017;131(1):49–58.

69. Minniti G, Amelio D, Amichetti M, Salvati M, Muni R, Bozzao A, et al. Patterns of failure and comparison of different target volume delineations in patients with glioblastoma treated with conformal radiotherapy plus concomitant and adjuvant temozolomide. Radiother Oncol. 2010;97(3):377–81.

70. ClinicalTrials.gov [Internet]. Identifier NCT03212742; 2019 Jan 16. Available from https://clinicaltrials.gov/ct2/show/NCT03212742?term=NCT03212742&rank=1.

71. Lesueur P, Lequesne J, Grellard J-M, Dugué A, Coquan E, Brachet P-E, et al. Phase I/IIa study of concomitant radiotherapy with olaparib and temozolomide in unresectable or partially resectable glioblastoma: OLA-TMZ-RTE-01 trial protocol. BMC Cancer. 2019;19(1):1–11.

72. Balazs EA. Ultrapure Hyaluronic Acid and the Use Thereof. U.S. Patent 4,141,973. 1979.

73. van Turnhout AAWM, Franke CJJ, Vriens-Nieuwenhuis EJC, van der Sluis WB. The use of SERI^{TM} Surgical Scaffolds in direct-to-implant reconstruction after skin-sparing mastectomy: A retrospective study on surgical outcomes and a systematic review of current literature. J Plast Reconstr Aesthetic Surg. 2018;71(5):644–50.

74. Sze JH, Brownlie JC, Love CA. Biotechnological production of hyaluronic acid: a mini review. 3 Biotech. 2016;6(1):1–9.

75. Shah JK, Potts MB, Sneed PK, Aghi MK, McDermott MW. Surgical Cavity Constriction and Local Progression Between Resection and Adjuvant Radiosurgery for Brain Metastases. Cureus. 2016;8(4).

76. The international pharmacopeia: 5.8 Methods of Sterilization. Eighth Edi. 2018. 1–3 p.

77. Rnjak-Kovacina J, Desrochers TM, Burke KA, Kaplan DL. The effect of sterilization on silk fibroin biomaterial properties. Macromol Biosci. 2015;15(6):861–74.

78. Reháková M, Bakoš D, Soldán M, Vizárová K. Depolymerization reactions of hyaluronic acid in solution. Int J Biol Macromol. 1994;16(3):121–4.

79. Rogers W. Sterilisation Techniques for Polymers in Sterilisation of Biomaterials and Medical Devices. S. Lerouge, A. Simmons E, editor. Woodhead Publishing, Sawston, Cambridge, UK; 2012. Ch.2.

80. Plikk P, Odelius K, Hakkarainen M, Albertsson AC. Finalizing the properties of porous scaffolds of aliphatic polyesters through radiation sterilization. Biomaterials. 2006;27(31):5335–47.

81. Kempner ES. Effects of High-Energy Electrons and Gamma Rays Directly on Protein Molecules. J Pharm Sci. 2001 Oct 1;90(10):1637–46.

82. Shimojo AAM, De Souza Brissac IC, Pina LM, Lambert CS, Santana MHA. Sterilization of auto-crosslinked hyaluronic acid scaffolds structured in microparticles and sponges. Biomed Mater Eng. 2015;26(3–4):183–91.

ANNEXE

European Journal of Pharmaceutics and Biopharmaceutics 125 (2018) 38–50

Contents lists available at ScienceDirect

European Journal of Pharmaceutics and Biopharmaceutics

journal homepage: www.elsevier.com/locate/ejpb

Research paper

Development of a non-toxic and non-denaturing formulation process for encapsulation of SDF-1α into PLGA/PEG-PLGA nanoparticles to achieve sustained release

Muhammad Haji Mansor[a,b], Mathie Najberg[a,c], Aurélien Contini[a], Carmen Alvarez-Lorenzo[c], Emmanuel Garcion[a,1], Christine Jérôme[b,1], Frank Boury[a,*]

[a] CRCINA, INSERM, Université de Nantes, Université d'Angers, Angers, France
[b] Center for Education and Research on Macromolecules (CERM), Université de Liège, Liège, Belgium
[c] Departamento de Farmacologia, Farmacia y Tecnología Farmacéutica, R & D Pharma Group, Facultad de Farmacia, Universidade de Santiago de Compostela, Santiago de Compostela, Spain

ARTICLE INFO

Keywords:
Stromal cell-derived factor-1α (SDF-1α)
Protein encapsulation
Polymeric nanoparticles
Sustained release

ABSTRACT

Chemokines are known to stimulate directed migration of cancer cells. Therefore, the strategy involving gradual chemokine release from polymeric vehicles for trapping cancer cells is of interest. In this work, the chemokine stromal cell-derived factor-1α (SDF-1α) was encapsulated into nanoparticles composed of poly-(lactic-co-glycolic acid) (PLGA) and a polyethylene glycol (PEG)-PLGA co-polymer to achieve sustained release. SDF-1α, and lysozyme as a model protein, were firstly precipitated to promote their stability upon encapsulation. A novel phase separation method utilising a non-toxic solvent in the form of isosorbide dimethyl ether was developed for the individual encapsulation of SDF-1α and lysozyme precipitates. Uniform nanoparticles of 200–250 nm in size with spherical morphologies were successfully synthesised under mild formulation conditions and conveniently freeze-dried in the presence of hydroxypropyl-β-cyclodextrin as a stabiliser. The effect of PLGA carboxylic acid terminal capping on protein encapsulation efficiency and release rate was also explored. Following optimisation, sustained release of SDF-1α was achieved over a period of 72 h. Importantly, the novel encapsulation process was found to induce negligible protein denaturation. The obtained SDF-1α nanocarriers may be subsequently incorporated within a hydrogel or other scaffolds to establish a chemokine concentration gradient for the trapping of glioblastoma cells.

1. Introduction

Stromal cell-derived factor-1α (SDF-1α) is a chemokine composed of 68 amino acids [1] that binds to its cognate receptor, C-X-C chemokine receptor type 4 (CXCR4) [2]. One of its important physiological functions is to retain high concentrations of CXCR4-expressing stem and progenitor cells within the bone marrow by creating a positive concentration gradient from the blood to this organ [3]. In the events of tissue damage, the SDF-1α expression at the injury site is elevated [4–6] in a simultaneous fashion to the increased SDF-1α degradation in the bone marrow [7,8] to allow mobilisation of the stem and progenitor cells and their subsequent chemoattraction to the site of damage. In addition to its roles in tissue repair and regeneration, SDF-1α-mediated chemotaxis is also implicated in tumour metastases. CXCR4-expressing cancerous cells that are present in the blood or lymphatic circulation after getting dislodged from the primary tumour site can be

---

Abbreviations: AFM, atomic force microscopy; BSA, bovine serum albumin; CXCR4, C-X-C chemokine receptor type 4; DL, drug loading; DMEM, Dulbecco's Modified Eagle's Medium; DMI, isosorbide dimethyl ether/dimethyl isosorbide; DMSO, dimethyl sulfoxide; EE, encapsulation efficiency; ELISA, enzyme-linked immunosorbent assay; FBS, foetal bovine serum; GBM, glioblastoma; HCl, hydrochloric acid; HPBCD, hydroxypropyl-β-cyclodextrin; ICH, International Conference on Harmonization; LNC, lipid nanocapsules; Mn, number-average molecular weight; Mw, weight-average molecular weight; NaCl, sodium chloride; NIH3T3, mouse fibroblast cell line NIH3T3; NMR, nuclear magnetic resonance; P188, poloxamer 188; PBS, phosphate-buffered saline; PDI, polydispersity index; PE, precipitation efficiency; PEG, polyethylene glycol; pI, isoelectric point; PLGA, poly-lactic-co- glycolic acid PLGA-COOH, poly-lactic-co- glycolic acid with uncapped carboxylic acid terminals; PLGA-COOR, poly-lactic-co- glycolic acid with capped carboxylic acid terminals; PS, polystyrene; PVA, polyvinyl alcohol; SD, standard deviation; SDF-1α, stromal cell-derived factor-1α; SEC, size exclusion chromatography; SEM, scanning electron microscopy; T_c, collapse temperature; TEM, transmission electron microscopy; Tris, tris(hydroxymethyl)-aminomethane; U87-MG, human malignant glioblastoma cell line U87-MG

[*] Corresponding author at: Cancer and Immunology Research Centre Nantes-Angers (CRCINA), INSERM U1232, Team GLIAD, Université d'Angers, IBS – CHU Angers, 4 rue Larrey, 49933 ANGERS CEDEX 9, France.

E-mail address: frank.boury@univ-angers.fr (F. Boury).

[1] Equivalent contribution.

https://doi.org/10.1016/j.ejpb.2017.12.020
Received 10 November 2017; Received in revised form 12 December 2017; Accepted 29 December 2017

chemoattracted to SDF-1α-secreting sites such as the bone marrow [9], liver [10] and lymph nodes [11] for future metastatic growth. This pathological role of SDF-1α has inspired the design of implants capable of creating a SDF-1α concentration gradient for trapping CXCR4-expressing cancerous cells relevant to multiple types of malignant cancers such as glioblastoma (GBM) [12], gastric carcinoma [13] and small-cell lung cancer [14].

Due to its solubility and rapid diffusion in physiological media, a sustained delivery of SDF-1α is a prerequisite for establishing its concentration gradient. Encapsulation of SDF-1α into polymeric nanoparticles is a credible strategy for achieving a gradual SDF-1α release at the site of application. In this regard, poly-(lactic-co-glycolic acid) (PLGA) is a polymer of choice for nanoparticle formulations, owing to its biocompatibility, biodegradability and most importantly, its status as a Food and Drug Administration-approved pharmaceutical excipient [15]. However, due to its hydrophobicity, the formation of stable PLGA nanoparticles often necessitates the use of amphiphilic surfactants such as polyvinyl alcohol (PVA) [16,17] and poloxamer 188 (P188) [18] in the formulation process. Although these surfactants are innocuous when used in isolation, residual PVA and P188 bound to the PLGA nanoparticle surfaces have been reported to induce toxicities especially at nanoparticle concentrations exceeding 1 mg/mL [19], which are relevant to many local applications of PLGA-based nanoparticles. The development of a PLGA-based nanoparticle formulation process that avoids or reduces the need for surfactants is therefore in demand.

To encapsulate hydrophilic drugs in hydrophobic PLGA matrices, the double emulsion (water/oil/water) process is often preferred [20,21]. While this process is excellent for encapsulating small hydrophilic molecules, problems can arise with drugs of complex structures such as proteins. The first step of this process that involves emulsification of a protein solution in the polymer-containing organic phase can lead to adsorption of protein molecules to the water/organic solvent interface and their subsequent unfolding. The structural instability of dissolved proteins is actually exaggerated by their conformational flexibility that makes it possible for their hydrophobic pockets to be externalised to make contact with the organic phase upon emulsification [22]. Thus, a possible solution to promote protein stability during encapsulation is by minimising their conformational mobility through the use of proteins in solid form. In this regard, techniques such as freeze-drying and spray-freeze-drying have been employed to produce fine protein particles for subsequent encapsulation [23,24]. However, these techniques themselves can induce substantial protein structural changes. On the other hand, proteins in solution can be precipitated by adding a water-miscible organic solvent [25]. This technique produces homogenous nano-sized protein particles without affecting protein structures and bioactivities, and therefore serves as a suitable protein treatment prior to encapsulation.

Currently, the encapsulation of proteins or peptides into PLGA nanoparticles typically involves the use of toxic halogenated solvents such as chloroform and dichloromethane as the polymer solvent [26–28]. Other common harmful PLGA solvents include acetonitrile [29], N-methylpyrrolidone [30], N,N-dimethylformamide and tetrahydrofuran [31]. These solvents belong to Class 2 according to the International Conference on Harmonization (ICH), which are harmful solvents that can pose serious threats to patient safety [32]. Less toxic solvents such as acetone [33], ethyl acetate [34] and dimethyl sulfoxide [30] are being increasingly used as alternatives. Nevertheless, they are still regarded as potential hazards to human health by the ICH. Differently, the safety of non-volatile water-miscible organic solvents such as glycofurol and isosorbide dimethyl ether (DMI) have been demonstrated *in vivo*. They have been recommended as solvents suitable for intravascular injections [35,36] due to their negligible toxicity. Thus, the use of these solvents for protein encapsulation into PLGA-based nanoparticles is well-motivated.

In the present study, an amphiphilic polyethylene glycol (PEG)-PLGA co-polymer was synthesised and used together with hydrophobic PLGA polymers to produce stable nanoparticles via a phase separation method without the use of conventional surfactants. In addition, the non-toxic DMI was utilised as a solvent for the PLGA polymers and the PEG-PLGA co-polymer. To the best of our knowledge, this is the first example of the use of this benign solvent to produce PLGA/PEG-PLGA nanoparticles. PLGA with capped or uncapped carboxylic acid terminals were combined with the PEG-PLGA co-polymer at different proportions to produce nanoparticles of different size distributions and surface charges. The nanoparticles were then freeze-dried in the presence of three excipients to explore the possibility of obtaining nanocarriers with a prolonged shelf-life. Following the optimisation of the PLGA/PEG-PLGA nanoparticle synthesis, lysozyme (14.3 kDa, isoelectric point: 11.35) was initially used as a model protein to optimise the encapsulation of SDF-1α (8.0 kDa, isoelectric point: 10.5). To preserve the protein bioactivity throughout the formulation process, lysozyme and SDF-1α precipitates were prepared by mixing respective protein solutions with glycofurol prior to encapsulation. Then, *in vitro* release of lysozyme and SDF-1α from the PLGA/PEG-PLGA nanoparticles was studied. The bioactivity of the released SDF-1α was subsequently assessed in terms of its capacity to induce migration of CXCR4-expressing human GBM cells (U87-MG). Finally, the cytocompatibility of the newly-developed nanoparticles was assessed *in vitro*.

2. Materials and methods

2.1. Materials

PLGA with capped carboxylic acid terminals and PEG-PLGA co-polymer were synthesised as described in Section 2.2. PLGA 75:25 with uncapped terminals (Resomer® RG752H, Mw = 9850 Da, polydispersity index (PDI) = 2.4), lysozyme of chicken egg white, *Micrococcus lysodeikticus*, glycofurol (tetraglycol or tetrahydrofurfuryl alcohol polyethyleneglycol ether), isosorbide dimethyl ether (dimethyl isosorbide), dimethyl sulfoxide (DMSO), sodium chloride, poloxamer 188 (Lutrol® F68), glycine, sucrose, trehalose, 37% hydrochloric acid, 10 M sodium hydroxide, tris(hydroxymethyl)aminomethane (Tris) base (Trizma®) and agarose with low gelling temperature were obtained from Sigma-Aldrich (Saint Quentin Fallavier, France). DL-lactide (Purasorb® DL) and glycolide (Purasorb® G) were obtained from Purac Biomaterials, Frankfurt, Germany. Bovine serum albumin fraction V was obtained from Roche Diagnostics (Mannheim, Germany), human SDF-1α from Miltenyi Biotech (Paris, France), hydroxypropyl-β-cyclodextrin (Kleptose® HPBCD) from Roquette (Lestrem, France), Dulbecco's phosphate-buffered saline (Biowhittaker®) from Lonza (Verviers, Belgium), and Dulbecco's Modified Eagle's Medium (Gibco® DMEM) from Thermo Fisher Scientific (Villebon sur Yvette, France). Ultrapure water dispensed from a Milli-Q® Advantage A10 system (Millipore, Paris, France) was used in all experiments.

2.2. Synthesis and characterization of PLGA with capped carboxylic acid terminals (PLGA-COOR) and PEG-PLGA co-polymer

2.2.1. Synthesis

The synthesis of PLGA-COOR was adapted from the ring-opening polymerization method described by Yoo and Park [37]. Briefly, a mixture of DL-lactide (Purasorb® DL) and glycolide (Purasorb® G) in the molar ratio of 3:1 was heated with the initiator benzyl alcohol to 140 °C under nitrogen atmosphere for complete melting. The use of this initiator would result in a benzyl group being the R-group in the PLGA-COOR product. Then, 0.04% (w/w) stannous octoate was added, and the reaction mixture was further heated to 180 °C. The temperature was maintained for 3 h for polymerization to take place under static vacuum. The polymer was then recovered by dissolution in dichloromethane before precipitation in heptane. The precipitate was subsequently filtered and dried at 25 °C for 24 h under vacuum. For the synthesis of PEG-PLGA co-polymer, the same procedure was adopted except that monomethoxy-PEG of number average molecular weight (Mn) of 5 kDa (Sigma-Aldrich) was used as an initiator instead of benzyl alcohol, and the precipitation of PEG-PLGA was carried out in diethyl ether chilled to −20 °C.

2.2.2. Characterization

^{1}H nuclear magnetic resonance (^{1}H NMR) spectra were recorded using a Bruker Avance® 400 apparatus (Bruker, Brussels, Belgium) to characterise the polymer/co-polymer composition and to estimate Mn. Deuterated DMSO and chloroform were used as solvents for PLGA-COOR and PEG-PLGA co-polymer respectively. Spectra were recorded at 400 MHz in the Fourier Transform mode at 25 °C with chemical shifts expressed in ppm with respect to the tetramethylsilane standard. The polymer/co-polymer was also characterized by size exclusion chromatography (SEC) using a Viscotek® TDA-305 equipment (Malvern, Worcestershire, UK). Polymer/co-polymer was dissolved in tetrahydrofuran at 5 mg/mL for elution at a flow rate of 1 mL/min at 45 °C. The weight-average molecular weight (Mw) and Mn were expressed with respect to polystyrene standards. The PDI of the polymer/co-polymer was subsequently obtained by calculating the ratio of Mw to Mn.

2.3. Preparation of lysozyme and SDF-1α precipitates

Proteins were precipitated using a technique adapted from Giteau et al. [25]. Briefly, lyophilized protein as provided by the supplier was dissolved in sodium chloride (NaCl) solution containing 20% (w/v) P188 as a protein protective agent. 25 µL of the protein solution was then added to 975 µL glycofurol in a 10 mL Nalgene® Oak Ridge High-Speed centrifuge tube (Thermo Fisher Scientific) prior to incubation in ice for 30 min. The optimal concentrations of protein and NaCl were investigated initially using lysozyme as a model protein. To evaluate the precipitation efficiency (PE), the formed suspension of protein precipitates was centrifuged at 12,800*g* for 30 min. The supernatant was carefully discarded and the pelleted protein precipitates were dissolved in 1 mL 0.05 M Tris-HCl buffer solution containing 0.1% (w/v) bovine serum albumin (BSA) and diluted for further quantification (see Section 2.7). PE was calculated using Eq. (1).

$$PE\,(\%) = \frac{Mass\ of\ protein\ recovered\ after\ precipitation}{Initial\ mass\ of\ protein\ used\ as\ a\ starting\ material} \times 100 \tag{1}$$

2.4. Preparation of lysozyme- and SDF-1α-loaded nanoparticles

Nanoparticles were formed using a phase separation method adapted from Tran et al. [17]. Briefly, PLGA-COOR, PLGA-COOH and PEG-PLGA co-polymer were dissolved separately in DMI at 12% (w/v). The three polymer solutions were mixed in different proportions to give a total volume of 300 µL. For protein encapsulation, 100 µL protein precipitate suspension in glycofurol consisting of either 25 µg lysozyme or 10 µg SDF-1α was added to the polymer solutions prior to magnetic stirring at 1300 rpm for 30 s. The theoretical drug loadings (DL), as calculated using Eq. (2), were 0.07% and 0.03% for lysozyme and SDF-1α respectively. For the synthesis of unloaded nanoparticles, the 100 µL protein precipitates was replaced with an equal volume of glycofurol alone. Then, 100 µL aqueous phase in the form of 0.05 M glycine-NaOH buffer solution was added under magnetic stirring to initiate phase separation. After 1 min, another 500 µL aqueous phase was added every 30 s for four times to enhance the phase separation process. The pH of the aqueous phase was varied to investigate the effect of protein solubility on encapsulation efficiencies. The formed nanoparticle suspension was diluted with water to 30 mL to allow diffusion of residual solvents out of the nanoparticles. After 1 h, the nanoparticle suspension was centrifuged for 30 min at 10,000*g*. The supernatant was discarded and the nanoparticle pellet was re-suspended in water. The centrifugation was repeated once to complete the purification process and the resultant nanoparticle suspension was concentrated to a final volume of 1 mL.

$$DL\,(\%) = \frac{Initial\ mass\ of\ protein\ used\ as\ a\ starting\ material}{Total\ mass\ of\ PLGA\ and\ PEG{-}PLGA} \times 100 \tag{2}$$

2.5. Freeze-drying of nanoparticles

After purification, 1 mL of nanoparticle suspension was transferred into a 20 mL glass vial. To ensure the stability of the nanoparticles throughout the freeze-drying process, 1 mL of cryoprotectant solution was added to the nanoparticle suspension to give a total volume of 2 mL and a final nanoparticle concentration of approximately 15 mg/mL. The cryoprotectants tested were HPBCD, trehalose and sucrose, at a final concentration of 5% (w/v). The vial was then immersed in liquid nitrogen (−196 °C) for 1 min to freeze the nanoparticle-cryoprotectant mixture, and subsequently placed on the shelf of the freeze-dryer pre-cooled to −35 °C for 2 h. The samples were subsequently lyophilized, alongside cryoprotectant-free nanoparticle samples as a control, in a Lyovax® GT freeze-dryer (Steris, Bordeaux, France) at −20 °C and 0.3 mbar for 16 h. The nanoparticle size was measured (as described in Section 2.6.1) before and after freeze-drying. The nanoparticles were assumed to be stable throughout the freeze-drying process if the ratio of final to initial size (S_f/S_i) and polydispersity index (PDI_f/PDI_i) is close to 1.

2.6. Nanoparticle characterization

2.6.1. Size distribution and zeta-potential

The nanoparticle size distribution was determined by a dynamic light scattering (DLS) technique whereas zeta-potentials were derived from electrophoretic mobility values using the Smoluchowski's approximation. Nanoparticle samples were prepared by dilution in water or 0.01 M NaCl solution for size and zeta-potential measurements respectively, to obtain concentrations suitable for analyses in a Nanosizer® ZS (Malvern) such that the attenuator value was in the range of 5–7. Each sample was measured in triplicate, with each measurement representing an average value of at least 10 runs. All measurements were made at 25 °C under automatic mode. Besides average particle size, the DLS protocol of Nanosizer® ZS produced a PDI value ranging between 0 and 1 that estimates the width of the size distribution.

2.6.2. Scanning electron microscopy (SEM), transmission electron microscopy (TEM) and atomic force microscopy (AFM)

The nanoparticle morphology was visualised under SEM (JSM 6310F, JEOL, Paris, France), TEM (JEM 1400, JEOL, Paris, France) and AFM (AutoProbe CP-Research, Veeco Digital Instruments, Santa Barbara, California, USA). A 2 µL drop of purified nanoparticle suspension at a concentration of 200 µg/mL was added onto the centre of a glass slide (for SEM and AFM) or carbon-coated nickel grid (for TEM), and left to dry overnight at room temperature. For SEM, the sample was coated with a gold layer of 5 nm thickness prior to observation while no coating was applied to TEM or AFM samples. For AFM, tapping mode (resonance frequency = 300 kHz) was used instead of contact mode to minimise sample damage upon observation.

For the observation of protein nanoprecipitates, the undiluted protein nanoprecipitate suspension was used to prepare samples for SEM, via the same procedure as the preparation of nanoparticle samples.

2.6.3. Protein encapsulation efficiency

Lyophilized protein-loaded nanoparticles, and unloaded nanoparticles as a control, were dissolved in 1 mL DMSO for 1 h before the addition of 3 mL 0.01 M HCl. The solution was left to stand for another hour for protein extraction from the nanoparticle fragments. The samples were then diluted for use in protein quantification assays (see Section 2.7). Encapsulation efficiency (EE) was calculated using Eq. (3).

$$EE\,(\%) = \frac{Mass\ of\ protein\ recovered\ from\ dissolved\ nanoparticles}{Initial\ mass\ of\ protein\ used\ as\ a\ starting\ material} \times 100 \tag{3}$$

2.7. *Protein quantification*

2.7.1. *Quantification of lysozyme*

Lysozyme was quantified using *Micrococcus lysodeikticus* cell suspension as a substrate as described by Morille et al. [38]. Briefly, 100 µL lysozyme solution or sample was added to 2.9 mL suspension of *M. lysodeikticus* (0.015% (w/v)) in 0.05 M Tris-HCl buffer solution (pH 7.4). After 4 h of incubation at 37 °C, the absorbance was measured at 450 nm. For the construction of a standard curve, the concentration of lysozyme solutions used was between 100 and 1000 ng/mL. 0.05 M Tris-HCl buffer solution (pH 7.4) was used to prepare several dilutions of the samples to obtain absorbance readings that were within the standard curve range.

2.7.2. *Quantification of SDF-1α*

SDF-1α was quantified using an enzyme-linked immunosorbent assay (ELISA) according to the supplier's instructions (R&D Systems, Lille, France). Briefly, SDF-1α capture antibody solution was added to a Nunc Maxisorp® 96-well microplate (Thermo Fisher Scientific) and incubated overnight to coat the wells. The microplate was then washed with 0.05% (w/v) Tween® 20 in phosphate-buffered saline (PBS) solution (pH 7.4), followed by a 1-hour incubation with PBS solution (pH 7.4) containing 1% (w/v) BSA to block the microplate. After washing, the kit standard and samples diluted in PBS (pH 7.4) containing 1% (w/v) BSA were added to the microplate for a 2-h incubation. Then, the microplate was washed before addition of a detection antibody solution for another 2-h incubation. The washing step was subsequently repeated prior to incubation with a streptavidin-horseradish peroxidase solution for 20 min. After the final wash, a substrate solution was added for another 20-min incubation. Finally, 2N sulphuric acid was added to terminate the enzymatic reaction followed by immediate measurement of absorbance at 450 nm. All incubations were done at room temperature.

2.8. *Assessment of SDF-1α bioactivity*

The bioactivity of the precipitated and released SDF-1α was assessed using the agarose drop migration assay as adapted from Milner et al. [39]. Briefly, U87-MG cells (American Tissue Culture Collection, Rockville, Maryland, USA), previously transfected to express CXCR4 receptor by Séhédic et al. [40], were seeded into a 24-well flat-bottomed culture plate (Nunc, Strasbourg, France) at a density of 1×10^5 cells per well and cultured in medium supplemented with 10% foetal bovine serum (FBS) and 1% penicillin/streptomycin. The wells were previously treated with 500 µL of a 10 µg/mL poly-D-lysine hydrobromide (Sigma-Aldrich) solution for 15 min at 37 °C and washed three times with PBS prior to cell seeding. After 72 h of incubation at 37 °C under a 5% CO_2 humidified atmosphere , the culture medium was removed and the cells were lysed by adding water (500 µL per well) to cover the well surfaces with a thin cell-derived matrix. After 20 min, the wells were washed three times with PBS and allowed to air-dry. Then, 2 µL of 1% (w/v) low gelling point agarose solution containing U87-MG cells at a density of 50×10^6 cells/mL was dropped onto the centre of each well and allowed to gel at 4 °C for 15 min. At this point, 400 µL of SDF-1α-free medium or medium supplemented with 40 ng/mL native/precipitated/released SDF-1α was added to the cell-laden agarose drops prior to incubation. After 72 h, optical microscopic images of the plan view of each well were taken. Cell migration was estimated by measuring the distance between the furthest-migrating cells and the edge of the cell-laden agarose drop. Measurements were made on four sides (north, east, south and west) of the drop using ImageJ software and subsequently averaged to obtain a representative value of a drop. Three drops were prepared for each medium condition in each experiment.

2.9. *In vitro protein release*

Protein-loaded nanoparticles, and unloaded nanoparticles as a control, were suspended in 2 mL buffer solution containing 0.1% (w/v) BSA as a protein stabilizer and kept in a 2 mL centrifuge tube. The tube was incubated at 37 °C in a shaking water bath (125 rpm). At pre-defined time intervals, the tube was centrifuged at 8500*g* for 30 min. 0.3 mL of the supernatant was collected and replaced with fresh buffer. The supernatant was stored at −20 °C until protein quantification (as described in Section 2.7 for lysozyme and SDF-1α) and biological activity assessment (as described in Section 2.8 for SDF-1α).

2.10. *In vitro cytotoxicity of nanoparticles*

In vitro cytotoxicity of unloaded PLGA/PEG-PLGA nanoparticles was evaluated using a resazurin-based assay adapted from Swed et al. [41]. NIH3T3 mouse fibroblast cell line was cultured at 37 °C and 5% CO_2 in medium supplemented with 10% FBS and 1% penicillin/streptomycin, and replaced every 3 days. The cells were seeded in a 96-well flat-bottomed culture plate (Nunc) at a density of 5.5×10^3 cells/well in 100 µL medium and incubated at 37 °C and 5% CO_2 for 24 h. At this point, 50 µL of the old medium was replaced with an equal volume of nanoparticle-containing fresh medium, to obtain final nanoparticle concentrations of 0.01, 0.1, 1 and 10 mg/mL. As a negative control, cells incubated with the medium alone were prepared. After 48 h of incubation (72 h post-seeding) in the presence or absence of nanoparticles, the entire medium was replaced with 100 µL fresh medium containing 44 µM resazurin. The resazurin-containing medium was also added in three wells of the assay plates (without cells), which served as blank. The plate was incubated for another 3 h 30 m. Cell viability was estimated from the fluorescence intensity of the reduced product of resazurin, called resorufin, which was measured using a ClarioStar microplate fluorometer (BMG Labtech GmbH, Ortenberg, Germany) at 545 nm excitation and 600 nm emission. All readings were normalised to those obtained with the nanoparticle-untreated cells.

In addition to the PLGA/PEG-PLGA nanoparticles, two other types of nanoparticles, namely lipid nanocapsules (LNC) and polystyrene (PS) nanoparticles, were tested in this assay to obtain information on the relative safety of the newly-developed nanoparticles. LNC (average size = 122 nm, PDI = 0.088) were prepared using a phase inversion method as discussed by Heurtault et al. [42]. PS nanoparticles (average size = 285 nm, PDI = 0.175) were purchased from Sigma-Aldrich.

2.11. *Statistical analysis*

Data are presented as the mean value ± standard deviation (SD) of at least three experiments ($n \geq 3$). One-way ANOVA with post-Dunnet's multiple comparison test with a threshold P-value of 0.05 was used to investigate any significant difference between multiple groups of data. In the figures, * indicates $P \leq 0.05$, ** indicates $P \leq 0.01$, *** indicates $P \leq 0.001$ and **** indicates $P \leq 0.0001$.

3. Results and discussion

3.1. *Characterization of PLGA-COOR and PEG-PLGA co-polymer*

^{1}H NMR spectrum of PLGA-COOR in Fig. 1 revealed the presence of lactide units at 5.19 ppm and 1.46 ppm, glycolide units at 4.91 ppm, and benzyl capping groups at 7.37 ppm. Using the signal at 7.37 ppm as

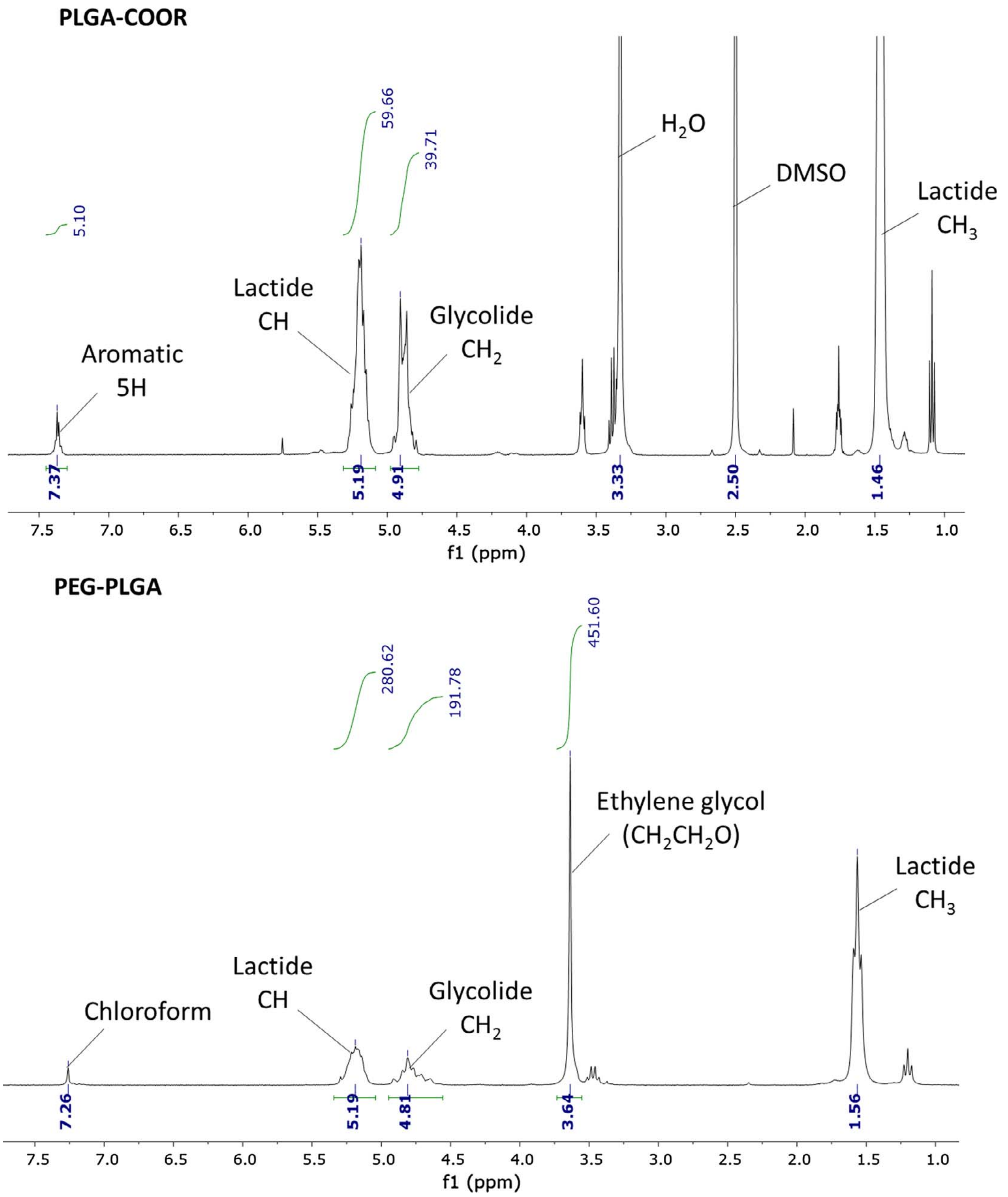

Fig. 1. ^{1}H NMR of PLGA-COOR and PEG-PLGA co-polymer in deuterated DMSO and chloroform respectively.

a reference for integration, Mn was calculated to be 5.5 kDa, with a lactide/glycolide molar percentage of 75/25. For the PEG-PLGA co-polymer, the signal at 3.64 ppm, which is characteristic of ethylene glycol units, indicated the successful co-polymerization of mono-methoxy-PEG 5 kDa to the lactide and glycolide units. Using this signal as a reference, the Mn of the co-polymer was 30.7 kDa (PEG 5 kDa – PLGA 25.7 kDa) whereas the lactide/glycolide molar percentage was calculated to be 75/25. On the other hand, SEC analyses showed that the Mw/Mn values were 11.2/5.7 kDa (PDI = 2.0) and 44.1/21.0 kDa (PDI = 2.1) for PLGA-COOR and PEG-PLGA co-polymer respectively. The disparity between the PEG-PLGA Mn values calculated using these two techniques could be attributed to the amphiphilic nature of the co-polymer [38,43,44] that may have modified the hydrodynamic volume to prolong the retention time, which subsequently produced an underestimated Mn value using SEC.

3.2. Lysozyme and SDF-1α precipitation

Due to the greater stability of proteins in their solid state, proteins dissolved in a salt solution containing P188 were precipitated through their addition to an organic solvent as a preparation for encapsulation. Glycofurol was the organic solvent of choice for two main reasons. Firstly, its water-miscibility enables an efficient separation of water from protein molecules to induce precipitation. Secondly, it has been used to precipitate many proteins without causing their denaturation [25,38,45,46]. P188 was added due to its ability to refold any unfolded protein [47] and also to reduce protein adsorption to the hydrophobic PLGA following encapsulation, which in turn may allow for greater cumulative release [38,48]. To minimise any potential toxicity, the amount of P188 used to precipitate the amount of protein sufficient for one nanoparticle formulation was kept at 500 µg. Proteins were initially dissolved in NaCl solution to neutralise the charged protein molecules and promote attractive hydrophobic interactions. The concentration of NaCl that would decrease the aqueous solubility of SDF-1α without

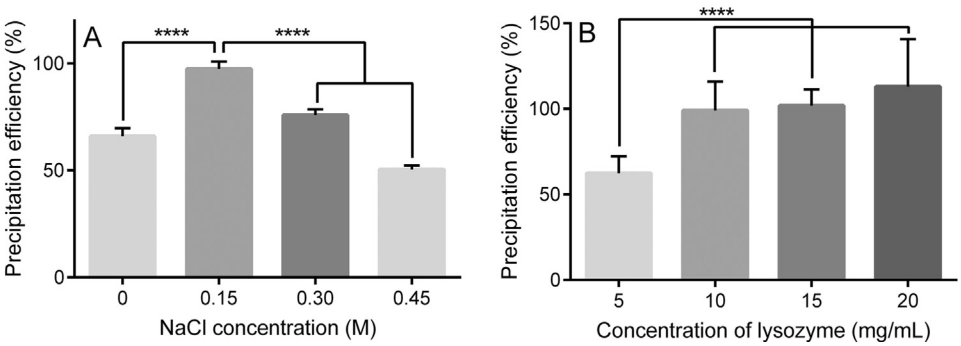

Fig. 2. Effect of (A) NaCl and (B) lysozyme concentrations on lysozyme precipitation efficiency. For (A), lysozyme concentration was fixed at 10 mg/mL whereas NaCl concentration was fixed at 0.15 M for (B). Statistical analysis was conducted to investigate any significant difference ($P \le 0.05$) in comparison to 0.15 M NaCl or 5 mg/mL lysozyme concentration for (A) and (B) respectively. **** indicates $P \le 0.0001$, n = 3 for each lysozyme precipitation condition.

causing its denaturation was investigated using lysozyme as a model protein. Following precipitation, the amount of bioactive lysozyme was quantified using the *Micrococcus lysodeikticus* assay. As shown in Fig. 2, 0.15 M NaCl resulted in a successful precipitation with a complete preservation of lysozyme bioactivity. Lower PE was obtained in the absence of NaCl, possibly due to the repulsion between charged protein molecules that hindered the formation of precipitates. On the other hand, PE decreased when the NaCl concentration was increased above 0.15 M. Although high concentrations of salt can reduce the aqueous solubility of a protein and facilitate precipitation, the excess charge neutralisation may simultaneously promote protein denaturation by allowing any unfolded protein molecules to spontaneously form aggregates and therefore preventing their re-folding [49]. On this basis, 0.15 M NaCl was used to precipitate SDF-1α. The effect of protein concentrations on PE was also investigated. PE values were greater with higher lysozyme concentrations, due to greater tendencies for protein molecules to collide and interact with one another. Although 10 mg/mL or higher lysozyme concentrations were identified to result in a maximum PE, it was not possible to dissolve SDF-1α in 0.15 M NaCl at these concentrations. Therefore, SDF-1α was precipitated at 2.67 mg/mL, which was the highest concentration that could be achieved without the appearance of visible protein solids. Using ELISA, the PE was calculated to be 91 ± 5%. More importantly, the bioactivity of the re-constituted SDF-1α precipitates was not significantly different from the native SDF-1α when tested using the agarose drop migration assay (Fig. 6B, C).

Following the optimisation of precipitation conditions, the morphology of the precipitates was observed under SEM. The precipitates of both proteins were mostly spherical in shape (Fig. 3). Furthermore, their size distributions (as estimated using the ImageJ software) were 57 ± 10 nm and 57 ± 25 nm for lysozyme and SDF-1α respectively. The sub-100 nm sizes of the protein precipitates make them ideal for subsequent encapsulation into the PLGA/PEG-PLGA nanoparticles.

3.3. Preparation and characterization of lysozyme- and SDF-1α-loaded nanoparticles

3.3.1. Optimisation of PLGA/PEG-PLGA nanoparticle synthesis

Due to the amphiphilic behaviour of PEG-PLGA, it was predicted that uniform and stable nanoparticles can be obtained by mixing this co-polymer with the hydrophobic PLGA. Using this combination instead of the co-polymer alone can provide additional means for controlling the nanoparticle physicochemical properties that are critical for protein encapsulation and release, such as the size and zeta-potential, by varying the chemical constituents of the PLGA component such as the number of uncapped carboxylic acid groups.

The physicochemical characteristics of unloaded nanoparticles made from different combinations of PEG-PLGA co-polymer and PLGA polymers are shown in Table 1. No homogeneous nanoparticle suspension could be obtained in the absence of PEG-PLGA (Formulations 1 & 5) whereas the size and PDI values decreased as the PEG-PLGA proportion was increased when used in combination with either PLGA-COOH (Formulations 2–4) or PLGA-COOR (Formulations 6–8). These observations confirmed the critical nanoparticle-stabilizing roles of the co-polymer to compensate for the lack of use of surfactants such as PVA and P188. Furthermore, zeta-potential values generally became less negative with increasing PEG-PLGA proportion, which can be explained by the increasing density of PEG layer on the nanoparticle surface that shields the negatively-charged PLGA carboxylic acid groups [50]. Based on these observations and literature data [51], the synthesised nanoparticles can be thought of to possess a structure consisting of a hydrophilic PEG layer surrounding a hydrophobic PLGA core.

Upon substituting PLGA-COOH with an equal proportion of PLGA-COOR, the nanoparticle size increased and zeta-potential values became less negative (Formulations 2 vs. 6, 3 vs. 7 and 4 vs. 8), which suggested that PLGA terminal capping has an effect on nanoparticle properties. To confirm this, PLGA-COOH and PLGA-COOR were combined with a fixed proportion of PEG-PLGA that is sufficient to produce uniform nanoparticles (Formulation 9 and 10). Taking together the results obtained when only either PLGA-COOH or PLGA-COOR was combined with PEG-PLGA (Formulations 4 and 8), it was confirmed

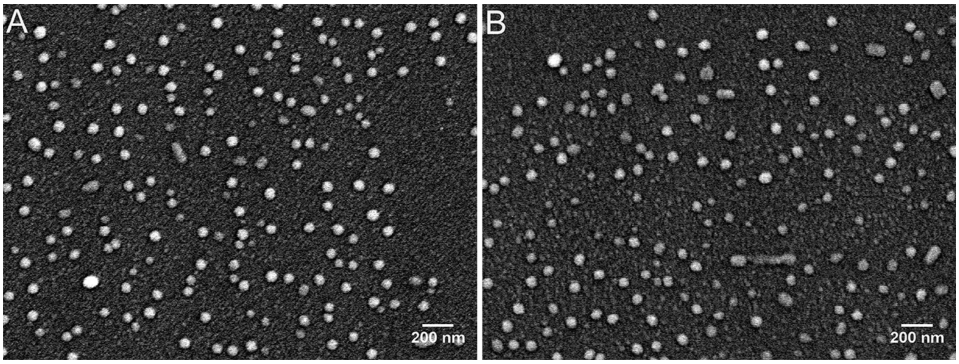

Fig. 3. Scanning electronic microscopy of (A) lysozyme and (B) SDF-1α nanoprecipitates.

Table 1
Average size, polydispersity index (PDI) and zeta-potential (ZP) of unloaded nanoparticle formulations. Data are presented as mean ± SD, n = 3.

Formulation number	Proportion (%)			Average size (nm)[a]	Average PDI[a]	Average ZP (mV)[b]		
	PLGA-COOH	PLGA-COOR	PEG-PLGA			pH 4	pH 7	pH 10
1	100	0	0			n.d.[c]		
2	92	0	8	599 ± 20	0.46 ± 0.08	−16.6 ± 1.0	−20.7 ± 2.2	−28.0 ± 2.4
3	75	0	25	279 ± 3	0.17 ± 0.03	−9.9 ± 0.8	−12.1 ± 1.3	−15.7 ± 1.5
4	67	0	33	202 ± 3	0.08 ± 0.05	−6.6 ± 1.0	−8.9 ± 0.8	−9.8 ± 0.7
5	0	100	0			n.d.[c]		
6	0	92	8	> 1000	1	−2.9 ± 0.5	−4.7 ± 0.4	−6.4 ± 0.6
7	0	75	25	691 ± 23	0.40 ± 0.05	−1.8 ± 0.1	−2.3 ± 0.3	−3.1 ± 0.4
8	0	67	33	255 ± 4	0.14 ± 0.04	−1.2 ± 0.2	−3.0 ± 0.6	−2.9 ± 0.2
9	33	33	33	215 ± 7	0.10 ± 0.03	−4.1 ± 0.2	−4.8 ± 0.5	−4.3 ± 0.3
10	17	50	33	236 ± 6	0.10 ± 0.02	−2.8 ± 0.4	−4.1 ± 0.6	−4.0 ± 0.4

[a] Purified nanoparticle suspension was diluted to 100 μg/mL in water prior to measurement.

[b] Purified nanoparticle suspension was diluted to 100 μg/mL in 0.01 M NaCl and 0.1 M HCl or NaOH was used to adjust the pH of the suspension to pH 4, 7 or 10 prior to measurement.

[c] n.d. = not determined, as no homogenous particle suspension was obtained.

that the nanoparticle size increased as the PLGA-COOH was gradually replaced with PLGA-COOR. Simultaneously, the zeta-potential values also became less negative. The largest zeta-potential change was seen in alkaline conditions (pH 10) due to deprotonation of all uncapped carboxylic acid groups. The greater abundance of uncapped carboxylic acid terminals found in nanoparticles made of higher PLGA-COOH proportions may lead to higher inter-particle electrostatic repulsions, which prevent particle collusion and consequently reduce the average size.

To ensure good colloidal stability, zeta potential values of greater than +30 mV or lower than −30 mV are generally regarded as ideal, as this ensures strong electrostatic repulsive forces between the nanoparticles [52]. In this work, the presence of the external PEG layer inevitably decreased the zeta potential magnitude of the PLGA/PEG-PLGA nanoparticles. Despite the loss in electrostatic stabilization, the nanoparticle suspension benefited from the steric stabilization conferred by the PEG chains. To verify this, Formulation 8 was suspended in 0.05 M Tris-HCl buffer (pH 7.4) containing 0.15 M NaCl at 1 mg/mL concentration and the suspension was kept at 37 °C. There were minimal changes in the average size of the nanoparticles after 20 days (Supplementary Fig. 1A). Interestingly, the zeta-potential values became increasingly negative with time (Supplementary Fig. 1B). It was likely that PEG-mediated steric repulsions provided the main stabilization force for freshly-produced nanoparticles. As the PLGA ester bonds gradually hydrolyzed to reveal more negatively-charged carboxylic acid terminals, the increasing magnitude of electrostatic repulsions prevented the formation of any aggregates.

3.3.2. *Freeze-drying of PLGA/PEG-PLGA nanoparticles*

Polyesters such as PLGA are prone to degradation by means of hydrolysis of the ester bonds, which may lead to leakage of the drug load encapsulated within polyester-based nanocarriers. Therefore, dehydration of PLGA-based nanoparticles, commonly by freeze-drying, is imperative to ensure their long-term stability. To protect the nanoparticles from freezing and drying stresses, cryoprotectants should be added to the nanoparticle suspension before freezing. Disaccharides such as sucrose and trehalose, and oligosaccharides such as HPBCD have been shown to be excellent protectants [53]. Nevertheless, it is also important that the drying temperature is maintained below the collapse temperature (T_c) of the protectant to prevent the collapse of the freeze-dried products [54], which may lead to prolonged nanoparticle reconstitution times [53,55] and higher residual humidity [56].

In this study, 5% (w/v) sucrose, trehalose and HPBCD with T_c of −32, −30 and −15 °C respectively [57,58] were used as protectants. The shelf temperature throughout the drying phase was fixed at −20 °C as this was the lowest temperature for water vaporization at 0.3 mbar, which was the lowest pressure achievable by the freeze-dryer used in this study. As predicted, the freeze-dried product containing either sucrose or trehalose appeared collapsed and required sonication for reconstitution while the non-collapsed HPBCD-stabilised product could be reconstituted completely by gentle agitation alone. The formulation collapse resulted in a decrease in the degree of porosity of the freeze-dried product, which subsequently reduced its surface area to volume ratio and hydration rate [56]. Nevertheless, all three protectants produced better results compared to that obtained from the lyophilization of nanoparticle suspension alone, confirming the protective roles of these excipients during freeze-drying.

Following reconstitution, the nanoparticle size and PDI were measured again to evaluate the protective effect of sucrose, trehalose and HPBCD. The highest protective effect, as demonstrated by the maximum preservation of nanoparticle size and PDI, was obtained with HPBCD (Table 2). It is likely that the volume shrinkage resulting from the collapse of the sucrose and trehalose matrices has reduced the distance of separation between the nanoparticles, allowing the PEG layers of neighbouring particles to interact and form stable crystalline bridges as reported in the literature [51,59]. Differently, in the presence

Table 2
Characterization of PLGA/PEG-PLGA nanoparticles (Formulation 8) before and after freeze-drying without any cryoprotectant or with sucrose, trehalose or HPBCD. Data are presented as mean ± SD, n = 3.

Protectant	Average size (nm)		Average PDI		S_f/S_i	PDI_f/PDI_i
	Before freeze-drying[a]	After freeze-drying[b]	Before freeze-drying[a]	After freeze-drying[b]		
–		n.d.[c]		n.d.[c]		
Sucrose	255 ± 8	308 ± 5	0.13 ± 0.01	0.22 ± .01	1.21	1.69
Trehalose		266 ± 5		0.19 ± 0.01	1.04	1.46
HPBCD		255 ± 3		0.14 ± 0.02	1.00	1.08

[a] Purified nanoparticle suspension was diluted to 100 μg/mL in water prior to measurement.

[b] Freeze-dried nanoparticles were re-suspended in 2 mL water and diluted to 100 μg/mL in the same diluent prior to measurement.

[c] n.d. = not determined, as the freeze-dried product could not be reconstituted completely even after 10 min sonication.

Table 3
Effect of pH of aqueous phase on encapsulation efficiencies of lysozyme. Data are presented as mean ± SD, n = 3.

Formulation number	pH of aqueous phase[a]	Encapsulation efficiency (%)	
		Lysozyme	SDF-1a
4	8.4	18.0 ± 0.8	34.3 ± 3.7
	9.4	28.1 ± 1.7	79.7 ± 4.1
	10.4	66.0 ± 1.6	107.7 ± 1.5
	11.4	107.0 ± 3.6	–

[a] 0.05 M glycine-NaOH buffer solution was used as the aqueous phase.

of HPBCD, the PLGA/PEG-PLGA nanoparticles were easily freeze-dried, which may be convenient for long-term storage and transportation. In future work, the protective effects of sucrose and trehalose can be re-evaluated by setting the drying temperature to be lower than their respective T_c to minimise dependency on the relatively costly HPBCD.

3.3.3. Lysozyme and SDF-1α encapsulation

3.3.3.1. Effect of pH of the aqueous phase on encapsulation efficiencies. Protein molecules have smaller net electrical charge and thus lower aqueous solubility when the pH is buffered near the protein's isoelectric point (pI). This may decrease the leakage of protein into the aqueous phase during the formulation process to subsequently maximise encapsulation efficiency. The results shown in Table 3 supported this hypothesis as both lysozyme and SDF-1α were encapsulated most successfully when the pH of the aqueous phase was buffered closest to their respective pI (lysozyme – 11.35; SDF-1α – 10.5). In addition to a decrease in aqueous solubility, it is likely that the smaller net charge also attenuated the electrostatic repulsions between protein molecules to allow the protein load to be compacted, which can facilitate its entrapment within the nanoparticles [60,61]. For these reasons, the pH of the aqueous phase was always set to the protein's pI in subsequent encapsulations.

3.3.3.2. Effect of PLGA carboxylic acid terminal capping on encapsulation efficiencies. Since both proteins and PLGA possess ionisable groups, electrostatic interactions can have a major influence on lysozyme and SDF-1α encapsulation. Due to the complexity associated with protein charge modifications, the proportions of PLGA-COOH and PLGA-COOR were altered accordingly to vary the number of ionisable groups in the nanoparticles instead. The encapsulation of both proteins decreased slightly when PLGA-COOH was substituted with an equal amount of PLGA-COOR (Formulation 4 vs. 8 in Table 4). These results suggested that protein-polymer electrostatic interactions can influence the protein encapsulation efficiencies. Although protein leakage during the encapsulation process can be minimised by adjusting the pH of the aqueous phase to be similar to the protein's pI, proteins located close to the nanoparticle surface can be lost during subsequent purification stages when the nanoparticles were suspended in non-buffered water. This is especially true since the presence of the outer hydrophilic PEG layer can facilitate the access of water to the PLGA core to cause dissolution of any loosely-trapped proteins [62]. However, the strong electrostatic interactions between the negatively-charged carboxylic acid terminals, which are more abundant in PLGA-COOH than in PLGA-COOR, and the positively-charged basic proteins such as lysozyme and SDF-1α can reduce protein loss. Interestingly, additional experiments with lysozyme (Formulation 9 and 10) and SDF-1α (Formulation 10) produced similar results as Formulation 4. Considering the very low protein loading involved, it seems that the inclusion of a small proportion of PLGA-COOH is sufficient to ensure that the nanoparticles have an adequate number of carboxylic acid groups to interact with the protein molecules for maximum encapsulation efficiency.

Table 4
Effect of the PLGA-COOH proportion on encapsulation efficiencies of lysozyme and SDF-1α. Data are presented as mean ± SD, n = 3 and 4 for lysozyme and SDF-1α respectively.

Formulation number	PLGA-COOH proportion (%)	Encapsulation efficiency (%)	
		Lysozyme	SDF-1a
4	67	107.0 ± 3.6	107.7 ± 1.5
8	0	89.6 ± 5.7	75.5 ± 2.2
9	33	108.2 ± 1.9	–
10	17	111.0 ± 3.9	104.0 ± 2.8

Table 5
Average size, polydispersity index (PDI) and zeta-potential (ZP) of lysozyme and SDF-1α-loaded nanoparticles. Data are presented as mean ± SD, n = 3.

Formulation number	Encapsulated protein	Average size (nm)[a]	Average PDI[a]	Average ZP (mV)[b]
4	Lysozyme	202 ± 5	0.09 ± 0.01	−9.7 ± 0.8
	SDF-1α	197 ± 2	0.08 ± 0.01	−9.6 ± 0.7
8	Lysozyme	253 ± 5	0.17 ± 0.03	−3.3 ± 0.3
	SDF-1α	259 ± 8	0.19 ± 0.01	−2.9 ± 0.2

[a] Purified nanoparticle suspension was diluted to 100 μg/mL in water prior to measurement.

[b] Purified nanoparticle suspension was diluted to 100 μg/mL in 0.01 M NaCl solution and the pH of the suspension was adjusted to pH 7 prior to measurement.

3.3.3.3. Physicochemical characteristics of protein-loaded nanoparticles. Protein encapsulation did not affect the size or zeta-potential of the nanoparticles regardless of the type of formulation or encapsulated protein (Table 5), possibly due to the low amount of protein being encapsulated. In terms of morphology, both the unloaded and SDF-1α-loaded nanoparticles appeared similar under the vacuum condition of SEM or TEM (Fig. 4). In addition, the image taken using AFM under a non-vacuum condition confirmed the consistent appearance of the SDF-1α-loaded nanoparticles regardless of the conditions under which the nanoparticles were observed and the differences in the sample treatment prior to observation.

3.4. In vitro protein release

Protein release was studied by suspending the nanoparticles in a buffer solution followed by centrifugation at pre-defined time intervals to collect the supernatant for protein quantification. Initially, lysozyme release patterns in different buffer solutions was studied. At the physiologically-relevant pH 7.4 (0.05 M Tris-HCl buffer), the proportion of PLGA-COOH in the nanoparticles was shown to affect the extent of lysozyme release (Fig. 5A). The highest release of encapsulated lysozyme was achieved with Formulation 8 (43%) whereas negligible protein release was observed with Formulation 4 even after 15 days. When a mixture of PLGA-COOH and PLGA-COOR was tested (Formulation 10), only 12% encapsulated lysozyme was successfully released. The lack of protein release from PLGA particles containing uncapped carboxylic end groups has been previously reported [38,41,63]. Concurrent measurement of zeta-potentials during the release study offered a possible explanation for this observation. Nanoparticles made from higher PLGA-COOH proportions had more negative zeta-potential values in the early stages of the release study (Fig. 5B). At pH 7.4, these nanoparticles are expected to establish electrostatic interactions with the positively-charged lysozyme molecules (pI = 11.35), which hinders their release. These interactions seem to be the governing factor for protein load entrapment, as no further protein release was observed despite the continuous degradation of PLGA matrices into acidic products, as inferred from the increasingly negative zeta-potential values of all the formulations, taking place throughout the release study period.

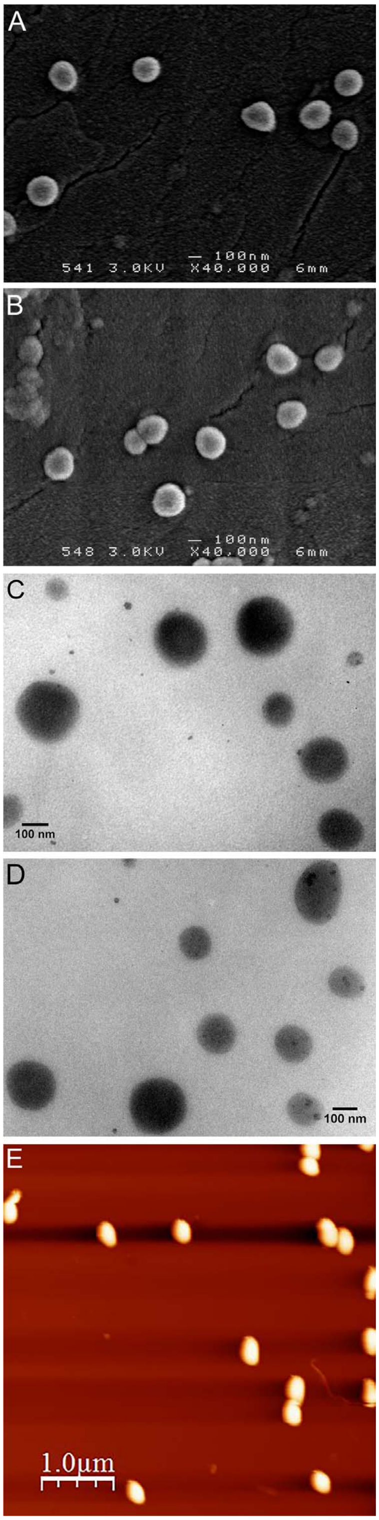

Fig. 4. Morphology of PLGA/PEG-PLGA nanoparticles. SEM and TEM images of (A, C) unloaded and (B, D) SDF-1α-loaded nanoparticles. (E) AFM image of SDF-1α-loaded nanoparticles.

To confirm the obstructive effect of lysozyme-PLGA electrostatic interactions on lysozyme release, the study was repeated in release medium buffered to pH 4.0 (0.01 M citrate buffer). It can be hypothesised that the excess protons present in the release medium will neutralise the PLGA carboxylic acid groups, which in turn should trigger the release of lysozyme molecules. As expected, release of lysozyme was enhanced regardless of the nanoparticle's PLGA-COOH proportion (Fig. 5C). However, incomplete release was still observed with Formulation 4, even after 30 days. It is likely that the high proportion of PLGA-COOH in this formulation led to incomplete neutralisation of the carboxylic acid groups, hindering complete lysozyme release. Besides pH, another factor that may affect lysozyme-PLGA electrostatic interactions is the concentration of cations in the release medium, as these ions can also displace lysozyme molecules from the PLGA carboxylic acid groups. As predicted, in the presence of 0.15 M sodium chloride, release of lysozyme at pH 7.4 was enhanced (Fig. 5D), recording levels similar to those obtained at acidic pH. These release medium conditions were selected for subsequent SDF-1α release study due to their physiological relevance.

Interestingly, although the biphasic release pattern seen in lysozyme release study was reproduced, the release of SDF-1α was reduced in all formulations (Fig. 6A). After 30 days, the nanoparticles were lyophilized and dissolved to quantify the amount of unreleased SDF-1α using ELISA. The sum of released SDF-1α and the unreleased proportion, was equal to 95–98% of the total encapsulated SDF-1α for all the studied formulations. SDF-1α may establish stronger electrostatic interactions with PLGA carboxylic acid groups than lysozyme because of the greater percentage of basic amino acid residues in the SDF-1α primary sequence, resulting in lower cumulative SDF-1α releases. Despite the multiple literature-approved measures taken in this study to reduce protein-polymer interactions, including protein precipitation in the presence of poloxamer 188 [38] and use of more hydrophilic polymer materials [63] in the form of PEG-PLGA co-polymer, additional approaches such as protein PEGylation [64,65] should be considered in future work to obtain more complete protein release. Nevertheless, the bioactivity of SDF-1α in the release sample collected up to 72 h (after which further SDF-1α release was negligible) was found to be similar to that of its native counterpart when assessed using the agarose drop migration assay (Fig. 6B, C), suggesting that the encapsulation process did not induce protein denaturation. In the context of patient safety, the preservation of protein bioactivity throughout formulation processes is imperative as denatured proteins tend to be more immunogenic than their native forms [66,67].

The biphasic release patterns observed in lysozyme and SDF-1α release studies were consistent with literature data on PEG-containing PLGA nanoparticles [61,68]. The initial burst release was due to the rapid liberation of proteins located adjacent to the nanoparticle surface, which was a consequence of the efflux of residual solvents during the purification step that drew most proteins away from the core of the nanoparticles. This stage was then followed by a slower release attributable to the diffusion of proteins from deeper parts of the nanoparticles. In relation to future work, the initial rapid SDF-1α release is useful for establishing a concentration gradient within a hydrogel to immediately induce chemotaxis of cancer cells while the subsequent gradual release may be beneficial to maintain the established gradient. It was also observed that the cumulative release curves began to plateau after 72 h. This relatively short duration of release was expected as the huge surface area to volume ratio of the nanoparticles contributed to a rapid protein release. However, as the SDF-1α-loaded nanoparticles are intended in the future to be incorporated within a hydrogel and not suspended directly in physiological fluids, literature data suggested that the release duration can be prolonged [69], which would allow more time for cancer cells to migrate into the hydrogel/nanoparticle composite implant to be trapped.

3.5. *In vitro cytotoxicity study*

Due to the innocuous nature of the solvent used in the formulation process and the well-reported safety of PLGA, the newly-developed nanoparticles are expected to exhibit negligible cytotoxicity. To prove this, NIH3T3 mouse embryonic fibroblasts were treated with unloaded PLGA/PEG-PLGA nanoparticles (Formulation 8) for 48 h. This cell line was chosen as it has been reported to be highly-sensitive to chemical-

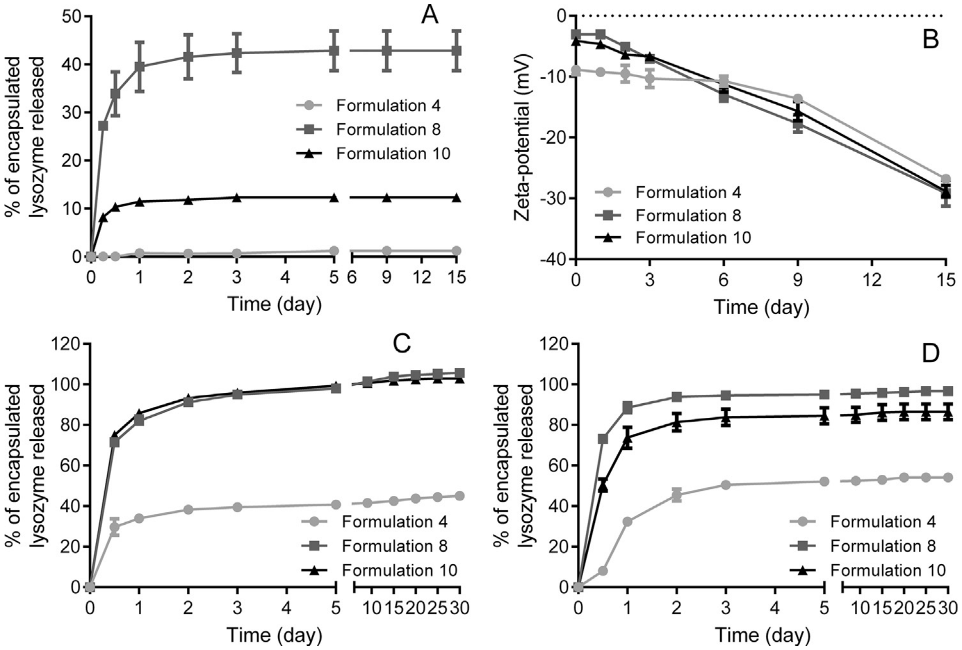

Fig. 5. Release study of lysozyme. (A) Cumulative release of lysozyme in 0.05 M Tris-HCl buffer at pH 7.4 and (B) concurrent changes in the zeta-potential value of different nanoparticle formulations. Nanoparticle suspension was diluted 200-fold in 0.01 M NaCl solution and the pH was adjusted to pH 7 prior to zeta-potential measurement. (C) Cumulative lysozyme release in 0.01 M citrate buffer at pH 4.0 or (D) 0.05 M Tris-HCl buffer at pH 7.4 containing 0.15 M NaCl. Each data point with error bar represents mean ± SD, n = 3 for each formulation.

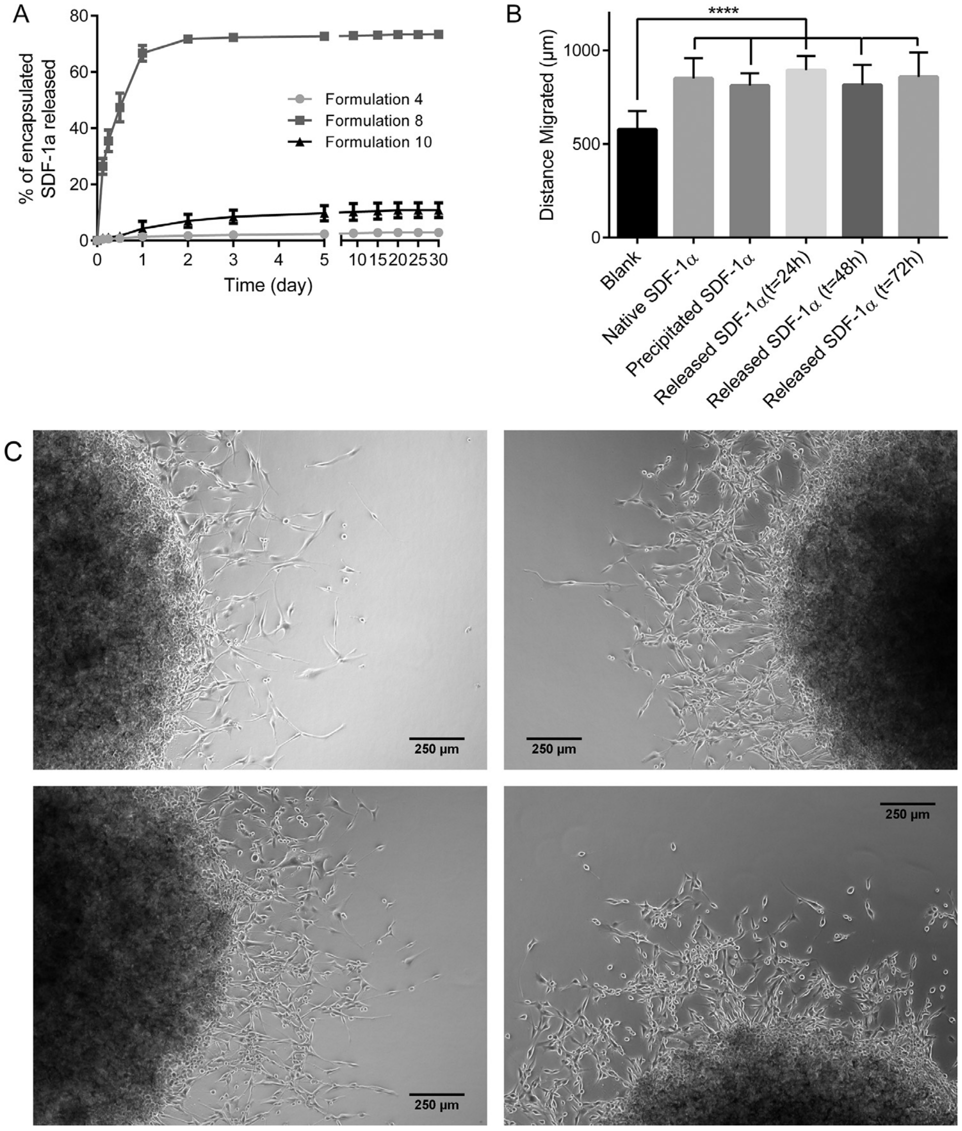

Fig. 6. Release study of SDF-1α and its biological activity assessment. (A) Cumulative release of SDF-1α in 0.05 M Tris-HCl buffer at pH 7.4 containing 0.15 M NaCl. Each data point with error bar represents mean ± SD, n = 4 for each formulation. (B) Distance migrated by U87-MG cells induced by the culture medium alone (Blank), or supplemented with 40 ng/mL native, precipitated or released SDF-1α collected from Formulation 8 at different time points of the release study. Statistical analysis was conducted to investigate any significant difference ($P \leq 0.05$) in comparison to the native SDF-1α. **** indicates $P \leq 0.0001$, n = 3 for each type of SDF-1α treatment. (C) Examples of optical microscopic images of U87-MG cell-laden agarose drops after 72 h treatment with culture medium alone (top left) or medium containing 40 ng/mL native (top right), precipitated (bottom left) or released SDF-1α (bottom right).

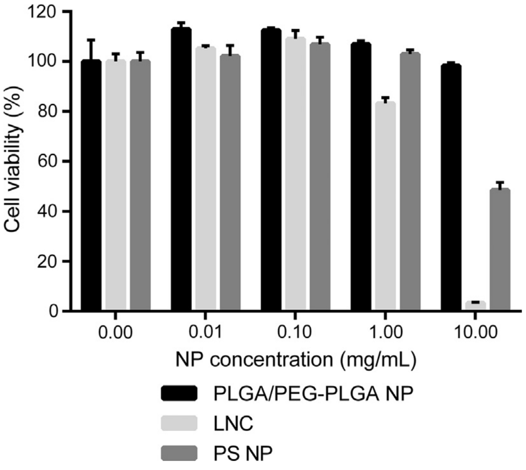

Fig. 7. Effect of different concentrations of PLGA/PEG-PLGA nanoparticles (Formulation 8), lipid nanocapsules (LNC) and polystyrene (PS) nanoparticles on the viability of NIH3T3 cells after 48 h incubation. n = 3 for each nanoparticle treatment.

induced toxicities [70]. Alongside PLGA/PEG-PLGA nanoparticles, lipid nanocapsules (LNC) and polystyrene (PS) nanoparticles, which have been widely utilised in various pharmaceutical research, were tested to investigate the relative cytocompatibility of the newly-developed nanocarriers. The range of nanoparticle concentrations for cell treatment in this study was set to 0.01–10 mg/mL to assess the suitability of the PLGA/PEG-PLGA nanoparticles for both systemic and local drug delivery applications. In comparison to the two reference nanoparticles, the PLGA/PEG-PLGA nanoparticles induced minimal cell deaths even at the highest concentration tested (Fig. 7). In addition, the LNC was found to be the most toxic between the three types of nanoparticles at high concentrations. Two studies reported similar findings [71,72] and suggested that the high amount of surfactant (up to 2.8% (w/v)) required to stabilise the LNC formulation is responsible for the high toxicity due to the ability of the hydrophilic and hydrophobic components of surfactant molecules to interact with the phosphate groups and fatty acid tails of lipid bilayer respectively to cause disruption of cellular membranes [73]. On the other hand, the PS nanoparticles exhibited intermediate cytotoxicity, possibly due to the lower amount of surfactant used in their formulation (up to 0.5% (w/v) as described by the manufacturer). Although one can speculate that the differences in the cytotoxicity can be attributed to other components of the three types of nanoparticles, as well as to differences in their physicochemical characteristics such as size and surface charge, the surfactant-free formulation process using non-toxic components developed in the present work can undoubtedly produce nanocarriers with excellent biocompatibility that are more suitable for local drug delivery applications compared to several other well-established alternatives.

4. Conclusion

This study reports on the development of novel SDF-1α nanocarriers composed of PLGA and a PEG-PLGA co-polymer. Following optimization using lysozyme as a model protein, SDF-1α was successfully precipitated and subsequently loaded into these nanoparticles under mild formulation conditions. SDF-1α was also released in its bioactive conformation in a gradual fashion. Furthermore, by changing the number of uncapped carboxylic acid groups in the PLGA core, the novel formulation process allows the production of nanoparticles with different physicochemical properties that influence encapsulation efficiencies and the extent of protein release. In addition, the use of non-toxic polymers and solvents ensured the excellent biocompatibility of the synthesised nanoparticles. Thus, the novel SDF-1α nanocarriers are promising for future cancer cell trapping applications and will be incorporated into a suitable hydrogel for studying chemotaxis of glioblastoma cells.

Declaration of interest

No conflict of interest exists.

Acknowledgement

Authors would like to thank the French Ministry of Higher Education and Research for their financial support (PhD Grant) and the National Funds for Scientific Research, Belgium (FNRS), MINECO (SAF2017-83118-R), AEI Spain and FEDER for additional financial assistance. The authors are thankful for the European financial support (EACEA) in the frame of the NanoFar program, an Erasmus Mundus Joint Doctorate (EMJD) program in nanomedicine and pharmaceutical innovation. This work was also supported by “La Région Pays-de-la-Loire”, by the “Institut National de la Santé et de la Recherche Médicale” (INSERM), by the “University of Angers” and the “University of Liège” and by the “Cancéropôle Grand-Ouest” though the ”glioblastoma“ and ”vectorization and radiotherapies“ networks. E. Garcion is also a member of the LabEx IRON “Innovative Radiopharmaceuticals in Oncology and Neurology” as part of the French government “Investissements d’Avenir” program and head the PL-BIO 2014-2020 INCA (Institut National du Cancer) project MARENGO - “MicroRNA agonist and antagonist Nanomedicines for GliOblastoma treatment: from molecular programmation to preclinical validation”. Finally the authors thank Dr D. Séhédic for the kind provision of CXCR4-expressing U87-MG human glioblastoma cell line and R. Mallet and R. Perrot of the SCIAM (Common service for Imaging and microscopy analysis, Angers, France) for SEM and TEM analyses.

Appendix A. Supplementary material

Supplementary data associated with this article can be found, in the online version, at https://doi.org/10.1016/j.ejpb.2017.12.020.

References

[1] M. De La Luz Sierra, F. Yang, M. Narazaki, O. Salvucci, D. Davis, R. Yarchoan, H.H. Zhang, H. Fales, G. Tosato, Differential processing of stromal-derived factor-1alpha and stromal-derived factor-1beta explains functional diversity, Blood 103 (2004) 2452–2459, http://dx.doi.org/10.1182/blood-2003-08-2857.

[2] M. Janowski, Functional diversity of SDF-1 splicing variants, Cell Adh. Migr. 3 (2009) 243–249.

[3] T. Sugiyama, H. Kohara, M. Noda, T. Nagasawa, Maintenance of the hematopoietic stem cell pool by CXCL12-CXCR4 chemokine signaling in bone marrow stromal cell niches, Immunity. 25 (2006) 977–988, http://dx.doi.org/10.1016/j.immuni.2006.10.016.

[4] T. Kitaori, H. Ito, E.M. Schwarz, R. Tsutsumi, H. Yoshitomi, S. Oishi, M. Nakano, N. Fujii, T. Nagasawa, T. Nakamura, Stromal cell-derived factor 1/CXCR4 signaling is critical for the recruitment of mesenchymal stem cells to the fracture site during skeletal repair in a mouse model, Arthritis Rheum. 60 (2009) 813–823, http://dx.doi.org/10.1002/art.24330.

[5] J. Deng, Z.M. Zou, T.L. Zhou, Y.P. Su, G.P. Ai, J.P. Wang, H. Xu, S.W. Dong, Bone marrow mesenchymal stem cells can be mobilized into peripheral blood by G-CSF in vivo and integrate into traumatically injured cerebral tissue, Neurol. Sci. 32 (2011) 641–651, http://dx.doi.org/10.1007/s10072-011-0608-2.

[6] Y. Kimura, M. Komaki, K. Iwasaki, M. Sata, Y. Izumi, I. Morita, Recruitment of bone marrow-derived cells to periodontal tissue defects, Front. Cell Dev. Biol. 2 (2014) 1–6, http://dx.doi.org/10.3389/fcell.2014.00019.

[7] J.-P. Lévesque, J. Henry, Y. Takamatsu, P.J. Simmons, L.J. Bendall, Disruption of the CXCR4/CXCL12 chemotactic interaction during, J. Clin. Invest. 110 (2003) 187–196, http://dx.doi.org/10.1172/JCI200315994.Introduction.

[8] L. Marquez-Curtis, A. Jalili, K. Deiteren, N. Shirvaikar, A.-M. Lambeir, A. Janowska-Wieczorek, Carboxypeptidase M expressed by human bone marrow cells cleaves the C-terminal lysine of stromal cell-derived factor-1α: another player in hematopoietic stem/progenitor cell mobilization? Stem Cells. 26 (2008) 1211–1220, http://dx.doi.org/10.1634/stemcells.2007-0725.

[9] A.M. Roccaro, A. Sacco, W.G. Purschke, M. Moschetta, C. Maasch, D. Zboralski, S. Zöllner, S. Vonhoff, P. Maiso, M.R. Reagan, S. Lonardi, M. Ungari, D. Eulberg, A. Kruschinski, A. Vater, G. Rossi, I.M. Ghobrial, Therapy 9 (2014) 118–128, http://dx.doi.org/10.1016/j.celrep.2014.08.042.SDF-1.

[10] R. Matsusue, H. Kubo, S. Hisamori, K. Okoshi, H. Takagi, K. Hida, K. Nakano, A. Itami, K. Kawada, S. Nagayama, Y. Sakai, Hepatic stellate cells promote liver

metastasis of colon cancer cells by the action of SDF-1/CXCR4 axis, Ann. Surg. Oncol. 16 (2009) 2645–2653, http://dx.doi.org/10.1245/s10434-009-0599-x.

[11] J.-P. Zhang, W.-G. Lu, F. Ye, H.-Z. Chen, C.-Y. Zhou, X. Xie, Study on CXCR4/SDF-1alpha axis in lymph node metastasis of cervical squamous cell carcinoma, Int. J. Gynecol. Cancer. 17 (2007) 478–483, http://dx.doi.org/10.1111/j.1525-1438.2007.00786.x.

[12] C.B. Stevenson, M. Ehtesham, K.M. McMillan, J.G. Valadez, M.L. Edgeworth, R.R. Price, T.W. Abel, K.Y. Mapara, R.C. Thompson, CXCR4 expression is elevated in glioblastoma multiforme and correlates with an increase in intensity and extent of peritumoral T2-weighted magnetic resonance imaging signal abnormalities, Neurosurgery 63 (2008) 560–569, http://dx.doi.org/10.1227/01.NEU.0000324896.26088.EF.

[13] B.-C. Zhao, Z.-J. Wang, W.-Z. Mao, H.-C. Ma, J.-G. Han, B. Zhao, H.-M. Xu, CXCR4/SDF-1 axis is involved in lymph node metastasis of gastric carcinoma, World J. Gastroenterol. 17 (2011) 2389–2396, http://dx.doi.org/10.3748/wjg.v17.i19.2389.

[14] M. Burger, A. Glodek, T. Hartmann, A. Schmitt-Gräff, L.E. Silberstein, N. Fujii, T.J. Kipps, J.A. Burger, Functional expression of CXCR4 (CD184) on small-cell lung cancer cells mediates migration, integrin activation, adhesion to stromal cells, Oncogene 22 (2003) 8093–8101, http://dx.doi.org/10.1038/sj.onc.1207097.

[15] F. Danhier, E. Ansorena, J.M. Silva, R. Coco, A. Le Breton, V. Préat, PLGA-based nanoparticles: An overview of biomedical applications, J. Control. Release 161 (2012) 505–522, http://dx.doi.org/10.1016/j.jconrel.2012.01.043.

[16] R.M. Mainardes, R.C. Evangelista, PLGA nanoparticles containing praziquantel: effect of formulation variables on size distribution, Int. J. Pharm. 290 (2005) 137–144, http://dx.doi.org/10.1016/j.ijpharm.2004.11.027.

[17] X. Song, Y. Zhao, W. Wu, Y. Bi, Z. Cai, Q. Chen, Y. Li, S. Hou, PLGA nanoparticles simultaneously loaded with vincristine sulfate and verapamil hydrochloride: systematic study of particle size and drug entrapment efficiency, Int. J. Pharm. 350 (2008) 320–329, http://dx.doi.org/10.1016/j.ijpharm.2007.08.034.

[18] M.K. Tran, A. Swed, F. Boury, Preparation of polymeric particles in CO_2 medium using non-toxic solvents: formulation and comparisons with a phase separation method, Eur. J. Pharm. Biopharm. 82 (2012) 498–507, http://dx.doi.org/10.1016/j.ejpb.2012.08.005.

[19] N. Grabowski, H. Hillaireau, J. Vergnaud, N. Tsapis, M. Pallardy, S. Kerdine-Römer, E. Fattal, Surface coating mediates the toxicity of polymeric nanoparticles towards human-like macrophages, Int. J. Pharm. 482 (2015) 75–83, http://dx.doi.org/10.1016/j.ijpharm.2014.11.042.

[20] E. Cohen-Sela, M. Chorny, N. Koroukhov, H.D. Danenberg, G. Golomb, A new double emulsion solvent diffusion technique for encapsulating hydrophilic molecules in PLGA nanoparticles, J. Control. Release 133 (2009) 90–95, http://dx.doi.org/10.1016/j.jconrel.2008.09.073.

[21] J. Liu, Z. Qiu, S. Wang, L. Zhou, S. Zhang, A modified double-emulsion method for the preparation of daunorubicin-loaded polymeric nanoparticle with enhanced *in vitro* anti-tumor activity, Biomed. Mater. 5 (2010) 65002, http://dx.doi.org/10.1088/1748-6041/5/6/065002.

[22] U. Bilati, E. Allémann, E. Doelker, Strategic approaches for overcoming peptide and protein instability within biodegradable nano- and microparticles, Eur. J. Pharm. Biopharm. 59 (2005) 375–388, http://dx.doi.org/10.1016/j.ejpb.2004.10.006.

[23] A. Sánchez, B. Villamayor, Y. Guo, J. McIver, M.J. Alonso, Formulation strategies for the stabilization of tetanus toxoid in poly(lactide-co-glycolide) microspheres, Int. J. Pharm. 185 (1999) 255–266, http://dx.doi.org/10.1016/S0378-5173(99)00178-7.

[24] J. Wang, K.M. Chua, C.H. Wang, Stabilization and encapsulation of human immunoglobulin G into biodegradable microspheres, J. Colloid Interface Sci. 271 (2004) 92–101, http://dx.doi.org/10.1016/j.jcis.2003.08.072.

[25] A. Giteau, M.C. Venier-Julienne, S. Marchal, J.L. Courthaudon, M. Sergent, C. Montero-Menei, J.M. Verdier, J.P. Benoit, Reversible protein precipitation to ensure stability during encapsulation within PLGA microspheres, Eur. J. Pharm. Biopharm. 70 (2008) 127–136, http://dx.doi.org/10.1016/j.ejpb.2008.03.006.

[26] B. Mukherjee, K. Santra, G. Pattnaik, S. Ghosh, Preparation, characterization and in-vitro evaluation of sustained release protein-loaded nanoparticles based on biodegradable polymers, Int. J. Nanomed. 3 (2008) 487–496, http://dx.doi.org/10.2147/IJN.S3938.

[27] T. Feczkó, J. Tóth, G. Dósa, J. Gyenis, Optimization of protein encapsulation in PLGA nanoparticles, Chem. Eng. Process. Process Intensif. 50 (2011) 757–765, http://dx.doi.org/10.1016/j.cep.2011.06.008.

[28] X. Jiang, H. Lin, D. Jiang, G. Xu, X. Fang, L. He, M. Xu, B. Tang, Z. Wang, D. Cui, F. Chen, H. Geng, Co-delivery of VEGF and bFGF via a PLGA nanoparticle-modified BAM for effective contracture inhibition of regenerated bladder tissue in rabbits, Sci. Rep. 6 (2016) 20784, http://dx.doi.org/10.1038/srep20784.

[29] M. Morales-Cruz, G.M. Flores-Fernández, M. Morales-Cruz, E.A. Orellano, J.A. Rodriguez-Martinez, M. Ruiz, K. Griebenow, Two-step nanoprecipitation for the production of protein-loaded PLGA nanospheres, Results Pharma Sci. 2 (2012) 79–85, http://dx.doi.org/10.1016/j.rinphs.2012.11.001.

[30] U. Bilati, E. Allémann, E. Doelker, Development of a nanoprecipitation method intended for the entrapment of hydrophilic drugs into nanoparticles, Eur. J. Pharm. Sci. 24 (2005) 67–75, http://dx.doi.org/10.1016/j.ejps.2004.09.011.

[31] L. Tang, J. Azzi, M. Kwon, M. Mounayar, R. Tong, Q. Yin, R. Moore, N. Skartsis, T.M. Fan, R. Abdi, J. Cheng, Immunosuppressive activity of size-controlled PEG-PLGA nanoparticles containing encapsulated cyclosporine A, J. Transplant. 2012 (2012) 1–9, http://dx.doi.org/10.1155/2012/896141.

[32] EMEA, ICH guideline Q3C (R6) on impurities: guideline for residual solvents, 2003. < http://www.ema.europa.eu/docs/en_GB/document_library/Scientific_guideline/2011/03/WC500104258.pdf > .

[33] A. Yang, L. Yang, W. Liu, Z. Li, H. Xu, X. Yang, Tumor necrosis factor alpha blocking peptide loaded PEG-PLGA nanoparticles: preparation and in vitro evaluation, Int. J. Pharm. 331 (2007) 123–132, http://dx.doi.org/10.1016/j.ijpharm.2006.09.015.

[34] J. Coleman, A. Lowman, Biodegradable nanoparticles for protein delivery: analysis of preparation conditions on particle morphology and protein loading, activity and sustained release properties, J. Biomater. Sci. Polym. Ed. ahead-of-p (2012) 1–23, doi: 10.1163/092050611X576648.

[35] O. Dudeck, O. Jordan, K.T. Hoffmann, A.F. Okuducu, K. Tesmer, T. Kreuzer-Nagy, D.A. Rüfenacht, E. Doelker, R. Felix, Organic solvents as vehicles for precipitating liquid embolics: a comparative angiotoxicity study with superselective injections of swine rete mirabile, Am. J. Neuroradiol. 27 (2006) 1900–1906.

[36] A. Boongird, N. Nasongkla, S. Hongeng, N. Sukdawong, W. Sa-Nguanruang, N. Larbcharoensub, Biocompatibility study of glycofurol in rat brains, Exp. Biol. Med. 236 (2011) 77–83, http://dx.doi.org/10.1258/ebm.2010.010219.

[37] H.S. Yoo, T.G. Park, Biodegradable polymeric micelles composed of doxorubicin conjugated PLGA – PEG block copolymer, J. Control. Release 70 (2001) 63–70.

[38] M. Morille, T. Van-Thanh, X. Garric, J. Cayon, J. Coudane, D. Noël, M.C. Venier-Julienne, C.N. Montero-Menei, New PLGA-P188-PLGA matrix enhances TGF-β3 release from pharmacologically active microcarriers and promotes chondrogenesis of mesenchymal stem cells, J. Control. Release 170 (2013) 99–110, http://dx.doi.org/10.1016/j.jconrel.2013.04.017.

[39] R. Milner, G. Edwards, C. Streuli, C. Ffrench-Constant, A role in migration for the alpha V beta 1 integrin expressed on oligodendrocyte precursors, J. Neurosci. 16 (1996) 7240–7252.

[40] D. Séhédic, I. Chourpa, C. Tétaud, A. Griveau, C. Loussouarn, S. Avril, C. Legendre, N. Lepareur, D. Wion, F. Hindré, F. Davodeau, E. Garcion, Locoregional Confinement and Major Clinical Benefit of ^{188}Re-Loaded CXCR4-Targeted Nanocarriers in an Orthotopic Human to Mouse Model of Glioblastoma, Theranostics 7 (2017) 4517–4536, http://dx.doi.org/10.7150/thno.19403.

[41] A. Swed, T. Cordonnier, A. Dénarnaud, C. Boyer, J. Guicheux, P. Weiss, F. Boury, Sustained release of TGF-β1 from biodegradable microparticles prepared by a new green process in CO2 medium, Int. J. Pharm. 493 (2015) 357–365, http://dx.doi.org/10.1016/j.ijpharm.2015.07.043.

[42] B.J.P. Heurtault, P. Saulnier, B. Pech, J.E. Proust, A novel phase inversion-based process for the preparation of lipid nanocarrier, Pharm. Res. 19 (2002) 875–880.

[43] F. Li, S. Li, M. Vert, Synthesis and rheological properties of polylactide/poly(ethylene glycol) multiblock copolymers, Macromol. Biosci. 5 (2005) 1125–1131, http://dx.doi.org/10.1002/mabi.200500143.

[44] A. Harrane, A. Leroy, H. Nouailhas, X. Garric, J. Coudane, B. Nottelet, PLA-based biodegradable and tunable soft elastomers for biomedical applications, Biomed. Mater. 6 (2011) 65006, http://dx.doi.org/10.1088/1748-6041/6/6/065006.

[45] A. Swed, T. Cordonnier, A. Dénarnaud, C. Boyer, J. Guicheux, P. Weiss, F. Boury, Sustained release of TGF-??1 from biodegradable microparticles prepared by a new green process in CO_2 medium, Int. J. Pharm. 493 (2015) 357–365, http://dx.doi.org/10.1016/j.ijpharm.2015.07.043.

[46] S. Kandalam, L. Sindji, G.J.-R. Delcroix, F. Violet, X. Garric, E.M. André, P.C. Schiller, M.-C. Venier-Julienne, A. des Rieux, J. Guicheux, C.N. Montero-Menei, Pharmacologically active microcarriers delivering BDNF within a hydrogel: novel strategy for human bone marrow-derived stem cells neural/neuronal differentiation guidance and therapeutic secretome enhancement, Acta Biomater. (2016), http://dx.doi.org/10.1016/j.actbio.2016.11.030.

[47] D. Mustafi, C.M. Smith, M.W. Makinen, R.C. Lee, Multi-block poloxamer surfactants suppress aggregation of denatured proteins, Biochim. Biophys. Acta – Gen. Subj. 1780 (2008) 7–15, http://dx.doi.org/10.1016/j.bbagen.2007.08.017.

[48] A. Paillard-Giteau, V.T. Tran, O. Thomas, X. Garric, J. Coudane, S. Marchal, I. Chourpa, J.P. Benoît, C.N. Montero-Menei, M.C. Venier-Julienne, Effect of various additives and polymers on lysozyme release from PLGA microspheres prepared by an s/o/w emulsion technique, Eur. J. Pharm. Biopharm. 75 (2010) 128–136, http://dx.doi.org/10.1016/j.ejpb.2010.03.005.

[49] S. James, J.J. McManus, Thermal and solution stability of lysozyme in the presence of sucrose, glucose, and trehalose, J. Phys. Chem. B 116 (2012) 10182–10188, http://dx.doi.org/10.1021/jp303898g.

[50] N. Pirooznia, S. Hasannia, A. Lotfi, M. Ghanei, Encapsulation of Alpha-1 antitrypsin in PLGA nanoparticles. In Vitro characterization as an effective aerosol formulation in pulmonary diseases, J. Nanobiotechnol. 10 (2012) 20, http://dx.doi.org/10.1186/1477-3155-10-20.

[51] F. De Jaeghere, E. Allémann, J. Feijen, T. Kissel, E. Doelker, R. Gurny, Freeze-drying and lyopreservation of diblock and triblock poly(lactic acid)-poly(ethylene oxide) (PLA-PEO) copolymer nanoparticles, Pharm. Dev. Technol. 5 (2000) 473–483, http://dx.doi.org/10.1081/PDT-100102031.

[52] S. Honary, F. Zahir, Effect of zeta potential on the properties of nano – drug delivery systems – a review (Part 2), Trop. J. Pharm. Al Res. 12 (2013) 265–273, http://dx.doi.org/10.4314/tjpr.v12i2.19.

[53] W. Abdelwahed, G. Degobert, H. Fessi, Investigation of nanocapsules stabilization by amorphous excipients during freeze-drying and storage, Eur. J. Pharm. Biopharm. 63 (2006) 87–94, http://dx.doi.org/10.1016/j.ejpb.2006.01.015.

[54] W. Abdelwahed, G. Degobert, S. Stainmesse, H. Fessi, Freeze-drying of nanoparticles: Formulation, process and storage considerations, Adv. Drug Deliv. Rev. 58 (2006) 1688–1713, http://dx.doi.org/10.1016/j.addr.2006.09.017.

[55] M. Sameti, G. Bohr, M.N.V. Ravi Kumar, C. Kneuer, U. Bakowsky, M. Nacken, H. Schmidt, C.M. Lehr, Stabilisation by freeze-drying of cationically modified silica nanoparticles for gene delivery, Int. J. Pharm. 266 (2003) 51–60, http://dx.doi.org/10.1016/S0378-5173(03)00380-6.

[56] S.M. Patel, T. Doen, M.J. Pikal, Determination of end point of primary drying in freeze-drying process control, AAPS PharmSciTech. 11 (2010) 73–84, http://dx.doi.org/10.1208/s12249-009-9362-7.

[57] W. Abdelwahed, G. Degobert, H. Fessi, A pilot study of freeze drying of poly

(epsilon-caprolactone) nanocapsules stabilized by poly(vinyl alcohol): formulation and process optimization, Int. J. Pharm. 309 (2006) 178–188, http://dx.doi.org/10.1016/j.ijpharm.2005.10.003.

[58] G. Yang, K. Gilstrap, A. Zhang, L.X. Xu, X. He, Collapse temperature of solutions important for lyopreservation of living cells at ambient temperature, Biotechnol. Bioeng. 106 (2010) 247–259, http://dx.doi.org/10.1002/bit.22690.

[59] F. De Jaeghere, E. Allémann, J.C. Leroux, W. Stevels, J. Feijen, E. Doelker, R. Gurny, Formulation and lyoprotection of poly(Lactic acid-co-ethylene oxide) nanoparticles: influence on physical stability and In vitro cell uptake, Pharm. Res. 16 (1999) 859–866, http://dx.doi.org/10.1023/A:1018826103261.

[60] N. Shamim, L. Hong, K. Hidajat, M.S. Uddin, Thermosensitive-polymer-coated magnetic nanoparticles: adsorption and desorption of Bovine Serum Albumin, J. Colloid Interface Sci. 304 (2006) 1–8, http://dx.doi.org/10.1016/j.jcis.2006.08.047.

[61] M.J. Santander-Ortega, N. Csaba, L. González, D. Bastos-González, J.L. Ortega-Vinuesa, M.J. Alonso, Protein-loaded PLGA-PEO blend nanoparticles: encapsulation, release and degradation characteristics, Colloid Polym. Sci. 288 (2010) 141–150, http://dx.doi.org/10.1007/s00396-009-2131-z.

[62] T. Morita, Y. Sakamura, Y. Horikiri, T. Suzuki, H. Yoshino, Protein encapsulation into biodegradable microspheres by a novel S/O/W emulsion method using poly (ethylene glycol) as a protein micronization adjuvant, J. Control. Release 69 (2000) 435–444, http://dx.doi.org/10.1016/S0168-3659(00)00326-6.

[63] L.J. White, G.T.S. Kirby, H.C. Cox, R. Qodratnama, O. Qutachi, F.R.A.J. Rose, K.M. Shakesheff, Accelerating protein release from microparticles for regenerative medicine applications, Mater. Sci. Eng. C 33 (2013) 2578–2583, http://dx.doi.org/10.1016/j.msec.2013.02.020.

[64] I.J. Castellanos, W. Al-Azzam, K. Criebenow, Effect of the covalent modification with poly(ethylene glycol) on α-chymotrypsin stability upon encapsulation in poly (lactic-co-glycolic) microspheres, J. Pharm. Sci. 94 (2005) 327–340, http://dx.doi.org/10.1002/jps.20243.

[65] K.D. Hinds, K.M. Campbell, K.M. Holland, D.H. Lewis, C.A. Piché, P.G. Schmidt, PEGylated insulin in PLGA microparticles. In vivo and in vitro analysis, J. Control. Release 104 (2005) 447–460, http://dx.doi.org/10.1016/j.jconrel.2005.02.020.

[66] S. Hermeling, D.J.A. Crommelin, H. Schellekens, W. Jiskoot, Structure-immunogenicity relationships of therapeutic proteins, Pharm. Res. 21 (2004) 897–903, http://dx.doi.org/10.1023/B:PHAM.0000029275.41323.a6.

[67] C. Maas, S. Hermeling, B. Bouma, W. Jiskoot, M.F.B.G. Gebbink, A role for protein misfolding in immunogenicity of biopharmaceuticals, J. Biol. Chem. 282 (2007) 2229–2236, http://dx.doi.org/10.1074/jbc.M605984200.

[68] J. Park, P.M. Fong, J. Lu, K.S. Russell, C.J. Booth, W.M. Saltzman, T.M. Fahmy, PEGylated PLGA nanoparticles for the improved delivery of doxorubicin, Nanomed. Nanotechnol., Biol. Med. 5 (2009) 410–418, http://dx.doi.org/10.1016/j.nano.2009.02.002.

[69] J. Liu, S.M. Zhang, P.P. Chen, L. Cheng, W. Zhou, W.X. Tang, Z.W. Chen, C.M. Ke, Controlled release of insulin from PLGA nanoparticles embedded within PVA hydrogels, J. Mater. Sci. Mater. Med. 18 (2007) 2205–2210, http://dx.doi.org/10.1007/s10856-007-3010-0.

[70] M. Xia, R. Huang, K.L. Witt, N. Southall, J. Fostel, M.H. Cho, A. Jadhav, C.S. Smith, J. Inglese, C.J. Portier, R.R. Tice, C.P. Austin, Compound cytotoxicity profiling using quantitative high-throughput screening, Environ. Health Perspect. 116 (2008) 284–291, http://dx.doi.org/10.1289/ehp.10727.

[71] C. Maupas, B. Moulari, A. Béduneau, A. Lamprecht, Y. Pellequer, Surfactant dependent toxicity of lipid nanocapsules in HaCaT cells, Int. J. Pharm. 411 (2011) 136–141, http://dx.doi.org/10.1016/j.ijpharm.2011.03.056.

[72] G. Le Roux, H. Moche, A. Nieto, J.P. Benoit, F. Nesslany, F. Lagarce, Cytotoxicity and genotoxicity of lipid nanocapsules, Toxicol. Vitr. 41 (2017) 189–199, http://dx.doi.org/10.1016/j.tiv.2017.03.007.

[73] M. Partearroyo, H. Ostolaza, Surfactant-induced cell toxicity and cell lysis: a study using B16 melanoma cells, Biochem. (1990) 1323–1328, http://dx.doi.org/10.1016/0006-2952(90)90399-6.

UNIVERSITE BRETAGNE LOIRE
BIOLOGIE SANTE

université angers

USC
UNIVERSIDADE DE SANTIAGO DE COMPOSTELA

Titre : Développement, caractérisation physico-chimique et évaluation biologique d'éponges lyophilisées de fibroïne de soie et acide hyaluronique pour le piégeage de cellules de glioblastome

Mots clés : Piège à cellules tumorales; biomimétisme cérébral; implant poreux; éponges composites

Résumé : Le glioblastome (GBM) est une tumeur dévastatrice du système nerveux central. Malgré un traitement agressif, les récidives sont inévitables et l'application d'une stratégie thérapeutique efficace deumeure un défi. Le concept révolutionnaire de piège à cellules cancéreuses peut offrir de nouvelles opportunités. L'objectif est d'attirer et de confiner les cellules cancéreuses résiduelles entourant la cavité chirurgicale dans un implant polymère biomimétique délivrant des molécules chimioattractantes. Le SDF-1α, également appelé CXCL12, se lie sélectivement au récepteur CXCR4 à la surface des cellules de GBM infiltrantes et peut être utile pour induire le recrutement de ces cellules. Des éponges lyophilisées ont été préparées en combinant de la fibroïne de soie (SF), de l'acide hyaluronique (HA), de la poly-L-lysine (PLL) et de l'héparine (hep) réticulée avec N-(3-diméthylaminopropyl)-N'-éthylcarbodiimide (EDC) et du N-hydroxysulfosuccinimide (NHS). Les éponges ont montré une porosité élevée (près de 90%) avec des diamètres de pores moyens de 60 µm et contenait jusqu'à 95% d'eau une fois hydraté et un module de Young inférieur à 6 kPa. De plus, l'addition de SF dans la formulation a permis d'augmenter la stabilité des éponges dans le PBS comparé à l'éponge HA-PLL. Les éponges SF-HA et SF-HA-hep étaient capables de conserver 75% et 93% de la protéine SDF-1α respectivement après 7 jours dans du PBS supplémenté en enzymes (hyaluronidase et héparinase). Des études in vivo ont montré que les éponges SF-HA et SF-HA-hep étaient bien tolérées dans le cerveau des rats et que l'éponge SF-HA-hep ne libérait pas de SDF-1α dans le cerveau après 7 jours.

Title: Development, physicochemical characterisation and biological evaluation of silk fibroin/hyaluronic acid freeze-dried sponges for the trapping of glioblastoma cells

Keywords: Tumour cell trap; brain biomimicry; porous scaffold; composite sponges

Abstract: Glioblastoma (GBM) is a devastating tumour of the central nervous system. Despite an aggressive treatment, recurrence is inevitable, and the application of an effective therapeutic strategy remains a challenge. The breakthrough concept of cancer cell trap may offer new hopes and opportunities. The goal is to attract and confine the residual cancer cells surrounding the surgical cavity in a biomimetic polymeric scaffold delivering chemoattractive molecules. The stromal cell-derived factor-1α (SDF-1α), also called CXCL12, binds selectively to the CXCR4 receptor on the surface of infiltrative GBM cells and may be useful for inducing chemotaxis and the recruitment of residual GBM cells. In this work, series of freeze-dried sponges were prepared by combining silk fibroin (SF), hyaluronic acid (HA), poly-L-lysine (PLL) and heparin crosslinked with N-(3-dimethylaminopropyl)-N′-ethylcarbodiimide hydrochloride (EDC) and N-hydroxysulfosuccinimide sodium salt (NHS). Sponges showed high porosity (near 90%) with mean pore diameters ca. 60 µm and contained up to 95% water once hydrated. They presented a soft texture close to the one of a brain with a Young's Modulus down to 6 kPa. Moreover, addition of SF in the formulation yielded sponges with greater stability in PBS than the HA-PLL sponges. SF-HA and SF-HA-hep sponges were able to retain 75% and 93% of the SDF-1α protein respectively after 7 days in PBS supplemented with enzymes (hyaluronidase and heparinase). *In vivo* studies showed that the SF-HA and SF-HA-hep sponges were well tolerated in rats' brain and that the SF-HA-hep sponge did not release SDF-1α after 7 days in the brain.